



**TECHNISCHE
UNIVERSITÄT
WIEN**

Dissertation

The Role of Sterics and Electronics of PNP Pincer Ligands in Iron(II) and Manganese(I) Chemistry

ausgeführt zum Zwecke der Erlangung des akademischen Grades eines

Doktors der technischen Wissenschaften (Dr.techn.)

unter der Leitung von

a.o.Univ.Prof. Dipl.-Ing. Dr.techn. Karl Kirchner

E163 Institut für Angewandte Synthesechemie (IAS)

eingereicht an der Technischen Universität Wien

Fakultät für Technische Chemie

von

Mathias Glatz MSc.

0731595.

Staudach 216

A-8230 Hartberg-Fürstenfeld

Wien, im April 2018



TECHNISCHE
UNIVERSITÄT
WIEN

Ich habe zur Kenntnis genommen, dass ich zur Drucklegung meiner Arbeit unter der Bezeichnung

Dissertation

nur mit Bewilligung der Prüfungskommission berechtigt bin.

Ich erkläre weiters Eides statt, dass Ich meine Dissertation nach den anerkannten Grundsätzen für wissenschaftliche Abhandlungen selbstständig ausgeführt habe und alle verwendeten Hilfsmittel, insbesondere die zugrunde gelegte Literatur, genannt habe.

Weiters erkläre Ich, dass ich dieses Dissertations-Thema bisher weder im In- noch Ausland (einer Beurteilerin/einem Beurteiler zur Begutachtung) in irgendeiner Form als Prüfungsarbeit vorgelegt habe und dass diese Arbeit mit der vom Begutachter beurteilten Arbeit übereinstimmt.

Wien, im April 2018

Danksagung

Zuallererst danke ich Karl Kirchner, der mir die Möglichkeit gab in Seiner Arbeitsgruppe mitzuarbeiten und diese über die Jahre hinweg auch zu prägen. Sein visionäres Ziel „geile Chemie“ mit „coolen Metallen“ zu machen, macht ihn zu einem Vorreiter auf dem Gebiet der nachhaltigen Katalyse. Das uneingeschränkte Vertrauen, das in Seinen Mitarbeiter vermittelt ein „Wir“ Gefühl welches einzigartig für „die Kirchners“ ist. Fleiß, Erfolg und gute Stimmung schließen sich in dieser Arbeitsgruppe keinesfalls aus. Durch Seine unkomplizierte und zielorientierte Mentalität kann top aktuelle Forschung auf hohem Niveau betrieben werden und mit den Top Universitäten der Welt mithalten. Karl ist weinsame Klasse.

Der größte Dank gilt meiner Familie, welche mir mein Leben lang ein stabiles und sicheres Fundament gesichert hat, auf dem ich meine Persönlichkeit und Ausbildung aufbauen konnte. Ich konnte mich immer voll und ganz auf meine Interessen konzentrieren – Schaden und Sorgen wurden verlässlich von meiner Mutter „Ranne“ und Schwester „Kata“ abgewendet. Zwar neigen sie noch gerne dazu meine Selbständigkeit zu unterschätzen, aber diese regelmäßige Art von Kritik ist immer noch eine Triebkraft um mich persönlich zu verbessern. Vorschläge und Konzepte müssen schon bombenfest sein, um etwas durchzusetzen.

Besonderen Dank verdient mein Kollege und Namensvetter Matthias Mastalir. Über die Jahre bildeten wir ein unzertrennliches Duo, welches in manchen Situationen „Beavis und Butthead“ ähnelte...nur eben auf akademischem Niveau. Von ihm habe ich die Fähigkeit Projekte und Ziele umzusetzen gelernt. Oft versinken wir bei unseren Eskapaden in unserer eigenen Welt und lachen stundenlang ohne dass uns jemand folgen kann. Im starken Kontrast dazu, sind wir zielstrebig bei der Arbeit, frei von Konkurrenzdenken und fokussiert. Wir waren stets bedacht, die enge menschliche Verbindung und Teamarbeit an unsere Schützlinge weitergeben. Wenn unser Humor auch manchmal sehr persönlich ausgefallen ist, so möchte ich darauf hinweisen, dass wir herzensliebe Kabarettisten sind – jeder bekommt etwas vom Fett ab.

Ich möchte allen Leuten danken, welche an der flüssigen Funktion der Arbeitsgruppe beteiligt waren. Zu nennen wären zunächst alle aktiven Kirchners, Matthias „welcher“ Mastalir, Nikolaus „Tequila“ Gorgas, Gerald „Leiberl aus“ Tomsu, Julian „Juli“ Brünig, Daniel „Beeendl“ Himmelbauer, Stefan Weber, Wolfgang Eder, Jan Pecak und Markus Rotter. Auch die tatkräftige Unterstützung meiner ehemaligen Mitarbeiter Sathy, Berni, Özgür, Sara, Holzi, Afrooz soll gewürdigt sein.

Dank gilt auch an die anderen Arbeitsgruppen, welche mit Messungen, Knowhow und Gerätschaften Hilfe geleistet haben. Schon als Ehrenmitglied angesehen ist dabei der Röntgenkristallograph Berthold „DJ Oaschloch“ Stöger, der unzählige Strukturen aufgelöst hat. Seine Ambition für kontrastreiche musikalische Unterstreichung unserer Abende hat unsere Herzen gewonnen. Dank an Christian Hametner, dessen Messungen am 600er NMR die Charakterisierung der Mangan-Komplexen erst ermöglichte. Danke liebe Esthi, Danny, Christian und Marco für die kurzfristige Aushilfe bei Ressourcen- und Materialknappheit.

Vielen Dank an Peter Weinberger, der unser persönlicher Liquidator in Zeiten der Not und Verzweiflung war. Deine Geschichten in der Kaffeerunde werden uns noch lange erheitern.

Danke Svenni, für die gewissenhafte Planung des Synthesepraktikums, dein verlässlichen Ratschläge und den Ruhepol den du im Stockwerk bildest.

Danke an alle Praktikanten und Studenten welche unter meiner Leitung an den Ergebnissen oder auch Erlebnissen teilgenommen haben. Danke Lena, Andi, Emil für das vorantreiben der Manganchemie. Meinen frühesten Studies Clara, Alex, Viktor, Steffi wünsche ich viel Erfolg und hoffe dass wir uns noch oft an der Uni sehen werden.

Ich danke meiner alten Lerngruppe aus Graz „die 3 lustigen 4“ welche meinen chemischen Hintergrund definiert hat. Ich hoffe dass wir es nach dem Doktorat irgendwann schaffen, unser lange prophezeites Spaßsemester zu absolvieren.

Danke für die allgegenwärtige Freundschaft meiner Kollegen aus der Steiermark, Lukas, Peter, Albin und Heli. Obwohl wir uns nur vereinzelt treffen, ist das Gefühl so als ob wir uns gerade erst am Vortag getroffen hätten.

Zuletzt ein Dank an das gesamte Personal der TU Wien welche ich hier nicht mehr namentlich unterbringen konnte. All die unterhaltsamen Erlebnisse, Diskussionen und Veranstaltungen sind eine Bereicherung welche man gewiss an keinem anderen Ort der Welt finden könnte! Die Ausbildung die ich erfahren durfte, werde ich stolz in die Welt hinaustragen.

Cheers!

Kurzfassung

Die Ablösung von Edelmetallen in der homogenen Katalyse durch unedle Metalle ist ein Hauptziel der metallorganischen Chemie. Es ist dabei notwendig ein kompatibles Ligandensystem bereitzustellen, um katalytische Aktivität zu erhalten. Der Einfluss von strukturierten Liganden auf unedle Metalle wird am Beispiel von Eisen(II) und Mangan(I) Verbindungen gezeigt. Die Grundlage dieser Forschung bilden dreizählige „Pincer“ Liganden mit einem Pyridin Fragment, welches mit zwei Phosphan-Donoren verbunden ist (PNP-Liganden). Die Liganden unterscheiden sich im Aufbau der Verknüpfung (CH₂, NH, NMe, O) sowie der Phosphan-Reste (PR₂).

Eine neue Klasse von Eisen(II) PNP Pincer Komplexen, mit zwei Pincer-Liganden unterschiedlicher Zähigkeit (zweizählig und dreizählig) wird präsentiert. Diese Komplexe der Formel $\kappa^3, \kappa^2\text{-[Fe(PNP)}_2\text{X}]^+$ sind nur in Gegenwart kleiner Phosphan-Reste (PR₂; R = Me, Et, *n*Pr, *n*Bu, Ph) und NH als Verknüpfung (Linker) im PNP Liganden zu beobachten. Die Bildung dieser Komplexe geschieht unabhängig von der Stöchiometrie. Im ³¹P {¹H} NMR erhält man ein A₂B Spin-System für die koordinierten Phosphane, und ein Singulett für den freien nicht koordinierten Phosphan-Rest. Die Kristallstrukturen zeigen, dass eine Wasserstoffbrückenbindung zwischen den NH Linkern und dem Pyridin Stickstoff die Struktur stabilisiert. Die verzerrte Oktaeder führt zu einer großen Spannung, welche den zweizählig koordinierten Liganden destabilisiert. Eine Umordnung zu Dreizähligkeit oder Ligandaustausch durch ein Kohlenmonoxid Molekül (CO) ist möglich. Carbonyl Komplexe der Form $[\text{Fe(PNP)(CO)X}_2]$ werden so erhalten, welche bei Hitzeeinwirkung wiederum leicht CO verlieren können. Dieser Effekt ist umso stärker, je größer die Phosphan-Reste sind.

Mangan(I) PNP Pincer Komplexe des Typs $[\text{Mn(PNP)(CO)}_2\text{H}]$ stellten sich als Katalysatoren für die selektive Hydrierung von Aldehyden heraus. Funktionelle Gruppen wie Ketone, Nitrile, Ester und Olefine werden dabei toleriert. Unter den verwendeten PNP Liganden, zeigten jene mit NH Linkern die besten Ergebnisse. Die Ergebnisse lassen schließen, dass die Bifunktionalität der Liganden, und Ligand-Metall Wechselwirkung eine wichtige Rolle für den Mechanismus spielen. Umsatzzahlen von bis zu 10.000 Substraten pro Molekül wurden erreicht. Die Hydrierung verläuft bei Raumtemperatur, ohne Zusätze in protischen Lösungsmitteln. Analoge Rhenium(I) PNP Pincer Komplexe $[\text{Re(PNP)(CO)}_2\text{H}]$ zeigten deutlich schlechtere Umsätze (<100). Die Hydrid-Komplexe aktivierten außerdem Kohlendioxid (CO₂) in einer 1,2-Addition, wobei Formiat-Komplexe erhalten werden.

Die Ergebnisse bieten einen Leitfaden der Fe(II) und Mn(I) Pincer Chemie, zur gezielten Anpassung derer chemischen Eigenschaften.

Abstract

Base metal catalysis is an emerging field in organometallic chemistry to replace precious metals by earth abundant metals. To achieve so, a suited ligand backbone to support the non-precious metals is needed, in order to get catalytic activity. The influence of well designed ligands on base metal chemistry is exemplified on a series of iron(II) and manganese(II) compounds. The research bases on tridentate “pincer” ligands with a pyridine backbone connected with two phosphine donors (PNP-ligands). The ligands vary in the set-up of linkers (CH₂, NH, NMe, O) and phosphine moiety PR₂.

A new class of iron(II) PNP pincer complexes, made up of two pincer ligands in different bonding modes (tridentate and bidentate) is described. The complexes of general formula $\kappa^3, \kappa^2\text{-[Fe(PNP)}_2\text{X]}^+$ are only observed when small phosphines (PR₂; R = Me, Et, *n*Pr, *n*Bu, Ph) and a NH linker is apparent in the PNP ligands. In solution, the formation is inevitable, even when altering the stoichiometry. The ³¹P {¹H} NMR gives rise to an A₂B spin system for the coordinated phosphines, and a singlet for the vacant, non-coordinating phosphine. The X-ray structures reveal that a hydrogen bonding between NH linker and the pyridine nitrogen is stabilizing the coordination geometry. The distorted octahedral structure leads to a high degree of stress, which makes the bidentate ligand labile. Rearrangement to tridentate mode and displacement by carbon monoxide (CO) are possible. Carbonyl complexes of type [Fe(PNP)(CO)X₂] are accessible, which are prone to CO release on thermal treatment, with increasing steric demand of the phosphine.

Manganese(I) PNP pincer complexes of type [Mn(PNP)(CO)₂H] were found to be pre-catalysts for the selective hydrogenation of aldehydes. Functional groups like ketones, nitriles, esters and olefins are tolerated. Among the selected PNP ligands, NH linkers delivered the best results. The results suggest that bifunctionality of the ligand along with ligand-metal cooperation is essential for the mechanism. Turnover numbers (TON) of up to 10,000 could be achieved. The hydrogenation proceeds at room temperature, without additives in protic media. Analogue rhenium(I) PNP pincer complexes [Re(PNP)(CO)₂H] had inferior performance below 100 TONs. Additionally, the hydrido complexes [Mn(PNP)(CO)₂H] and [Re(PNP)(CO)₂H] activate carbon dioxide (CO₂) at ambient conditions. The 1,2-addition of CO₂ leads to a series of formate complexes of the types [Mn(PNP)(CO)₂(OCHO)] and [Re(PNP)(CO)₂(OCHO)].

In summary, these results offer a guide for Mn(I) and Fe(II) pincer chemistry allowing to alter the chemical properties in a modular fashion.

Contents

1	Introduction	1
1.1	Pincer Ligands.....	1
1.1.1	Pincer Complexes.....	2
1.1.2	Pyridine based PNP Pincer Ligands	3
1.2	Phosphine Ligands.....	4
1.2.1	Phosphine Building Blocks.....	4
1.3	Carbon Monoxide – Carbonyl Complexes	5
1.4	Iron(II) PNP Pincer Chemistry	6
1.4.1	Aromatic Backbones	7
1.4.2	Denticity of PNP Pincer Ligands	8
1.4.3	Application in Catalysis	9
1.4.4	Anionic Fe(II) PNP Pincer Complexes	12
1.5	Manganese(I) PNP Pincer Chemistry.....	13
1.5.1	Manganese(I) PNP Pincer Complexes	13
1.5.2	Catalytic Applications.....	15
2	Results and Discussion.....	19
2.1	Contributed Manuscripts.....	19
2.2	Context of Contributions	20
2.3	Original Manuscripts.....	22
3	Conclusion and Closing Words	83
4	State of Contribution	85
5	References.....	86
6	List of Figures	91
7	Abbreviation	92
8	Reprint Permissions.....	93
9	Curriculum Vitae (CV)	102

1 Introduction

The field of organometallic chemistry is generally considered as a discipline that combines organic (ligand) and inorganic (metal) frameworks to design molecules of a distinct structure. Further transformations on the obtained intermediates often lead to characteristics of severe interest. Especially transition metals pose remarkable reactivities. These include the activation of chemical bonds, a vital requirement for catalysts. Metal based asymmetric catalysis was honored with the Nobel Prize for chemistry in 2001. Organometallic compounds of noble metals, especially those of the platinoid group (Ru, Rh, Pd, Os, Ir, Pt) exhibited astonishing reactivity so far and new synthetic pathways were allowed. While highly active, many compounds proved to be stable enough for a convenient usage.

However, for economic and ecologic reasons, this research field is slowly parting ways from precious metals. Major drawbacks are increasing costs, limited abundance and none the less, health issues because of toxicity on very low levels. Throughout the years, this became a turning point, where research focuses on environmentally benign metals.¹ Especially the 1st row transition metals offer a nice selection of “non-toxic” and earth abundant elements. Base-metal chemistry is untenably overtaking the spotlight. Iron (Fe) and manganese (Mn) are among the two most common transition metals in the earth crust.² Catalysts based on these metals are of virtually endless supply and low price would relieve superb benefits.

To achieve so, ligands and metal precursors have to suit well. It is necessary to develop leading structures which enable a structured study on these components. This work contributes fundamental results to the understanding of the underlying chemical properties of such compounds.

1.1 Pincer Ligands

Pincer ligands or pincers are tridentate chelate ligands that utilize a meridional bonding geometry, which means that all coordinative bonds to the central atom (usually a metal) are in plane. The name pincer originates from its imaginative fixation of the metal center like a pincer tongs and was introduced by van Koten in 1989.³ Figure 1 demonstrates the basic structure of pincer ligands. Three donor groups (D^{1,2} and E) are linked together by any desired framework (Y). The surrounding backbone may be made up of rigid aromates or flexible aliphatic chains. Via coordinative bonding of a lone pair, a desired central atom (M) may be stabilized.⁴

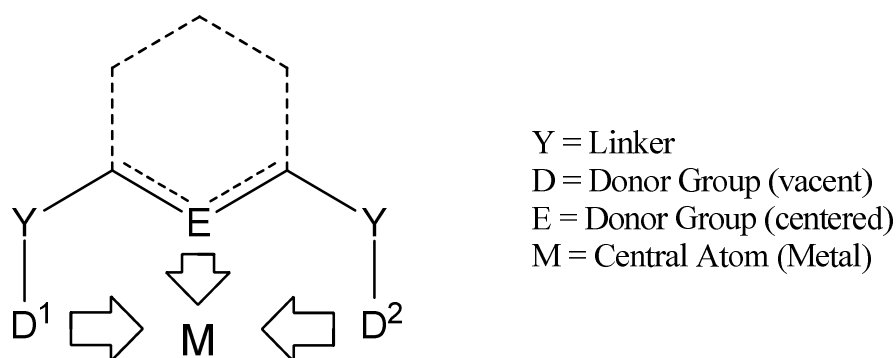


Figure 1: Basic structure of a pincer ligand and coordination to a metal center

For simplicity, groups of pincers are termed after its three donor atoms, generally denominated as DED. The characters, entitle the element-symbols of the donor atoms, most often C, N, P, S or O. Figure 1 displays a selection of common pincer ligands including their abbreviation. The charge of the pincers may also be altered according to the application, including anionic, neutral and (infrequent) cationic functionalities.⁵

1.1.1 Pincer Complexes

Pincer complexes are made up of their parent ligands. The “first” pincer complexes are always related to the syntheses of Moulton and Shaw, back in 1976.⁶ The nature of this complex class was studied into the early 80’s (Figure 2).⁷ These complexes exhibit an anionic PCP pincer backbone which resulted from C-H activation of a benzene or “CH₂” fragment. Since this was accomplished in alcoholic solvents, the driving force is not a deprotonation. This habit is naturally exclusive for noble metals (Rh, Ir, Pt) which is the reason why pincer chemistry stepwise emerged from precious metal coordination chemistry.

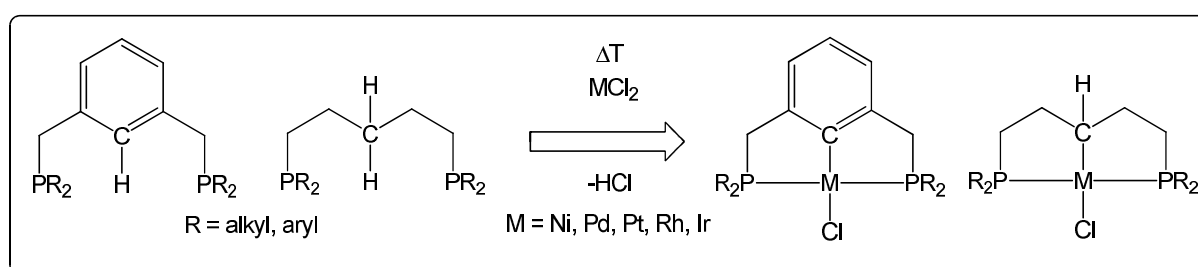


Figure 2: Synthesis of PCP pincer complexes by Shaw

For most pincer complexes, a five-membered metallacycle is the most favored, but depending on the ligand and size of the metal, also six-membered metallacycles are possible. Shaw and coworkers reported exceptional high thermal stability which is a huge benefit in organometallic catalysis. Numerous manuscripts comprise the sheer potential and finesse of precious pincer complexes, in countless applications as catalysts, switches and sensors.⁸ These include activation of small molecules,

transfer hydrogenations, cross-couplings, hydrogenations, oxidations and many more (Figure 3).

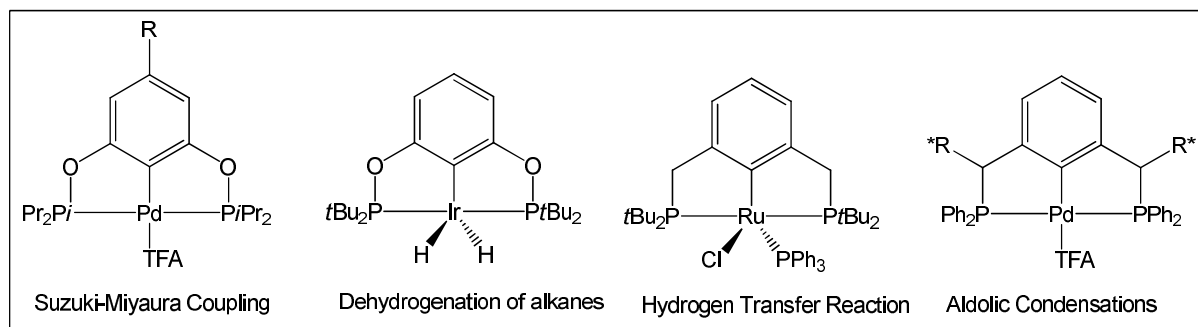


Figure 3: Applications of precious metal pincer complexes

1.1.2 Pyridine based PNP Pincer Ligands

Among the class of PNP pincers, the aromatic pyridine is known since before the works of Shaw. Based on a 2,6-Lutidine PNP pincer, Nelson *et al.* characterized a series of 1st row transition metal PNP pincer complexes.⁹ It wasn't until Sacco *et al.* that these complexes were utilized in noticeable reactions like water-gas-shift and Pd-chemistry.¹⁰ Meanwhile, the pyridine motive underwent considerable popularity in modern pincer chemistry. Despite its plain structure, a 2,6-substituted pyridine frame has many possibilities to systematically alter the ligand profile (Figure 4).

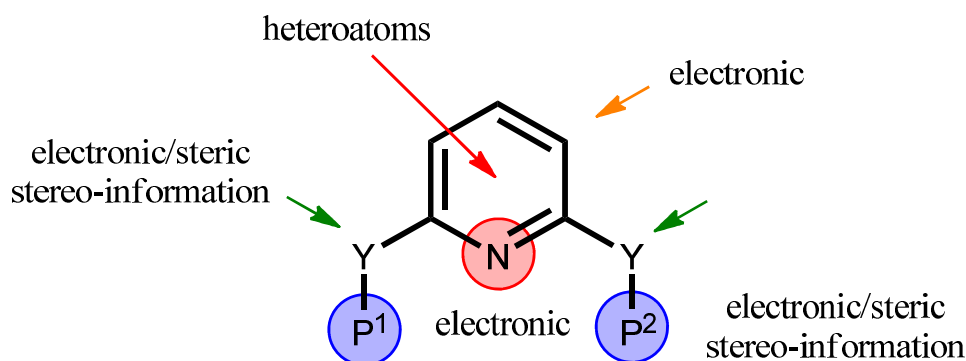


Figure 4: Versatility of 2,6-substituted pyridine moiety

- Modifying the 3, 4 or 5 position changes electronics and solubility
- Introducing additional hetero atoms (N, O) influences the π -electron density
- Linkers Y can vary in bulkiness, chirality and electron withdrawing habits
- Donors P^{1,2} can be adjusted to any means, once the leading structure is set

Pyridine precursors, for the synthesis of PNP pincer ligands fulfill all features, which are desired in comparative catalytic applications: Stability, simplicity, tunability and cost efficiency (low price, good availability). The selection of the ligands, used in this work, originates from these indispensable benefits (Figure 5).¹¹

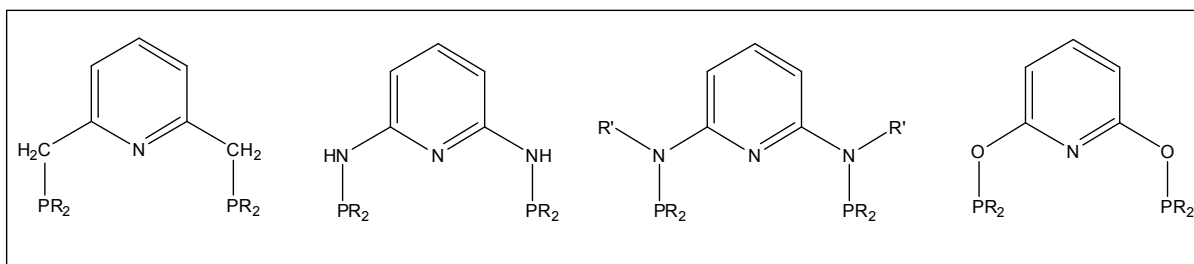


Figure 5: PNP pincer ligands used in this work

1.2 Phosphine Ligands

Noticeably, the listing of pincer-complexes was imbued with phosphorus containing ligands. Indeed, the presence of phosphines is inevitable for many of the praised homogeneous catalysts.¹² Compared to nitrogen, phosphorus is a soft Lewis base and tends to form stronger bonds towards soft transition metals. Tertiary phosphines PR_3 are considered as strong σ -donors but weak π -acceptors.¹³ This effect can be increased by electron donating groups EDG (silyl or alkyl) or decreased by electron withdrawing groups EWG (alkoxy, aryl, amino). This thermodynamic impact makes it possible to shape the nature of the metal center for successful catalysis. At the same time, kinetic impact can be adjusted by the size of the phosphine, without much change in electronics. These parameters have been summarized in an extensive review by Chadwick Tolman.¹⁴ An additional advantage of phosphines as ligand, is the excellent sensitivity of the ^{31}P nucleus in nuclear magnet resonance (NMR) spectroscopy.¹⁵ Combined with its natural abundancy of 100%, this is a superb method for characterization of intermediates and facilitates the study of reactive intermediates. Even small amounts may be traced in solution and pathways can be monitored in real time.

1.2.1 Phosphine Building Blocks

Planning the synthesis of ligands usually involves a retrosynthetic analysis to figure out alternative routes for a successful implementation.¹⁶ The synthesis of a 2,6-lutidine PNP pincer may be executed from two different synthetic approaches (Figure 6).

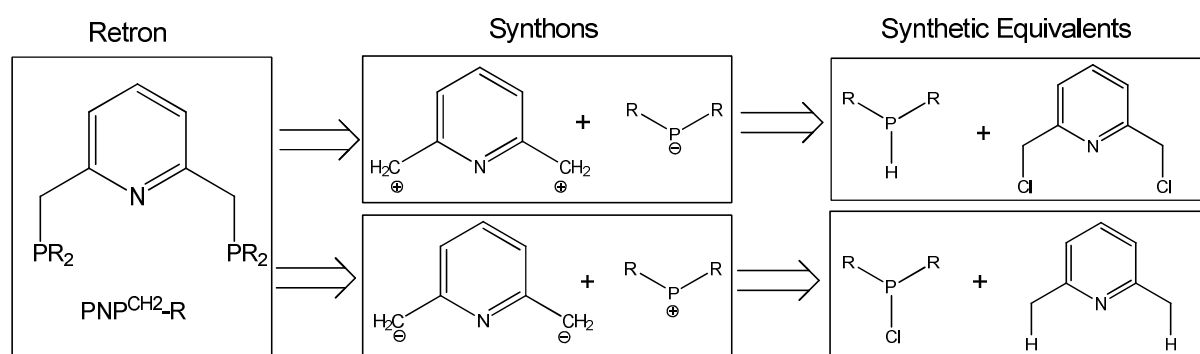


Figure 6: Retrosynthetic analysis of a PNP pincer with CH_2 linkers

For the building block of the phosphine rest PR_2 , two synthons are plausible – a nucleophilic and an electrophilic. This also counts for the 2,6-lutidine. The decision is naturally made after considering convenience, costs, supply and sustainability. In this case, both synthetic routes are reported in literature – still after modifications either could fail.

The practical aspect about tertiary phosphine precursors is the great variety of procedures to convert one synthon into another (Figure 7). The most important precursors are chlorophosphines and secondary phosphines since they are atom economic and straight forward. Chemical vendors have many of the commonly used chlorophosphines (usually cheaper) and secondary phosphines in stock. Both can be interconverted by strong chlorinating agents/strong reducing hydrides.¹⁷

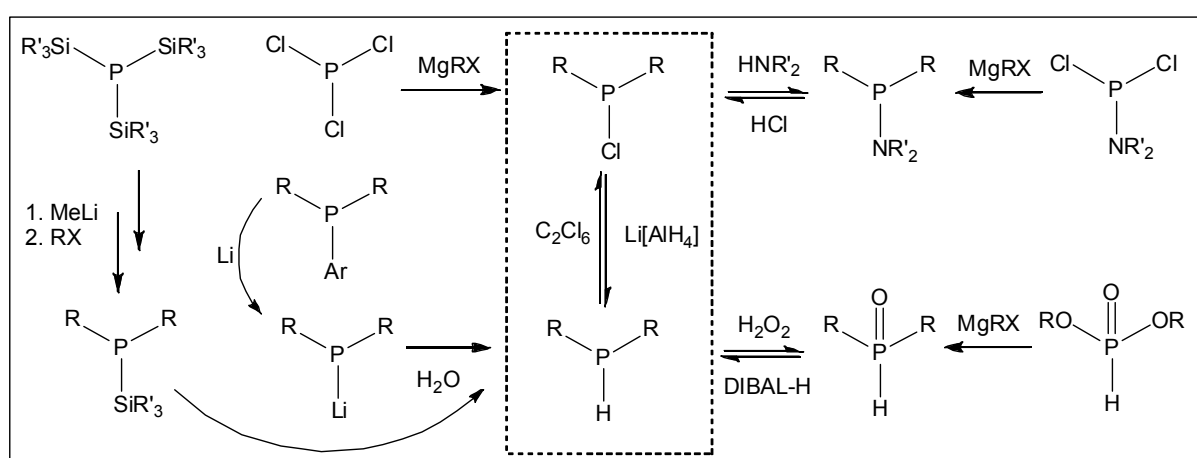


Figure 7: Synthetic concept for the preparation of tertiary phosphine precursors

Grignard alkylation of cheap PCl_3 is a very robust technique for a majority of phosphineprecursors.¹⁸ Size and electronic composition of R may need alternative routes through aminophosphines. The P-H bond is then cleaved cleanly by dry HCl gas.¹⁹ A smooth way to secondary phosphines, avoiding sensitive starting materials, is the alkylation of dialkoxyphosphites followed by reduction of the phosphine oxide with DIBAL-H.²⁰ A special synthetic case is the reduction of tertiary phosphines with Li when one aryl group (Ar) is apparent.²¹ Chiral phosphines usually need a synthetic approach via silylphosphino precursors.²²

1.3 Carbon Monoxide – Carbonyl Complexes

Carbon monoxide (CO) is a gaseous molecule of little reactivity in absence of oxidizing agents. However, to the human body (respiration cycle), CO is a serious threat because of its irreversible affinity to the heme molecule.²³ Homoleptic carbonyl complexes were studied very early in history. Metalcarbonyl research was initiated after the innovative protocol of Ludwig Mond, who isolated nickel of high purity from an equilibrium with nickel tetracarbonyl $[Ni(CO)_4]$.²⁴ Nowadays, CO plays a key role as a spectator/non-innocent ligand in catalysis and organometallic chemistry.²⁵

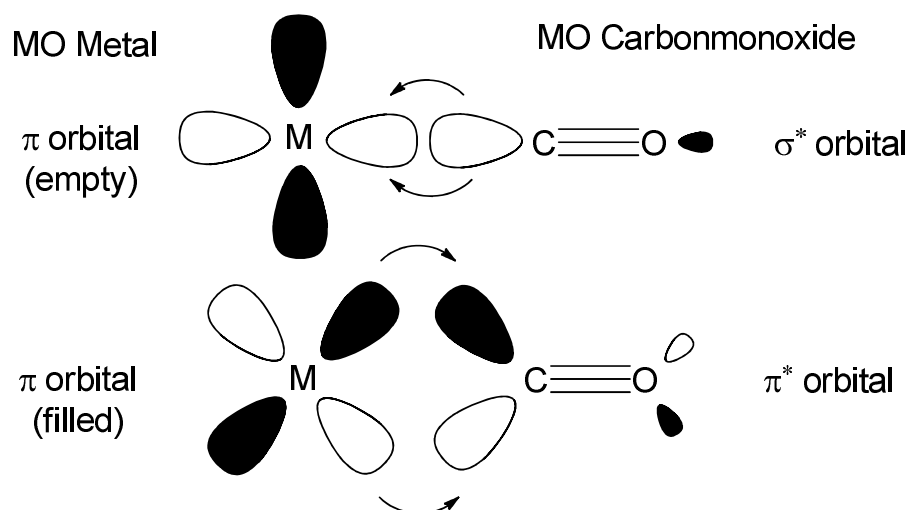


Figure 8: Illustration of σ -donor/ π -acceptor interaction in metal-CO complexes

The prowess of CO as a stabilizing ligand lies in the nature of its π^* molecule orbital (MO). Molecule orbitals of metals may interact in two ways with CO (Figure 8).

- The σ^* molecule orbital of CO is centered at the carbon atom and filled with 2 electrons. Through centrosymmetric interaction with an empty d-orbital of the metal (M) electron density can be transferred to the metal center. This effect has usually little overall influence.
- The π^* MO of CO is also centered at the C-atom and empty. Electrons of an electron-rich metal center can be shifted into this empty orbital, resulting in thermodynamic stabilization, which favors a low spin state of the metal. This effect has tremendous consequences on the stability of the overall complex.

The reversible binding of CO combined with a color change is a subject of molecular gas sensors and switches.²⁶

1.4 Iron(II) PNP Pincer Chemistry

First catalytic applications of iron complexes grounded on the Lewis acidic character of the metal center in ionic iron salts, e.g. halides, sulfates and oxides. Until today, iron oxides as heterogeneous contact-catalysts, are indispensable in the production of ammonia via Haber-Bosch process.²⁷ Iron undergoes changes in oxidation states easily, which makes characterization challenging. “Quick-shot” approaches with crude iron oxides, delivered reasonable results in cross couplings, but the true reactive species is unknown. Through time and experience, it was figured out, that chelating ligands improve the stability of the catalysts. This was the initiator for the quest towards well defined iron complexes.²⁸ Pincer ligands offer a toolbox of stabilizing ligands with easy tunability, which unfolded the true capacity of this underrated metal.²⁹ A very pronounced feature is the hydrogenation of multiple bonds of polar nature like aldehydes, ketones, nitriles, esters, nitrates and even carbon dioxide.

Traditional mechanisms of related precious metal catalysts estimate that the formation and breaking of bonds happens exclusively at the metal center. Non-precious metals like iron usually need a cooperative agent, which helps shuttling protons/electrons. Often, pincer ligands already have integrated aiding functionalities like NH, CH₂ and conjugated aromatic systems. The terms “non-innocent” or “bifunctional” ligand are favorably used in this context.³⁰ All these circumstances propel the investigations of many research groups to utilize the full potential of iron complexes.

1.4.1 Aromatic Backbones

A classic structural motif of Fe(II) PNP pincer complexes is the pentacoordinated iron PNP dihalide [Fe(PNP)(X₂)]. These high spin complexes ($s = 5/2$) are 16-electron complexes of distorted square pyramidal geometry (Figure 9).

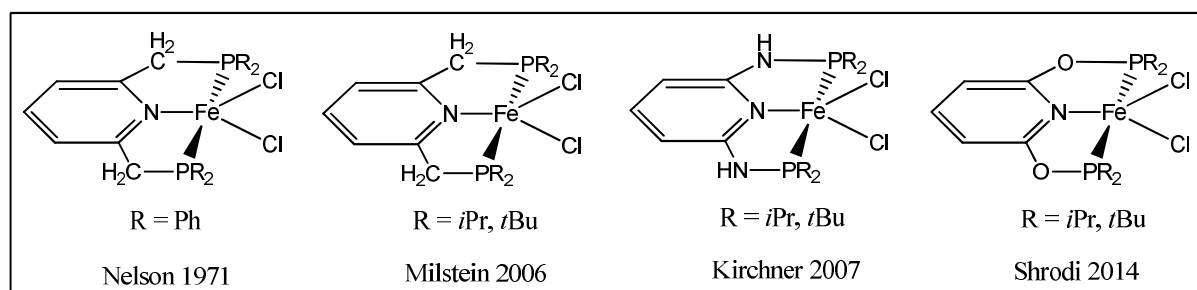


Figure 9: Selection of pentacoordinated Fe(II) PNP dichloro complexes

Aromatic pyridine-based pincers are the most frequently reported amongst them, with variations of the linker group (CH₂, NH, O). Although the earliest examples date back to the works of Nelson and Sacco, it wasn't before the mid 2000s that the reactivity of Fe(II) pincer complexes was studied (Figure 10). These studies rely on sterically demanding alkyl-phosphine moieties PR₂.³¹

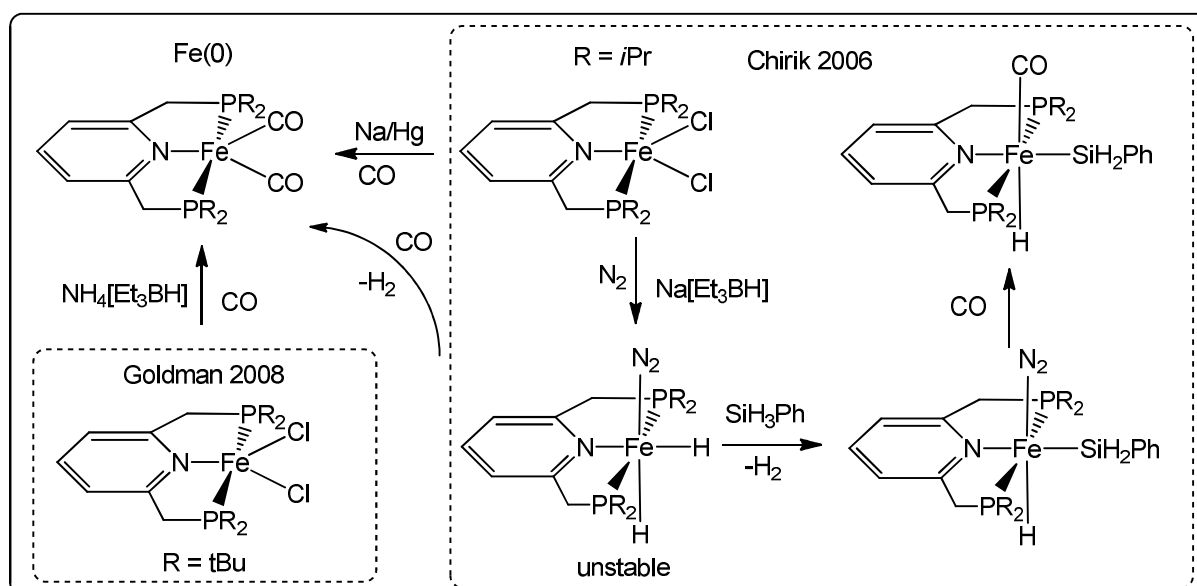


Figure 10: Synthesis of Fe(0) PNP biscarbonyl complexes

The isolation of stable Fe(0) PNP complexes was achieved by Chirik and Goldman, by reduction of Fe(II) PNP halides under CO atmosphere. Other highly reduced species were often too sensitive for full characterization. These results point out, that CO is a vital π -acceptor ligand to stabilize the electron rich Fe(0) center of d^8 -configuration. The geometry of $[\text{Fe}(\text{PNP})(\text{CO})_2]$ depicts perfect trigonal-bipyramidal geometry. They are diamagnetic, 18 electron complexes and the carbonyls show two stretching frequencies in IR-spectroscopy.³²

Fe(II) PNP carbonyl complexes are also accessible in a very convenient way. Unsaturated Fe(II) PNP halides readily bind CO in solid state and solution.³³ The reaction is accompanied by a color change from yellow to bright red/blue and may be monitored by the naked eye. The early works of the Kirchner group devoted several papers on these studies. The resulting complexes $[\text{Fe}(\text{PNP})(\text{Cl}_2)\text{CO}]$ are air-stable, octahedral 18 electron complexes. Two isomers (*cis* or *trans*) are observed, depending on the media (solid state, solution). Notably, this is a reversible process, since $[\text{Fe}(\text{PNP})\text{Cl}_2]$ is formed when heat and vacuum are applied (Figure 11).

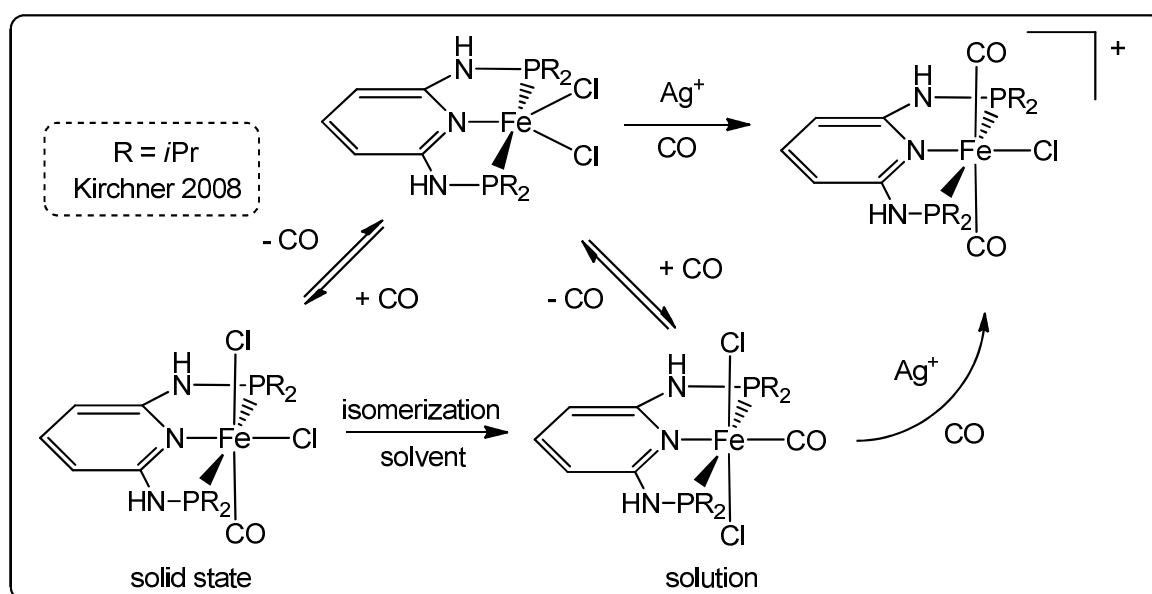


Figure 11: Reversible binding of CO by an iron(II) PNP pincer complex

Abstraction of a halide is achieved by silver(I) salts, which are strong halide scavengers. Under CO atmosphere, the vacant coordination site is occupied by a CO molecule. In absence of CO, the complex disproportionates to $[\text{Fe}(\text{PNP})\text{Cl}_2]$ and $[\text{Fe}(\text{PNP})(\text{CO})_2\text{Cl}]^+$. The process is irreversible, and only the *trans*-isomer was observed. In a very recent published work it was devoted, that also the *cis*-isomer is formed, after irradiation with visible light.³⁴

1.4.2 Denticity of PNP Pincer Ligands

In coordination chemistry, the term of denticity, describes the number of donors in one ligand, which are bound to the metal center. The notation κ ("kappa"), a greek

letter, and a subscript n ($n = 1, 2, 3, \dots$) is used for clarification. Pincers are expected to adopt a tridentate (κ^3) bonding mode, but in Fe(II) pincer complexes also other bonding modes (κ^2) have been observed (Figure 12).³⁵

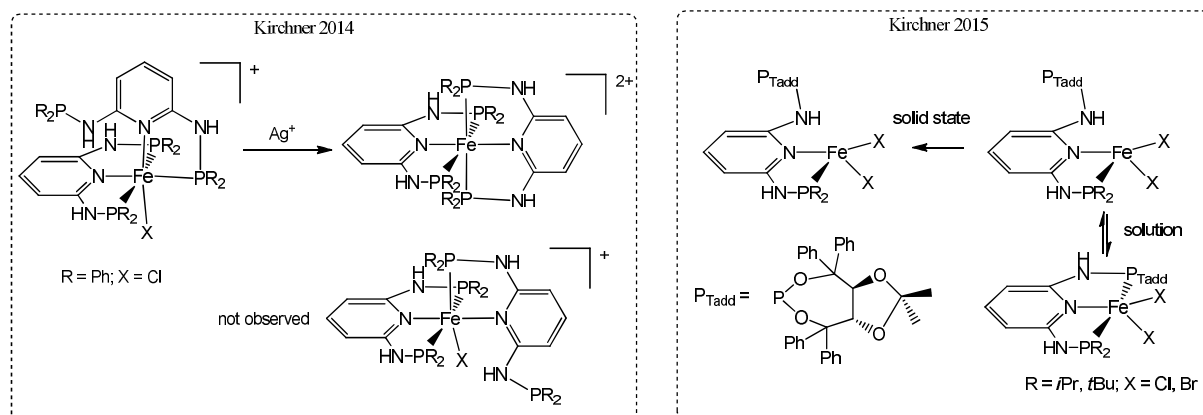


Figure 12: Fe(II) PNP pincer complexes with bidentate (κ^2) bonding modes

One example is a cationic octahedral Fe(II) complex, chelated by two 2,6-diaminopyridine PNP ligands. Remarkably, one pincer acts as tridentate, and the other as bidentate ligand, with the pyridines in *cis* configuration. The $^{31}\text{P}\{^1\text{H}\}$ NMR displays a A_2B spin system for the coordinated PR_2 , and a singlet for the vacant, non bonding PR_2 . Offering an additional coordination site by Ag(I)-salts or coordinating solvents, a dicationic complex of general formula $[\text{Fe}(\text{PNP})_2]^{2+}$ is formed. The other example uses a non-symmetrical PNP* pincer ligand, with one chiral phosphinite moiety. In solid state, apparently a tetrahedral complex of type $[\text{Fe}(\text{PN})\text{-P}^*\text{X}_2]$ is present, while in solution an equilibrium with the pentacoordinated $[\text{Fe}(\text{PNP}^*)\text{X}_2]$ exists.

1.4.3 Application in Catalysis

Applications in catalysis were still not quite ready. Fe(II) PNP carbonyls were too stable and Fe(0) carbonyls were too reactive for a convenient usage. However, these precursors were key for the breakthrough of Fe(II) pincer complexes in catalysis. Substitution of halides by hydrides and hydrido-equivalents uncovered a remarkable pool of highly active and selective catalysts in reductive chemistry.

Reduction of Aldehydes and Ketones to Alcohols

Hydrogenation uses molecular H_2 for saturation of multiple bonds. This reaction is unmatched in terms of sustainability, since it provides an atom efficiency of nearly 100 %. The activation barrier is very high at ambient conditions and needs a catalyst to get going. Transfer hydrogenation uses an alcohol, most commonly *iso*-propanol, as a “ H_2 ” source. Several Fe(II) PNP pincer hydrides have been developed, which are efficient pre-catalysts for hydrogenation and transfer hydrogenation.³⁶

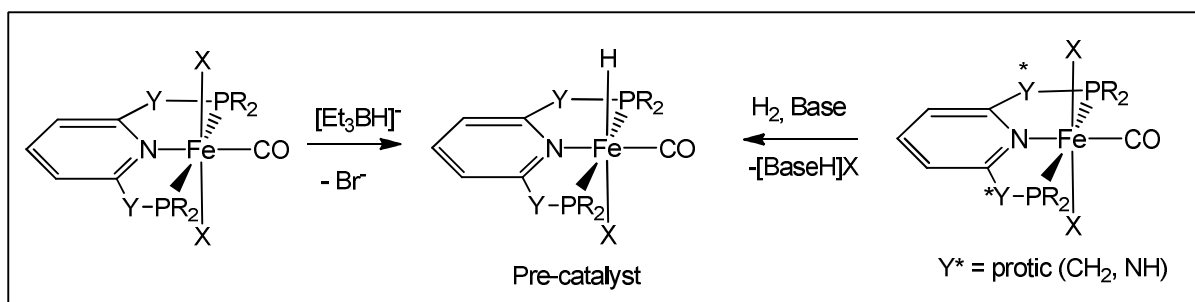


Figure 13: Pre-catalysts for hydrogenation of ketones and aldehydes

The Fe(II) PNP hydrido carbonyls in Figure 13 are prepared from their parent dibromo carbonyls via ligand exchange by H^- . Borohydrides and alkyl-borohydrides are popular reagents used for this reaction. But, hydrido complexes may also be formed in situ after addition of base in H_2 atmosphere. Notably, no related chloro compounds are reported.

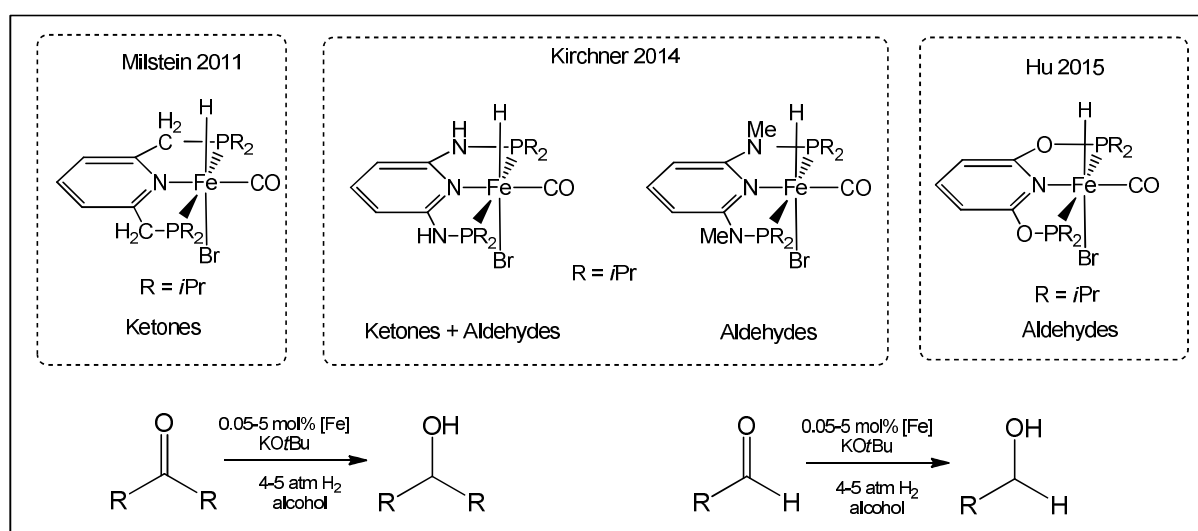


Figure 14: Pre-catalysts for hydrogenation of ketones and aldehydes

The pre-catalysts in Figure 14 are suited for the reduction of some carbonyl functionalities. Typical reaction conditions are very mild, with ambient temperatures and H_2 pressure. A common mutuality is the need of a strong base, especially at low catalyst loadings. The estimated role of the base is depending on the ligand system. Milstein proposed a deprotonation of the ligand, followed by cooperative activation of H-H bond. Kirchner proved the formation of a dihydrido species which is supposed to be the active catalyst in his cycle.

Reduction of ketones and aldehydes by hydrosilylation and aqueous workup was done by the group of Findlater.³⁷ The active catalyst was generated in situ, also by an alkyl borohydride agent (Figure 15).

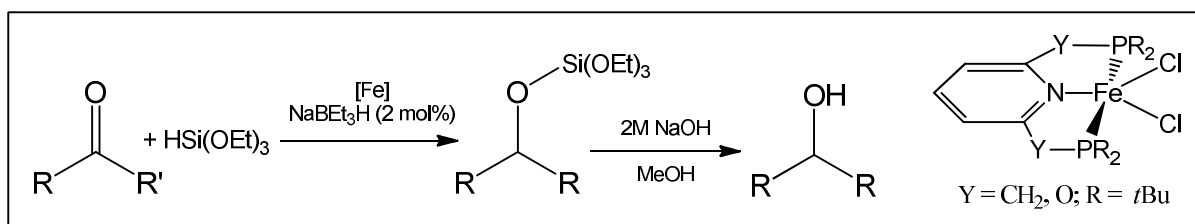


Figure 15: Hydrosilylation of secondary alcohols

Reduction of Carbon Dioxide

Carbon dioxide is a sustainable source for C1-buildingblocks, and in its reduced form (formaldehyde) also a futuristic candidate for energy storage.³⁸ Fe(II) formates are isolated as intermediates in a catalytic cycle of carbon dioxide reduction by dihydrogen.³⁹ Milstein's pyrazine based Fe(II) complexes activate and bind molecular CO in a ligand-metal cooperated mechanism under basic condition. Also base-triggered is Gonsalvi's pyridine based Fe(II) system via outer-sphere mechanism (Figure 16).

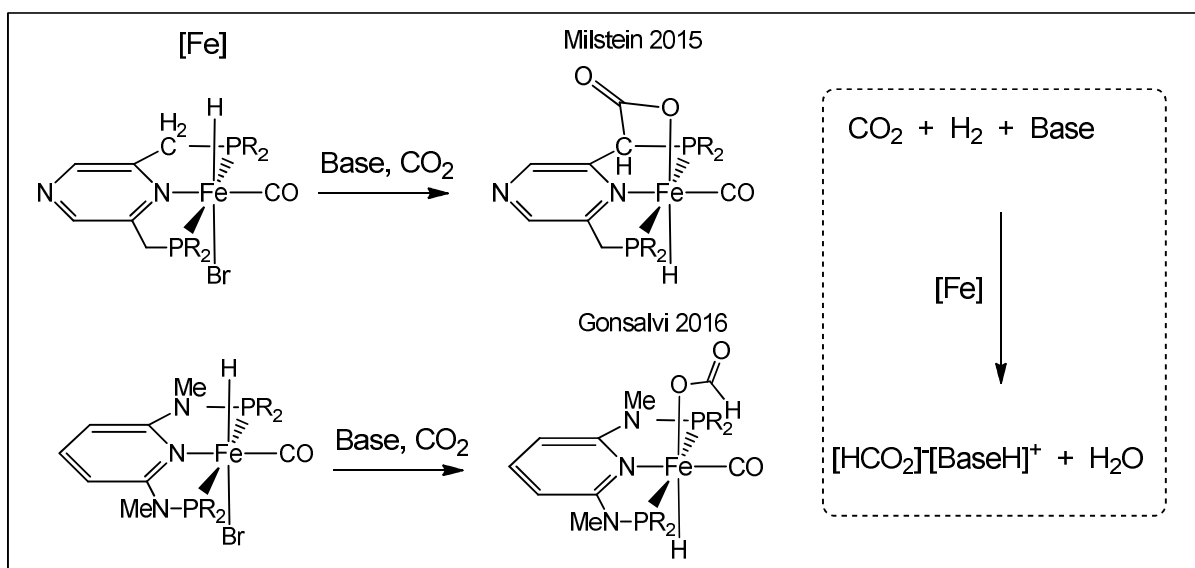


Figure 16: Hydrogenation of CO₂ catalyzed by Fe(II) PNP pincer complexes

Aliphatic Backbones

Iron PNP complexes based on aliphatic backbones like bis(phosphino)ethylamine, were established later on a time scale. A situational drawback is the flexibility of alkyl-chains. Compared to rigid aromatic structures, these tend to change coordination geometry after breakage of bonds. On the other hand, the bifunctionality of NH, directly at the metal center reveals new possibilities.⁴⁰

None the less, Fe(II) PNP pincer complexes on basis of bis(phosphino)ethylamine have shown impressive results in reduction of imines and dehydrogenation of methanol.⁴¹

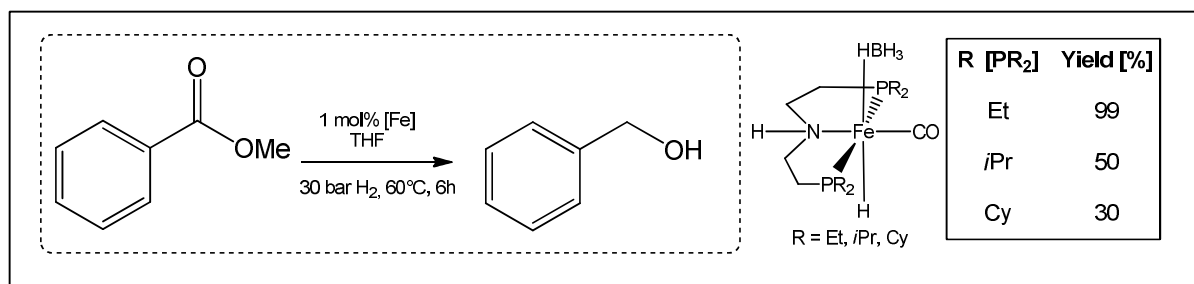


Figure 17: Hydrogenation of esters to alcohols catalyzed by Fe(II) PNP pincer complex

The reduction of esters by molecular hydrogen was performed in parallel works by the groups of Beller and Guan (Figure 17).⁴² This was done by highly activated hydrido-borohydrido Fe(II) PNP pincer complexes. The reaction displayed in Figure 17 does not proceed in absence of a bifunctional NH group. After replacement by a non-protic NMe functionality, no conversion was achieved at all.

1.4.4 Anionic Fe(II) PNP Pincer Complexes

Compared to neutral PNP pincer ligands, anionic PNP pincer ligands are less studied. Pyrrole backbones are far more electron rich than pyridines. The anionic charge poses a severe difference on the structural and electronic behavior of Fe(II). As proved in the publications of Mindiola, Caulton and Nishibayashi, the Fe(II) metal center adopts a tetra-coordinate state, either planar or pyramidal.⁴³ The high spin state of Fe(II) is very favorable in tetra-coordinate motives and CO is only bound upon treatment with strong reducing agents, yielding rarely seen Fe(I) species. The electron rich metal center of Nishibayashi activated the triple bond of molecular dinitrogen (Figure 18).

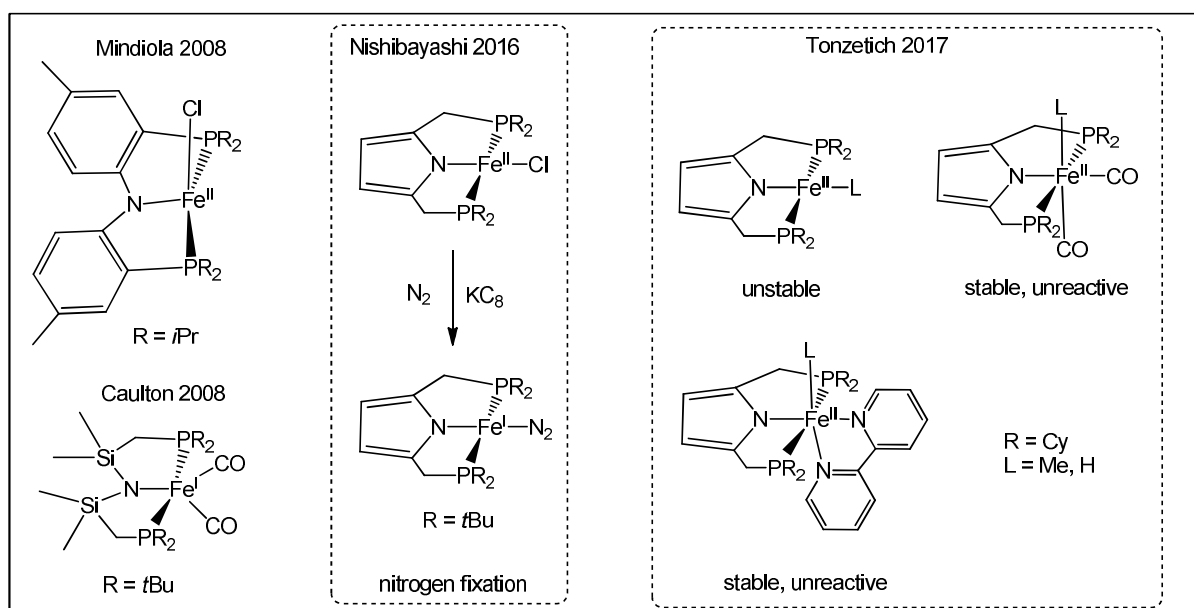


Figure 18: Iron PNP complexes with anionic ligand system

A series of works from the group of Tonzetich elaborated the challenge of pyrrole based PNP pincers.⁴⁴ The pyrrole-based Fe(II) PNP pincer complexes pose a

disadvantageous balance of stability and reactivity. Fe(II) PNP hydrides are too reactive for application, while dicarbonyls are too stable and hence unreactive. A supporting chelating ligand (bipyridine) trims just the right equilibrium.

1.5 Manganese(I) PNP Pincer Chemistry

Traditionally, manganese complexes are seen as redox-active compounds with a wide spectrum of stable oxidation states. In homogeneous catalysis, manganese is most well-known for oxidation reactions, especially in combination with salen ligands. Also, C-C coupling reactions are facilitated by manganese halides. All these reactions are usually based on higher oxidation states II-III. The utilization of manganese in lower oxidation states 0-I is still a very young field of research. Although C-H and C-X activations are achieved, the catalyst loadings need to be very high.⁴⁵ This is a result of low stability, reflected by a poor turnover number (TON). The characteristics of pincers pose promising possibilities for improvements. Fundamental research on manganese(I) chemistry is urgent for a better understanding. Very recent reviews summarize the latest development of Mn(I) PNP pincer complexes for catalytic applications like hydrogenation, aminoalkylation, hydrosilylation, etc.⁴⁶

1.5.1 Manganese(I) PNP Pincer Complexes

Manganese (I) compounds have d^6 electron configuration and are isoelectronic with Fe(II). The preferred coordination geometry is 6, especially in combination with π -acceptors like CO ligands. The most prominent manganese(I) precursor is manganese pentacarbonyl bromide $Mn(CO)_5Br$. It has superior stability towards oxidation and hydrolysis than the chloro analogue $Mn(CO)_5Cl$. Both are commercially available from common vendors. It may also be prepared from the cheaper dimanganese decacarbonyl $Mn_2(CO)_{10}$ (Figure 19).

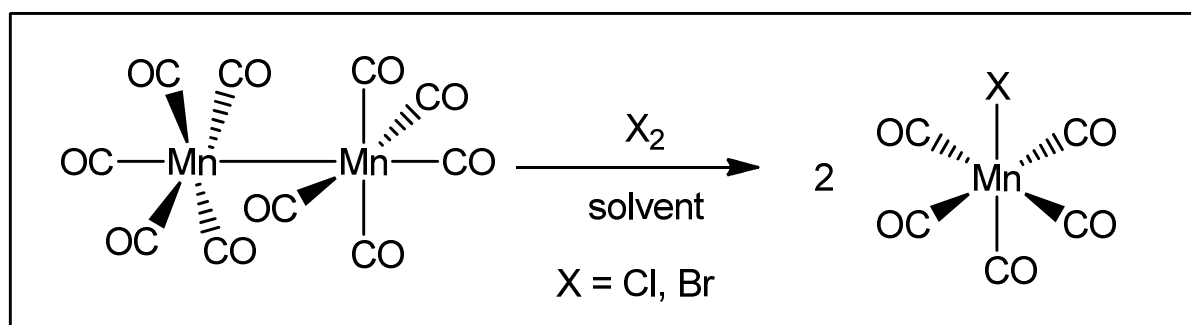


Figure 19: Synthesis of manganese-pentacarbonyl halide

Notably, $Mn_2(CO)_{10}$ is octahedral, with staggered conformation and has no bridging carbonyls.⁴⁷ Addition of chlorine gas or bromine into a solution of $Mn_2(CO)_{10}$ in a non-polar solvent yields $Mn(CO)_5X$ ($X = Cl, Br$) quantitatively.⁴⁸ The group of Nocera was the first one to synthesize Mn PNP pincer complexes from $Mn(CO)_5Br$ to obtain

neutral complexes of type $[\text{Mn}(\text{PNP})(\text{CO})_3]$. The PNP ligand consists of an amidobisphosphine system which was deprotonated beforehand. Alternatively, the same product was obtained from $\text{Mn}_2(\text{CO})_{10}$ in a non-innocent redox involvement of the ligand (Figure 20).⁴⁹

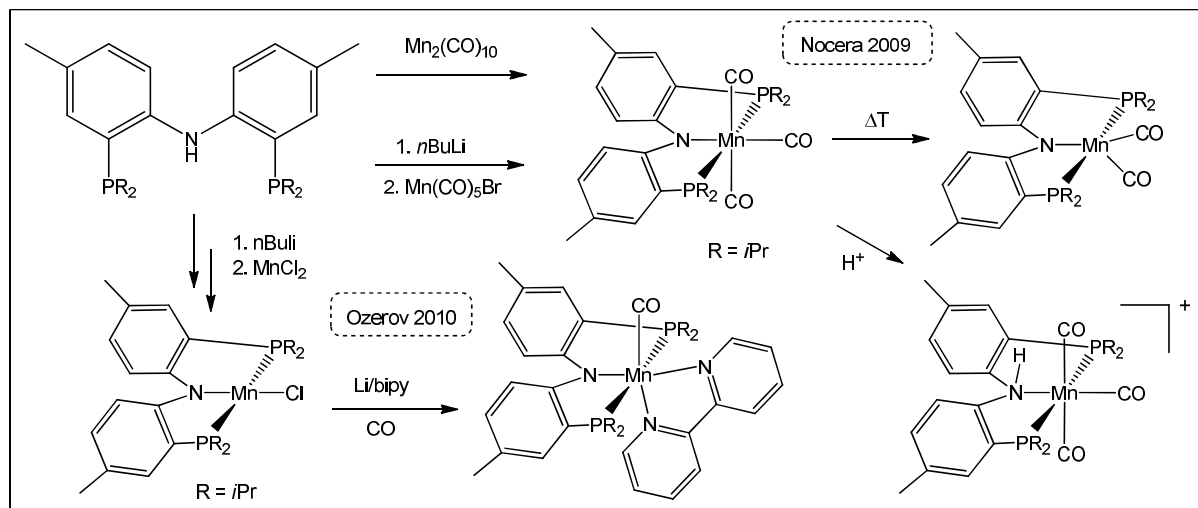


Figure 20: The first manganese(I) PNP pincer complexes by Nocera and Ozerov

Even though the complex was described to be very stable, a few reactivities have been observed. Thermal treatment resulted in the release of CO, obtaining a pentacoordinated 16 electron complex $[\text{Mn}(\text{PNP})(\text{CO})_2]$. The complex was isolated as a mixture with starting materials, but could be characterized by NMR spectroscopy. These kind of 16 electron carbonyl complexes are rare, and not observed for isoelectronic Fe(II). A cationic complex of type $[\text{Mn}(\text{PNP})(\text{CO})_3]^+$ was isolated after addition of triflic acid. The amido group in the backbone is protonated in this process. The indirect entry to a Mn(I) PNP pincer complex was achieved by the group of Ozerov.⁵⁰ Using the same amido diphosphine PNP ligand, they were able to obtain a tetracoordinated Mn(II) PNP chloride complex. Reduction with lithium-bipyridyl under CO atmosphere yielded $[\text{Mn}(\text{PNP})(\text{CO})(\text{bipy})]$.

2016 was the breakthrough year of Mn(I) pincer chemistry – several research groups independently developed Mn(I) pincer catalysts, based on well-developed pincer ligands established in Fe(II) chemistry.

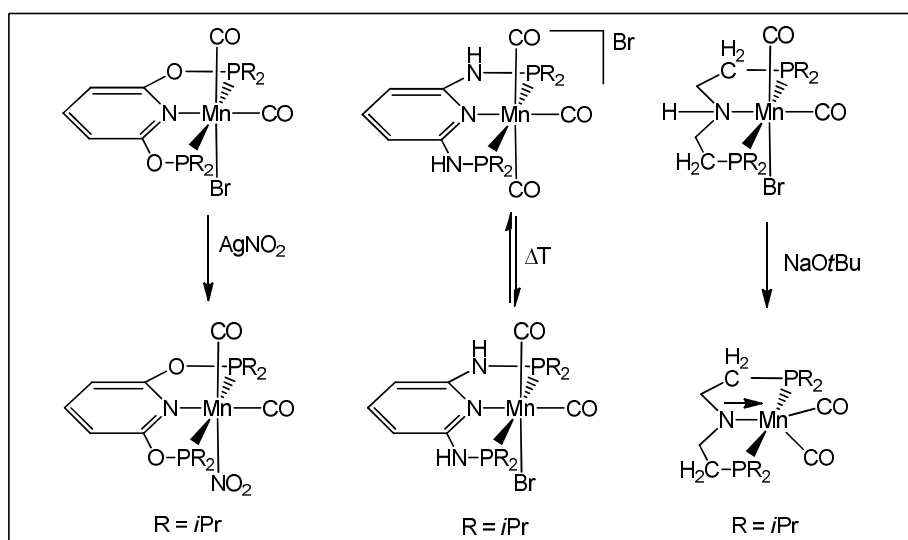


Figure 21: Reactivities of neutral Mn(I) PNP pincer complexes

Boncella and Tondreau contributed pioneering findings on aromatic and aliphatic Mn(I) PNP pincer complexes (Figure 21).⁵¹ Complexes of general formula *cis*-[Mn(PNP)(CO)₂Br] are generally the preferred isomers – no *trans* configurations were observed. Cationic manganese tricarbonyl complexes [Mn(PNP)(CO)₃]Br may be converted to [Mn(PNP)(CO)₂Br] at higher temperatures. Coordinating counter ions like nitrite (NO_2^-) can replace bromide as a ligand. Deprotonation of an aliphatic PNP ligand backbone, enforced the formation of a five-coordinated 16 electron complex like reported by Nocera in pure form.

1.5.2 Catalytic Applications

In a very short time span, manganese (I) PNP pincer complexes were established as pre-catalysts in parallel studies, employing reductive catalysis. Among the latest reports are hydrogenation of ketones and aldehydes to alcohols, as well as nitriles to obtain amines. The inverted reaction was also reported - dehydrogenation of alcohols combined with amine coupling (Figure 22).⁵²

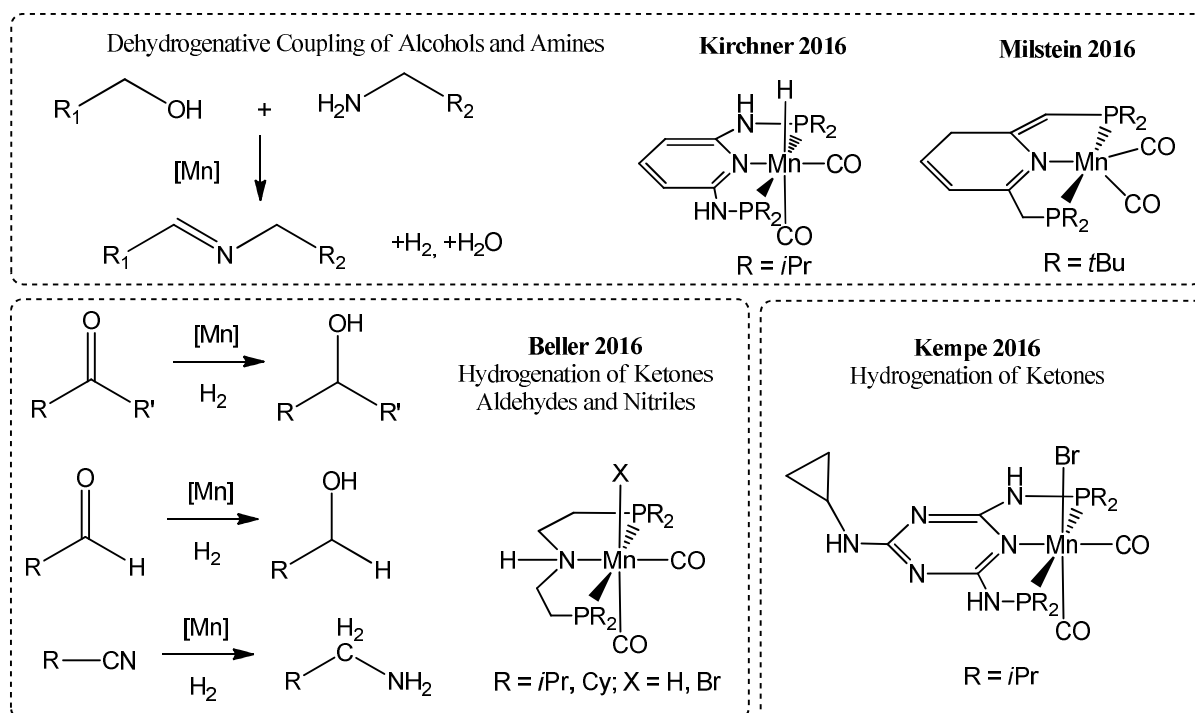


Figure 22: Mn(I) PNP pincer complexes in reductive chemistry

All of the complexes from the groups of Kirchner, Milstein, Beller and Kempe hold a protic site in the ligand backbone. The reaction conditions are rather harsh, elaborating high temperatures and strong base in excess. The pre-catalysts are either bromo, hydrido or neutral carbonyl Mn(I) complexes. A projected intermediate in all mechanisms is a hydrido species of general formula $[\text{Mn}(\text{PNP})(\text{CO})_2\text{H}]$. The hydrido complex is generated in situ at the given conditions after addition of dihydrogen by a deprotonated complex of type $[\text{Mn}(\text{PNP}^{\text{H}})(\text{CO})_2]$ (Figure 23).

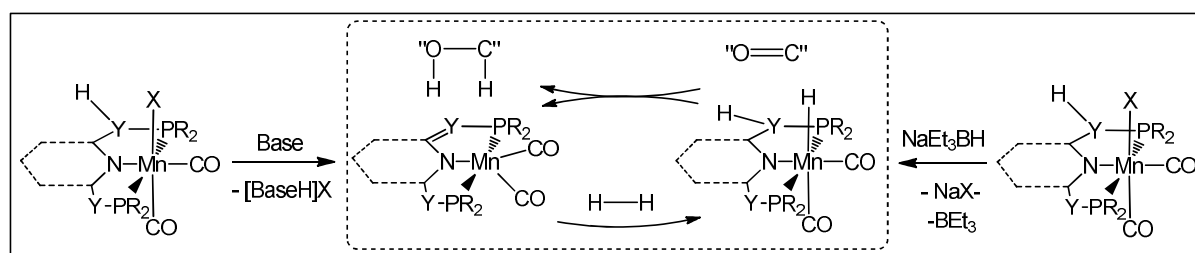


Figure 23: Formal mechanism of the hydrogenation mechanism on C=O double bond

Formally, the “H₂” fragment is transferred via metal-ligand cooperation to the unsaturated double/triple bond. In fact, the dihydrogen transfer is mediated by the solvent, presumably in an outer-sphere mechanism. This reflects the need of bifunctional backbones. Kirchner’s work evidenced, that the replacement of NH linkers by NMe linkers annihilates the catalytic activity.

Multicomponent Synthesis of Heterocycles

The subsequent cascade of dehydrogenation/hydrogenation is utilized in a beautiful example of heterocycle-synthesis.⁵³ The Mn(I) PNP pincer systems of Kempe and Kirchner excelled in multiple component reactions, yielding pyrimidines and

quinolines (Figure 24). The selective C-C and C-N bond formation is the result of consecutive dehydrogenation and condensation steps.

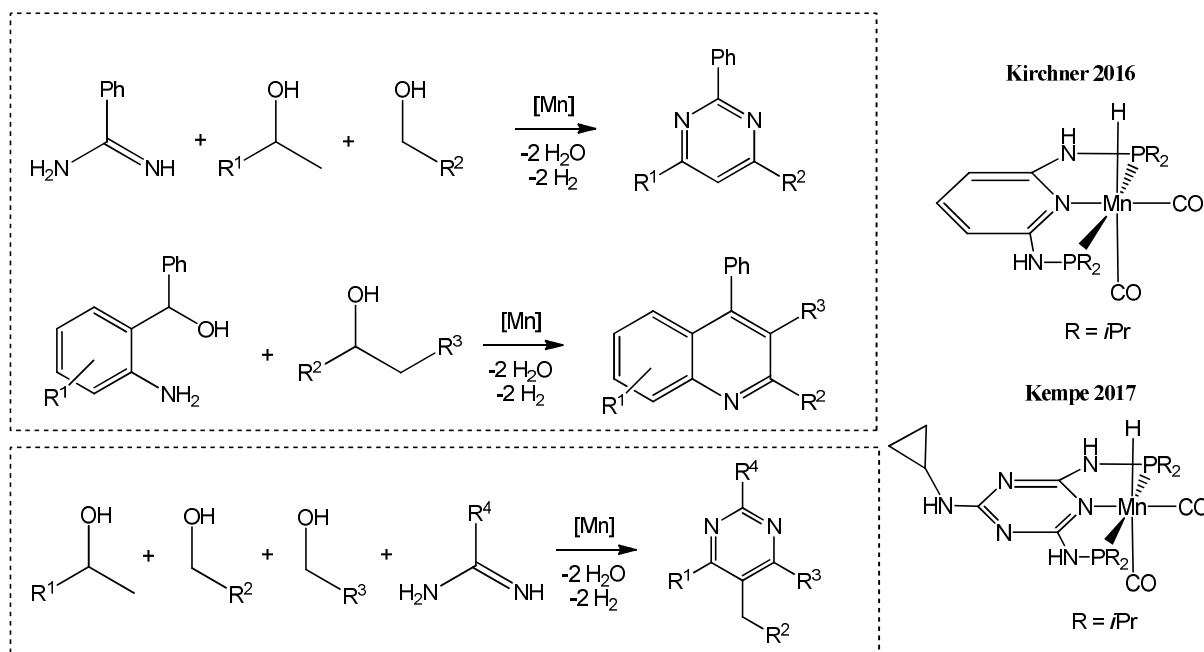


Figure 24: Multicomponent pyrimidine and quinoline synthesis catalyzed by Mn(I) PNP pincer complexes

As commented by Kempe, these kind of reactions are only matched by the noble metals ruthenium and iridium apart from that. The activity of triazine based complexes was significantly higher. The equilibrium of the reaction is driven by the release of two molecules of water and dihydrogen.

Hydrogen-borrowing Mechanism

Making use of alcohols as sustainable carbon building blocks is a worthy method in green chemistry. Methanol is a bulk chemical in sheer unlimited supply at low price and of superior degradability on nature. Three research groups separately developed methods to incorporate methanol as a C₁ source for methylation of amines, and aminomethylation of aromatic compounds (Figure 25).⁵⁴

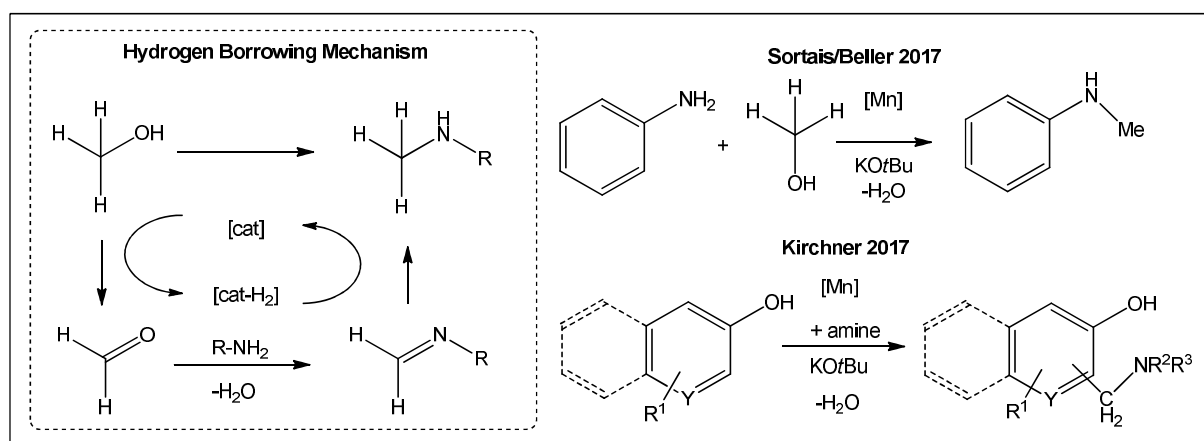


Figure 25: Alkylation of amines by methanol, catalyzed by Mn(I)

These reactions need very high amounts of base, often to the same quantity as substrate. This is accounted to the removal of water from the equilibrium, which is generated throughout the reaction. The methylations were limited to anilines and other activated amino groups. An interesting note from Beller is, that the reaction does not proceed in presence of nitrile functions.

Formate Complexes of Manganese (I)

The promising role of carbon dioxide has already been discussed in section “Fe(II) PNP Pincer Chemistry”. Sortais was the first one, to describe a Mn(I) PNP formiato complex, which catalyzed the decomposition of formic acid. Gonsalvi and Kirchner used their previous motif of Fe(II) PNP pincers and copied the concept successfully on Mn(I), for hydrogenation of carbon dioxide (Figure 26).⁵⁵

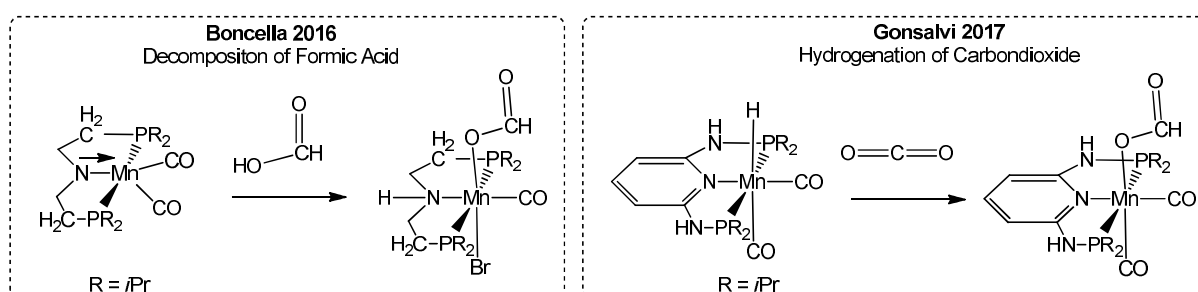


Figure 26: Synthesis of Mn(I) PNP formate pincer complexes

The formiato complexes were accessible via two different synthetic routes - protonation of a deprotonated 16 electron carbonyl complex with formic acid, or insertion of molecular CO₂ into a Mn-H bond. Boncellas decomposition of formic acid runs *via* dehydrogenation and dehydration, but is inhibited by the addition of Lewis acids. Gonsalvis dehydrogenation of carbon dioxide is improved by the addition of LiOTf as a co-catalyst. High turnover numbers (TONs) up to 10.000 are reported. Bifunctionality of the ligand is a critical requirement. The analogue complex having NMe linkers performed worse, to a factor of 10.

2 Results and Discussion

2.1 Contributed Manuscripts

Manuscript #1

"Iron(II) complexes featuring κ^3 - and κ^2 -bound PNP pincer ligands – the significance of sterics"

Glatz M.; Bichler B.; Mastalir M.; Stöger B.; Weil M.; Mereiter K.; Pittenauer E.; Allmaier G.; Veiros L. F.; Kirchner K. *Dalton Trans.* **2015**, 44, 281-294.

Manuscript #2

"Fe(II) Carbonyl Complexes Featuring Small to Bulky PNP Pincer Ligands – Facile Substitution of κ^2 P,N-Bound PNP Ligands by Carbon Monoxide"

Glatz M.; Holzacker C.; Bichler B.; Mastalir M.; Stöger B.; Mereiter K.; Weil M.; Veiros L. F.; Mösch-Zanetti N. C.; Kirchner K. *Eur. J. Inorg. Chem.* **2015**, 5053-5065.

Manuscript #3

"Synthesis and characterization of cationic dicarbonyl Fe(II) PNP pincer complexes"

Glatz M.; Schröder-Holzacker C.; Bichler B.; Stöger B.; Mereiter K.; Veiros L. F.; Kirchner K. *Monatsh. Chem.* **2016**, 147, 1713-1719.

Manuscript #4

"Chemoselective Hydrogenation of Aldehydes under Mild, Base-Free Conditions - Manganese Outperforms Rhenium"

Glatz M.; Stöger B.; Himmelbauer D.; Veiros L. F.; Kirchner K. *ACS Catal.* **2018**, 8, 4009-4016.

Manuscript #5

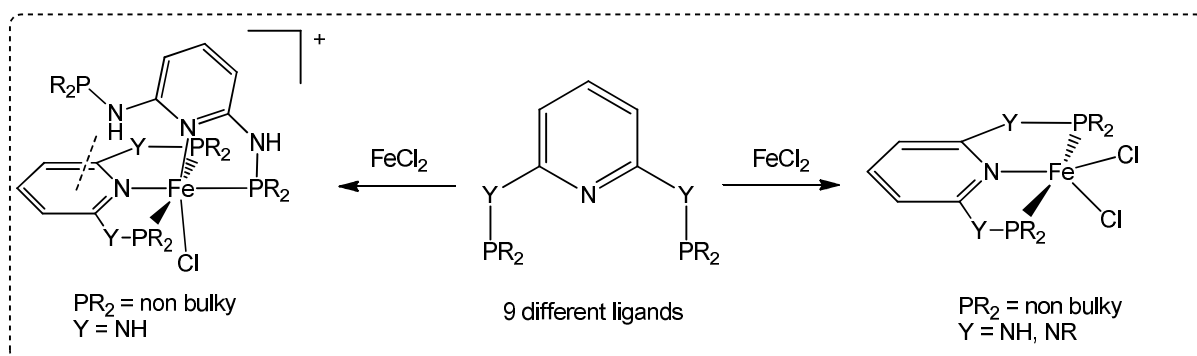
"Reaction of Carbon Dioxide with Hydride Mn and Re PNP Pincer Complexes"

Glatz M., Haager L.; Pecak J.; Stöger B.; Kirchner K. *Organometallics* **2018**, manuscript in preparation.

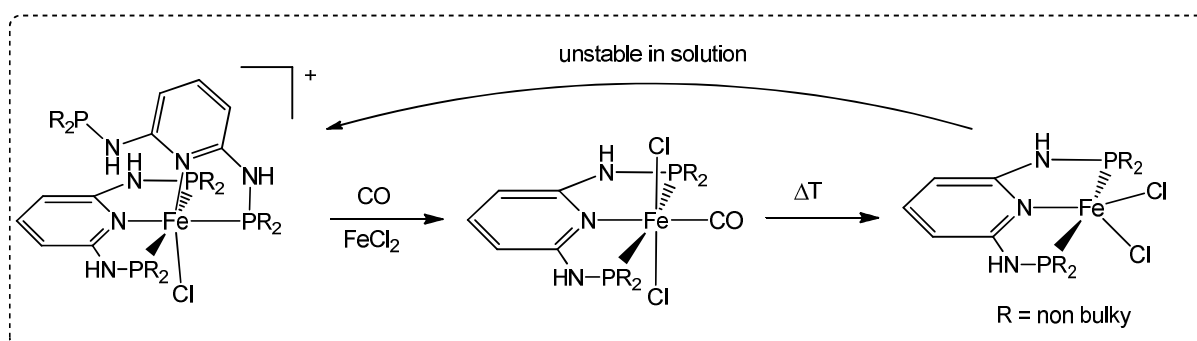
2.2 Context of Contributions

The objective of this work, was to investigate the reactivity of Fe(II) and Mn(I) PNP pincer complexes on a fundamental basis. The ligand properties were changed via modifications on the phosphine and linker moiety.

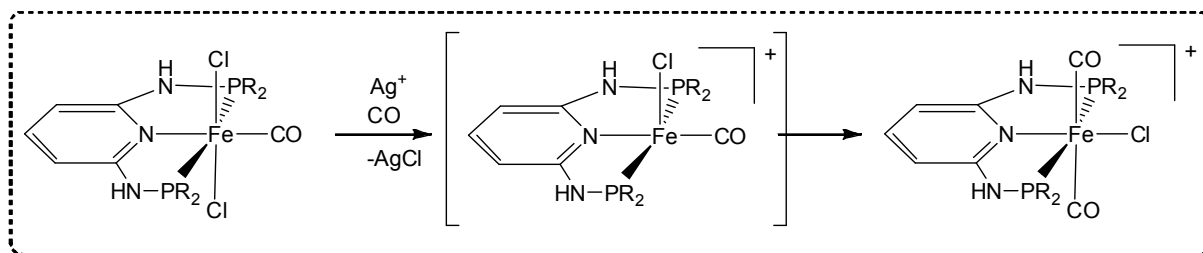
Manuscript 1# focuses on the nature of κ^3, κ^2 -[Fe(PNP)₂Cl]⁺ complexes. A series of 9 different ligands confirm the evidence, that this species is a pure result of sterics, and not electronics. According to crystal structure, there are also hydrogen bonding interactions between the pyridine aromate and NH linker. In some cases, alkylation of the NH linker resulted in hydrolysis of P-N bond and led to similar results.



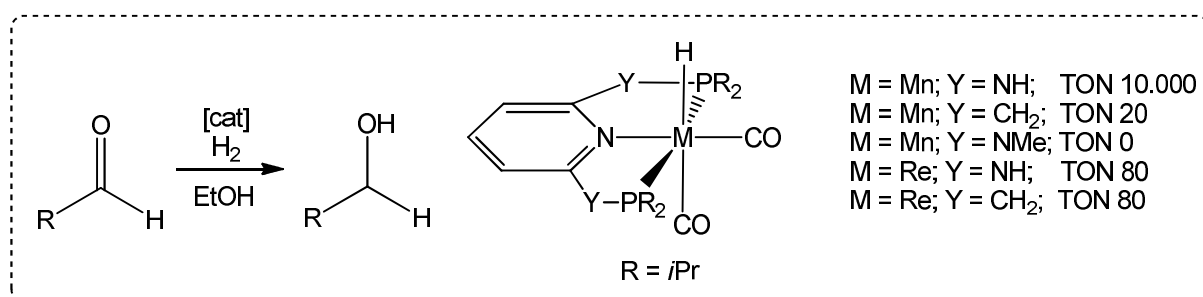
Manuscript 2# describes the reactivity of κ^3, κ^2 -[Fe(PNP)₂Cl]⁺ complexes. The pincer in bidentate coordination mode is labile, and can be substituted by CO yielding [Fe(PNP)(CO)₂Cl] complexes. These were not accessible for small phosphines by any other procedure beforehand. Further, the carbonyl ligand is also labile and can be released upon heating [Fe(PNP)(CO)₂Cl]. The bulkier the PR₂ moiety, the lower the temperature required for CO release. [Fe(PNP)Cl₂] with sterically less demanding phosphine donors were found to be unstable in solution, and dissociate into the original κ^2, κ^3 configuration.



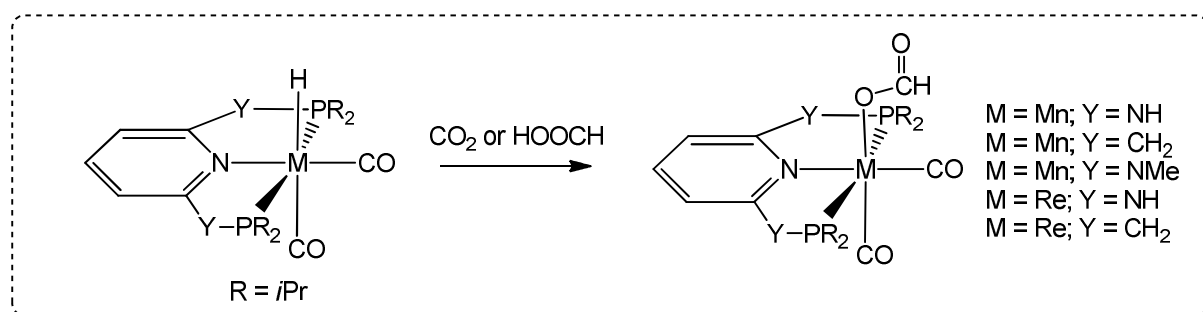
In **Manuscript 3#** a series of octahedral biscarbonyl Fe(II) PNP pincer complexes are prepared by halide abstraction under CO atmosphere. The resulting compound [Fe(PNP)(CO)₂Cl]⁺ always adopts a *trans* configuration independent of the ligand system.



Manuscript 4# covers novel results on the catalytic application of 2,6-diaminopyridine based Mn(I) PNP pincer complex, for highly selective hydrogenation of aldehydes. Other functions like ketones, esters and nitriles were tolerated. The catalyst achieved turn over numbers up to 10000. After modifications on the linker Y or metal center M (M = Re), the activity shrank drastically. The reaction proceeded only in protic solvents, and additional base improved the overall performance.



In **Manuscript 5#**, the hydrido complexes [Mn(PNP)(CO)₂H] described previously, were applied in the activation of molecular CO₂. Five formate complexes of Mn and Re, of general formula [M(PNP)(CO)₂(OCHO)] were characterized. The binding of CO₂ excelled at room temperature at 1 atm.



2.3 Original Manuscripts

Manuscript #1

“Iron(II) complexes featuring κ^3 - and κ^2 -bound PNP pincer ligands – the significance of sterics”

Glatz M.; Bichler B.; Mastalir M.; Stöger B.; Weil M.; Mereiter K.; Pittenauer E.; Allmaier G.; Veiros L. F.; Kirchner K. *Dalton Trans.* **2015**, 44, 281-294.

Reproduced by permission of The Royal Society of Chemistry

Cite this: *Dalton Trans.*, 2015, **44**, 281Iron(II) complexes featuring κ^3 - and κ^2 -bound PNP pincer ligands – the significance of sterics†Mathias Glatz,^a Bernhard Bichler,^a Matthias Mastalir,^a Berthold Stöger,^b Matthias Weil,^b Kurt Mereiter,^b Ernst Pittenauer,^b Günter Allmaier,^b Luis F. Veiros^c and Karl Kirchner^{*a}

Treatment of anhydrous FeX_2 ($X = \text{Cl}, \text{Br}$) with 2 equiv. of the sterically little demanding N,N' -bisphosphino-2,6-diaminopyridine based PNP ligands – featuring Ph, biphenol (BIPOL), Me, Et, $n\text{Pr}$, and $n\text{Bu}$ substituents at the phosphorus sites and H, Me, and Ph substituents at the N-linkers – afforded diamagnetic cationic octahedral complexes of the general formula $[\text{Fe}(\kappa^3\text{-}P,N,P\text{-PNP})(\kappa^2\text{-}P,N\text{-PNP})X]^+$ featuring a $\kappa^2\text{-}P,N$ bound PNP ligand. With the sterically more encumbered N -methylated ligand $\text{PNP}^{\text{Me}}\text{-Ph}$ the related complex $[\text{Fe}(\kappa^3\text{-}P,N,P\text{-PNP}^{\text{Me}}\text{-Ph})(\kappa^2\text{-}P,N\text{-PNP}^{\text{HMe}}\text{-Ph})\text{Cl}]^+$ rather than $[\text{Fe}(\kappa^3\text{-}P,N,P\text{-PNP}^{\text{Me}}\text{-Ph})\text{Cl}_2]^+$ was formed. This reaction was accompanied by P–N bond cleavage, thereby forming the $\kappa^2\text{-}P,N$ -bound N -diphenylphosphino- N,N' -methyl-2,6-diaminopyridine ligand. In contrast, with the N -phenylated ligands $\text{PNP}^{\text{Ph}}\text{-Et}$ and $\text{PNP}^{\text{Ph}}\text{-}n\text{Pr}$, despite small Et and $n\text{Pr}$ substituents at the phosphorus sites, complexes $[\text{Fe}(\kappa^3\text{-}P,N,P\text{-PNP}^{\text{Ph}}\text{-Et})\text{Cl}_2]^+$ and $[\text{Fe}(\kappa^3\text{-}P,N,P\text{-PNP}^{\text{Ph}}\text{-}n\text{Pr})\text{Cl}_2]^+$ were formed, revealing that sterics can be also controlled by substituent variations at the amino N-sites. Depending on the solvent, complexes featuring $\kappa^2\text{-}P,N$ -bound ligands undergo facile rearrangement reactions to give dicationic complexes of the type $[\text{Fe}(\kappa^3\text{-}P,N,P\text{-PNP})_2]^{2+}$ where both PNP ligands are bound in a $\kappa^3\text{-}P,N,P$ -fashion. In the presence of either Ag^+ or Na^+ salts as halide scavengers this reaction takes place within a few minutes. The pendant PR_2 arm of the $\kappa^3\text{-}\kappa^2$ -complexes is readily oxidized to the corresponding phosphine sulfides upon treatment with elemental sulfur. This was exemplarily shown for $[\text{Fe}(\kappa^3\text{-}P,N,P\text{-PNP-}n\text{Pr})(\kappa^2\text{-}P,N\text{-PNS-}n\text{Pr})\text{Cl}]^+$. Halide abstraction afforded the dicationic bis-chelated octahedral Fe(II) complex $[\text{Fe}(\kappa^3\text{-}P,N,P\text{-PNP})_2]^{2+}$ together with the free SNP ligand rather than $[\text{Fe}(\kappa^3\text{-}P,N,P\text{-PNP-}n\text{Pr})(\kappa^3\text{-}S,P,N\text{-PNS-}n\text{Pr})]^{2+}$.

Received 17th September 2014,

Accepted 17th October 2014

DOI: 10.1039/c4dt02866j

www.rsc.org/dalton

Introduction

Neutral pyridine-based ENE pincer ligands, where E is a (hetero)donor atom, are widely utilized in transition metal chemistry due to their combination of stability, activity and variability.¹ They typically enforce a meridional $\kappa^3\text{-}E,N,E$ coordination mode provided that three coordination sites are accessible at the metal center. As far as iron ENE complexes are concerned, an important class of compounds are coordinatively unsaturated 16e high-spin square-pyramidal complexes

of the type $[\text{Fe}(\text{ENE})\text{X}_2]$ ($X = \text{Cl}, \text{Br}$) obtained from Fe(II) halides with stoichiometric amounts of ENE ligands. Examples of prominent ENE ligands are bis(imino)pyridines (**I**),^{2–4} bis(phosphinomethyl)pyridines (**II**), bis(amino)pyridines (**III**),^{5–7} 6-phosphinomethyl-2,2'-bipyridines (**IV**),⁸ bis(imidazolylidene)pyridines (**V**),⁹ terpyridines (**VI**)¹⁰ and bis(phosphinito)pyridines (**VII**)¹¹ as shown in Chart 1. In most cases bulky R substituents such as $i\text{Pr}$ or $t\text{Bu}$ are required for avoiding the formation of bis-chelated dicationic low-spin complexes of the type $[\text{Fe}(\text{ENE})_2]^{2+}$. Some of these $[\text{Fe}(\text{ENE})\text{X}_2]$ complexes turned out to be highly active catalysts for polymerization reactions or are valuable precursors for Fe(0) complexes which, for instance, are useful catalysts for hydrogenation¹² and hydrosilylation¹³ reactions.

We are currently focusing on the synthesis and reactivity of iron complexes containing PNP pincer ligands based on the 2,6-diaminopyridine scaffold (**VIII**).¹⁴ In these ligands the aromatic pyridine ring and the phosphine moieties are linked *via* NH, N -alkyl, or N -aryl linkers. In the course of our studies we discovered¹⁴ that Fe(II) halides react with bulky PNP ligands N,N' -bis(di-*iso*-propylphosphino)-2,6-diaminopyridine (PNP-*iPr*) and N,N' -bis(di-*tert*-butylphosphino)-2,6-diaminopyridine (PNP-*tBu*) to give the expected mono-chelated high-spin

^aInstitute of Applied Synthetic Chemistry, Vienna University of Technology, Getreidemarkt 9, A-1060 Vienna, Austria. E-mail: kkirch@mail.tuwien.ac.at

^bInstitute of Chemical Technologies and Analytics, Vienna University of Technology, Getreidemarkt 9, A-1060 Vienna, Austria

^cCentro de Química Estrutural, Instituto Superior Técnico, Universidade de Lisboa, Av. Rovisco Pais No. 1, 1049-001 Lisboa, Portugal

† Electronic supplementary information (ESI) available: Synthetic details of compounds **1e**, **1f**, **2fBPh**^{Me}₄, **2gBF**₄, **2hBF**₄, **5dBF**₄, **5eBF**₄, and **5fBF**₄. CCDC 1005380 (**2eBPh**^{Me}₄), 1005381 (**2fBPh**^{Me}₄), 1005382 (**3**), 1005385 (**5aCl**), 1005384 (**5bCF**₃SO₃), 1005387 (**5cCF**₃SO₃), 1005386 (**5dBPh**₄), and 1024076 (**5eBF**₄). For ESI and crystallographic data in CIF or other electronic format see DOI: 10.1039/c4dt02866j

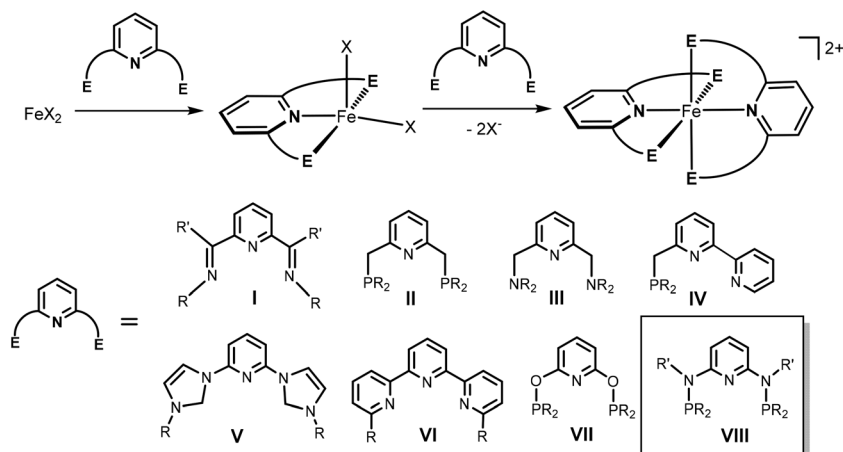
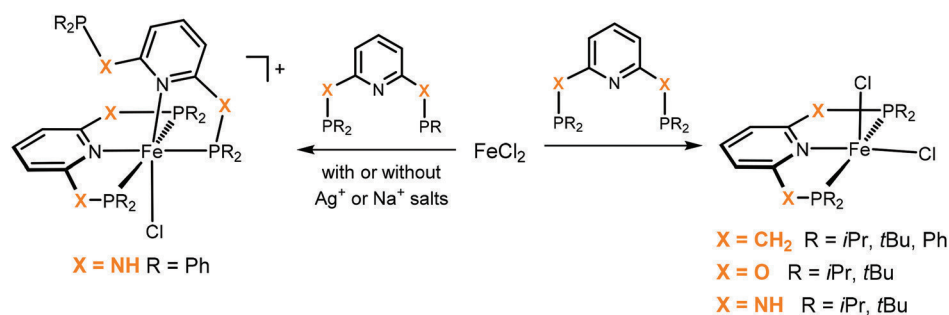


Chart 1



Scheme 1

complexes $[\text{Fe}(\text{PNP})\text{X}_2]$, while with *N,N'*-bis(diphenylphosphino)-2,6-diaminopyridine (PNP-Ph), the bis-chelated octahedral $\text{Fe}(\text{II})$ complex $[\text{Fe}(\kappa^3\text{-}P,N,P\text{-PNP-Ph})(\kappa^2\text{-}P,N\text{-PNP-Ph})\text{Cl}]^+$ (**2a**)¹⁵ was formed exclusively where the PNP pincer ligands are coordinated in a $\kappa^3\text{-}P,N,P$ - and $\kappa^2\text{-}P,N$ -fashion (Scheme 1). These reactions were not sensitive to the ratio of the reactants. It has to be noted that the reaction of FeCl_2 with $\text{PNP}^{\text{CH}_2}\text{-Ph}$ (Chart 1, type **II**) yields the pentacoordinate complex $[\text{Fe}(\text{PNP}^{\text{CH}_2}\text{-Ph})\text{Cl}_2]$ revealing striking differences between CH_2 and NH spacers in pyridine-based PNP pincer ligands (Scheme 1).

In continuation of our studies on iron PNP complexes, we report here on the synthesis and reactivity of a series of octahedral $\text{Fe}(\text{II})$ complexes where PNP pincer ligands are coordinated in a $\kappa^3\text{-}P,N,P$ - and $\kappa^2\text{-}P,N$ -fashion. In order to answer the question whether the formation of these complexes is sterically or electronically driven, we utilize PNP ligands with both weakly and strongly electron donating PR_2 substituents that, with the exception of *N*-methylated and *N*-phenylated ligands, are sterically non-demanding (Chart 2). The bulkiness of these ligands, based on their cone angles estimated from crystallographic

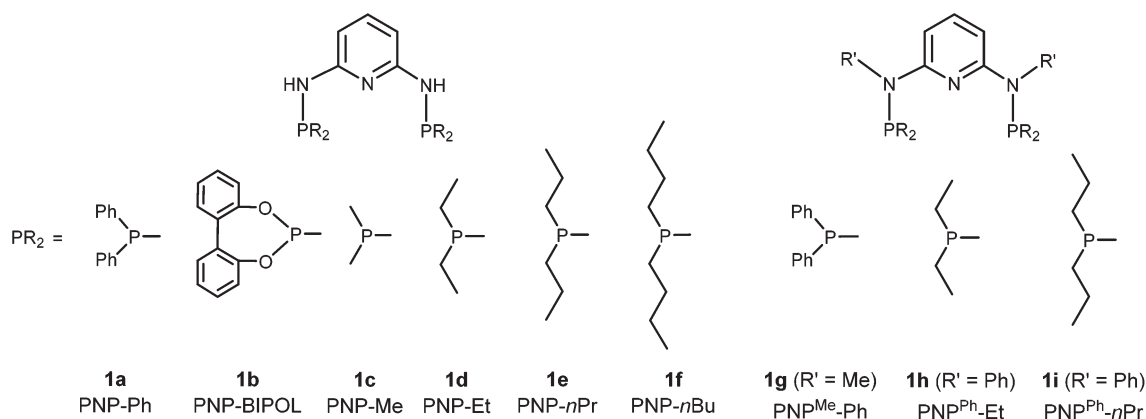


Chart 2

data^{16–18} by the procedure of Mingos *et al.*,¹⁹ decreases roughly in the order PNP^{Ph}-*n*Pr \approx PNP^{Ph}-Et (120) > PNP^{Me}-Ph (105) > PNP-*n*Bu \approx PNP-*n*Pr \approx PNP-Et \approx PNP-Ph (100) > PNP-BIPOL (95) > PNP-Me (90). For comparison, the cone angles of previously reported PNP ligands PNP-*t*Bu, PNP^{Me}-*i*Pr, and PNP-*i*Pr are 130, 120, and 115, respectively.

Results and discussion

Synthesis of Fe(II) complexes featuring κ^3 and κ^2 -bound PNP pincer ligands

Treatment of anhydrous FeCl₂ with 2 equiv. of the ligands PNP-Ph (**1a**), PNP-BIPOL (**1b**), PNP-Me (**1c**), PNP-Et (**1d**), PNP-*n*Pr (**1e**), and PNP-*n*Bu (**1f**) in THF at room temperature for 4 h afforded diamagnetic emerald green cationic octahedral complexes of the general formula [Fe(κ^3 -*P,N,P*-PNP)(κ^2 -*P,N*-PNP)Cl]⁺ (**2a–c,e,g,h**) in essentially quantitative yields (Scheme 2). The reaction of **1a** with FeCl₂ was described recently in a preliminary communication.¹⁵ Analogous bromide complexes [Fe(κ^3 -*P,N,P*-PNP)(κ^2 -*P,N*-PNP)Br]⁺ (**2d,f**) were obtained in a similar fashion by straightforward complexation of the ligands **1c** and **1d** with anhydrous ferrous dibromide.

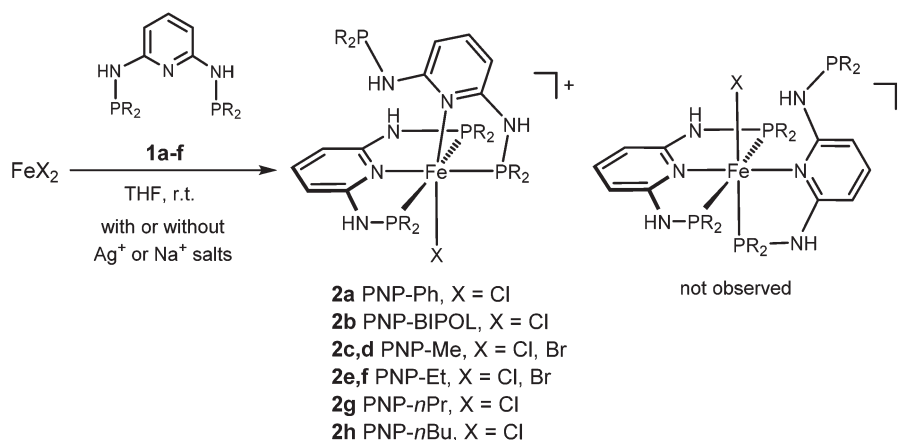
The formation of these complexes occurs independently of whether 1 or 2 equiv. of ligands are used. However, in the first case substantial amounts of unreacted FeX₂ remained which also form paramagnetic haloferrate counterions [FeX₄]^{2–}. All reactions are selective and the formation of only one isomer was observed where the pyridine moiety of the κ^2 -*P,N* bound PNP ligand is *trans* to the halide ligand. With the exception of **2a** and **2b**, all complexes containing chloride and bromide counterions were poorly soluble in most common solvents. In some cases, soluble, stable, and crystalline complexes were afforded upon counterion exchange with halide scavengers such as AgBF₄ (**2a**), Na{B[C₆H₄-4-Me]₄} (NaBPh^{Me}₄) (**2e**, **2f**), and NaBF₄ (**2g**, **2h**). However, in the case of **2b**, **2c**, and **2d** this procedure led to fast ligand rearrangement reactions (*vide infra*).

Most complexes were fully characterized by a combination of ¹H and ³¹P{¹H} NMR spectroscopy and elemental analysis.

Complexes **2e–2h** were also characterized by ¹³C{¹H} NMR spectroscopy. The instability and poor solubility of **2c** and **2d** precluded the recording of NMR spectra. While the ¹H NMR spectra were not very informative, the ³¹P{¹H} NMR spectra revealed in all cases an A₂B pattern for the κ^3 - and κ^2 bound PNP ligands as well as a singlet for the pendant PR₂-NH-arm of the κ^2 -bound PNP ligand.²⁰ Accordingly, in most cases, ³¹P{¹H} NMR chemical shifts and *J*_{PP} coupling constants had to be derived from simulations as exemplarily shown for **2g** in Fig. 1.

DFT calculations (see the Computational details section) performed for complexes **2a**, **2c**, and **2d** are in agreement with the experimental data, indicating that the experimentally observed isomer (denoted **A**) is thermodynamically more stable by 6.9, 5.2, and 4.4 kcal mol^{–1}, respectively, than the unobserved isomer **B** (Fig. 2). This stability difference is essentially due to steric effects, as shown in the space filling models for complexes **2a**, **2c**, and **2d** in Fig. 3 where it is clear that the ligand environment around the Cl ligand is more congested in isomer **B**.

Moreover, in the case of complex **2a**, the stereochemical stress around the Cl ligand in isomer **B** is reflected in the Cl–Fe–X angle, X being the atom *trans* to N_{py} of the κ^3 -*P,N,P* bound PNP ligand. This angle is 88° in **A** and becomes 104° in **B** showing that the Cl ligand is considerably bent towards the κ^3 -*P,N,P* bound PNP ligand in the latter species. This geometrical constraint has clear consequences for the bonding of the two isomers. Thus, the κ^3 -*P,N,P* bound PNP ligand binds strongly to the metal in **B** in order to compensate for the weakening of the coordination of the κ^2 -*P,N* bound PNP ligand due to the repulsion with the Cl ligand in that molecule. This effect is clear in the Fe–N_{py} bond involving the κ^3 -*P,N,P* bound PNP ligand which is weaker in **A** (*d* = 2.116 Å, WI = 0.27) than in **B** (*d* = 2.032 Å, WI = 0.37).²¹ On the other hand, in the latter the Fe–N_{py} bond of the κ^2 -*P,N* bound PNP ligand is much weaker with a distance of 2.198 Å. The Fe–Cl bond is also weaker in **B** as a result of the stereochemical repulsion. The Fe–Cl distance in **B** is 2.382 Å, compared with 2.376 Å in **A**, and the difference in bond strength is even more evident



Scheme 2

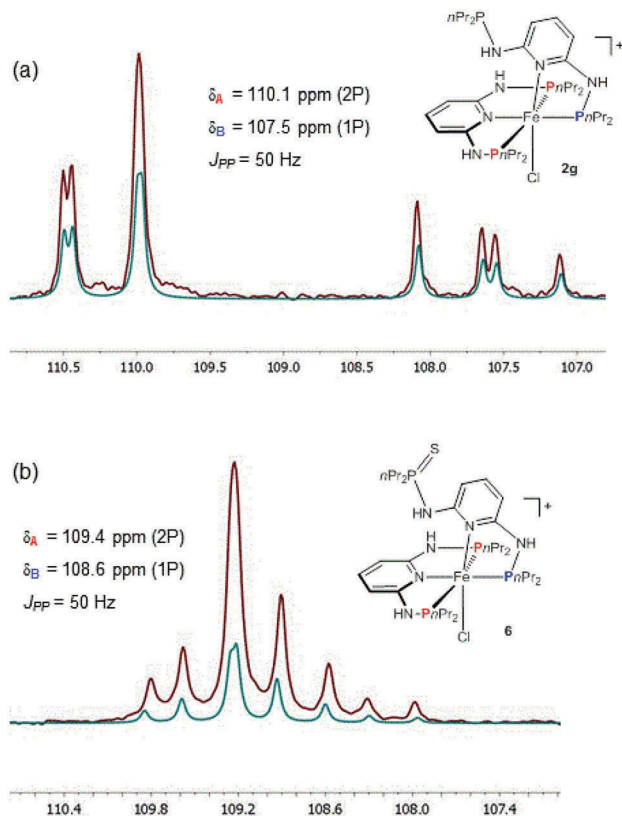


Fig. 1 Experimental (red) and simulated (blue) $^{31}\text{P}\{^1\text{H}\}$ NMR spectra of **2g** and **6** (A_2B spin system, signal of the pendant $\text{PnPr}_2\text{NH-}$ and $\text{S=PnPr}_2\text{NH-}$ arms are not shown).

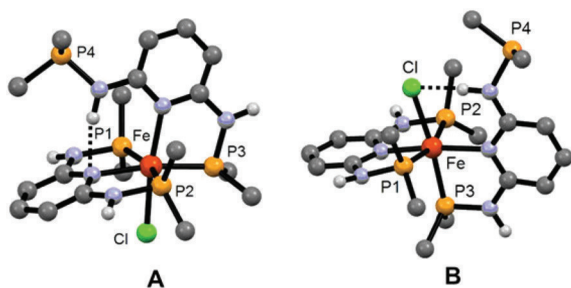


Fig. 2 Optimized B3LYP geometries of the two possible isomers **A** and **B** of $[\text{Fe}(\kappa^3\text{-P,N,P-PNP-Ph})(\kappa^2\text{-P,N-PNP-Ph})\text{Cl}]^+$ (**2a**). Most hydrogen atoms are omitted and only *ipso* carbon atoms of the Ph substituents are shown for clarity.

from the corresponding Wiberg indices being 0.39 in **B** and 0.46 in **A**. The different coordination strength of the two PNP ligands in each complex is also reflected in the charges of those ligands. Accordingly, in **A** the overall charges (NPA, see the Computational details section) of the $\kappa^3\text{-PNP}$ and $\kappa^2\text{-PNP}$ ligands are 0.86 and 0.56, while in **B** these values are 0.89 and 0.49, respectively. This indicates that comparing **A** with **B** the $\kappa^3\text{-P,N,P}$ bound PNP ligand becomes a stronger donor in **B** (more positive) while the opposite happens with the $\kappa^2\text{-P,N}$ bound PNP ligand. It is interesting to note that the intramolecular H-bond does not explain the stability difference because

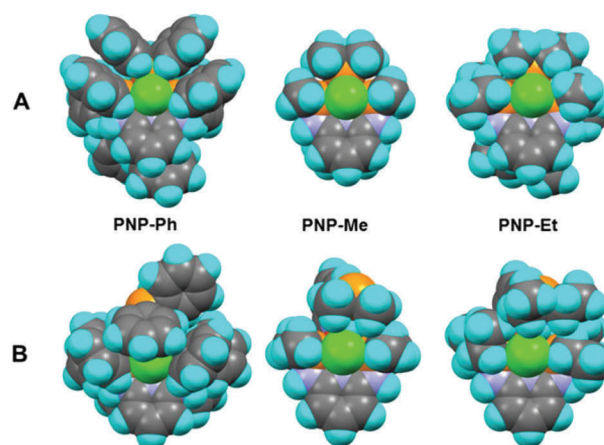


Fig. 3 Space filling representation of optimized B3LYP geometries of the two possible isomers **A** and **B** of **2a** (Ph), **2c** (Me) **2d** (Et), and viewed along the Fe–Cl bond to illustrate steric crowding around the Cl ligand (green).

it is actually stronger in the case of **B** ($\text{Cl}\cdots\text{H-N}$) as can be seen, for example, from the N–H bonds (covalent) in both cases. This bond is weaker in **B** ($d = 1.027 \text{ \AA}$) than in **A** ($d = 1.015 \text{ \AA}$), which is also apparent from the respective Wiberg indices for the H-bond being 0.02 for $\text{N}\cdots\text{HN}$ in **A** and 0.09 for $\text{Cl}\cdots\text{HN}$ in **B**.

In an attempt to prevent the coordination of a second PNP ligand we utilized the *N*-methylated and *N*-phenylated ligands $\text{PNP}^{\text{Me}}\text{-Ph}$ (**1g**), $\text{PNP}^{\text{Ph}}\text{-Et}$ (**1h**) and $\text{PNP}^{\text{Ph}}\text{-nPr}$ (**1i**) assuming that $\kappa^2\text{-P,N}$ -coordination of these ligands is highly unlikely due to unfavorable steric interactions with the pyridine unit of the $\kappa^3\text{-P,N,P}$ -bound ligand. The reaction with two equiv. of **1g** proceeded differently than expected, yielding the cationic complex $[\text{Fe}(\kappa^3\text{-P,N,P-PNP}^{\text{Me}}\text{-Ph})(\kappa^2\text{-P,N-PN}^{\text{HMe}}\text{-Ph})\text{Cl}]^+$ (**3**) as shown in Scheme 3. This reaction is accompanied by P–N bond cleavage, thereby forming the new $\kappa^2\text{-P,N}$ -bound *N*-diphenylphosphino-*N,N'*-methyl-2,6-diaminopyridine ligand. This reaction may be facilitated by adventitious water. The fate of the “ PPh_2 ” moiety was not investigated but it is not uncommon that amino-phosphines bearing phenyl substituents at the phosphorus site are prone to hydrolysis, forming for instance Ph_2POH .²² On the other hand, treating anhydrous FeCl_2 with 1 or 2 equiv. of **1h** and **1i** in THF at room temperature afforded the pentacoordinated high-spin complexes $[\text{Fe}(\text{PNP}^{\text{Ph}}\text{-Et})\text{Cl}_2]$ (**4a**) and $[\text{Fe}(\text{PNP}^{\text{Ph}}\text{-nPr})\text{Cl}_2]$ (**4b**), respectively, in 97 and 95% isolated yields (Scheme 4). This type of complex is well established. At room temperature, solution magnetic moment measurements of complexes **4a** and **4b** in a CH_2Cl_2 solution were consistent with these complexes having four unpaired electrons ($\mu_{\text{eff}} = 4.9$ and $4.8\mu_{\text{B}}$, Evans' method). Accordingly, these complexes display large paramagnetic shifted and very broad ^1H NMR and $^{13}\text{C}\{^1\text{H}\}$ NMR signals and were thus not very informative. $^{31}\text{P}\{^1\text{H}\}$ NMR signals could not be detected.

The solid state structures of **2fBPh**^{Me}₄ and **3** determined by single-crystal X-ray diffraction are depicted in Fig. 4 and 5 with selected bond distances given in the captions. The structure of

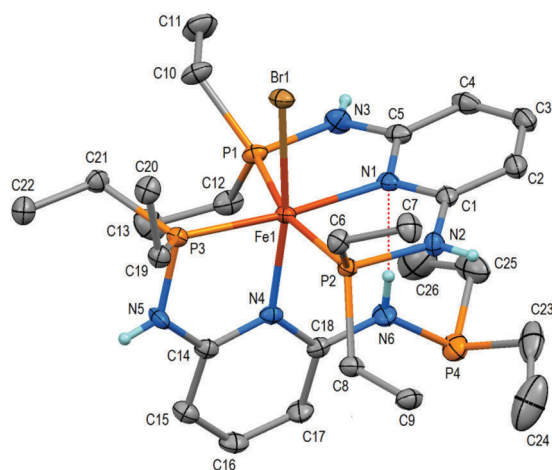
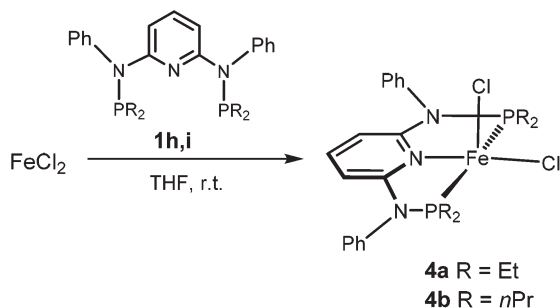
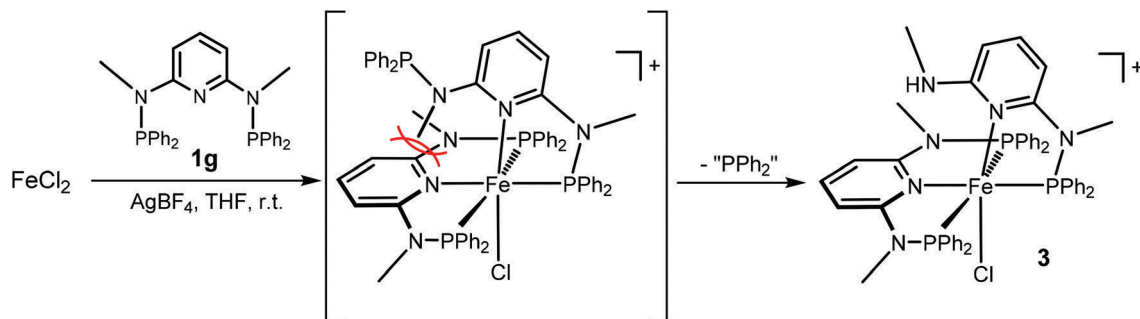


Fig. 4 Structural view of $[\text{Fe}(\kappa^3\text{-P,N,P-PNP-Et})(\kappa^2\text{-P,N-PNP-Et})\text{Br}]\text{BPhMe}_4 \cdot 3\text{THF}$ ($2\text{fBPhMe}_4 \cdot 3\text{THF}$) showing 50% thermal ellipsoids (most H-atoms, solvents and BPhMe_4^- are omitted for clarity). Selected bond lengths (Å) and bond angles (°): Fe(1)–P(1) 2.243(1), Fe(1)–P(2) 2.2521(9), Fe(1)–P(3) 2.189(1), Fe(1)–N(1) 2.063(2), Fe(1)–N(4) 2.117(2), Fe(1)–Br(1) 2.4878(9), P(1)–Fe(1)–P(2) 163.98(3), N(1)–Fe(1)–P(3) 171.38(6), Br(1)–Fe(1)–N(4) 171.03(6).

2eBPhMe_4 is provided in the ESI.† The coordination geometry around the iron center of 2eBPhMe_4 , 2fBPhMe_4 , and **3** corresponds to a characteristically distorted octahedron agreeing well with that in the previously reported complex 2aBF_4 of $[\text{Fe}(\kappa^3\text{-P,N,P-PNP-Ph})(\kappa^2\text{-P,N-PNP-Ph})\text{Cl}]\text{BF}_4 \cdot 2\text{THF} \cdot \text{Et}_2\text{O}$.¹⁴ A view of the complex core of these four structures is shown in Fig. 6 together with the mean values and ranges of selected geometric

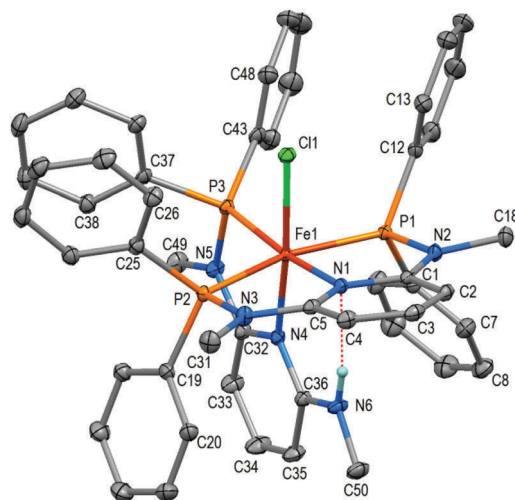


Fig. 5 Structural view of $[\text{Fe}(\kappa^3\text{-P,N,P-PNP}^{\text{Me}}\text{-Ph})(\kappa^2\text{-P,N-PN}^{\text{NHMe}}\text{-Ph})\text{Cl}]\text{BF}_4$ (**3**) showing 50% thermal ellipsoids (most H-atoms and BF_4^- are omitted for clarity). Selected bond lengths (Å) and bond angles (°): Fe(1)–P(1) 2.233(4), Fe(1)–P(2) 2.2410(4), Fe(1)–P(3) 2.1833(4), Fe(1)–N(1) 2.0472(9), Fe(1)–N(4) 2.0668(9), Fe(1)–Cl(1) 2.3323(3), P(1)–Fe(1)–P(2) 163.97(1), N(1)–Fe(1)–P(3) 171.60(3), Cl(1)–Fe(1)–N(4) 173.32(3).

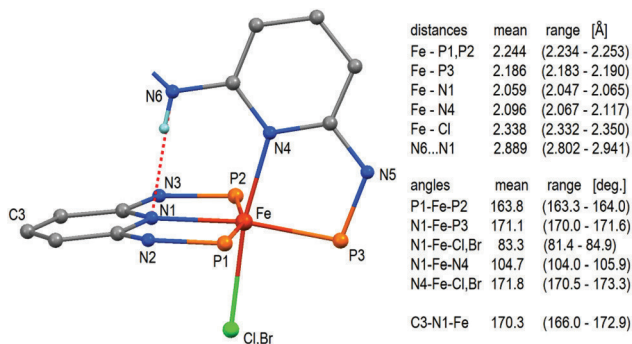


Fig. 6 Representation of the complex cores of four $[\text{Fe}(\kappa^3\text{-PNP})(\kappa^2\text{-PN-P})](\text{Cl,Br})$ -type complexes in compounds $2\text{aBF}_4 \cdot 2\text{THF} \cdot \text{Et}_2\text{O}$,¹⁵ $2\text{eBPhMe}_4 \cdot 3\text{THF}$, $2\text{fBPhMe}_4 \cdot 3\text{THF}$, and **3** and with mean values and ranges of bond lengths and bond angles. The red dotted line indicates an N–H...N hydrogen bond.

data. The bond lengths about iron are in narrow ranges irrespective of whether there is an aryl- or an alkyl-PNP ligand. The Fe–P bonds of the κ^3 -bonded ligand adopt normal values

of 2.244 Å on average and are modestly longer than the bonds to the κ^2 -bonded PNP ligand (mean value 2.186 Å). Likewise the Fe–N bonds to the pyridine nitrogen N1 of the κ^3 -bonded ligand are systematically shorter than those to N4 of the κ^2 -bonded PNP ligand. The NH group (with N6) of the dangling arm of the κ^2 -bonded PNP ligand is in all four complexes directed to the pyridine nitrogen N1 showing N6–N1 distances between 2.802 and 2.941 Å indicative of a stabilizing intramolecular hydrogen bond. This interaction is unusual because it seems to represent a hybrid between a classical N–H...N and an N–H... π interaction. This interaction is also responsible for the fact that the pyridine ring of N1 is bent away from N6 so that the angle C3–N1–Fe (Fig. 6) is about 170° whereas in normal κ^3 -bonded Fe(PNP) complexes this angle is always very close to 180°.

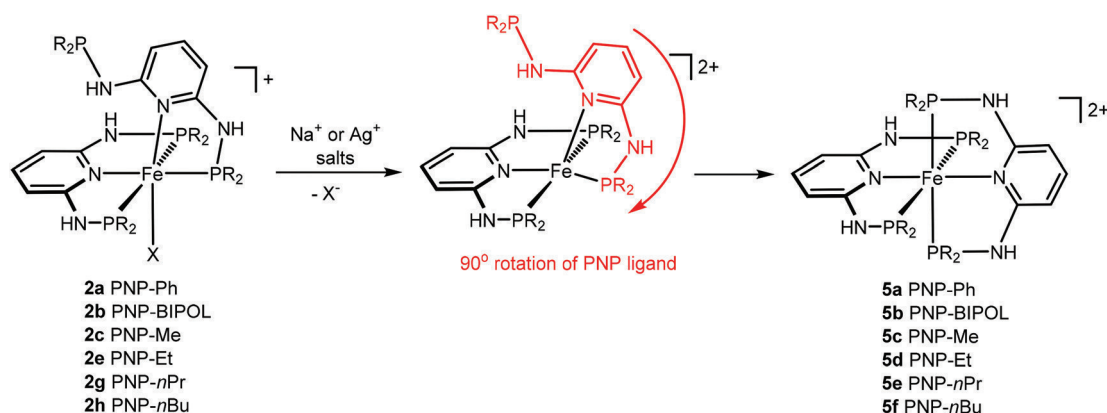
Reactivity of Fe(II) complexes featuring κ^3 and κ^2 -bound PNP pincer ligands

$[\text{Fe}(\kappa^3\text{-}P,N,P\text{-PNP-Ph})(\kappa^2\text{-}P,N,P\text{-PNP-Ph})\text{Cl}]^+$ (**2a**) is stable in THF for several days, but readily rearranges in CH_3CN (within a few minutes) and CH_2Cl_2 (within a few hours) to give $[\text{Fe}(\kappa^3\text{-}P,N,P\text{-PNP-Ph})_2]^{2+}$ (**5a**). This process involves halide dissociation and a 90° rotation of the κ^2 -bound PNP ligand. In the presence of halide scavengers this reaction proceeds in all common solvents within a few minutes (Scheme 5). Complex **5a** (as BF_4^- salt, **5aBF}_4) has already been prepared by an alternative method recently.¹⁶ It has to be noted that an analogous complex $[\text{Fe}(\text{PNP}^{\text{CH}_2}\text{-Ph})_2]^{2+}$ bearing CH_2 -spacers between the pyridine ring and the PPh_2 moieties was reported.²³ In the case of $[\text{Fe}(\kappa^3\text{-}P,N,P\text{-PNP-BIPOL})(\kappa^2\text{-}P,N,P\text{-PNP-BIPOL})\text{Cl}]^+$ (**2b**) rapid decomposition took place in all common solvents such as CH_2Cl_2 , CH_3CN , or THF also in the absence of halide scavengers such as AgCF_3SO_3 . However, fortunately from this mixture in THF as a solvent, small amounts of crystals of **5bCF}_3\text{SO}_3 suitable for an X-ray diffraction study could be obtained by slow solvent evaporation. Other decomposition products could not be identified. The complex $[\text{Fe}(\kappa^3\text{-}P,N,P\text{-PNP-Me})(\kappa^2\text{-}P,N,P\text{-PNP-Me})\text{Cl}]^+$ (**2c**) is unstable in solution and readily forms the dicationic complex $[\text{Fe}(\kappa^3\text{-}P,N,P\text{-PNP-Me})_2]^{2+}$ (**5c**) even in the absence of halide scavengers. Perhaps unexpectedly,****

in contrast to **2c** the Et, *n*Pr, and *n*Bu-analog complexes $[\text{Fe}(\kappa^3\text{-}P,N,P\text{-PNP-Et})(\kappa^2\text{-}P,N,P\text{-PNP-Et})\text{Cl}]^+$ (**2e**), $[\text{Fe}(\kappa^3\text{-}P,N,P\text{-PNP-}n\text{Pr})(\kappa^2\text{-}P,N,P\text{-PNP-}n\text{Pr})\text{Cl}]^+$ (**2g**), and $[\text{Fe}(\kappa^3\text{-}P,N,P\text{-PNP-}n\text{Bu})(\kappa^2\text{-}P,N,P\text{-PNP-}n\text{Bu})\text{Cl}]^+$ (**2h**), respectively, are stable in solution for several days without any noticeable rearrangement reactions. In the presence of halide scavengers, however, the dicationic complexes $[\text{Fe}(\kappa^3\text{-}P,N,P\text{-PNP-Et})_2]^{2+}$ (**5d**), $[\text{Fe}(\kappa^3\text{-}P,N,P\text{-PNP-}n\text{Pr})_2]^{2+}$ (**5e**) and $[\text{Fe}(\kappa^3\text{-}P,N,P\text{-PNP-}n\text{Bu})_2]^{2+}$ (**5f**) are readily formed. Since the electron donating properties of these PNP ligands are very similar, the observed reactivity differences may be due to steric reasons. Cone angles determined from crystallographic data reveal that PNP-Me is the sterically least demanding ligand in this series.

With the exception of **5b**, all complexes of the type $[\text{Fe}(\kappa^3\text{-}P,N,P\text{-PNP})_2]^{2+}$ were characterized by ^1H and $^{31}\text{P}\{^1\text{H}\}$ NMR spectroscopy and elemental analysis. In the case of complexes **5c–f**, $^{13}\text{C}\{^1\text{H}\}$ NMR spectra were also recorded. Complexes **5a** and **5c–f** exhibit a singlet resonance in the $^{31}\text{P}\{^1\text{H}\}$ NMR spectrum at 98.2, 108.3, 119.0, 114.2, and 115.0 ppm, respectively. In the ^1H NMR spectrum the NH protons give rise to a slightly broadened singlet in the range 7–8 ppm. All other resonances are unremarkable and are not discussed here.

ESI-MS enables the detection and study of not only reaction substrates and products but also short-lived reaction intermediates and decomposition products as they are present in solution. Accordingly, solutions of $[\text{Fe}(\kappa^3\text{-}P,N,P\text{-PNP-Ph})(\kappa^2\text{-}P,N,P\text{-PNP-Ph})\text{Cl}]\text{Cl}$ (**2aCl**) and $[\text{Fe}(\kappa^3\text{-}P,N,P\text{-PNP-Et})(\kappa^2\text{-}P,N,P\text{-PNP-Et})\text{Cl}]\text{Cl}$ (**2eCl**) in CH_3OH were subjected to ESI-MS analysis in the positive ion mode. The most abundant signal observed corresponds to the intact complexes **2a** and **2e** ($[\text{M}]^+$) at m/z 1045.4 and 661.2, respectively, emphasizing the relative stability of this complex. Further, small signals were found at m/z 505.2 and 313.1, respectively, assignable to the doubly charged complexes $[\text{Fe}(\kappa^3\text{-}P,N,P\text{-PNP-Ph})_2]^{2+}$ (**5a**) and $[\text{Fe}(\kappa^3\text{-}P,N,P\text{-PNP-Et})_2]^{2+}$ (**5e**), $[\text{M} - \text{Cl}]^{2+}$, where the chloride ligand is dissociated. Moreover, weak signals were detected at m/z 568.2 and 376.1, respectively, due to loss of a PNP ligand, $[\text{M} - \text{PNP}]^+$. The ESI full scan mass spectrum of **2eCl** in CH_3OH is depicted in Fig. 7. The fragmentation of the selected **2a** and **2e** ions $[\text{M}]^+$ with m/z 1045.4 and 661.2 by low energy collision-induced



Scheme 5

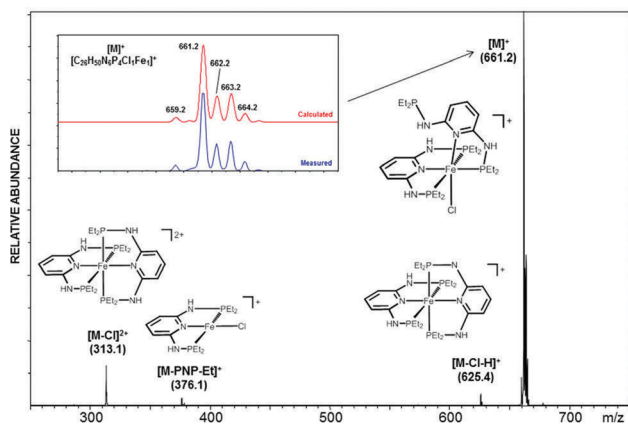


Fig. 7 Positive-ion full scan ESI-MS of $[\text{Fe}(\kappa^3\text{-P,N,P-PNP-Et})(\kappa^2\text{-P,N-PNP-Et})\text{Cl}]\text{Cl}$ (**2eCl**) in CH_3OH . The inset shows the isotope pattern match for **2eCl** ($[\text{M}]^+$).

dissociation (CID) in an ion trap analyzer resulted in the formation of ions with m/z 568.2 and 376.1, respectively, due to the loss of one PNP ligand ($[\text{M} - \text{PNP}]^+$). The results of the ESI-MS studies again support that both the halide and the $\kappa^2\text{-P,N}$ -bound PNP ligands are substitutionally labile.

Structural views of the $[\text{Fe}(\kappa^3\text{-P,N,P-PNP})_2]^{2+}$ complexes **5aCl**, **5bCF₃SO₃**, **5cCF₃SO₃**, **5dBPh₄**, and **5eBF₄** are depicted in Fig. 8–12 with selected bond distances given in the caption. The five complexes show modestly distorted and relatively uniform octahedral coordination figures about Fe, each coordinated by two N in axial and four P in equatorial disposition. The Fe–N bond distances vary between 1.956 and 2.032 Å, the mean value being 1.995 Å, and the N–Fe–N bond angles are nearly straight, varying between 178.23 and 180°. The Fe–P bond lengths are short for the complex **5bCF₃SO₃** with the phosphite ligands (mean value of Fe–P of 2.183 Å), intermediate

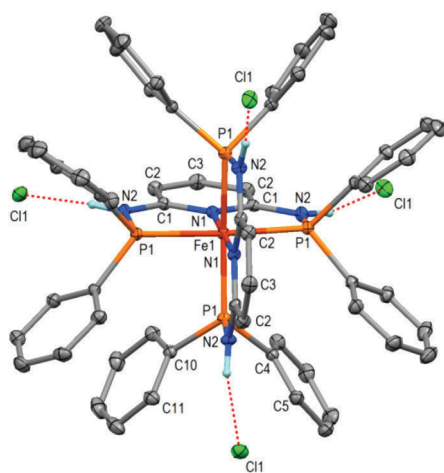


Fig. 8 Structural diagram of $[\text{Fe}(\kappa^3\text{-P,N,P-PNP-Ph})_2](\text{Cl})_2\cdot\text{solv}$ (**5aCl**·solv) showing only N-bonded H-atoms and 40% ellipsoids. The complex has point symmetry S_4 with C3-N1-Fe1-N1-C3 as the axial direction. Selected bond distances and angles (Å, °): Fe1-N1 1.9563(12) (2x), Fe1-P1 2.2520(3) (4x); N1-Fe1-N1 180.0, N1-Fe1-P1 84.47(1) (4x), P1-Fe1-P1 168.93(1) (2x); hydrogen bond $\text{N2}\cdots\text{Cl1}$ 3.140(1) (4x).

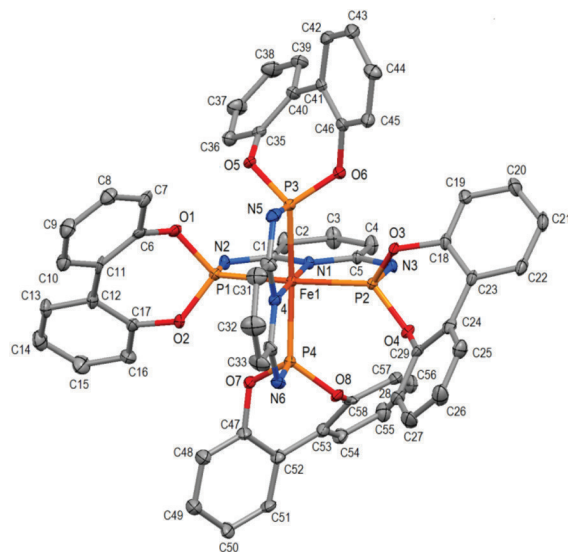


Fig. 9 Structural diagram of $[\text{Fe}(\kappa^3\text{-P,N,P-PNP-BIPOL})_2](\text{CF}_3\text{SO}_3)_2\cdot 6.5\text{THF}$ (**5bCF₃SO₃**·6.5THF) showing 50% ellipsoids. Most H-atoms, BF_4 anions and THF solvent molecules are omitted for clarity. Selected bond distances and angles (Å, °): Fe1-N4 1.967(7), Fe1-N1 1.969(6), Fe1-P4 2.180(2), Fe1-P1 2.181(2), Fe1-P2 2.182(2), Fe1-P3 2.189(2), N1-Fe1-N4 179.2(3), P1-Fe1-P2 167.47(9), P3-Fe1-P4 167.45(9).

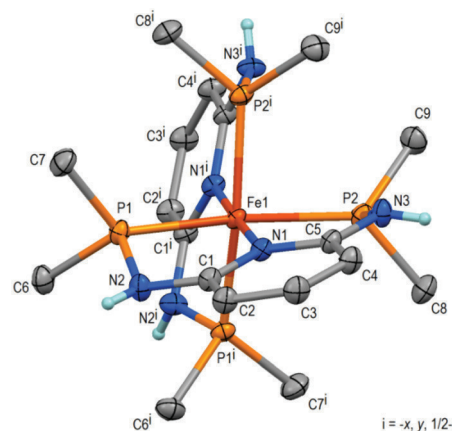


Fig. 10 Structural view of $[\text{Fe}(\kappa^3\text{-P,N,P-PNP-Me})_2](\text{CF}_3\text{SO}_3)_2\cdot 2\text{Me}_2\text{CO}$ (**5cCF₃SO₃**·2Me₂CO) (most H-atoms, acetone solvent molecules and CF_3SO_3^- are omitted for clarity). Selected bond lengths (Å) and bond angles (°): Fe(1)-P(1) 2.2748(5), Fe(1)-P(2) 2.2758(5), Fe(1)-N(1) 1.9973(14), P(1)-Fe(1)-P(2) 163.38(2) N(1)-Fe(1)-N(1) 178.23(9).

for the PPh_2 -based ligand in **5aCl** (Fe–P of 2.252 Å), and longest for the P(alkyl)_2 -based ligands of complexes **5cCF₃SO₃**, **5dBPh₄**, and **5eBF₄** (mean values of Fe–P of 2.275, 2.292, and 2.274 Å for PMe_2 in **5cCF₃SO₃**, PEt_2 in **5dBPh₄**, and PnPr_2 in **5eBF₄**). The *trans*-bond angles P–Fe–P deviate notably from 180° by varying between 154.92 (**5eBF₄**) and 168.93° (**5aCl**). Despite the relatively uniform FeN_2P_4 octahedra, there are significant differences between the complexes with respect to the planarity of the chelate rings Fe–P–N–C–N–(Fe) and, related with this, whether the two pyridine rings of each complex are

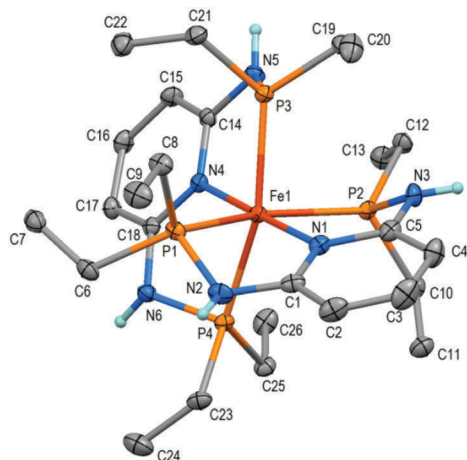


Fig. 11 Structural view of $[\text{Fe}(\kappa^3\text{-P,N,P-PNP-Et})_2(\text{BPh}_4)_2] \cdot 0.5\text{Et}_2\text{O}$ (**5dBPh**₄·0.5Et₂O) (most H-atoms, solvent and BPh₄⁻ are omitted for clarity). Selected bond lengths (Å) and bond angles (°): Fe(1)–P(1) 2.2804(4), Fe(1)–P(2) 2.2873(4), Fe(1)–P(3) 2.2898(6), Fe(1)–P(4) 2.3096(6), Fe(1)–N(1) 2.025(1), Fe(1)–N(4) 2.013(1), P(1)–Fe(1)–P(2) 157.93(2), P(3)–Fe(1)–P(4) 158.39(2).

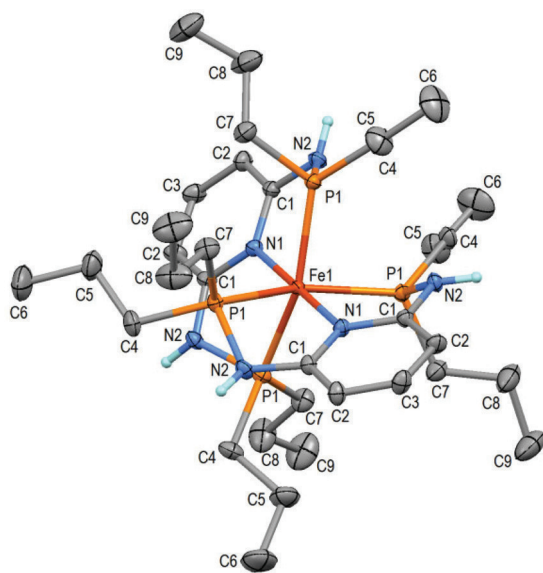


Fig. 12 Structural view of $[\text{Fe}(\kappa^3\text{-P,N,P-PNP-nPr})_2](\text{BF}_4)_2 \cdot 2\text{Me}_2\text{CO}$ (**5eBF**₄·2Me₂CO) (most H-atoms, solvent and BF₄⁻ are omitted for clarity). The complex has symmetry 222 (*D*₂) with Fe, N1, and C3 on one 2-fold axis. Selected bond lengths (Å) and bond angles (°): Fe–N1 2.0317(13) (2 \times), Fe–P1 2.2740(3) (4 \times), N1–Fe–N1 180.0, *trans*-P1–Fe–P1 154.92(1) (2 \times).

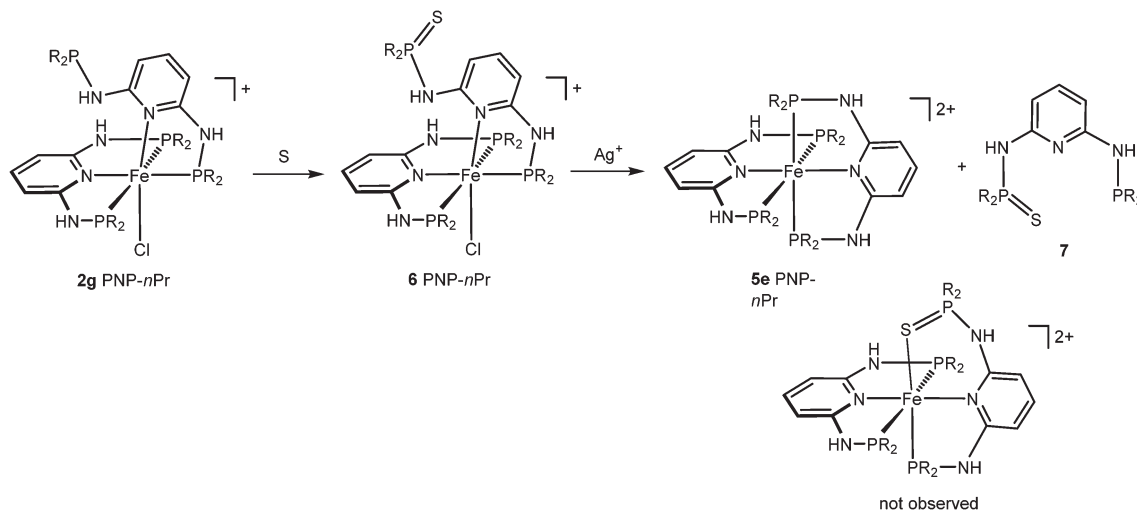
oriented in a mutually perpendicular direction or whether they are less inclined to each other. The first case with mutually perpendicular pyridine rings is represented by the PPh₂-based complex **5aCl**. In it the phenyl rings of adjacent PPh₂ groups are most relaxed when they are in pair-wise stabilizing π - π contacts (*cf.* Fig. 8). The ideal point symmetry of such a complex would be $\bar{4}2m$ (*D*_{2d}) from which complex **5aCl** deviates only a little and has point symmetry $\bar{4}$ (*S*₄) instead. Like in complex

5aCl the chelate rings in complex **5bCF**₃SO₃ are essentially flat and the two pyridine rings subtend an interplanar angle of 88.6°. Due to the steric features of the bipol ligand the complex in **5bCF**₃SO₃ adopts approximately the symmetry 222 (*D*₂). In the P(alkyl)₂-based complexes **5cCF**₃SO₃, **5dBPh**₄, and **5eBF**₄ the chelate rings about Fe are distinctly non-planar and the two pyridine rings are mutually inclined at angles of 57.78° (**5cCF**₃SO), 41.56° (**5dBPh**₄), and 34.61° (**5eBF**₄), which decrease with increasing alkyl chain length (**5cCF**₃SO₃: Me; **5dBPh**: Et, **5eBF**₄: *n*-Pr). In the same order the P–Fe–P *trans*-angles diminish from 163.38° *via* 157.17° to 154.92°. These changes, in pyridine interplanar angles and P–Fe–P *trans*-angles, are considered to be largely due to the increased steric demand of the alkyl substituents of phosphorus.

The pendant arm of complexes **2** may be readily oxidized to the respective phosphine oxides and sulfides in the presence of hydrogen peroxide and elemental sulfur. This was exemplarily examined for **2g**. While oxidation with hydrogen peroxide led to several unidentified decomposition products, the reaction with 1 equiv. of sulfur afforded cleanly $[\text{Fe}(\kappa^3\text{-P,N,P-PNP-nPr})(\kappa^2\text{-P,N-PNS-nPr})\text{Cl}]^+$ (**6**) in 91% isolated yield (Scheme 6). This complex features a new $\kappa^2\text{-P,N}$ -bound SNP ligand as is apparent from the ³¹P{¹H} NMR spectrum. Oxidation of the phosphorus atom of the pendant PnPr₂-NH-arm to give an S=PnPr₂-NH-moiety is accompanied by a high field shift from 27.5 to 64.6 ppm. The phosphorus atoms of the coordinated $\kappa^3\text{-PNP}$ and $\kappa^2\text{-SNP}$ ligands again give rise to a characteristic A₂B pattern (Fig. 1). Interestingly, treatment of **6** with 1 equiv. of AgBF₄ did not result in coordination of the phosphine sulfide moiety to give $[\text{Fe}(\kappa^3\text{-P,N,P-PNP-nPr})(\kappa^2\text{-S,P,N-PNS-nPr})\text{Cl}]^+$ but led to liberation of the SNP ligand and formation of the known homoleptic dicationic complex **5e** (Scheme 6).

Conclusion

In the present paper, we investigated the reaction of iron(II) halides with a series of PNP pincer ligands based on the 2,6-diaminopyridine scaffold. The steric bulk of PNP ligands prepared thus far decreases in the order PNP-*t*Bu (130) > PNP^{Me}-*i*Pr (120) \approx PNP^{Ph}-*n*Pr \approx PNP^{Ph}-Et (120) > PNP-*i*Pr (115) > PNP^{Me}-Ph (105) > PNP-*n*Bu \approx PNP-*n*Pr \approx PNP-Et \approx PNP-Ph (100) > PNP-BIPOL (95) > PNP-Me (90). With PNP ligands, which are sterically less demanding than PNP-*i*Pr, complexes of the type $[\text{Fe}(\kappa^3\text{-P,N,P-PNP})(\kappa^2\text{-P,N-PNP})\text{X}]^+$ (X = Cl, Br) were formed, while with the bulkier ligands, pentacoordinate complexes $[\text{Fe}(\kappa^3\text{-P,N,P-PNP})\text{X}_2]$ were obtained. In the case of the first, the PNP pincer ligands are coordinated in a $\kappa^3\text{-P,N,P}$ - and $\kappa^2\text{-P,N}$ -fashion, respectively, and adopt a strongly distorted octahedral geometry as established by X-ray crystallography. Obviously related to these distortions is their reactivity undergoing, upon halide dissociation, a facile rearrangement reaction to give the dicationic complexes $[\text{Fe}(\kappa^3\text{-P,N,P-PNP})_2]^{2+}$ where now both PNP ligands are bound in a $\kappa^3\text{-P,N,P}$ -fashion. This reaction proceeds only in the case of the smaller PNP ligands (PNP-Ph, PNP-BIPOL, PNP-Me), while with the bulkier



Scheme 6

ones (PNP-*n*Bu, PNP-*n*Pr, PNP-Et) the presence of a halide scavenger is required. The outcome of these investigation strongly suggests that the formation and reactivity of $[\text{Fe}(\kappa^3\text{-}P,N,P\text{-PNP})\text{-}(\kappa^2\text{-}P,N\text{-PNP})\text{X}]^+$ complexes are controlled by the steric bulk of the PNP ligands rather than their electronic properties.

Experimental section

General

All manipulations were performed under an inert atmosphere of argon using Schlenk techniques or in an MBraun inert-gas glovebox. The solvents were purified according to standard procedures.²⁴ The deuterated solvents were purchased from Aldrich and dried over 4 Å molecular sieves. The ligands *N,N'*-bis(dibenzo[*d,f*][1,3,2]dioxaphosphine)-2,6-diaminopyridine (PNP-BIPOL) (**1b**)¹⁷ and *N,N'*-bis(diphenylphosphino)-*N,N'*-dimethyl-2,6-diaminopyridine (PNP^{Me}-Ph)¹⁶ (**1g**), and $[\text{Fe}(\kappa^3\text{-}P,N,P\text{-PNP-Ph})(\kappa^2\text{-}P,N\text{-PNP-Ph})\text{Cl}]\text{Cl}$ (**2aCl**)¹⁵ were prepared according to the literature. ¹H, ¹³C{¹H}, and ³¹P{¹H} NMR spectra were recorded on Bruker AVANCE-250, AVANCE-300 DPX, and AVANCE-400 spectrometers. ¹H and ¹³C{¹H} NMR spectra were referenced internally to residual protio-solvent and solvent resonances, respectively, and are reported relative to tetramethylsilane ($\delta = 0$ ppm). ³¹P{¹H} NMR spectra were referenced externally to H₃PO₄ (85%) ($\delta = 0$ ppm). Room-temperature solution (CH₂Cl₂) magnetic moments were determined by ¹H NMR spectroscopy using the method of Evans.²⁵

All mass spectrometric measurements were performed on an Esquire 3000^{plus} 3D-quadrupole ion trap mass spectrometer (Bruker Daltonics, Bremen, Germany) in positive-ion mode by means of electrospray ionization (ESI). Mass calibration was done with a commercial mixture of perfluorinated trialkyl-triazines (ES Tuning Mix, Agilent Technologies, Santa Clara, CA, USA). All analytes were dissolved in methanol "hypergrade for LC-MS Lichrosolv" quality (Merck, Darmstadt, Germany) to form a concentration of roughly 1 mg mL⁻¹. Direct infusion

experiments were carried out using a Cole Parmer model 74900 syringe pump (Cole Parmer Instruments, Vernon Hills, IL, USA) at a flow rate of 2 $\mu\text{L min}^{-1}$. Full scan and MS/MS (low energy CID) scans were measured in the range m/z 100–1100 with the target mass set to m/z 1000. Further experimental conditions include: drying gas temperature: 150 °C; capillary voltage: -4 kV; skimmer voltage: 40 V; octapole and lens voltages: according to the target mass set. Helium was used as a buffer gas for full scans and as a collision gas for MS/MS scans in the low energy CID mode. The activation and fragmentation width for tandem mass spectrometric (MS/MS, CID) experiments was set to 6 Da to cover the main isotope cluster for fragmentation. The corresponding fragmentation amplitude ranged from 0.4 to 0.6 V in order to keep a precursor ion intensity of low abundance in the resulting MS/MS spectrum. All mass calculations are based on the lowest mass (*i.e.* the most abundant) iron isotope (⁵⁶Fe-isotope). Mass spectra and CID spectra were averaged during a data acquisition time of 1 to 2 min and one analytical scan consisted of five successive micro scans, resulting in 50 and 100 analytical scans, respectively, for the final full scan mass spectrum or the MS/MS spectrum.

***N,N'*-Bis(dimethylphosphino)-2,6-diaminopyridine (PNP-Me) (1c).** A suspension of 2,6-diaminopyridine (500 mg, 4.6 mmol) in THF (20 mL) was cooled to 0 °C and NEt₃ (1.3 mL, 9.2 mmol) was added. Then a solution of Me₂PCL (0.88 g, 9.90 mmol) in THF (10 mL) was added slowly *via* a dropping-funnel. The mixture was then allowed to reach room temperature and stirred for 12 h. The mixture was filtrated over Celite and washed with THF (5 mL). After removal of the solvent under reduced pressure, a pale red oil was obtained which afforded white crystals in the freezer at -20 °C. Yield: 0.93 g (89%). Anal. Calcd for C₉H₁₇N₃P₂ (229.20). C, 47.16; H, 7.48; N, 18.33. Found: C, 46.98; H, 7.81; N, 18.27. ¹H NMR (δ , CDCl₃, 20 °C): 7.25 (t, $J_{\text{HH}} = 8.5$ Hz, 1H, py⁴), 6.25 (d, $J_{\text{HH}} = 8.3$ Hz, 2H, py^{3,5}), 4.35 (s, broad, 2H, NH), 1.26 (d, $J_{\text{HP}} = 4.5$ Hz, 2H, CH₃). ¹³C{¹H} NMR (δ , CDCl₃, 20 °C): 157.4 (py), 139.5 (d, $J_{\text{CP}} =$

16.3 Hz, py), 97.8 (py), 6.1 (d, $J_{CP} = 8.0$ Hz, CH_3). $^{31}P\{^1H\}$ NMR (δ , $CDCl_3$, 20 °C): 14.1.

***N,N'*-Bis(diethylphosphino)-2,6-diaminopyridine (PNP-Et) (1d)**. A suspension of 2,6-diaminopyridine (590 mg, 5.4 mmol) in toluene (15 mL) was cooled to 0 °C and NEt_3 (1.5 mL, 10.8 mmol) was added. Then a solution of Et_2PCL (1.34 g, 10.8 mmol) in toluene (10 mL) was added slowly *via* a dropping-funnel. The mixture was then allowed to reach room temperature and stirred for 12 h. The mixture was filtered over Celite and washed with toluene (5 mL). After removal of the solvent under reduced pressure, a pale red oil was obtained which afforded white crystals in the freezer at -20 °C. Yield: 1.46 g (96%). Anal. Calcd for $C_{13}H_{25}N_3P_2$ (285.31): C, 54.73; H, 8.83; N, 14.73. Found: C, 54.53; H, 8.91; N, 14.70. 1H NMR (δ , $CDCl_3$, 20 °C): 7.25 (t, $J_{HP} = 8.4$ Hz, 1H, py⁴), 6.37 (d, $J_{HP} = 8.1$ Hz, 2H, py^{3,5}), 4.26 (d, $J_{HP} = 9.3$ Hz, 2H, NH), 1.55 (dq, $J_{HH} = 7.4$ Hz, $J_{HP} = 14.3$ Hz, 8H, CH_2), 1.05 (dt, $J_{HH} = 7.6$ Hz, $J_{HP} = 15.3$ Hz, 12H, CH_3). $^{13}C\{^1H\}$ NMR (δ , $CDCl_3$, 20 °C): 158.7 (d, $J_{CP} = 18.1$ Hz, py), 139.2 (s, py), 98.1 (d, $J_{CP} = 17.7$ Hz, py), 23.6 (d, $J_{CP} = 11.9$ Hz, CH_2), 8.5 (d, $J_{CP} = 13.0$ Hz, CH_3). $^{31}P\{^1H\}$ NMR (δ , $CDCl_3$, 20 °C): 33.2.

***N,N'*-Bis(ethylphosphino)-*N,N'*-diphenyl-2,6-diaminopyridine (PNP^{Ph}-Et) (1h)**. **1h** was prepared analogously to **1d** with *N,N'*-diphenyl-2,6-diaminopyridine (500 mg, 1.9 mmol) and Et_2PCL (480 mg, 3.8 mmol) as the starting materials. After workup the product is obtained as a white solid. Yield: 770 mg (90%). Anal. Calcd for $C_{25}H_{33}N_3P_2$ (437.50): C, 68.63; H, 7.60; N, 9.60. Found: C, 68.33; H, 7.87; N, 9.50. 1H NMR (δ , $CDCl_3$, 20 °C): 7.38 (m, 4H, Ph), 7.22 (t, $J_{HH} = 7.2$ Hz, 1H, py⁴), 7.08 (m, 6H, Ph), 5.99 (d, $J_{HH} = 8.0$ Hz, 2H, py^{3,5}), 1.78 (m, 4H, CH_2), 1.28 (m, 4H, CH_2), 1.04 (m, 12H, CH_3). $^{13}C\{^1H\}$ NMR (δ , $CDCl_3$, 20 °C): 160.2 (d, $J_{CP} = 11.9$ Hz, py), 137.7 (py), 130.1 (Ph), 130.0 (Ph), 129.2 (Ph), 125.9 (Ph), 102.0 (d, $J_{CP} = 8.9$ Hz, py), 21.3 (d, $J_{CP} = 13.8$ Hz, CH_2), 9.6 (d, $J_{CP} = 18.3$ Hz, CH_3). $^{31}P\{^1H\}$ NMR (δ , $CDCl_3$, 20 °C): 57.1.

***N,N'*-Bis(*n*-propylphosphino)-*N,N'*-diphenyl-2,6-diaminopyridine (PNP^{Ph}-*n*Pr) (1i)**. **1i** was prepared analogously to **1d** with *N,N'*-diphenyl-2,6-diaminopyridine (500 mg, 1.9 mmol) and Et_2PCL (580 mg, 3.8 mmol) as the starting materials. After workup the product is obtained as a pale-yellow solid. Yield: 860 mg (92%). Anal. Calcd for $C_{29}H_{41}N_3P_2$ (493.60): C, 70.56; H, 8.37; N, 8.51. Found: C, 70.34; H, 8.44; N, 8.69. 1H NMR (δ , $CDCl_3$, 20 °C): 7.34 (m, 4H, Ph), 7.20 (m, 1H, py⁴), 7.05 (d, $J_{HH} = 7.6$ Hz, 6H, Ph), 5.98 (d, $J_{HH} = 7.9$ Hz, 2H, py^{3,5}), 1.86 (m, 4H, CH_2), 1.50–1.39 (m, 8H, CH_2), 1.25–1.17 (m, 4H, CH_2), 0.95 (dt, $J_{HH} = 7.1$ Hz, $J_{HP} = 2.5$ Hz, 12H, CH_3). $^{13}C\{^1H\}$ NMR (δ , $CDCl_3$, 20 °C): 160.3 (d, $J_{CP} = 10.4$ Hz, py), 144.4 (Ph), 137.6 (py), 130.1 (Ph), 129.2 (Ph), 125.7 (Ph), 102.0 (d, $J_{CP} = 9.1$ Hz, py), 31.3 (d, $J_{CP} = 15.6$ Hz, CH_2), 19.0 (d, $J_{CP} = 18.3$ Hz, CH_2), 15.8 (d, $J_{CP} = 13.3$ Hz, CH_3). $^{31}P\{^1H\}$ NMR (δ , $CDCl_3$, 20 °C): 49.6.

$[Fe(\kappa^3\text{-}P,N,P\text{-PNP-BIPOL})(\kappa^2\text{-}P,N\text{-PNP-BIPOL})Cl]Cl$ (2bCl). To a suspension of anhydrous $FeCl_2$ (58 mg, 0.46 mmol) in THF (15 mL), PNP-BIPOL (**1b**) (500 mg, 0.93 mmol) was added and the mixture was stirred for 4 h. The resulting green solution was evaporated to dryness and the remaining green solid was washed with diethyl ether (30 mL) and dried under vacuum.

Yield: 422 mg (90%). Anal. Calcd for $C_{58}H_{42}Cl_2FeN_6O_8P_4$ (1201.64): C, 57.97; H, 3.52; N, 6.99. Found: C, 57.77; H, 3.49; N, 7.11. 1H NMR (δ , CD_2Cl_2 , 20 °C): 7.66–7.00 (m, 31 H), 6.85 (d, $J_{HH} = 7.5$ Hz, 4H, py), 6.56 (d, $J_{HP} = 7.5$ Hz, 3H, NH), 6.40 (t, 2H, py), 6.13 (d, $J_{HP} = 7.5$ Hz, 1H, NH). $^{31}P\{^1H\}$ NMR (δ , CD_2Cl_2 , 20 °C): A₂B spin system, $\delta_A = 192.4$ (2P), $\delta_B = 182.1$ (1P), $J_{PP} = 110$ Hz (shifts and J_{PP} determined from simulations), 146.2 (1P).

$[Fe(\kappa^3\text{-}P,N,P\text{-PNP-Me})(\kappa^2\text{-}P,N\text{-PNP-Me})Cl]Cl$ (2cCl). A solution of PNP-Me (**1c**) (100 mg, 0.44 mmol) in acetone (8 mL) was reacted with anhydrous $FeCl_2$ (27 mg, 0.22 mmol) and was stirred for 6 h, whereupon a green precipitate was formed. The solid was filtered and washed with acetone (5 mL), diethyl ether (5 mL), and dried under vacuum. Yield: 120 mg (95%). Anal. Calcd for $C_{18}H_{34}Cl_2FeN_6P_4$ (585.15): C, 36.95; H, 5.86; N, 14.36. Found: C, 36.67; H, 5.97; N, 14.40.

$[Fe(\kappa^3\text{-}P,N,P\text{-PNP-Me})(\kappa^2\text{-}P,N\text{-PNP-Me})Br]Br$ (2dBr). This compound was prepared analogously to **2c** using **1c** (100 mg, 0.44 mmol) and anhydrous $FeBr_2$ (46 mg, 0.22 mmol) as the starting materials. Yield: 139 mg (95%). Anal. Calcd for $C_{18}H_{34}Br_2FeN_6P_4$ (674.05): C, 32.07; H, 5.08; N, 12.47. Found: C, 32.24; H, 4.94; N, 11.81.

$[Fe(\kappa^3\text{-}P,N,P\text{-PNP-Et})(\kappa^2\text{-}P,N\text{-PNP-Et})Cl]BPh^Me_4$ (2eBPh^{Me}₄). A solution of PNP-Et (**1d**) (200 mg, 0.70 mmol) and $FeCl_2$ (44 mg, 0.35 mmol) in THF (10 mL) was stirred for 1 h at room temperature. A green precipitate was formed which was collected on a glass frit, washed with THF (5 mL) and dried under vacuum. Yield: 232 mg (95%) of $[Fe(\kappa^3\text{-}P,N,P\text{-PNP-Et})(\kappa^2\text{-}P,N\text{-PNP-Et})Cl]Cl$. Anal. Calcd for $C_{26}H_{50}Cl_2FeN_6P_4$ (697.36): C, 44.78; H, 7.23; N, 12.05. Found: C, 44.23; H, 6.94; N, 12.06. In order to obtain a soluble complex, this compound was suspended in 8 mL of THF and $NaBPh^Me_4$ was added (139 mg, 0.35 mmol). After stirring for 30 min the solution was evaporated to dryness and the residue was resolved in CH_2Cl_2 (10 mL) and filtered over Celite. The solvent was then removed under reduced pressure and the green solid was washed with *n*-hexane (10 mL) and dried under vacuum. Crystals of **2eBPh^{Me}₄** were grown from a THF solution by slow diffusion of diethyl ether. Yield 323 mg (89%). Anal. Calcd for $C_{54}H_{78}ClFeN_6P_4 \cdot C_{12}H_{24}O_3$ (1253.58): C, 63.24; H, 8.20; N, 6.70. Found: C, 62.98; H, 8.94; N, 6.56. 1H NMR (δ , CD_2Cl_2 , 20 °C): 8.21 (s, 2H, NH), 7.92 (s, 1H, NH), 7.54 (t, $J_{HP} = 8.1$ Hz, 1H, py), 7.30 (m, 8H, Ph), 7.06 (t, $J_{HP} = 7.8$ Hz, 1H, py), 6.79 (m, 8H, Ph), 6.64 (d, $J_{HP} = 8.0$ Hz, 2H, py), 6.36 (dd, $J_{HP} = 4.8$ Hz, 1H, py), 6.07 (d, $J_{HP} = 7.7$ Hz, 1H, py), 4.91 (d, $J_{HP} = 9.5$ Hz, 1H, NH), 2.85–2.54 (m, 8H, CH_2), 2.51–2.34 (m, 4H, CH_2), 2.15 (s, 12H, CH_3), 2.07–2.00 (m, 18H, CH_3), 1.38–1.31 (m, CH_2), 1.10–0.85 (m, CH_3). $^{31}P\{^1H\}$ NMR (δ , CD_2Cl_2 , 20 °C): the A₂B spin system, $\delta_A = 114.4$ (2P), $\delta_B = 111.4$ (1P), $J_{PP} = 50$ Hz (shifts and J_{PP} determined from simulations), 36.3 (1P).

$[Fe(\kappa^3\text{-}P,N,P\text{-PNP}^Me\text{-Ph})(\kappa^2\text{-}P,N\text{-PN}^NHMe\text{-Ph})Cl]BF_4$ (3). To a suspension of anhydrous $FeCl_2$ (127 mg, 1.0 mmol) in THF (10 mL), PNP^{Me}-Ph (**1g**) (1.02 g, 2.00 mmol) and $AgBF_4$ (195 mg, 1.0 mmol) were added and the mixture was stirred for 4 h. The solvent was removed under reduced pressure and the remaining green solid was dissolved in CH_2Cl_2 . The white

precipitate (AgCl) was removed by filtration over Celite and the solution was evaporated under reduced pressure. The remaining green solid was washed twice with diethyl ether (10 mL) and dried under vacuum. Yield: 950 mg (94%). Crystals of **3** were grown by slow diffusion of diethyl ether into a solution of THF. Anal. Calcd for $C_{50}H_{49}BClF_4FeN_6P_3$ (1005.00): C, 59.76; H, 4.91; N, 8.36. Found: C, 59.83; H, 4.86; N, 8.31. 1H NMR (δ , CD_2Cl_2 , 20 °C): 6.80–8.10 (m, 41H, py, Ph), 2.97 (bs, 9H, CH_3). $^{31}P\{^1H\}$ (δ , CD_2Cl_2 , 20 °C): A_2B spin system, $\delta_A = 128.1$ (2P), $\delta_B = 122.6$ (1P), $J_{PP} = 46$ Hz (shifts and J_{PP} determined from simulations).

$[Fe(\kappa^3-P,N,P-PNP^{Ph}-Et)(Cl)_2]$ (**4a**). A suspension of **1h** (100 mg, 0.23 mmol) and anhydrous $FeCl_2$ (29 mg, 0.23 mmol) in THF (7 mL) was stirred for 1 h. After that the solvent was removed under reduced pressure and a yellow solid was obtained which was washed with 10 mL of *n*-hexane and dried under vacuum. Yield: 125 mg (97%). Anal. Calcd for $C_{25}H_{33}Cl_2FeN_3P_2$ (564.25): C, 53.22; H, 5.89; N, 7.45. Found: C, 53.33; H, 5.83; N, 7.71. $\mu_{eff} = 4.9\mu_B$.

$[Fe(\kappa^3-P,N,P-PNP^{Ph}-nPr)(Cl)_2]$ (**4b**). This complex was prepared analogously to **4a** using $PNP^{Ph}-nPr$ (**1i**) (150 mg, 0.30 mmol) in THF (7 mL) and anhydrous $FeCl_2$ (38 mg, 0.30 mmol) as reactants. Yield: 180 mg (95%). Anal. Calcd for $C_{29}H_{41}Cl_2FeN_3P_2$ (620.35): C, 56.15; H, 6.66; N, 6.77. Found: C, 56.00; H, 6.53; N, 6.87. $\mu_{eff} = 4.8\mu_B$.

$[Fe(\kappa^3-P,N,P-PNP-Ph)_2](Cl)_2$ (**5aCl**). A solution of complex **2aCl** (50 mg) in 5 mL of CH_3CN was stirred for 15 min, whereupon the color changed from green to red. The solvent was evaporated and the remaining red solid was washed with diethyl ether and dried in a vacuum. Yield: 45 mg (90% yield). All spectral data for **5aCl** were identical with those of the authentic sample **5aBF₄** reported previously.¹⁶ Crystals for X-ray diffraction were obtained by slow solvent evaporation from a mixture of methanol and diethyl ether.

$[Fe(\kappa^3-P,N,P-PNP-BIPOL)_2](CF_3SO_3)_2$ (**5bCF₃SO₃**). Small amounts of crystals of **5bCF₃SO₃** suitable for X-ray crystallography could be obtained by reacting **2bCl** in THF with two equiv. of $AgCF_3SO_3$ followed by solvent evaporation. However, this complex could not be isolated in a pure form and crystals were taken from a mixture of several intractable solid products.

$[Fe(\kappa^3-P,N,P-PNP-Me)_2](BF_4)_2$ (**5cBF₄**). A solution of **1c** (100 mg, 0.44 mmol) and anhydrous $FeCl_2$ (27 mg, 0.22 mmol) in acetone (10 mL) was stirred for 1 h. After that, $AgBF_4$ (86 mg, 0.44 mmol) was added and the mixture was stirred for an additional hour whereupon the color of the solution changed from green to purple. The solution was filtered over Celite, and the solvent was removed under reduced pressure. The purple solid was washed with 15 mL of *n*-hexane and was then dried under vacuum. Yield: 144 mg (95%). Anal. Calcd for $C_{18}H_{34}FeFeN_6P_4B_2F_8$ (687.85): C, 31.43; H, 4.98; N, 12.22. Found: C, 30.79; H, 4.80; N, 11.98. 1H NMR (δ , acetone- d_6 , 20 °C): 7.48 (s, 4H, NH), 7.22 (t, $J_{HH} = 9.5$ Hz, 2H, py), 6.17 (d, $J_{HH} = 9.5$ Hz, 4H, py), 2.10 (s, 24H, CH_3). $^{13}C\{^1H\}$ NMR (δ , acetone- d_6 , 20 °C): 162.4 (py), 140.0 (py), 100.3 (py), 23.3 (t, $J_{CP} = 18$ Hz, CH_3). $^{31}P\{^1H\}$ NMR (δ , acetone- d_6 , 20 °C): 108.3. Crystals suitable for X-ray crystallography were grown with

$CF_3SO_3^-$ as the counterion (analogously prepared with $AgCF_3SO_3$ as a halide scavenger) from an acetone solution by slow diffusion of diethyl ether.

$[Fe(\kappa^3-P,N,P-PNP-nPr)(\kappa^2-P,N-PNS-nPr)Cl]BF_4$ (**6**). To a solution of $PNP-nPr$ (**1e**) (200 mg, 0.59 mmol) in acetone (7 mL), anhydrous $FeCl_2$ (37 mg, 0.29 mmol) and $NaBF_4$ (28 mg, 0.25 mmol) were added and the mixture was stirred for 1 h. Elemental sulfur (8.0 mg, 0.25 mmol) was then added and the solution was stirred for an additional 2 h. The green suspension was then filtered over Celite and the solution was evaporated to dryness. The remaining solid was washed with diethyl ether (5 mL) and *n*-hexane (10 mL). The remaining green powder was dried in a vacuum. Yield: 204 mg (91%). Anal. Calcd for $C_{34}H_{66}BClF_4FeN_6P_4S$ (892.99): C, 45.73; H, 7.45; N, 9.42. Found: C, 45.81; H, 7.39; N, 9.36. 1H NMR (δ , acetone- d_6 , 20 °C): 8.14 (s, 2H, NH), 7.89 (s, 1H, NH), 7.48 (m, 1H, py^4), 7.22 (m, 1H, py^4), 6.64 (m, 2H, $py^{3,5}$), 6.33 (m, 1H, py^3), 5.88 (d, $J_{HH} = 7.8$ Hz, py^5), 4.96 (s, 1H, NH), 2.70–2.18 (m, 4H, CH_2), 1.88–1.39 (m, 4H, CH_2), 1.10–0.90 (m, 15H, CH_2 , CH_3), 0.64 (m, 3H, CH_3). $^{13}C\{^1H\}$ NMR (δ , acetone- d_6 , 20 °C): 164.6 (m, py), 164.3–164.5 (m, py), 140.8 (py), 138.0 (py), 101.3 (py), 100.7 (py), 100.1 (py), 37.4 (m, CH_2), 34.0 (CH_2), 32.9 (CH_2), 30.8 (d, $J_{CP} = 10.8$ Hz, CH_2), 17.1–14.3 (CH_2 , CH_3). $^{31}P\{^1H\}$ NMR (δ , acetone- d_6 , 20 °C): the A_2B spin-system, $\delta_A = 109.4$ (2P), $\delta_B = 108.6$ (1P), $J_{PP} = 50$ Hz (shifts and J_{PP} determined from simulations), 64.6 (1P).

X-ray structure determination

X-ray diffraction data were collected at $T = 100$ K in a dry stream of nitrogen on Bruker Kappa APEX II (complexes **2eBPh^{Me}₄**, **2fBPh^{Me}₄**, **3**, **5aCl**, **5bCF₃SO₃**, **5cCF₃SO₃**, **5dBPh₄**, and **5eBF₄**) diffractometer systems using graphite-monochromatized Mo-K α radiation ($\lambda = 0.71073$ Å) and fine sliced φ - and ω -scans. Data were reduced with the program SAINT-Plus²⁶ and corrections for absorption and detector effects were applied with the program SADABS.²⁵ The structures of complexes **2fBPh^{Me}₄**, **5aCl**, **5bCF₃SO₃**, and **5dBPh₄** were solved with direct methods and refined with the SHELXTL program package.²⁷ The structures of complexes **2eBPh^{Me}₄**, **3**, **5cCF₃SO₃**, and **5eBF₄** were solved with charge-flipping implemented in SUPERFLIP²⁸ and refined using Jana2006.²⁹ All refinements were against F^2 data. Non-hydrogen atoms were refined anisotropically. The H atoms connected to C atoms were placed in calculated positions and thereafter refined as riding on the parent atoms. H atoms connected to N atoms were mostly located in difference Fourier maps and freely refined. Molecular graphics were generated with the program MERCURY.³⁰ Crystal data and experimental details are given in the ESI (Table S1† and CIF).

Variata: seven of the eight crystal structures concerned solvates, namely: **2eBPh^{Me}₄·3THF**, **2fBPh^{Me}₄·3THF**, **5aCl-solv** (solv = CH_3OH , Et_2O), **5bCF₃SO₃·6.5THF**, **5cCF₃SO₃·2Me₂CO**, **5dBPh₄·0.5Et₂O**, and **5eBF₄·2Me₂CO**. Only compound **3** was an unsolvated tetrafluoroborate salt. Complexes **2eBPh^{Me}₄·3THF** and **2fBPh^{Me}₄·3THF**, a chloride and a bromide complex, represent an isostructural pair. A small peak in the difference

Fourier map of $2\text{eBPh}^{\text{Me}}_4\cdot 3\text{THF}$ was attributed to a partially oxidized uncoordinated phosphine P atom. The site was therefore refined as a partially occupied isotropic O atom, whereby the occupancy refined to 0.162(7). Complex $5\text{aCl}\cdot\text{sol}$: the solvent in this solid, a mixture of methanol and diethyl ether, was disordered and was therefore removed from the structure factors with the procedure SQUEEZE of the program PLATON³¹ prior to concluding the refinement. Complex $5\text{bCF}_3\text{SO}_3\cdot 6.5\text{THF}$: this was a weakly scattering solvent-rich material with 6.5 THF molecules per formula unit. One THF was disordered about the centre of symmetry and one of the two CF_3SO_3 groups was orientation disordered. This highly desolvation-prone material scattered only to θ ca. 25° and gave somewhat meagre *R* values for a lastly very reasonable crystal structure. Complex $5\text{cCF}_3\text{SO}_3\cdot 2\text{Me}_2\text{CO}$: In this crystal structure the Fe complex $5\text{cCF}_3\text{SO}_3\cdot 2\text{Me}_2\text{CO}$ and one acetone molecule are located on 2-fold axes (point symmetry C_2) while another acetone molecule is disordered about an inversion. Complex $5\text{dBPh}_4\cdot 0.5\text{Et}_2\text{O}$: In this crystal structure the diethyl ether molecule is disordered about an inversion. $5\text{eBPh}_4\cdot 2\text{Me}_2\text{CO}$: in this crystal structure the Fe complex has point symmetry $222 (D_2)$ and the ordered acetone molecule has point symmetry $2 (C_2)$.

Computational details

All calculations were performed using the GAUSSIAN 09 software package³² on the Phoenix Linux Cluster of the Vienna University of Technology. The optimized geometries were obtained with the B3LYP functional,³³ without symmetry constraints. That functional includes a mixture of Hartree-Fock³⁴ exchange with DFT³⁵ exchange–correlation, given by Becke's three parameter functional with the Lee, Yang and Parr correlation functional, which includes both local and non-local terms. The basis set used for the geometry optimizations consisted of the Stuttgart/Dresden ECP (SDD) basis set³⁶ to describe the electrons of iron, and a standard 6-31G** basis set³⁷ for all other atoms. A Natural Population Analysis (NPA)³⁸ and the resulting Wiberg indices²¹ were used to study the electronic structure and bonding of the optimized species.

The inclusion of dispersion effects by means of the Grimme DFT-D3 method³⁹ with Becke and Johnson short distance damping⁴⁰ rises the stability difference between the two isomers of complex **2a** from 6.9 to 9.0 kcal mol⁻¹ (**A** remaining the most stable). Also, for comparison, geometry optimizations of the two isomers of **2a** were performed with the M06 functional leading to same conclusions and a stability difference of 6.1 kcal mol⁻¹. The M06 functional is a hybrid meta-GGA functional developed by Truhlar and Zhao,⁴¹ and it was shown to perform very well for transition metal systems, providing a good description of weak and long range interactions.⁴²

Acknowledgements

Financial support by the Austrian Science Fund (FWF) is gratefully acknowledged (project no. P24202-N17) and LFV acknowledges the Fundação para a Ciência e Tecnologia (Projecto Estratégico – PEst-OE/QUI/UI0100/2013). The X-ray Center of the Vienna

University of Technology is acknowledged for financial support and for providing access to the single-crystal diffractometer.

References

- For reviews on pincer complexes, see: (a) M. Albrecht and G. van Koten, *Angew. Chem., Int. Ed.*, 2001, **40**, 3750; (b) M. E. van der Boom and D. Milstein, *Chem. Rev.*, 2003, **103**, 1759; (c) J. T. Singleton, *Tetrahedron*, 2003, **59**, 1837; (d) P. Bhattacharya and H. Guan, *Comments Inorg. Chem.*, 2011, **32**, 88; (e) S. Schneider, J. Meiners and B. Askevold, *Eur. J. Inorg. Chem.*, 2012, 412; (f) *The Chemistry of Pincer Compounds*, ed. D. Morales-Morales and C. M. Jensen, Elsevier, Amsterdam, 2007; (g) D. Benito-Garagorri and K. Kirchner, *Acc. Chem. Res.*, 2008, **41**, 201.
- (a) B. L. Small, M. Brookhart and M. A. Bennett, *J. Am. Chem. Soc.*, 1998, **120**, 4049; (b) Y. Chen, R. Chen, C. Qian, X. Dong and J. Sun, *Organometallics*, 2003, **22**, 4312; (c) G. J. P. Britovsek, J. England, S. K. Spitzmesser, A. J. P. White and D. J. Williams, *Dalton Trans.*, 2005, 945.
- (a) G. J. P. Britovsek, V. C. Gibson, B. S. Kimberley, P. J. Maddox, S. J. McTavish, G. A. Solan, A. J. P. White and D. J. Williams, *Chem. Commun.*, 1998, 849; (b) G. J. P. Britovsek, M. Bruce, V. C. Gibson, B. S. Kimberley, P. J. Maddox, S. Mastroianni, S. J. McTavish, C. Redshaw, G. A. Solan, S. Stromberg, A. J. P. White and D. J. Williams, *J. Am. Chem. Soc.*, 1999, **121**, 8728.
- S. C. Bart, E. Lobkovsky and P. J. Chirik, *J. Am. Chem. Soc.*, 2004, **126**, 13749.
- (a) W. V. Dahlhoff and S. M. Nelson, *J. Chem. Soc. A*, 1971, 2184; (b) P. Giannoccaro, G. Vasapollo, C. F. Nobile and A. Sacco, *Inorg. Chim. Acta*, 1982, **61**, 69; (c) G. Müller, M. Klinga, M. Leskelä and B. Rieger, *Z. Anorg. Allg. Chem.*, 2002, **628**, 2839.
- (a) J. Zhang, M. Gandelman, D. Herrman, G. Leituss, L. J. W. Shimon, Y. Ben-David and D. Milstein, *Inorg. Chim. Acta*, 2006, **359**, 1955; (b) R. J. Trovitch, E. Lobkovsky and P. J. Chirik, *Inorg. Chem.*, 2006, **45**, 7252.
- E. M. Pelczar, T. J. Emge, K. Krogh-Jespersen and A. S. Goldman, *Organometallics*, 2008, **27**, 5759.
- (a) L. Zhang, D. Peng, X. Leng and Z. Huang, *Angew. Chem., Int. Ed.*, 2013, **52**, 3676; (b) T. Zell, P. Milko, K. L. Fillman, Y. Diskin-Posner, T. Bendikov, M. A. Iron, G. Leituss, Y. Ben-David, M. L. Neidig and D. Milstein, *Chem. – Eur. J.*, 2014, **20**, 4403.
- A. A. Danopoulos, N. Tsoureas, J. A. Wright and M. E. Light, *Organometallics*, 2004, **23**, 166.
- J. S. Judge, W. M. Reiff, G. M. Intille, P. Ballway and W. A. Baker Jr., *J. Inorg. Nucl. Chem.*, 1967, **29**, 1711.
- W.-S. W. DeRieux, A. Wong and Y. Schrodi, *J. Organomet. Chem.*, 2014, 772–773, 60.
- (a) R. J. Trovitch, E. Lobkovsky, E. Bill and P. J. Chirik, *Organometallics*, 2008, **27**, 1470; (b) S. K. Russell, J. M. Darmon, E. Lobkovsky and P. J. Chirik, *Inorg. Chem.*, 2010, **49**, 2782.

- 13 (a) A. M. Tondreau, E. Lobkovsky and P. J. Chirik, *Org. Lett.*, 2008, **10**, 2789; (b) A. M. Tondreau, J. M. Darmon, B. M. Wile, S. K. Floyd, E. Lobkovsky and P. J. Chirik, *Organometallics*, 2009, **28**, 3928; (c) A. M. Tondreau, C. C. H. Atienza, J. M. Darmon, C. Milsmann, H. M. Hoyt, K. J. Weller, S. A. Nye, K. M. Lewis, J. Boyer, J. G. P. Delis, E. Lobkovsky and P. J. Chirik, *Organometallics*, 2012, **31**, 4886; (d) S. K. Russell, C. Milsmann, E. Lobkovsky, T. Weyhermüller and P. J. Chirik, *Inorg. Chem.*, 2011, **50**, 3159; (e) A. M. Tondreau, C. C. H. Atienza, K. J. Weller, S. A. Nye, K. M. Lewis, J. G. P. Delis and P. J. Chirik, *Science*, 2012, **335**, 567.
- 14 (a) D. Benito-Garagorri, J. Wiedermann, M. Pollak, K. Mereiter and K. Kirchner, *Organometallics*, 2007, **26**, 217; (b) D. Benito-Garagorri, M. Puchberger, K. Mereiter and K. Kirchner, *Angew. Chem., Int. Ed.*, 2008, **47**, 9142; (c) D. Benito-Garagorri, L. G. Alves, M. Puchberger, K. Mereiter, L. F. Veiros, M. J. Calhorda, M. D. Carvalho, L. P. Ferreira, M. Godinho and K. Kirchner, *Organometallics*, 2009, **28**, 6902.
- 15 B. Bichler, M. Glatz, B. Stöger, K. Mereiter, L. F. Veiros and K. Kirchner, *Dalton Trans.*, 2014, **43**, 14517.
- 16 S. R. M. M. de Aguiar, B. Stöger, E. Pittenauer, G. Allmaier, M. Puchberger, L. F. Veiros and K. Kirchner, *J. Organomet. Chem.*, 2014, **760**, 74.
- 17 D. Benito-Garagorri, E. Becker, J. Wiedermann, W. Lackner, M. Pollak, K. Mereiter, J. Kisala and K. Kirchner, *Organometallics*, 2006, **25**, 1900.
- 18 Ö. Öztöpcü, C. Holzhacker, M. Puchberger, M. Weil, K. Mereiter, L. F. Veiros and K. Kirchner, *Organometallics*, 2013, **32**, 3042.
- 19 T. E. Müller and D. M. P. Mingos, *Transition Met. Chem.*, 1995, **20**, 533.
- 20 R. J. Abraham, J. Fisher and P. Loftus, *Introduction to NMR Spectroscopy*; John Wiley & Sons, Ltd., New York, 1988.
- 21 (a) WI represents the Wiberg index. Wiberg indices are electronic parameters related to the electron density between two atoms, which scale as bond strength indicators. They can be obtained from a Natural Population Analysis (b) K. B. Wiberg, *Tetrahedron*, 1968, **24**, 1083.
- 22 S. Pavlik, K. Mereiter, M. Puchberger and K. Kirchner, *Organometallics*, 2005, **24**, 3561.
- 23 P. Giannoccaro, G. Vasapollo, C. F. Nobile and A. Sacco, *Inorg. Chim. Acta*, 1982, **61**, 69.
- 24 D. D. Perrin and W. L. F. Armarego, *Purification of Laboratory Chemicals*, Pergamon, New York, 3rd edn, 1988.
- 25 (a) S. K. Sur, *J. Magn. Reson.*, 1989, **82**, 169; (b) D. F. Evans, *J. Chem. Soc.*, 1959, 2003.
- 26 *Computer programs APEX2, SMART, SAINT, SADABS, and SHELXTL*, Bruker AXS Inc., Madison, WI, 2012.
- 27 G. M. Sheldrick, *Acta Crystallogr., Sect. A: Fundam. Crystallogr.*, 2008, **64**, 112.
- 28 L. Palatinus and G. Chapuis, *J. Appl. Crystallogr.*, 2007, **40**, 786.
- 29 V. Petříček, M. Dušek and L. Palatinus, *JANA2006. Institute of Physics, Czech Republic, Praha*, 2006.
- 30 C. F. Macrae, P. R. Edgington, P. McCabe, E. Pidcock, G. P. Shields, R. Taylor, M. Towler and J. van de Streek, *J. Appl. Crystallogr.*, 2006, **39**, 453.
- 31 A. L. Spek, *Acta Crystallogr., Sect. D: Biol. Crystallogr.*, 2009, **65**, 148.
- 32 M. J. Frisch, G. W. Trucks, H. B. Schlegel, G. E. Scuseria, M. A. Robb, J. R. Cheeseman, G. Scalmani, V. Barone, B. Mennucci, G. A. Petersson, H. Nakatsuji, M. Caricato, X. Li, H. P. Hratchian, A. F. Izmaylov, J. Bloino, G. Zheng, J. L. Sonnenberg, M. Hada, M. Ehara, K. Toyota, R. Fukuda, J. Hasegawa, M. Ishida, T. Nakajima, Y. Honda, O. Kitao, H. Nakai, T. Vreven, J. A. Montgomery Jr., J. E. Peralta, F. Ogliaro, M. Bearpark, J. J. Heyd, E. Brothers, K. N. Kudin, V. N. Staroverov, R. Kobayashi, J. Normand, K. Raghavachari, A. Rendell, J. C. Burant, S. S. Iyengar, J. Tomasi, M. Cossi, N. Rega, J. M. Millam, M. Klene, J. E. Knox, J. B. Cross, V. Bakken, C. Adamo, J. Jaramillo, R. Gomperts, R. E. Stratmann, O. Yazyev, A. J. Austin, R. Cammi, C. Pomelli, J. W. Ochterski, R. L. Martin, K. Morokuma, V. G. Zakrzewski, G. A. Voth, P. Salvador, J. J. Dannenberg, S. Dapprich, A. D. Daniels, Ö. Farkas, J. B. Foresman, J. V. Ortiz, J. Cioslowski and D. J. Fox, *Gaussian 09, Revision A.02*, Gaussian, Inc., Wallingford, CT, 2009.
- 33 (a) A. D. Becke, *J. Chem. Phys.*, 1993, **98**, 5648; (b) B. Miehlich, A. Savin, H. Stoll and H. Preuss, *Chem. Phys. Lett.*, 1989, **157**, 200; (c) C. Lee, W. Yang and G. Parr, *Phys. Rev. B: Condens. Matter*, 1988, **37**, 785.
- 34 W. J. Hehre, L. Radom, P. v. R. Schleyer and J. A. Pople, *Ab Initio Molecular Orbital Theory*, John Wiley & Sons, New York, 1986.
- 35 R. G. Parr and W. Yang, *Density Functional Theory of Atoms and Molecules*, Oxford University Press, New York, 1989.
- 36 (a) U. Haeusermann, M. Dolg, H. Stoll and H. Preuss, *Mol. Phys.*, 1993, **78**, 1211; (b) W. Kuechle, M. Dolg, H. Stoll and H. Preuss, *J. Chem. Phys.*, 1994, **100**, 7535; (c) T. Leininger, A. Nicklass, H. Stoll, M. Dolg and P. Schwerdtfeger, *J. Chem. Phys.*, 1996, **105**, 1052.
- 37 (a) A. D. McLean and G. S. Chandler, *J. Chem. Phys.*, 1980, **72**, 5639; (b) R. Krishnan, J. S. Binkley, R. Seeger and J. A. Pople, *J. Chem. Phys.*, 1980, **72**, 650; (c) P. J. Hay, *J. Chem. Phys.*, 1977, **66**, 4377; (d) K. Raghavachari and G. W. Trucks, *J. Chem. Phys.*, 1989, **91**, 1062; (e) R. C. Binning and L. A. Curtiss, *J. Comput. Chem.*, 1995, **103**, 6104; (f) M. P. McGrath and L. Radom, *J. Chem. Phys.*, 1991, **94**, 511.
- 38 (a) J. E. Carpenter and F. Weinhold, *J. Mol. Struct. (THEOCHEM)*, 1988, **169**, 41; (b) J. E. Carpenter, PhD thesis, University of Wisconsin, Madison, WI, 1987; (c) J. P. Foster and F. Weinhold, *J. Am. Chem. Soc.*, 1980, **102**, 7211; (d) A. E. Reed and F. Weinhold, *J. Chem. Phys.*, 1983, **78**, 4066; (e) A. E. Reed and F. Weinhold, *J. Chem. Phys.*, 1983, **78**, 1736; (f) A. E. Reed, R. B. Weinstock and F. Weinhold, *J. Chem. Phys.*, 1985, **83**, 735; (g) A. E. Reed, L. A. Curtiss and F. Weinhold, *Chem. Rev.*, 1988, **88**, 899; (h) F. Weinhold

- and J. E. Carpenter, *The Structure of Small Molecules and Ions*, Plenum, 1988, p. 227.
- 39 S. Grimme, J. Antony, S. Ehrlich and H. J. Krieg, *Chem. Phys.*, 2010, **132**, 154104.
- 40 (a) A. D. Becke and E. R. J. Johnson, *Chem. Phys.*, 2005, **122**, 154101; (b) E. R. Johnson and A. D. Becke, *J. Chem. Phys.*, 2005, **123**, 24101; (c) E. R. Johnson and A. D. Becke, *J. Chem. Phys.*, 2006, **124**, 174104.
- 41 Y. Zhao and D. G. Truhlar, *Theor. Chem. Acc.*, 2008, **120**, 215.
- 42 (a) Y. Zhao and D. G. Truhlar, *Acc. Chem. Res.*, 2008, **41**, 157; (b) Y. Zhao and D. G. Truhlar, *Chem. Phys. Lett.*, 2011, **502**, 1.

Manuscript #2

“Fe(II) Carbonyl Complexes Featuring Small to Bulky PNP Pincer Ligands – Facile Substitution of κ^2 P,N-Bound PNP Ligands by Carbon Monoxide”

Glatz M.; Holzacker C.; Bichler B.; Mastalir M.; Stöger B.; Mereiter K.; Weil M.; Veiros L. F.; Mösch-Zanetti N. C.; Kirchner K. *Eur. J. Inorg. Chem.* **2015**, 5053-5065.

Reproduced by permission of The Royal Society of Chemistry

DOI:10.1002/ejic.201500646

Fe^{II} Carbonyl Complexes Featuring Small to Bulky PNP Pincer Ligands – Facile Substitution of κ^2P,N -Bound PNP Ligands by Carbon Monoxide

Mathias Glatz,^[a] Christian Holz hacker,^[a] Bernhard Bichler,^[a] Matthias Mastalir,^[a] Berthold Stöger,^[b] Kurt Mereiter,^[b] Matthias Weil,^[b] Luis F. Veiros,^[c] Nadia C. Mös ch-Zanetti,^[d] and Karl Kirchner*^[a]

Keywords: Iron / Pincer ligands / N,P ligands / Carbonyl ligands / Density functional calculations

Complexes *trans*- and *cis*-[Fe(κ^3P,N,P -PNP)(CO)Cl₂] bearing sterically demanding to small PNP ligands based on the 2,6-diaminopyridine scaffold are synthesized. The aromatic pyridine ring and the phosphine PR₂ moieties are connected through NH, *N*-alkyl, or *N*-aryl linkers. For bulky PNP ligands, with the exception of the ligands with *t*Bu₂ units, these complexes are obtained upon the treatment of [Fe(κ^3P,N,P -PNP)Cl₂] with CO. With small PNP ligands, such complexes are not accessible directly owing to the formation of [Fe(κ^3P,N,P -PNP)(κ^2P,N -PNP)Cl]Cl. These complexes liberate the κ^2 -*P,N*-bound PNP ligand in the presence of CO to yield [Fe(κ^3P,N,P -PNP)(CO)Cl₂] in yields of less than 50%. High yields are achieved by reacting FeCl₂ with PNP ligands

under a CO atmosphere. For structural and reactivity comparisons, [Fe(κ^3P,N,P -PNP-Ph)(κ^2P,N -PN-Ph)Cl]⁺ was prepared, and this complex does not react with CO. In contrast to the reactions in solution, in the solid state, complexes [Fe(κ^3P,N,P -PNP)Cl₂] with NH linkers are also converted quantitatively into *trans*- or *cis*-[Fe(κ^3P,N,P -PNP)(CO)(Cl)₂] upon treatment with CO, as indicated by a color change and by IR spectroscopy monitoring. Those with *N*-alkyl and *N*-aryl linkers did not react with CO. To rationalize why most [Fe(κ^3P,N,P -PNP)Cl₂] complexes react readily with CO but those with *t*Bu substituents do not, the additions of CO to [Fe(κ^3P,N,P -PNP-*i*Pr)Cl₂] and [Fe(κ^3P,N,P -PNP-*t*Bu)Cl₂] were investigated by DFT calculations.

Introduction

Neutral pyridine-based PNP pincer ligands are utilized widely in transition-metal chemistry owing to their combination of stability, activity, and variability.^[1] They typically enforce a meridional κ^3 -*P,N,P* coordination mode if three coordination sites are accessible at the metal center. An important class of iron PNP complexes are the coordinatively unsaturated 16e high-spin square-pyramidal complexes of the type [Fe(κ^3P,N,P -PNP)X₂] (X = Cl, Br) obtained from Fe^{II} halides with stoichiometric amounts of PNP ligands.

Examples of prominent PNP ligands are bis(phosphino-methyl)pyridines^[2–4] and bis(phosphinito)pyridines.^[5] In most cases, bulky R substituents such as *i*Pr or *t*Bu are required to avoid the formation of bis-chelated dicationic low-spin complexes of the type [Fe(κ^3P,N,P -PNP)₂]²⁺.

We are currently focusing on the synthesis and reactivity of non-precious-metal complexes containing PNP pincer ligands^[1] based on the 2,6-diaminopyridine scaffold with the aromatic pyridine ring and the phosphine moieties connected through NH, *N*-alkyl, or *N*-aryl linkers. An advantage of these ligands over PNP pincers bearing CH₂ or O linkers is that the substituents of the phosphine and amine sites can be systematically varied in a modular fashion. In particular, the nature of the linker has a decisive effect on reaction outcomes.^[6] With bulky PNP ligands such as PNP-*i*Pr (**1a**) or PNP-*t*Bu (**1c**), the typical monochelated high-spin complexes [Fe(κ^3P,N,P -PNP)X₂] (type **I**) are formed (Scheme 1).^[7] Such complexes add CO to give *trans*-[Fe(κ^3P,N,P -PNP)(CO)X₂], *cis*-[Fe(κ^3P,N,P -PNP)(CO)X₂], or both (Scheme 2).^[8]

These reactions are of interest, as CO addition is fully reversible both in solution and in the solid state and accompanied by both color and spin-state changes and might, thus, be useful for CO sensors.^[9,10] The general effect of

[a] Institute of Applied Synthetic Chemistry, Vienna University of Technology,

Getreidemarkt 9, 1060 Vienna, Austria

E-mail: kkirchner@mail.tuwien.ac.at

http://www.ias.tuwien.ac.at

[b] Institute of Chemical Technologies and Analytics, Vienna University of Technology,

Getreidemarkt 9, 1060 Vienna, Austria

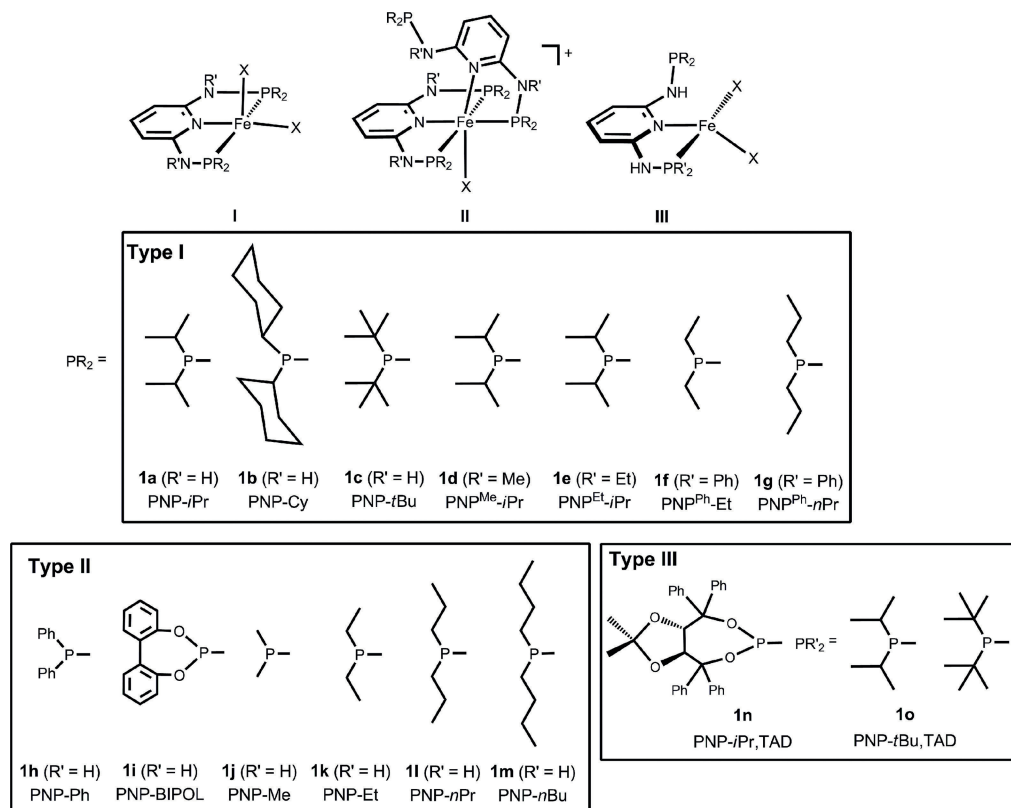
[c] Centro de Química Estrutural, Instituto Superior Técnico, Universidade de Lisboa,

Av. Rovisco Pais No. 1, 1049-001 Lisboa, Portugal

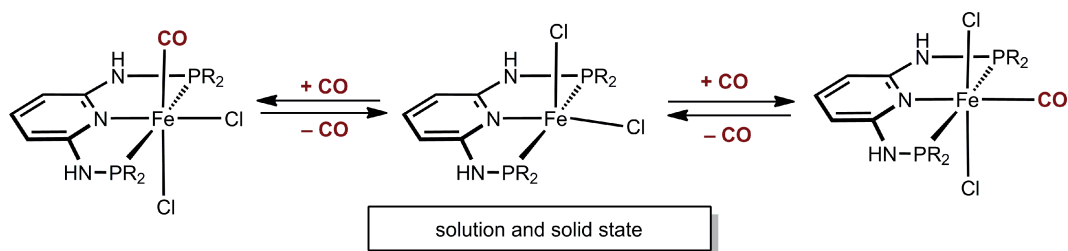
[d] Institute of Chemistry, University of Graz,

Schubertstrasse 1, 8010 Graz, Austria

Supporting information and ORCID(s) from the author(s) for this article are available on the WWW under <http://dx.doi.org/10.1002/ejic.201500646>.



Scheme 1. Overview of PNP ligands (the labeling of the complexes refers to the letters of the ligands depicted here) and classification of their reaction behavior with FeX₂ (X = Cl, Br).



Scheme 2.

spin-state changes upon CO coordination to transition-metal complexes is well described.^[11,12] Several examples of reversible and irreversible carbonylation reactions of Fe^{II} complexes have been reported.^[13–16] In contrast, with smaller pincer ligands such as PNP-Ph (**1g**) or PNP-Et (**1j**), irrespective of the stoichiometry, diamagnetic bis-chelated octahedral complexes of the type [Fe(κ^3P,N,P -PNP)(κ^2P,N -PNP)X]⁺ (X = Cl, Br; type **II**) are obtained in which the PNP pincer ligands are coordinated in κ^3P,N,P and κ^2P,N fashions.^[8a,8b] The use of asymmetrically substituted PNP ligands **1n** and **1o**, which are based on *R,R*-TADDOL in combination with bulky *i*Pr and *t*Bu substituents, leads to the formation of complexes of the type [Fe(κ^2P,N -PNP-R,TAD)X₂] (type **III**), in which the PNP ligand is coordinated in an unexpected κ^2P,N fashion. Interestingly, equi-

libria between [Fe(κ^2P,N -PNP-R,TAD)X₂] and [Fe(κ^3P,N,P -PNP-R,TAD)X₂] complexes have been observed in solution.^[17]

In continuation of our studies on iron PNP complexes, we report here on the synthesis and reactivity of octahedral Fe^{II} carbonyl complexes bearing both sterically undemanding as well as new bulky PNP ligands and discuss the impact of the NR linker on the outcome of these reactions. In addition, we show that the removal of CO from solid samples of [Fe(κ^3P,N,P -PNP(CO)Cl₂)] at elevated temperatures (under vacuum) allows the preparation of [Fe(κ^3P,N,P -PNP)Cl₂] complexes, which are not accessible by conventional methods for small PNP ligands owing to the formation of [Fe(κ^3P,N,P -PNP)(κ^2P,N -PNP)Cl]⁺ (type **II**).^[8a,8b]

Results and Discussion

Reactions Involving Bulky PNP Ligands

The treatment of anhydrous FeCl_2 with 1 equiv. of the respective PNP ligand (**1a–1g**) in tetrahydrofuran (THF) at room temperature afforded the pentacoordinate coordinatively unsaturated complexes $[\text{Fe}(\kappa^3P,N,P\text{-PNP})\text{Cl}_2]$ (**3a–3g**) in high isolated yields (Scheme 3). The syntheses of $[\text{Fe}(\kappa^3P,N,P\text{-PNP-}i\text{Pr})\text{Cl}_2]$ (**3a**) and $[\text{Fe}(\kappa^3P,N,P\text{-PNP-}t\text{Bu})\text{Cl}_2]$ (**3c**) were reported elsewhere.^[7,8] These complexes are thermally robust pale yellow solids that are air-stable both in the solid state and in solution for several days. The effective magnetic moments of **3a**, **3b**, **3f**, and **3g** are in the range 4.9–5.0 μ_B , as determined in the solid state by superconducting quantum interference device (SQUID) magnetometry or with a Faraday balance and in solution by the Evans method.^[27] Accordingly, they typically adopt a high-spin configuration with a typical quintet ground state (four unpaired electrons). All of the complexes display contact-shifted ^1H NMR spectra, but some exhibit relatively narrow linewidths at room temperature, and the expected ligand resonances for **3a**, **3c**, **3d**, and **3e** could be assigned on the basis of integration. The molecular structures of **3d** and **3e** were determined by X-ray crystallography. Structural views are depicted in Figures 1 and 2, and selected bond lengths and angles are given in the captions. The iron centers have distorted square-pyramidal coordination geometries; the iron atoms lie 0.686 (**3d**) and 0.683 Å (**3e**) out of the basal planes defined by N1–P1–Cl1–P2, and Cl2 forms the apex of the pyramid. The bond lengths and angles of **3d** and **3e** are in good accord with the solid-state structure of $[\text{Fe}(\kappa^3P,N,P\text{-PNP-}i\text{Pr})\text{Cl}_2]$ (**3a**). Particularly characteristic for all of these complexes are the comparatively long Fe–N and Fe–P bonds, which clearly indicate that they are in the high-spin state; low-spin Fe PNP complexes have Fe–N and Fe–P bonds ca. 0.2 Å shorter. In contrast, the Fe–Cl bonds are quite insensitive to the spin state, but the equatorial Fe–Cl1 bond is always systematically longer by ca. 0.1 Å than the apical Fe–Cl2 bond.

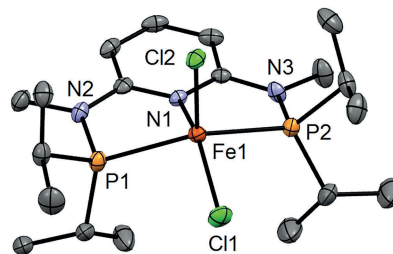


Figure 1. Structural view of $[\text{Fe}(\kappa^3P,N,P\text{-PNP}^{\text{Me-}i\text{Pr}})\text{Cl}_2]\cdot 0.5\text{THF}$ (**3d** $\cdot 0.5\text{THF}$) showing 50% thermal ellipsoids (H atoms and solvent molecules omitted for clarity). Selected bond lengths [Å] and angles [°]: Fe1–N1 2.290(3), Fe1–Cl1 2.3473(10), Fe1–Cl2 2.3012(10), Fe1–P1 2.4637(11), Fe1–P2 2.4432(11), N1–Fe1–Cl1 145.45(8), N1–Fe1–Cl2 107.81(8), Cl1–Fe1–Cl2 106.71(4), P1–Fe1–P2 140.89(4).

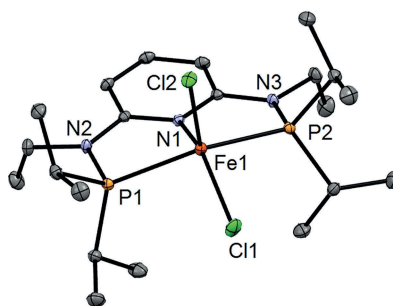
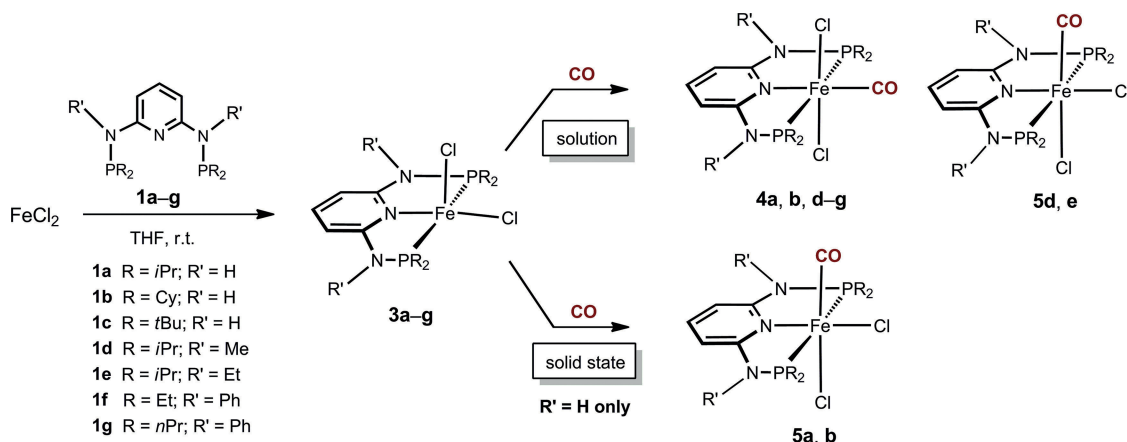


Figure 2. Structural view of $[\text{Fe}(\kappa^3P,N,P\text{-PNP}^{\text{Et-}i\text{Pr}})\text{Cl}_2]$ (**3e**) showing 50% thermal ellipsoids (H atoms omitted for clarity). Selected bond lengths [Å] and angles [°]: Fe1–N1 2.2296(7), Fe1–Cl1 2.3694(3), Fe1–Cl2 2.3003(4), Fe1–P1 2.4343(4), Fe1–P2 2.4307(3), N1–Fe1–Cl1 140.86(2), N1–Fe1–Cl2 112.45(2), Cl1–Fe1–Cl2 106.681(10), P1–Fe1–P2 145.125(9).

Complexes **3a**, **3b**, **3f**, and **3g** react readily with the strong π -acceptor ligand CO in solution to afford selectively the *trans* complexes $[\text{Fe}(\kappa^3P,N,P\text{-PNP-}i\text{Pr})(\text{CO})(\text{Cl})_2]$ (**4a**), $[\text{Fe}(\kappa^3P,N,P\text{-PNP-Cy})(\text{CO})\text{Cl}_2]$ (**4b**), $[\text{Fe}(\kappa^3P,N,P\text{-PNP}^{\text{Ph-Et}})(\text{CO})\text{Cl}_2]$ (**4f**), and $[\text{Fe}(\text{PNP}^{\text{Ph-}n\text{Pr}})(\text{CO})\text{Cl}_2]$ (**4g**) in excellent yields (75–96%), as shown in Scheme 3. Complex **3c** did not react with CO, whereas **3d** and **3e** afforded mixtures



Scheme 3.

of *trans*- and *cis*-[Fe(κ^3P,N,P -PNP^{M_c}-*i*Pr)(CO)Cl₂] (**4d/4e** and **5d/5e**). All of the compounds are air-stable in the solid state but slowly decompose in solution upon exposure to air. Complexes **4** were characterized by ¹H and ³¹P{¹H} NMR spectroscopy, IR spectroscopy, and elemental analysis. In most cases, the ¹³C{¹H} NMR spectra were also recorded. The *trans* and *cis* isomers **4d/4e** and **5d/5e** can be readily distinguish on the basis of their ¹³C{¹H} and ³¹P{¹H} NMR spectra. The ¹³C{¹H} NMR spectra of the *trans*-chloro complexes **4d** and **4e** give rise to one set of signals for the isopropyl methine and methyl carbon atoms, which is consistent with a complex of C_{2v} symmetry with a *trans*-dichloro arrangement. For the *cis*-dichloro arrangement of **5d** and **5e** (C_s symmetry), two sets of signals are observed for these carbon atoms. Moreover, the ³¹P{¹H} NMR resonances of the *trans*-chloro complexes are typically low-field-shifted by ca. 12–14 ppm relative to the resonances of the respective *cis*-chloro compounds. The isomers could not be distinguished by IR spectroscopy. In addition to the spectroscopic characterization, the solid-state structures of **4b** and **4f** were determined by single-crystal X-ray diffraction. Structural views are depicted in Figures 3 and 4, and selected bond lengths and angles given in the captions.

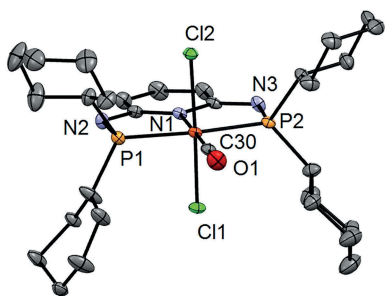


Figure 3. Structural view of *trans*-[Fe(κ^3P,N,P -PNP-Cy)(CO)Cl₂] \cdot 2DMSO \cdot Et₂O (**4b** \cdot 2DMSO \cdot Et₂O; DMSO = dimethyl sulfoxide) showing 50% thermal ellipsoids (H atoms and solvent molecules omitted for clarity). Selected bond lengths [Å] and angles [°]: Fe1–Cl1 2.3041(9), Fe1–Cl2 2.3362(9), Fe1–P1 2.2433(9), Fe1–P2 2.2463(9), Fe1–N1 1.9935(17), Fe1–C30 1.765(2), Cl1–Fe1–Cl2 173.19(2), Cl1–Fe1–N1 86.83(5), Cl2–Fe1–N1 86.36(5), N1–Fe1–C30 179.54(8), P1–Fe1–P2 167.74(2).

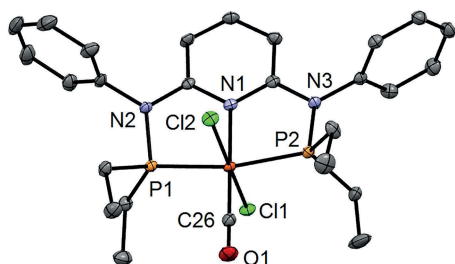


Figure 4. Structural view of *trans*-[Fe(κ^3P,N,P -PNP^{ph}-Et)(CO)Cl₂] (**4f**) showing 50% thermal ellipsoids (H atoms and a second independent complex omitted for clarity). Selected bond lengths [Å] and angles [°]: Fe1–Cl1 2.3156(3), Fe1–Cl2 2.3172(3), Fe1–P1 2.2157(3), Fe1–P2 2.2146(3), Fe1–N1 2.0061(7), Fe1–C26 1.7602(8), Cl1–Fe1–Cl2 175.041(9), Cl1–Fe1–N1 88.73(2), Cl2–Fe1–N1 86.49(2), N1–Fe1–C26 177.45(3), P1–Fe1–P2 167.126(10).

The exposure of solid **3a** and **3b** to 1 bar of gaseous CO at room temperature results in rapid quantitative conversion to solid *cis*-[Fe(κ^3P,N,P -PNP-*i*Pr)(CO)(Cl)₂] (**5a**) and *cis*-[Fe(κ^3P,N,P -PNP-Cy)(CO)Cl₂] (**5b**) as the sole products, as indicated by a color change from light yellow to deep red (Scheme 3). In contrast, the bulky complex **3c** as well as complexes **3d–3g**, which feature NMe, NEt, and NPh linkers between the pyridine ring and the PR₂ moieties, did not react with CO in the solid state. The exclusive formation of **5a** and **5b** in the solid state was confirmed by ¹H and ³¹P{¹H} solution NMR spectroscopy and IR spectroscopy. The recording of solution ¹³C{¹H} NMR spectra was precluded, as the *cis* isomers transform quantitatively within ca. 30 min into the respective *trans* complexes **4a** and **4b** (the mechanism of this process was discussed recently).^[8b]

To rationalize why **3a** (as well as **3b** and **3d–3g**) reacted readily with CO to afford complexes of the type [Fe(κ^3P,N,P -PNP)(CO)Cl₂] but **3c** did not, the addition of CO to **3a** and **3c** was investigated through DFT calculations, and the energy profiles obtained are presented in Figures 5^[18] and 6. The addition of carbon monoxide to these complexes is a “spin-forbidden” or “non-adiabatic” reaction as there is a change in spin state from the reagent to the product. Although **3a** and **3c** have a spin-quintet (*S* = 2) ground state, *trans*-[Fe(κ^3P,N,P -PNP-*i*Pr)(CO)Cl₂] (**4a**) and the elusive *trans*-[Fe(κ^3P,N,P -PNP-*t*Bu)(CO)Cl₂] (**4c**) exist as spin-singlet molecules (*S* = 0). The energy profile associated with such a reaction goes through a minimum-energy crossing point (MECP) of the two potential energy surfaces (PES) involved.^[19] Once that point is reached, there is a given probability for the system to change spin state and

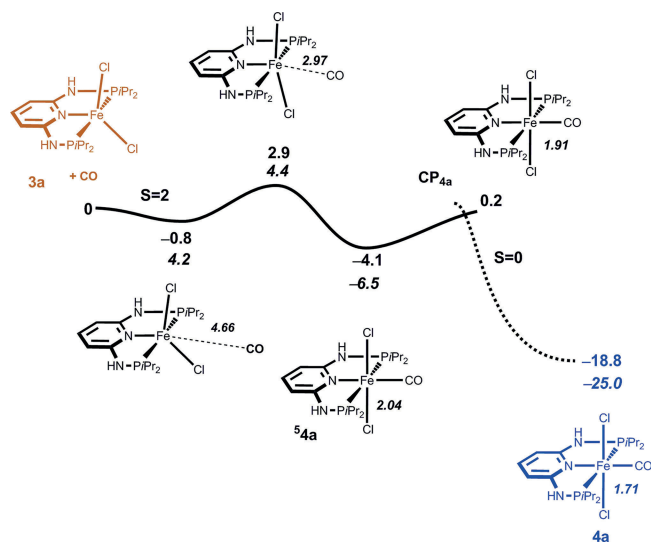


Figure 5. Energy profile (OPBE) for the addition of CO to [Fe(κ^3P,N,P -PNP-*i*Pr)(CO)Cl₂] (**3a**) to yield *trans*-[Fe(κ^3P,N,P -PNP-*i*Pr)(CO)Cl₂] (**4a**). The energy values [kcal/mol] are relative to the separate reagents, and the values in italics represent the free energy corrected for dispersion effects (DFT-D3). The plain curve corresponds to the spin-quintuplet PES (*S* = 2), and the dashed curve corresponds to the spin-singlet PES (*S* = 0). The Fe–C(CO) distance [Å] along the reaction coordinate is indicated.

hop from one PES to the other and, thus, give rise to the “spin-forbidden” reaction.^[20]

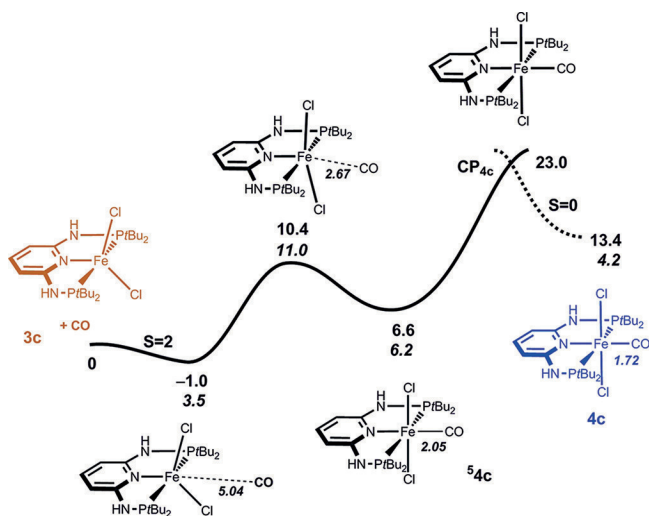


Figure 6. Energy profile (OPBE) for the addition of CO to $[\text{Fe}(\kappa^3P,N,P\text{-PNP-}t\text{Bu})\text{Cl}_2]$ (**3c**) to yield the elusive complex $\text{trans-}[\text{Fe}(\kappa^3P,N,P\text{-PNP-}t\text{Bu})(\text{CO})\text{Cl}_2]$ (**4c**). The energy values [kcal/mol] are relative to the separate reagents, and the values in italics represent the free energy corrected for dispersion effects (DFT-D3). The plain curve corresponds to the spin-quintuplet PES ($S = 2$), and the dashed curve corresponds to the spin-singlet PES ($S = 0$). The Fe–C(CO) distance [\AA] along the reaction coordinate is indicated.

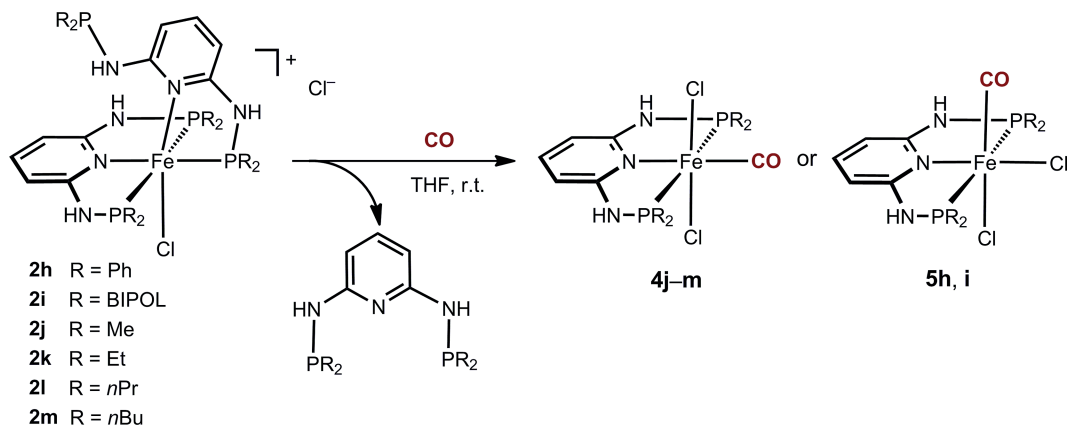
From the separated reactants and following the $S = 2$ PES, a van der Waals pair forms between the two reacting molecules, CO and $[\text{Fe}(\kappa^3P,N,P\text{-PNP-}i\text{Pr})\text{Cl}_2]$ or $[\text{Fe}(\kappa^3P,N,P\text{-PNP-}t\text{Bu})\text{Cl}_2]$, with a rather long Fe–C(CO) distance (4.66 and 5.04 \AA , respectively), and the stabilization of the system is correspondingly small ($\Delta E = -0.8$ and -1.0 kcal/mol, respectively). From here, the high-spin isomers of the products ($^5\mathbf{4a}$ and $^5\mathbf{4c}$) form in a single step over accessible energy barriers ($\Delta E^\ddagger = 3.7$ and 11.4 kcal/mol). Although the formation of $^5\mathbf{4a}$ is exothermic with $\Delta E = -3.3$ kcal/mol, the equivalent step for $^5\mathbf{4c}$ is thermodynamically unfavorable ($\Delta E = 7.6$ kcal/mol); therefore, intermediate $^5\mathbf{4c}$ is less stable than the corresponding pair of reactants. After the formation of the high-spin CO adduct ($^5\mathbf{4a}$ or $^5\mathbf{4c}$), the last step of the mechanism corresponds to a spin change in each case. For the species with the less bulky ligand (PNP-*i*Pr, **1a**), the MECP between the two potential energy surfaces (CP_{4a}) is easily reached and has an associated energy barrier of $\Delta E = 4.3$ kcal mol⁻¹. Once the crossing point CP_{4a} is reached and the hopping between surfaces is accomplished, the system follows the $S = 0$ PES downhill until the final product forms, that is, low-spin ($S = 0$) $\text{trans-}[\text{Fe}(\kappa^3P,N,P\text{-PNP-}i\text{Pr})(\text{CO})\text{Cl}_2]$ (**4a**). The overall process is favorable thermodynamically, as **4a** is 18.8 kcal/mol more stable than the initial reagents. In sharp contrast, in the profile obtained for the species with the bulkier ligand (PNP-*t*Bu, **1c**), the last step is clearly unfavorable and has a high barrier of 16.4 kcal/mol. Moreover, the putative final product **4c** is 13.4 kcal/mol less stable than the initial reagents.

Importantly, the overall balance for the reactions with free-energy values corrected for dispersion effects (values in italics in Figures 5 and 6) indicates that the addition of CO to the PNP-*i*Pr complex, **3a**, is clearly exergonic ($\Delta G = -25.0$ kcal mol⁻¹), whereas the equivalent reaction for the complex with the bulkier ligand (**3c**) is endergonic ($\Delta G = 4.2$ kcal mol⁻¹). This indicates a thermodynamically unfavorable process for the last reaction and is in good accord with the experimental result, as the formation of the CO adduct for the PNP-*t*Bu species was not observed, in contrast to the outcome for the PNP-*i*Pr system.

Reactions with Sterically Less Demanding PNP Ligands

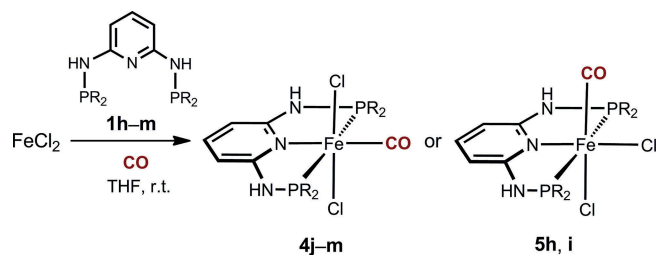
Complexes of the type $[\text{Fe}(\kappa^3P,N,P\text{-PNP})\text{Cl}_2]$ (**3**) with small PNP ligands are not accessible directly from the reaction of FeCl_2 with 1 equiv. of PNP ligand owing the formation of complexes $[\text{Fe}(\kappa^3P,N,P\text{-PNP})(\kappa^2P,N\text{-PNP})\text{Cl}]^+$ (**2**). However, preliminary reactivity studies revealed^[6a] that complexes **2** are substitutionally labile. This was shown for $[\text{Fe}(\kappa^3P,N,P\text{-PNP-Ph})(\kappa^2P,N\text{-PNP-Ph})\text{Cl}]^+$ (**2h**) with the poorly coordinating BF_4^- counterion, which readily adds carbon monoxide to afford the cationic *trans*-dicarbonyl complex $\text{trans-}[\text{Fe}(\kappa^3P,N,P\text{-PNP-Ph})(\text{CO})_2\text{Cl}]^+$ with the liberation of the κ^2P,N -bound PNP ligand. This methodology is used here to obtain Fe PNP carbonyl complexes of the type $[\text{Fe}(\kappa^3P,N,P\text{-PNP})(\text{CO})\text{Cl}_2]$ with small PNP ligands. Accordingly, the treatment of $[\text{Fe}(\kappa^3P,N,P\text{-PNP})(\kappa^2P,N\text{-PNP})\text{Cl}]^+$ (**2h–2m**; in this case as chloride salts) with CO in THF at room temperature resulted in the dissociation of the κ^2P,N -bound PNP ligand and the formation of the carbonyl complexes $\text{trans-}[\text{Fe}(\kappa^3P,N,P\text{-PNP})(\text{CO})\text{Cl}_2]$ (**4j–4m**) and $\text{cis-}[\text{Fe}(\kappa^3P,N,P\text{-PNP})(\text{CO})\text{Cl}_2]$ (**5h** and **5i**) albeit in yields of less than 50%, as shown in Scheme 4. The reaction is complete within several minutes for **2h** and **2i** but requires several hours for **2j–2m**. For **2i** in CH_2Cl_2 , it has to be noted that the *trans* isomer (**4i**) is formed selectively.

High yields of **4** and **5** could be achieved by reacting anhydrous FeCl_2 with 1 equiv. of the respective PNP ligand (**1h–1m**) under a CO atmosphere in THF or CH_2Cl_2 at room temperature (Scheme 5). Complexes **4** and **5** were characterized through a combination of ^1H , $^{13}\text{C}\{^1\text{H}\}$, and $^{31}\text{P}\{^1\text{H}\}$ NMR spectroscopy; IR spectroscopy; and elemental analysis. In addition to the spectroscopic characterization, the solid-state structures of **4j**, **4k**, **4l**, and **5h** were determined by single-crystal X-ray diffraction. ORTEP diagrams are depicted in Figures 7, 8, 9, and 10, and selected bond lengths and angles are given in the captions. The iron centers in all $\text{trans-}[\text{Fe}(\kappa^3P,N,P\text{-PNP})(\text{CO})\text{Cl}_2]$ complexes **4b**, **4j**, **4k**, **4l**, and **4f** have modestly distorted octahedral coordination geometries. The mean bond lengths and angles of these five complexes with their estimated standard deviations (esd's) are Fe–C 1.763(2) \AA , Fe–N 2.003(5) \AA , Fe–P 2.228(10) \AA , Fe–Cl 2.319(8) \AA , P–Fe–P 167.0(5) $^\circ$, and N–Fe–Cl 87.8(10) $^\circ$. These values are in good accord with those of the two previously reported complexes of this



Scheme 4.

type.^[7,8a] The coordination geometry of the iron center in *cis*-[Fe(κ^3P,N,P -PNP-Ph)(CO)Cl₂] (**4h**) is also octahedral, and the bond lengths are similar to those of the *trans* complexes. In the *cis* complex, a modest *trans* effect of the CO group on the Fe–Cl₂ bond can be noted (Fe–Cl₂ 2.346 Å compared with Fe–Cl₁ 2.317 Å). In compensation for this, the Fe–N bond in **4h** is slightly shorter (Fe–N 1.980 Å) than those in the *trans* complexes.



Scheme 5.

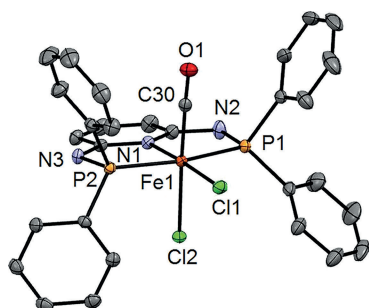


Figure 7. Structural view of *cis*-[Fe(κ^3P,N,P -PNP-Ph)(CO)Cl₂]·3DMSO (**5h**·3DMSO) showing 50% thermal ellipsoids (H atoms and solvent molecules omitted for clarity). Selected bond lengths [Å] and angles [°]: Fe1–Cl1 2.3173(4), Fe1–Cl2 2.3461(4), Fe1–P1 2.2248(4), Fe1–P2 2.2279(4), Fe1–N1 1.9798(11), Fe1–C30 1.7569(14), C30–Fe1–Cl1 85.89(4), C30–Fe1–Cl2 177.79(4), N1–Fe1–Cl1 176.80(4), N1–Fe1–Cl2 84.60(3), Cl1–Fe1–Cl2 92.287(13), P1–Fe1–P2 167.215(15).

In the ¹³C{¹H} NMR spectra, the CO ligands exhibit a single low-intensity triplet resonance in the range δ = 216–224 ppm. The IR spectra of the complexes bearing alkyl substituents show one strong band in the range $\tilde{\nu}$ = 1937–

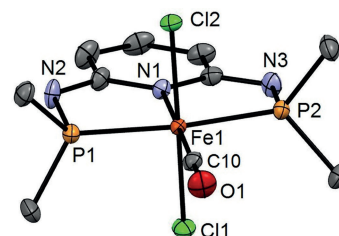


Figure 8. Structural view of *trans*-[Fe(κ^3P,N,P -PNP-Me)(CO)Cl₂]·Et₂O (**4j**·Et₂O) showing 50% thermal ellipsoids (H atoms and solvent molecules omitted for clarity). Selected bond lengths [Å] and angles [°]: Fe1–Cl1 2.3190(10), Fe1–Cl2 2.3179(10), Fe1–P1 2.2233(11), Fe1–P2 2.2241(10), Fe1–N1 2.004(3), Fe1–C10 1.762(4), Cl1–Fe1–Cl2 176.47(4), C10–Fe1–N1 178.84(16), N1–Fe1–Cl1 87.94(9), N1–Fe1–Cl2 88.53(9), P1–Fe1–P2 166.76(4).

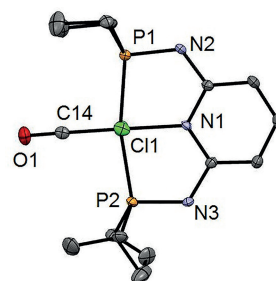


Figure 9. Structural view of *trans*-[Fe(κ^3P,N,P -PNP-Et)(CO)Cl₂] (**4k**) showing 50% thermal ellipsoids (H atoms omitted for clarity). Selected bond lengths [Å] and angles [°]: Fe1–Cl1 2.3179(8), Fe1–Cl2 2.3178(8), Fe1–P1 2.2273(8), Fe1–P2 2.2284(8), Fe1–N1 2.0068(19), Fe1–C14 1.762(3), Cl1–Fe1–Cl2 177.88(3), Cl1–Fe1–N1 89.68(6), Cl2–Fe1–N1 88.22(6), P1–Fe1–P2 166.80(3), N1–Fe1–C14 179.08(11).

1965 cm^{−1}, whereas those with aryl substituents exhibit the CO stretching frequency at $\tilde{\nu}$ = 1985–2001 cm^{−1}; this significant shift to lower wavenumbers indicates that the latter are much weaker donors (cf. $\tilde{\nu}$ = 2143 cm^{−1} for free CO).

In all of the complexes featuring NH linkers, CO binding is fully reversible, and heating solid samples of **4j–4m** or **5h** at 60–150 °C for ca. 40 min under vacuum leads to the complete regeneration of **3h** and **3j–3m**, which react again with CO in the solid state to give **4j–4m** or **5h**. The BIPOL

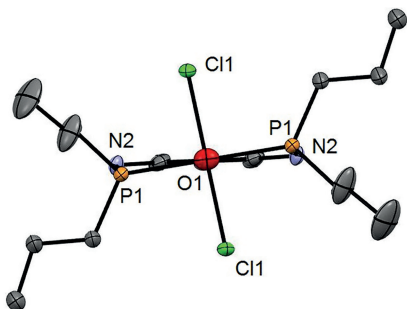


Figure 10. Structural view of *trans*-[Fe(κ^3P,N,P -PNP-*n*Pr)(CO)Cl₂] (**4i**) showing 50% thermal ellipsoids (H atoms omitted for clarity). Selected bond lengths [Å] and angles [°]: Fe1–Cl1 2.3241(4), Fe1–P1 2.2272(4), Fe1–N1 2.0015(17), Fe1–C10 1.765(2), Cl1–Fe1–Cl1 175.040(17), P1–Fe1–P1 166.408(18), Cl1–Fe1–N1 87.520(11), Cl1–Fe1–N1 87.520(11), N1–Fe1–C10 180.0(5).

complexes **4i** and **5i** are exceptions and decompose at elevated temperatures with CO release to form intractable materials. Qualitatively, CO is most easily liberated from the

complexes with bulky substituents such as [Fe(κ^3P,N,P -PNP-Cy)(CO)Cl₂] (**4b**), which requires ca. 60 °C, whereas those with small substituents such as [Fe(κ^3P,N,P -PNP-Me)(CO)Cl₂] (**4j**) require up to 200 °C. The reversibility of this reaction in the solid state has been elucidated by time-resolved infrared spectroscopy, through which the stretching vibration of the coordinated CO ligand in **4** and **5** was monitored. This “on” and “off” process can be repeated for at least four cycles without any noticeable decomposition, as shown in Figure 11 for **3h** and **5h**. In contrast to **3a–3g**, complexes **3h** and **3j–3m** bearing small PNP ligands are very air-sensitive in the solid state. In solution, they rapidly rearrange to form **2h** and **2j–2m** together with intractable materials (Scheme 6). The formation of **3h** and **3j–3m** was confirmed by their reaction with CO and the reformation of the respective complexes **4** and **5**. In addition, the solid-state magnetic moments μ_{eff} were exemplarily determined for **3h** and **3j** to be 5.3 and 5.2 μ_{B} , respectively, which are consistent with the expected d⁶ high-spin configuration (four unpaired electrons).

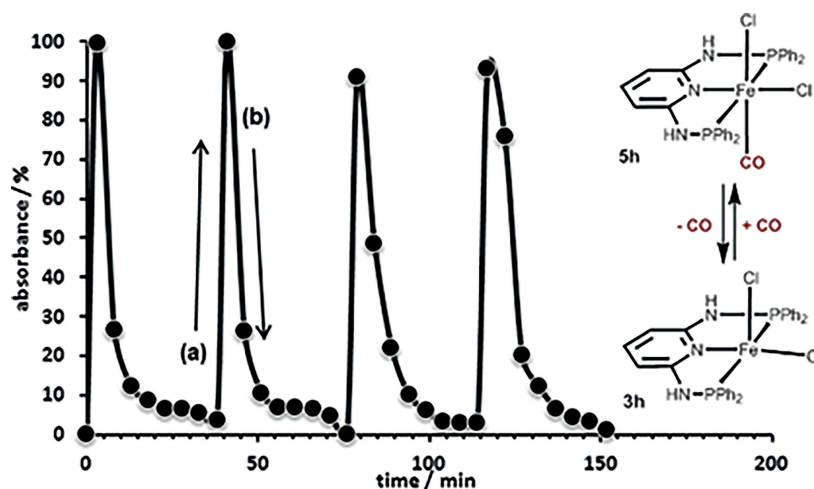
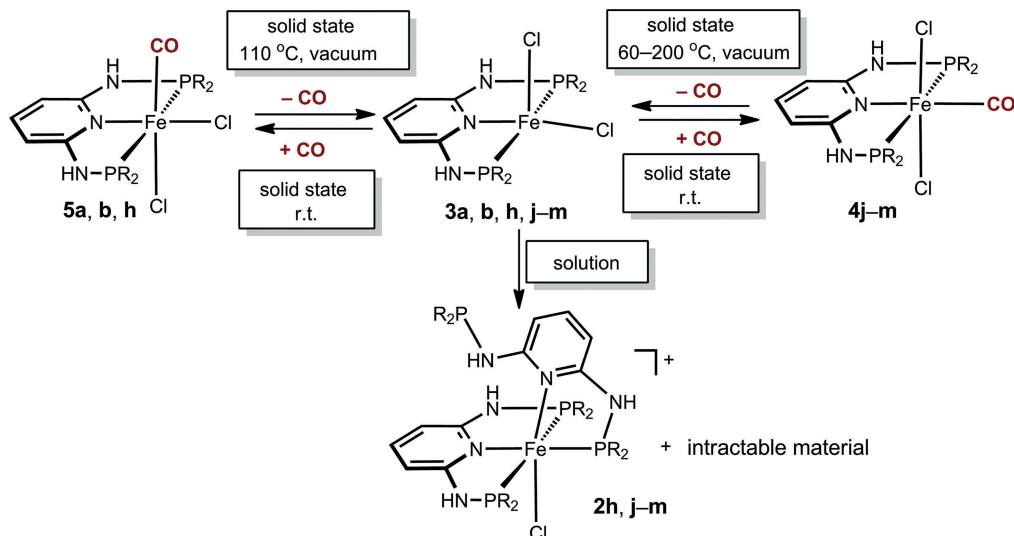
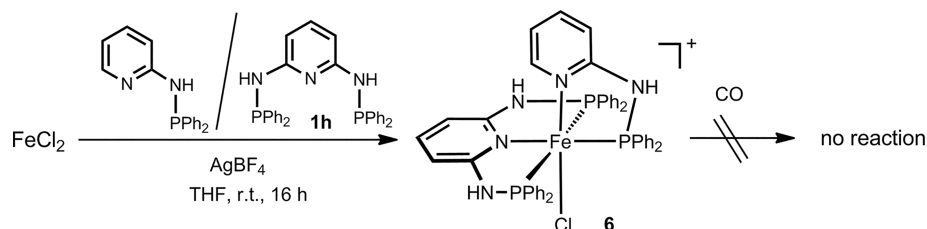


Figure 11. Time-dependent (a) increase of the ν_{CO} stretching frequency of **5h** at $\tilde{\nu} = 1985 \text{ cm}^{-1}$ upon exposure of **3h** to pure CO at 25 °C and ambient pressure and (b) decrease of this absorption band as the temperature increases from 25 to 110 °C under vacuum.



Scheme 6.



Scheme 7.

For structural and reactivity comparisons, we also prepared the related complex $[\text{Fe}(\kappa^3P,N,P\text{-PNP-Ph})(\kappa^2P,N\text{-PN-Ph})\text{Cl}]\text{BF}_4$ (**6**) by reacting anhydrous FeCl_2 with 1 equiv. of **1h** and PN-Ph in the presence of 1 equiv. of AgBF_4 (Scheme 7). The pyridine moiety of the PN-Ph ligand in this compound lacks a substituent at the second *ortho* position, and it does not react with CO even after 48 h. This complex was characterized through a combination of ^1H and $^{31}\text{P}\{^1\text{H}\}$ NMR spectroscopy and elemental analysis. Although the ^1H and $^{13}\text{C}\{^1\text{H}\}$ NMR spectra were not very informative, the $^{31}\text{P}\{^1\text{H}\}$ NMR spectra revealed a characteristic A_2B pattern^[21] of multiplets centered at $\delta_A = 112.5$ ppm and $\delta_B = 111.9$ ppm with a $J_{P,P}$ coupling constant of 50 Hz, which can be assigned to the two phosphorus atoms of the κ^3 -bound PNP ligand and the phosphorus atom of κ^2 -bound PN ligand, respectively. The solid-state structure of **6** determined by single-crystal X-ray diffraction is depicted in Figure 12, and selected bond lengths given in the caption. The coordination geometry around the iron center of **6** corresponds to a slightly distorted octahedron with N1-Fe1-P3 , Cl1-Fe1-N4 , and P1-Fe1-P2 angles of 178.1, 178.8, and 164.0°, respectively. The first two angles are significantly different to those of the related complexes $[\text{Fe}(\kappa^3P,N,P\text{-PNP})(\kappa^2P,N\text{-PNP})\text{Cl}]^+$ (**2h** and **2k**), which are on average 171.1 and 171.8°, as the NH group of the dangling arm of the κ^2 -bound PNP ligand is directed to the pyridine nitrogen atom to form an intramolecular hydrogen interaction. This causes the pyridine ring

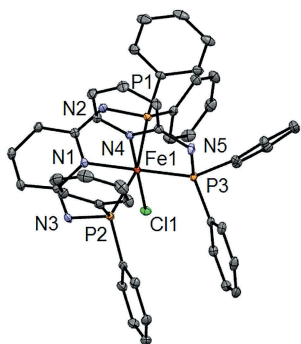


Figure 12. Structural view of $[\text{Fe}(\kappa^3P,N,P\text{-PNP-Ph})(\kappa^2P,N\text{-PN-Ph})\text{Cl}]\text{BF}_4 \cdot 2\text{THF}$ (**6**·2THF) showing 50% thermal ellipsoids (H atoms, BF_4^- anion, and solvent molecules omitted for clarity). Selected bond lengths [Å] and angles [°]: Fe1-Cl1 2.3333(4), Fe1-P1 2.2787(4), Fe1-P2 2.2534(4), Fe1-P3 2.1864(4), Fe1-N1 2.0170(11), Fe1-N4 1.9932(11), Cl1-Fe1-P3 , 94.737(13), Cl1-Fe1-N1 86.95(3), Cl1-Fe1-N4 178.83(3), P1-Fe1-P2 163.996(15), P1-Fe1-P3 97.932(14), N1-Fe1-N4 93.51(4).

of N1 to be bent away from N6 so that the angle C3-N1-Fe is ca. 170°, whereas this angle is very close to 180° (179.8°) in **6**. Accordingly, this distortion may be responsible for the lability of the κ^2 -bound PNP ligand in complexes **2**.

Conclusions

We have prepared *trans*- and *cis*- $[\text{Fe}(\kappa^3P,N,P\text{-PNP})(\text{CO})\text{Cl}_2]$ complexes bearing both sterically demanding and small PNP ligands based on the 2,6-diaminopyridine scaffold in which the aromatic pyridine ring and the phosphine PR_2 moieties are connected through NH, *N*-alkyl, or *N*-aryl linkers. For bulky PNP ligands, with the exception of complexes with *PtBu*₂ units, these complexes are obtained upon the treatment of $[\text{Fe}(\kappa^3P,N,P\text{-PNP})\text{Cl}_2]$ with CO in THF or CH_2Cl_2 solutions. On the other hand, with small PNP ligands, such complexes are not directly accessible owing to the formation of $[\text{Fe}(\kappa^3P,N,P\text{-PNP})(\kappa^2P,N\text{-PNP})\text{Cl}]\text{Cl}$. These complexes are substitutionally labile and liberate the κ^2 -*P,N*-bound PNP ligand in the presence of CO to yield the desired complexes $[\text{Fe}(\kappa^3P,N,P\text{-PNP})(\text{CO})\text{Cl}_2]$ in yields of less than 50%. High yields of $[\text{Fe}(\kappa^3P,N,P\text{-PNP})(\text{CO})\text{Cl}_2]$ could be achieved by reacting anhydrous FeCl_2 with 1 equiv. of the respective PNP ligand under a CO atmosphere. For structural and reactivity comparisons, we also prepared the related complex $[\text{Fe}(\kappa^3P,N,P\text{-PNP-Ph})(\kappa^2P,N\text{-PN-Ph})\text{Cl}]^+$, in which the pyridine moiety of the PN-Ph ligand lacks a substituent at the second *ortho* position. This complex does not react with CO. In the solid state, complexes $[\text{Fe}(\kappa^3P,N,P\text{-PNP})\text{Cl}_2]$ with NH linkers are also converted quantitatively into *trans*- or *cis*- $[\text{Fe}(\kappa^3P,N,P\text{-PNP})(\text{CO})(\text{Cl})_2]$ upon treatment with CO, as indicated by a color change of the material and by IR spectroscopy monitoring. On the other hand, all complexes with NMe, NEt, and NPh linkers did not react with CO. Finally, to rationalize why most $[\text{Fe}(\kappa^3P,N,P\text{-PNP})\text{Cl}_2]$ complexes react readily with CO but those with *tBu* substituents do not, the additions of CO to $[\text{Fe}(\kappa^3P,N,P\text{-PNP-}i\text{Pr})\text{Cl}_2]$ and $[\text{Fe}(\kappa^3P,N,P\text{-PNP-}t\text{Bu})\text{Cl}_2]$ was investigated by DFT calculations, which revealed a thermodynamically unfavorable process for the latter reaction.

Experimental Section

General: All manipulations were performed under an inert atmosphere of argon by using Schlenk techniques or in an MBraun in-

ert-gas glovebox. The solvents were purified according to standard procedures.^[22] The deuterated solvents were purchased from Aldrich and dried with molecular sieves (4 Å). The ligand *N*-diphenylphosphino-2-aminopyridine (PN-Ph),^[23] all PNP ligands (**1a**, **1c–1m**), and complexes [Fe(κ^3P,N,P -PNP-Ph)(κ^2P,N -PNP-Ph)Cl]Cl (**2h**), [Fe(κ^3P,N,P -PNP-BIPOL)(κ^2P,N -PNP-BIPOL)Cl]Cl (**2i**), [Fe(κ^3P,N,P -PNP-Me)(κ^2P,N -PNP-Me)Cl]Cl (**2j**), [Fe(κ^3P,N,P -PNP-Et)(κ^2P,N -PNP-Et)Cl]Cl (**2k**), [Fe(κ^3P,N,P -PNP-*n*Pr)(κ^2P,N -PNP-*n*Pr)Cl]Cl (**2l**), and [Fe(κ^3P,N,P -PNP-*n*Bu)(κ^2P,N -PNP-*n*Bu)Cl]Cl (**2m**) were prepared according to the literature procedures.^[18a,8b]

The ^1H , $^{13}\text{C}\{^1\text{H}\}$, and $^{31}\text{P}\{^1\text{H}\}$ NMR spectra were recorded with Bruker AVANCE-250, AVANCE-300 DPX, and AVANCE-400 spectrometers. The ^1H and $^{13}\text{C}\{^1\text{H}\}$ NMR spectra were referenced internally to residual protio solvent and solvent resonances, respectively, and are reported relative to tetramethylsilane ($\delta = 0$ ppm). The $^{31}\text{P}\{^1\text{H}\}$ NMR spectra were referenced externally to H_3PO_4 (85%; $\delta = 0$ ppm). Microanalysis was performed by Microanalytical Laboratories, University of Vienna.

The room-temperature solution magnetic moments were determined by ^1H NMR spectroscopy by the Evans method.^[24] The solid-state magnetic susceptibility measurements were performed with a Johnson Matthey MSB Auto1 magnetic balance, which was calibrated with the standard complex [HgCo(SCN)₄]. From the measured volume susceptibilities χ_V and the sample densities, the mass susceptibilities χ_g and effective magnetic moments μ_{eff} were obtained.

***N,N'*-Bis(dicyclohexyl)-2,6-diaminopyridine (PNP-Cy, 1b)**: To a suspension of 2,6-diaminopyridine (390 mg, 3.6 mmol) in toluene (10 mL), NEt_3 (2.0 mL, 14.4 mmol) was added. A solution of PCy_2Cl (1.68 g, 7.2 mmol) in toluene (10 mL) was added slowly with a dropping funnel. The mixture was then stirred at 70 °C for 48 h. After that, the solution was filtered through Celite. The solid was washed with toluene (10 mL), and the combined solution was evaporated to dryness. The crude product was recrystallized from toluene/*n*-hexane at –20 °C, yield 1.80 g (99%). $\text{C}_{29}\text{H}_{49}\text{N}_3\text{P}_2$ (501.68): calcd. C 69.43, H 9.85, N 8.38; found C 69.35, H 9.78, N 8.44. ^1H NMR (CDCl_3 , 20 °C): $\delta = 7.20$ (t, $J_{\text{H,H}} = 8.2$ Hz, 1 H, py), 6.37 (d, $J_{\text{H,H}} = 6.5$ Hz, 2 H, py), 4.40 (br. s, 2 H, NH), 1.72–1.64 (18 H, Cy), 1.53–1.42 (m, 8 H, Cy), 1.19 (18 H, Cy) ppm. $^{13}\text{C}\{^1\text{H}\}$ NMR (CDCl_3 , 20 °C): $\delta = 159.3$ (py), 139.4 (p), 97.9 (d, $J_{\text{C,P}} = 19.3$ Hz, py), 36.0 (d, $J_{\text{C,P}} = 11.3$ Hz, CH), 28.8 (d, $J_{\text{C,P}} = 17.6$ Hz, CH_2), 27.2 (CH_2), 27.0 (d, $J_{\text{C,P}} = 3.6$ Hz, CH_2), 26.8 (CH_2), 26.7 (CH_2), 26.3 (CH_2) ppm. $^{31}\text{P}\{^1\text{H}\}$ NMR (CDCl_3 , 20 °C): $\delta = 41.6$ ppm.

[Fe(κ^3P,N,P -PNP-Cy)Cl₂] (3b): PNP-Cy (**1b**) (200 mg, 0.40 mmol) and anhydrous FeCl_2 (50 mg, 0.40 mmol) were stirred in THF (10 mL) for 1 h. The yellow suspension was evaporated to dryness, and the solid was washed with *n*-hexane (15 mL). The yellow powder was dried under reduced pressure, yield 240 mg (96%). $\text{C}_{29}\text{H}_{49}\text{Cl}_2\text{FeN}_3\text{P}_2$ (628.42): calcd. C 55.43, H 7.86, N 6.69; found C 55.35, H 7.78, N 6.71. $\mu_{\text{eff}} = 4.8(1) \mu_{\text{B}}$.

[Fe(κ^3P,N,P -PNP^{Me}-iPr)Cl₂] (3d): A suspension of anhydrous FeCl_2 (120 mg, 0.95 mmol) and PNP^{Me}-iPr (**1d**; 350 mg, 0.95 mmol) in THF (15 mL) was stirred at room temperature for 12 h. The solvent was then removed under vacuum, and the remaining solid was redissolved in CH_2Cl_2 (15 mL). The insoluble materials were removed by filtration. The volume of the solution was reduced to ca. 0.5 mL, and the product was precipitated by the addition of *n*-pentane (40 mL). After filtration, the yellow product was washed twice with *n*-pentane (10 mL) and dried under vacuum, yield 360 mg (77%). $\text{C}_{19}\text{H}_{37}\text{Cl}_2\text{FeN}_3\text{P}_2$ (496.22): calcd. C 45.99, H

7.52, N 8.47; found C 46.11, H 7.48, N 8.39. ^1H NMR (CD_2Cl_2 , 20 °C): $\delta = 183.51$ [br s, 4 H, $\text{CH}(\text{CH}_3)_2$], 68.66 (s, 2 H, $\text{py}^{3,5}$), 24.79 (s, 6 H, NCH_3), 9.44 [br s, 12 H, $\text{CH}(\text{CH}_3)_2$], 3.00 [br s, 12 H, $\text{CH}(\text{CH}_3)_2$], –17.37 (s, 1 H, py^4) ppm.

[Fe(κ^3P,N,P -PNP^{Et}-iPr)Cl₂] (3e): This complex was prepared analogously to **3d** with FeCl_2 (112 mg, 0.88 mmol) and PNP^{Et}-iPr (**1e**; 350 mg, 0.88 mmol) as starting materials, yield 346 mg (75%). $\text{C}_{21}\text{H}_{41}\text{Cl}_2\text{FeN}_3\text{P}_2$ (524.27): calcd. C 48.11, H 7.88, N 8.02; found C 48.00, H 7.93, N 7.96. ^1H NMR (CD_2Cl_2 , 20 °C): $\delta = 192.61$ [br s, 4 H, $\text{CH}(\text{CH}_3)_2$], 72.45 (s, 2 H, $\text{py}^{3,5}$), 37.54 (s, 4 H, NCH_2CH_3), 5.89 [br s, 12 H, $\text{CH}(\text{CH}_3)_2$], 3.88 [br s, 12 H, $\text{CH}(\text{CH}_3)_2$], 2.17 (br s, 6 H, NCH_2CH_3), –19.67 (s, 1 H, py^4) ppm.

[Fe(κ^3P,N,P -PNP^{Ph}-Et)Cl₂] (3f): This compound was prepared analogously to **3b** with PNP^{Ph}-Et (**1f**; 197 mg, 0.45 mmol) and anhydrous FeCl_2 (57 mg, 0.45 mmol) as starting materials, yield 246 mg (97%). $\text{C}_{25}\text{H}_{33}\text{Cl}_2\text{FeN}_3\text{P}_2$ (564.25): calcd. C 53.22, H 5.90, N 7.45; found C 53.15, H 5.98, N 7.51. $\mu_{\text{eff}} = 5.0(1) \mu_{\text{B}}$.

[Fe(κ^3P,N,P -PNP^{Ph}-*n*Pr)Cl₂] (3g): This compound was prepared analogously to **3b** from PNP^{Ph}-*n*Pr (**1g**; 222 mg, 0.45 mmol) and anhydrous FeCl_2 (57 mg, 0.45 mmol), yield 265 mg (95%). $\text{C}_{29}\text{H}_{41}\text{Cl}_2\text{FeN}_3\text{P}_2$ (620.36): calcd. C 56.15, H 6.66, N 6.77; found C 56.22, H 6.72, N 6.84. $\mu_{\text{eff}} = 5.0(1) \mu_{\text{B}}$.

***trans*-[Fe(κ^3P,N,P -PNP-Cy)(CO)Cl₂] (4b)**: Carbon monoxide was bubbled into a solution of anhydrous FeCl_2 (63 mg, 0.50 mmol) and PNP-Cy (**1b**) (250 mg, 0.50 mmol) in THF (10 mL) for ca. 5 min, whereupon the reaction mixture turned from yellow to violet, and the mixture was stirred for 1 h. After the removal of the solvent under reduced pressure, the remaining solid was washed twice with *n*-hexane (10 mL) and dried under vacuum, yield 307 mg (94%). $\text{C}_{30}\text{H}_{49}\text{Cl}_2\text{FeN}_3\text{OP}_2$ (656.43): calcd. C 54.89, H 7.52, N 6.40; found C 54.93, H 7.69, N 6.26. ^1H NMR ($[\text{D}_6]\text{DMSO}$, 20 °C): $\delta = 8.35$ (s, 2 H, NH), 7.38 (t, $^3J_{\text{H,H}} = 7.6$ Hz, 1 H, py^4), 6.42 (d, $^3J_{\text{H,H}} = 7.7$ Hz, 2 H, $\text{py}^{3,5}$), 3.32 (m, 4 H, CH), 2.16 (d, $J_{\text{H,H}} = 10.9$ Hz, 4 H, CH_2), 2.05 (d, $J_{\text{H,H}} = 9.0$ Hz, 4 H, CH_2), 1.93–1.42 (m, 18 H, CH_2), 1.25–1.04 (m, 14 H, CH_2) ppm. $^{13}\text{C}\{^1\text{H}\}$ NMR ($[\text{D}_6]\text{DMSO}$, 20 °C): $\delta = 223.9$ (t, $^2J_{\text{C,P}} = 21.2$ Hz, CO), 162.9 (vt, $^2J_{\text{C,P}} = 9.4$ Hz, $\text{py}^{2,6}$), 139.6 (py^4), 98.6 ($\text{py}^{3,5}$), 36.4 (vt, $^1J_{\text{C,P}} = 11.2$ Hz, CH), 28.3 (CH_2), 27.8–24.7 (m, CH_2), 18.4 (CH_2), 17.1 (CH_2), 12.7 (CH_2) ppm. $^{31}\text{P}\{^1\text{H}\}$ NMR ($[\text{D}_6]\text{DMSO}$, 20 °C): $\delta = 113.5$ ppm. IR [attenuated total reflectance (ATR)]: $\tilde{\nu} = 1952$ (ν_{CO}) cm^{-1} .

***cis*-[Fe(κ^3P,N,P -PNP-Cy)(CO)Cl₂] (5b)**: Carbon monoxide was passed over **3b** (100 mg, 0.160 mmol) for ca. 15 min, whereupon the solid changed from yellow to red, yield 104 mg (quantitative). $\text{C}_{30}\text{H}_{49}\text{Cl}_2\text{FeN}_3\text{OP}_2$ (656.43): calcd. C 54.89, H 7.52, N 6.40; found C 54.98, H 7.59, N 6.30. ^1H NMR ($[\text{D}_6]\text{DMSO}$, 20 °C): $\delta = 8.12$ (s, 2 H, NH), 7.01 (t, $^3J_{\text{H,H}} = 8.4$ Hz, 1 H, py^4), 5.95 (d, $^3J_{\text{H,H}} = 7.8$ Hz, 2 H, $\text{py}^{3,5}$), 3.55 (m, 4 H, CH), 2.16 (d, $J_{\text{H,H}} = 10.9$ Hz, 4 H, CH_2), 2.05 (d, $J_{\text{H,H}} = 9.0$ Hz, 4 H, CH_2), 1.93–1.42 (m, 18 H, CH_2), 1.25–1.04 (m, 14 H, CH_2) ppm. $^{31}\text{P}\{^1\text{H}\}$ NMR ($[\text{D}_6]\text{DMSO}$, 20 °C): $\delta = 96.2$ ppm. IR (ATR): $\tilde{\nu} = 1946$ (ν_{CO}) cm^{-1} .

***cis/trans*-[Fe(κ^3P,N,P -PNP^{Me}-iPr)(CO)Cl₂] (4d, 5d)**: CO was bubbled through a solution of **3d** (250 mg, 0.50 mmol) in CH_2Cl_2 (15 mL) for 5 min. An immediate color change from yellow to dark red was observed. The volume of the solvent was reduced to ca. 0.5 mL, and the product was precipitated by the addition of *n*-pentane (40 mL). The red product was collected by filtration, washed twice with *n*-pentane (10 mL), and dried under vacuum. A 28:72 mixture of the *cis/trans* isomers **4d/5d** was obtained, yield 226 mg (86%). $\text{C}_{20}\text{H}_{37}\text{Cl}_2\text{FeN}_3\text{OP}_2$ (524.23): calcd. C 45.82, H 7.11, N 8.02; found C 45.65, H 7.18, N 7.93.

trans-[Fe(κ^3P,N,P -PNP^{Me}-iPr)(CO)Cl₂]: ¹H NMR (CD₂Cl₂, 20 °C): δ = 7.66 (t, ³J_{H,H} = 8.3 Hz, 1 H, py⁴), 6.33 (d, ³J_{H,H} = 8.3 Hz, 2 H, py^{3,5}), 3.24 (vt, ³J_{P,H} = 1.6 Hz, 6 H, NCH₃), 2.87 [m, 4 H, CH(CH₃)₂], 1.56 [dd, ²J_{P,H} = 15.8, ³J_{H,H} = 7.1 Hz, 12 H, CH(CH₃)₂], 1.25 [dd, ²J_{P,H} = 14.3, ³J_{H,H} = 7.2 Hz, 12 H, CH(CH₃)₂] ppm. ¹³C{¹H} NMR (CD₂Cl₂, 20 °C): δ = 223.9 (t, ²J_{C,P} = 22.1 Hz, CO), 163.9 (vt, ²J_{C,P} = 10.4 Hz, py^{2,6}), 140.0 (py⁴), 98.5 (vt, ³J_{C,P} = 3.4 Hz, py^{3,5}), 36.8 (vt, ²J_{C,P} = 2.5 Hz, NCH₃), 29.9 [vt, ¹J_{C,P} = 10.5 Hz, CH(CH₃)₂], 21.0 [CH(CH₃)₂], 19.1 [vt, ²J_{C,P} = 2.4 Hz, CH(CH₃)₂] ppm. ³¹P{¹H} NMR (CD₂Cl₂, 20 °C): δ = 143.7 ppm. IR (ATR): $\tilde{\nu}$ = 1960 (ν_{C=O}) cm⁻¹.

cis-[Fe(κ^3P,N,P -PNP^{Me}-iPr)(CO)Cl₂]: ¹H NMR (CD₂Cl₂, 20 °C): δ = 7.26 (t, ³J_{H,H} = 8.2 Hz, 1 H, py⁴), 5.84 (d, ³J_{H,H} = 8.3 Hz, 2 H, py^{3,5}), 3.48 [m, 2 H, CH(CH₃)₂], 3.01 (vt, ³J_{P,H} = 1.6 Hz, 6 H, NCH₃), 2.87 [m, 2 H, CH(CH₃)₂], 1.60–1.46 [m, 18 H, CH(CH₃)₂], 1.35 [dd, ²J_{P,H} = 13.7, ³J_{H,H} = 7.1 Hz, 6 H, CH(CH₃)₂] ppm. ¹³C{¹H} NMR (CD₂Cl₂, 20 °C): δ = 220.3 (t, ²J_{C,P} = 28.9 Hz, CO), 163.9 (vt, ²J_{C,P} = 8.6 Hz, py^{2,6}), 138.9 (py⁴), 97.6 (vt, ³J_{C,P} = 2.9 Hz, py^{3,5}), 36.0 (vt, ²J_{C,P} = 2.3 Hz, NCH₃), 31.5 [vt, ¹J_{C,P} = 8.6 Hz, CH(CH₃)₂], 29.0 [vt, ¹J_{C,P} = 9.7 Hz, CH(CH₃)₂], 19.8 [CH(CH₃)₂], 18.7 [CH(CH₃)₂], 18.1 [vt, ²J_{C,P} = 4.1 Hz, CH(CH₃)₂] ppm. ³¹P{¹H} NMR (CD₂Cl₂, 20 °C): δ = 128.2 ppm. IR (ATR): $\tilde{\nu}$ = 1937 (ν_{C=O}) cm⁻¹.

trans/cis-[Fe(κ^3P,N,P -PNP^{Et}-iPr)(CO)Cl₂] (4e, 5e): This complex was prepared analogously to **4d** with **3e** (250 mg, 0.48 mmol) as the starting material. A 13:87 mixture of the *cis/trans* isomers **4e** and **5e** was obtained, yield 230 mg (87%). C₂₂H₄₁Cl₂FeN₃O₂ (552.28): calcd. C 47.85, H 7.48, N 7.61; found C 47.79, H 7.51, N 7.68.

trans-[Fe(κ^3P,N,P -PNP^{Et}-iPr)(CO)Cl₂]: ¹H NMR (CD₂Cl₂, 20 °C): δ = 7.70 (t, ³J_{H,H} = 8.3 Hz, 1 H, py⁴), 6.42 (d, ³J_{H,H} = 8.3 Hz, 2 H, py^{3,5}), 3.80 (m, 4 H, NCH₂CH₃), 2.99 [m, 4 H, CH(CH₃)₂], 1.60 [dd, ³J_{P,H} = 14.5, ³J_{H,H} = 7.1 Hz, 12 H, CH(CH₃)₂], 1.45 [dd, ³J_{P,H} = 15.8, ³J_{H,H} = 7.4 Hz, 12 H, CH(CH₃)₂], 1.35 (t, ³J_{H,H} = 7.0 Hz, 6 H, NCH₂CH₃) ppm. ¹³C{¹H} NMR (CD₂Cl₂, 20 °C): δ = 224.1 (t, ²J_{C,P} = 22.5 Hz, CO), 163.0 (vt, ²J_{C,P} = 10.3 Hz, py^{2,6}), 139.6 (py⁴), 98.7 (vt, ³J_{C,P} = 3.5 Hz, py^{3,5}), 42.5 (vt, ²J_{C,P} = 2.5 Hz, NCH₂CH₃), 27.1 [vt, ¹J_{C,P} = 10.3 Hz, CH(CH₃)₂], 21.5 [CH(CH₃)₂], 18.4 [CH(CH₃)₂], 13.2 (NCH₂CH₃) ppm. ³¹P{¹H} NMR (CD₂Cl₂, 20 °C): δ = 142.8 ppm. IR (ATR): $\tilde{\nu}$ = 1950 (ν_{C=O}) cm⁻¹.

cis-[Fe(κ^3P,N,P -PNP^{Et}-iPr)(CO)Cl₂]: ¹H NMR (CD₂Cl₂, 20 °C): δ = 7.31 (t, ³J_{H,H} = 8.3 Hz, 1 H, py⁴), 5.93 (d, ³J_{H,H} = 8.3 Hz, 2 H, py^{3,5}), 3.84–3.75 [m, 6 H, NCH₂CH₃, CH(CH₃)₂], 3.16 [m, 2 H, CH(CH₃)₂], 1.60 [dd, ³J_{P,H} = 14.5, ³J_{H,H} = 7.1 Hz, 12 H, CH(CH₃)₂], 1.45 [dd, ³J_{P,H} = 15.8, ³J_{H,H} = 7.4 Hz, 12 H, CH(CH₃)₂], 1.31 (t, ³J_{H,H} = 7.0 Hz, 6 H, NCH₂CH₃) ppm. ¹³C{¹H} NMR (CD₂Cl₂, 20 °C): δ = 224.1 (t, ²J_{C,P} = 22.5 Hz, CO), 163.0 (vt, ²J_{C,P} = 10.3 Hz, py^{2,6}), 138.4 (s, py⁴), 98.0 (vt, ³J_{C,P} = 3.0 Hz, py^{3,5}), 42.0 (vt, ²J_{C,P} = 2.4 Hz, NCH₂CH₃), 30.2 [vt, ¹J_{C,P} = 8.7 Hz, CH(CH₃)₂], 27.8 [vt, ¹J_{C,P} = 9.5 Hz, CH(CH₃)₂], 21.9 [vt, ²J_{C,P} = 4.1 Hz, CH(CH₃)₂], 19.2 [CH(CH₃)₂], 18.8 [CH(CH₃)₂], 17.5 [vt, ²J_{C,P} = 4.0 Hz, CH(CH₃)₂], 13.0 (NCH₂CH₃) ppm. ³¹P{¹H} NMR (CD₂Cl₂, 20 °C): δ = 127.8 ppm. IR (ATR): $\tilde{\nu}$ = 1942 (ν_{C=O}) cm⁻¹.

trans-[Fe(κ^3P,N,P -PNP^{Ph}-Et)(CO)Cl₂] (4f): This compound was prepared analogously to **4b** with PNP^{Ph}-Et (**1f**; 140 mg, 0.32 mmol) and anhydrous FeCl₂ (140 mg, 0.32 mmol) as the starting materials, yield 180 mg (95%). Crystals were grown by the slow diffusion of *n*-pentane into a THF solution. C₂₆H₃₃Cl₂FeN₃O₂ (592.26): calcd. C 52.73, H 5.62, N 7.09; found C 52.82, H 5.49, N 7.01. ¹H NMR ([D₆]acetone, 20 °C): δ = 7.63 (m, 6 H, Ph^{3,4,5}), 7.34 (d, ³J_{H,H} = 6.9 Hz, 4 H, Ph^{2,6}), 7.26 (t, ³J_{H,H} = 8.3 Hz, 1 H, py⁴), 5.61 (d, ³J_{H,H} = 7.9 Hz, 2 H, py^{3,5}), 2.60 (m, 4 H, CH₂), 2.19 (m, 4 H, CH₂), 1.33 (m, 12 H, CH₃) ppm. ¹³C{¹H} NMR ([D₆]acetone, 20 °C): δ

= 222.4 (t, ²J_{C,P} = 23.1 Hz, CO), 163.9 (vt, ²J_{C,P} = 11.8 Hz, py^{2,6}), 139.4 (s, py⁴), 139.3 (vt, ²J_{C,P} = 2.8 Hz, Ph¹), 130.7 (Ph), 130.6 (Ph), 128.9 (Ph⁴), 100.7 (py^{3,5}), 20.4 (vt, ¹J_{C,P} = 13.5 Hz, CH₂), 8.0 (CH₃) ppm. ³¹P{¹H} NMR ([D₆]acetone, 20 °C): δ = 137.3 ppm. IR (ATR): $\tilde{\nu}$ = 1959 (ν_{CO}) cm⁻¹.

trans-[Fe(κ^3P,N,P -PNP^{Ph}-nPr)(CO)Cl₂] (4g): This compound was prepared analogously to **4b** with PNP^{Ph}-nPr (**1g**; 160 mg, 0.32 mmol) and anhydrous FeCl₂ (140 mg, 0.32 mmol) as the starting materials, yield 195 mg (94%). C₃₁H₄₁Cl₂FeN₃O₂ (648.37): calcd. C 55.57, H 6.37, N 6.48; found C 55.55, H 6.31, N 6.52. ¹H NMR ([D₆]acetone, 20 °C): δ = 7.57 (m, 6 H, Ph^{3,4,5}), 7.31–6.85 (m, 5 H, Ph^{2,6}, py⁴), 5.57 (d, ³J_{H,H} = 7.4 Hz, 2 H, py^{3,5}), 2.54 (m, 4 H, CH₂), 2.00 (m, 4 H, CH₂), 1.62 (m, 8 H, CH₂), 1.08 (t, ³J_{H,H} = 6.7 Hz, 12 H, CH₃) ppm. ¹³C{¹H} NMR ([D₆]acetone, 20 °C): δ = 222.4 (t, ²J_{C,P} = 23.0 Hz, CO), 163.8 (vt, ²J_{C,P} = 11.9 Hz, py^{2,6}), 139.5 (py⁴), 139.4 (vt, ²J_{C,P} = 2.7 Hz, Ph¹), 130.8 (Ph), 130.6 (Ph), 129.0 (Ph⁴), 100.8 (vt, ³J_{C,P} = 2.6 Hz, py^{3,5}), 17.6 (CH₂), 15.8 (vt, ¹J_{C,P} = 8.4 Hz, CH₂), 15.0 (CH₃) ppm. ³¹P{¹H} NMR ([D₆]acetone, 20 °C): δ = 133.0 ppm. IR (ATR): $\tilde{\nu}$ = 1958 (ν_{CO}) cm⁻¹.

cis-[Fe(κ^3P,N,P -PNP-Ph)(CO)Cl₂] (5h): To a suspension of anhydrous FeCl₂ (100 mg, 0.79 mmol) in THF, the ligand PNP-Ph (**1h**) was added, and CO gas was immediately bubbled through the solution for ca. 5 min. The mixture was stirred for 4 h, whereupon the suspension turned red. The solvent was removed under reduced pressure, and the red solid was washed with Et₂O (10 mL) and dried under vacuum, yield 93%. C₃₀H₂₅Cl₂FeN₃O₂ (623.24): calcd. C 56.99, H 3.99, N 6.65; found C 57.11, H 3.89, N 6.71. ¹H NMR ([D₆]acetone, 20 °C): δ = 9.01 (m, 2 H, NH), 8.28 (m, 4 H), 8.08 (m, 4 H), 7.45 (m, 6 H), 7.37 (m, 6 H), 7.0 (m, 1 H, py⁴), 6.51 (d, ³J_{H,H} = 5.8 Hz, 2 H, py^{3,5}) ppm. ¹³C{¹H} NMR ([D₆]acetone, 20 °C): δ = 216.9 (t, ²J_{C,P} = 29.0 Hz, CO), 162.3 (vt, ²J = 9.5 Hz, py^{2,6}), 139.2 (py⁴), 133.0 (vt, ²J = 5.5 Hz, Ph^{2,6}), 131.8 (vt, ¹J_{C,P} = 6.3 Hz, Ph¹), 130.2 (Ph), 130.1 (Ph), 138.3 (Ph), 127.5 (Ph), 99.4 (t, ³J_{C,P} = 4.6 Hz, py^{3,5}) ppm. ³¹P{¹H} NMR ([D₆]acetone, 20 °C): δ = 88.0 ppm. IR (ATR): $\tilde{\nu}$ = 1985 (ν_{CO}) cm⁻¹.

trans-[Fe(κ^3P,N,P -PNP-BIPOL)(CO)Cl₂] (4i): Carbon monoxide was bubbled into a suspension of anhydrous FeCl₂ (118 mg, 0.93 mmol) and PNP-BIPOL (**1i**) (500 mg, 0.93 mmol) in CH₂Cl₂ (10 mL) for ca. 5 min, whereupon the reaction mixture turned from green to pink, and the mixture was stirred for 4 h. After the removal of the solvent under reduced pressure, the remaining solid was washed twice with CH₂Cl₂ (10 mL) and dried under vacuum, yield 650 mg (91%). Crystals were grown in THF at –20 °C. C₃₀H₂₁Cl₂FeN₃O₅P₂ (692.20): calcd. C 52.05, H 3.06, N 6.07; found C 52.15, H 3.21, N 6.11. ¹H NMR ([D₆]acetone, 20 °C): δ = 9.70 (m, 2 H, NH), 7.77 (m, 5 H, Ph, py⁴), 7.52 (m, 12 H, Ph), 6.82 (d, ³J_{H,H} = 6.4 Hz, 2 H, py^{3,5}) ppm. ¹³C{¹H} NMR ([D₆]acetone, 20 °C): δ = 216.6 (t, ²J_{C,P} = 32.5 Hz, CO), 158.6 (vt, ²J_{C,P} = 14.0 Hz, py^{2,6}), 141.3 (py⁴), 130.2 (Ph), 129.8 (Ph), 129.7 (Ph), 126.4 (Ph⁴), 122.6 (Ph⁶), 101.4 (vt, ³J_{C,P} = 4.5 Hz, py^{3,5}) ppm. ³¹P{¹H} NMR ([D₆]acetone, 20 °C): δ = 190.9 ppm. IR (ATR): $\tilde{\nu}$ = 1991 (ν_{CO}) cm⁻¹.

cis-[Fe(κ^3P,N,P -PNP-BIPOL)(CO)Cl₂] (5i): Carbon monoxide was bubbled into a solution of anhydrous FeCl₂ (118 mg, 0.93 mmol) and PNP-BIPOL (**1i**) (500 mg, 0.93 mmol) in THF (10 mL) for ca. 5 min, whereupon the reaction mixture turned from yellow to red and was stirred for 1 h. After the removal of the solvent under reduced pressure, the remaining solid was washed twice with toluene (10 mL) and Et₂O (10 mL) and dried under vacuum, yield 630 mg (89%). C₃₀H₂₁Cl₂FeN₃O₅P₂ (692.20): calcd. C 52.05, H 3.06, N 6.07; found C 51.98, H 3.18, N 6.04. ¹H NMR ([D₆]acetone, 20 °C): δ = 9.69 (m, 2 H, NH), 7.77 (m, 5 H, Ph, py⁴), 7.51

(m, 12 H, Ph), 6.82 (m, 2 H, py^{3,5}) ppm. ¹³C{¹H} NMR ([D₆]acetone, 20 °C): δ = 216.5 (t, ²J_{C,P} = 31.5 Hz, CO), 158.5 (py^{2,6}), 141.9 (py⁴), 130.2 (Ph), 130.1 (Ph), 130.0 (Ph), 126.8 (Ph⁴), 122.7 (Ph⁶), 101.4 (m, py^{3,5}) ppm. ³¹P{¹H} NMR ([D₆]acetone, 20 °C): δ = 190.9 ppm. IR (ATR): ν̄ = 2001 (ν_{CO}) cm⁻¹.

trans-[Fe(κ³P,N,P-PNP-Me)(CO)Cl₂] (4j): The ligand PNP-Me (**1j**; 150 mg, 0.65 mmol) was added portionwise to a suspension of anhydrous FeCl₂ (83 mg, 0.65 mmol) in THF (7 mL) over a period of 5 min as CO was bubbled through the solution. The mixture was then stirred for 4 h. The violet solid was then collected on a glass frit, washed with THF (7 mL) and *n*-hexane (7 mL), and dried under vacuum, yield 245 mg (98%). Crystals of **4c** were grown by the slow diffusion of *n*-pentane into a THF solution. C₁₀H₁₇Cl₂FeN₃OP₂ (383.96): calcd. C 31.28, H 4.46, N 10.94; found C 31.25, H 4.33, N 11.01. ¹H NMR ([D₆]DMSO, 20 °C): δ = 8.64 (m, 2 H, NH), 7.40 (t, ³J_{H,H} = 8.2 Hz, 1 H, py⁴), 6.27 (d, ³J_{H,H} = 8.0 Hz, py^{3,5}), 1.85 (t, ²J_{H,P} = 3.9 Hz, 12 H, CH₃) ppm. ¹³C{¹H} NMR ([D₆]acetone, 20 °C): δ = 221.3 (t, ²J_{C,P} = 23.8 Hz, CO), 161.9 (vt, ²J_{C,P} = 10.1 Hz, py^{2,6}), 139.8 (py⁴), 98.1 (vt, ²J_{C,P} = 4.1 Hz, py^{3,5}), 14.7 (vt, ¹J_{C,P} = 15.5 Hz, CH₃) ppm. ³¹P{¹H} NMR ([D₆]DMSO, 20 °C): δ = 107.8 ppm. IR (ATR): ν̄ = 1959 (ν_{CO}) cm⁻¹.

trans-[Fe(κ³P,N,P-PNP-Et)(CO)Cl₂] (4k): This compound was prepared analogously to **4j** with PNP-Et (**1k**; 200 mg, 0.70 mmol) and anhydrous FeCl₂ (88 mg, 0.70 mmol) as the starting materials, yield 300 mg (97%). Crystals were grown by the slow diffusion of *n*-pentane into a THF/DMSO solution. C₁₄H₂₅Cl₂FeN₃OP₂ (440.07): calcd. C 38.21, H 5.73, N 9.55; found C 38.25, H 5.61, N 9.48. ¹H NMR ([D₆]DMSO, 20 °C): δ = 8.61 (m, 2 H, NH), 7.37 (m, 1 H, py⁴), 6.30 (d, ³J_{H,H} = 6.0 Hz, 2 H, py^{3,5}), 2.08 (m, 8 H, CH₂), 1.26 (m, 12 H, CH₃) ppm. ¹³C{¹H} NMR ([D₆]DMSO, 20 °C): δ = 221.1 (t, ²J_{C,P} = 23.5 Hz, CO), 160.5 (vt, ²J_{C,P} = 9.9 Hz, py^{2,6}), 138.2 (py⁴), 96.8 (vt, ³J_{C,P} = 4.8 Hz, py^{3,5}), 15.4 (vt, ¹J_{C,P} = 14.0 Hz, CH₂), 6.12 (CH₃) ppm. ³¹P{¹H} NMR ([D₆]DMSO, 20 °C): δ = 119.1 ppm. IR (ATR): ν̄ = 1965 (ν_{CO}) cm⁻¹.

trans-[Fe(κ³P,N,P-PNP-*n*Pr)(CO)Cl₂] (4l): A suspension of PNP-*n*Pr (**1k**; 230 mg, 0.67 mmol) and anhydrous FeCl₂ (85 mg, 0.67 mmol) in CH₂Cl₂ (10 mL) was purged with CO for 5 min. The mixture was stirred for 14 h, whereupon a violet powder formed. The powder was collected on a glass frit, washed with *n*-hexane (15 mL), and dried under vacuum, yield 307 mg (92%). Crystals were grown by the slow diffusion of *n*-pentane into a THF solution. C₁₈H₃₃Cl₂FeN₃OP₂ (496.17): calcd. C 43.57, H 6.70, N 8.47; found C 43.52, H 6.74, N 8.52. ¹H NMR ([D₆]acetone, 20 °C): δ = 7.7 (m, 2 H, NH), 7.34 (t, ³J_{H,H} = 7.8 Hz, py⁴), 6.34 (d, ³J_{H,H} = 7.8 Hz, py^{3,5}), 2.46–2.13 (m, 8 H, CH₂), 1.93 (m, 4 H, CH₂), 1.77 (m, 4 H, CH₂), 1.02 (t, ³J_{H,H} = 7.1 Hz, 12 H, CH₃) ppm. ¹³C{¹H} NMR ([D₆]acetone, 20 °C): δ = 223.5 (t, ²J_{C,P} = 23.1 Hz, CO), 162.8 (py^{2,6}), 140.4 (py⁴), 99.4 (py^{3,5}), 28.1 (vt, ¹J_{C,P} = 13.7 Hz, CH₂), 17.9 (CH₃), 16.4 (vt, ²J_{C,P} = 7.0 Hz, CH₂) ppm. ³¹P{¹H} NMR ([D₆]acetone, 20 °C): δ = 116.3 ppm. IR (ATR): ν̄ = 1950 (ν_{CO}) cm⁻¹.

trans-[Fe(κ³P,N,P-PNP-*n*Bu)(CO)Cl₂] (4m): This compound was prepared analogously to **4j** with PNP-*n*Bu (**1m**; 230 mg, 0.58 mmol) and anhydrous FeCl₂ (73 mg, 0.58 mmol) as the starting materials, yield 291 mg (91%). C₂₂H₄₁Cl₂FeN₃OP₂ (552.28): calcd. C 47.84, H 7.48, N 7.61; found C 47.79, H 7.56, N 7.54. ¹H NMR ([D₆]acetone, 20 °C): δ = 7.88 (m, 2 H, NH), 7.26 (m, 1 H, py⁴), 6.34 (d, ³J_{H,H} = 7.1 Hz, 2 H, py^{3,5}), 2.38–2.13 (m, 6 H, CH₂), 1.75 (m, 8 H, CH₂), 1.38 (m, 10 H, CH₂), 0.87 (t, ³J_{H,H} = 7.2 Hz, 12 H, CH₃) ppm. ¹³C{¹H} NMR ([D₆]acetone, 20 °C): δ = 222.6 (t, ²J_{C,P} = 23.5 Hz, CO), 161.9 (vt, ²J_{C,P} = 9.7 Hz, py^{2,6}), 139.2 (py⁴), 98.4

(py^{3,5}), 25.3 (CH₂), 24.5 (vt, ¹J_{C,P} = 13.9 Hz, CH₂), 24.1 (vt, ²J_{C,P} = 7.0 Hz, CH₂), 13.1 (CH₃) ppm. ³¹P{¹H} NMR ([D₆]acetone, 20 °C): δ = 116.8 ppm. IR (ATR): ν̄ = 1953 (ν_{CO}) cm⁻¹.

[Fe(κ³P,N,P-PNP-Ph)(κ²P,N-PN-Ph)Cl]BF₄ (6): Anhydrous FeCl₂ (127 mg, 1.0 mmol), PNP-Ph (**1g**; 480 mg, 1.0 mmol), PN-Ph (280 mg, 1.0 mmol), and AgBF₄ (195 mg, 1.0 mmol) were stirred in THF (10 mL) for 4 h. The mixture turned green, and a white precipitate formed. The solid was removed by filtration through Celite, and the solution was evaporated to dryness. The obtained green powder was washed twice with Et₂O (10 mL), yield 900 mg (96%). C₄₆H₄₀BClF₄FeN₅P₃ (933.88): calcd. C 59.16, H 4.32, N 7.50; found C 59.19, H 4.40, N 7.82. ¹H NMR ([D₆]acetone, 20 °C): δ = 9.27 (m, 1 H, NH), 8.67 (m, 2 H, NH), 7.81 (m, 6 H, Ph), 7.37 (m, 8 H, Ph, py⁴), 7.26–7.00 (m, 16 H, Ph, py^{2,6}), 7.00–6.73 (m, 6 H, Ph) ppm. ³¹P{¹H} NMR ([D₆]acetone, 20 °C): A₂B spin-system: δ_A = 112.5, δ_B = 111.9 ppm, ²J_{P,P} = 50 Hz (shifts and J_{P,P} determined from simulation).

General Procedure for the Decarbonylation of [Fe(κ³P,N,P-PNP)-(CO)Cl₂] (4j–4m, 5h): The decarbonylation was performed in the solid state. A defined portion of **4j–4m** or **5h** (ca. 100 mg) was placed into a Schlenk tube and then heated in an oil bath (60–200 °C) under vacuum, whereupon the color changed from red to pale yellow. The completion of this reaction was established by IR spectroscopy when the CO stretching band was no longer observed.

X-ray Structure Determination: The X-ray diffraction data of **3d**, **3e**, **4b**, **4e**, **4j**, **4k**, **4l**, **5h**, and **6** were collected at T = 100 K in a dry stream of nitrogen with a Bruker Kappa APEX II diffractometer system with graphite-monochromated Mo-K_α radiation (λ = 0.71073 Å) and fine-sliced φ and ω scans. The data were reduced to intensity values with SAINT. Crystals of **4e** were systematically twinned by reflection at (001). Both domains were integrated concurrently with overlapping information. An absorption correction was applied with the multiscan approach implemented in SADABS or TWINABS.^[25] The structures were solved by direct methods implemented in SHELXS^[26] or charge flipping implemented in SUPERFLIP^[27] and refined with SHELXL or JANA2006.^[28] Non-hydrogen atoms were refined anisotropically. The H atoms connected to C atoms were placed in calculated positions and thereafter refined as riding on the parent atom. Molecular graphics were generated with the program MERCURY.^[29] The crystal data and experimental details are given in Table S1.

CCDC-1050950 (for **3d**), -1050951 (for **3e**), -1050952 (for **4b**), -1050953 (for **4f**), -1015364 (for **5h**), -1050954 (for **4j**), -1050955 (for **4k**), -1050956 (for **4l**), and -1005383 (for **6**) contain the supplementary crystallographic data for this paper. These data can be obtained free of charge from The Cambridge Crystallographic Data Centre via www.ccdc.cam.ac.uk/data_request/cif.

Computational Details: Calculations were performed with the GAUSSIAN 09 software package,^[30] and the OPBE functional^[31] was used without symmetry constraints. This functional combines the Handy OPTX modification of the Becke exchange functional with the gradient-corrected correlation functional of Perdew, Burke, and Ernzerhof and is accurate in the calculation of spin-state energy splitting for first-transition-row species and, in particular, for iron complexes.^[32] The optimized geometries were obtained with the Stuttgart/Dresden ECP (SDD) basis set^[33] to describe the electrons of the iron atom. For all other atoms, a standard 6-31G** basis set was employed.^[34] Transition-state optimizations were performed with the synchronous transit-guided quasi-Newton method (STQN) developed by Schlegel et al.,^[35] following a thorough search of the potential energy surfaces (PES). Frequency calculations were performed to confirm the nature of the stationary points,

which yielded one imaginary frequency for the transition states and none for the minima. Each transition state was further confirmed by following its vibrational mode downhill on both sides and obtaining the minima presented on the energy profiles.

The MECPs between the PES of two different spin states were determined by using a code developed by Harvey et al.^[36] This code consists of a set of shell scripts and Fortran programs that use the Gaussian results of energies and gradients of both spin states to produce an effective gradient pointing towards the MECP.

Electronic energy values are presented in the profiles and discussed in the text because MECPs are not stationary points and, hence, a standard frequency analysis is not applicable. However, the free-energy values are also presented for all stationary points for comparison purposes. Those values were obtained from the electronic energies at 298.15 K and 1 atm by using zero-point-energy and thermal-energy corrections based on structural and vibration frequency data and were further corrected for dispersion effects by the Grimme DFT-D3 method^[37] with Becke and Johnson short-distance damping.^[38]

Supporting Information (see footnote on the first page of this article): Complete crystallographic data and technical details.

Acknowledgments

Financial support by the Austrian Science Fund (FWF) is gratefully acknowledged (project number P24202-N17). L. F. V. acknowledges the Portuguese Fundação para a Ciência e Tecnologia (FCT) (UID/QUI/00100/2013) for support. The X-ray center of the Vienna University of Technology is acknowledged for financial support and for providing access to the single-crystal diffractometer.

- [1] For reviews on pincer complexes, see: a) M. Albrecht, G. van Koten, *Angew. Chem. Int. Ed.* **2001**, *40*, 3750; *Angew. Chem.* **2001**, *113*, 3866; b) M. E. van der Boom, D. Milstein, *Chem. Rev.* **2003**, *103*, 1759; c) J. T. Singleton, *Tetrahedron* **2003**, *59*, 1837; d) P. Bhattacharya, H. Guan, *Comments Inorg. Chem.* **2011**, *32*, 88; e) S. Schneider, J. Meiners, B. Askevold, *Eur. J. Inorg. Chem.* **2012**, 412; f) D. Morales-Morales, C. M. Jensen (Eds.), *The Chemistry of Pincer Compounds*, Elsevier, Amsterdam, **2007**; g) D. Benito-Garagorri, K. Kirchner, *Acc. Chem. Res.* **2008**, *41*, 201.
- [2] a) W. V. Dahlhoff, S. M. Nelson, *J. Chem. Soc. A* **1971**, 2184; b) P. Giannoccaro, G. Vasapollo, C. F. Nobile, A. Sacco, *Inorg. Chim. Acta* **1982**, *61*, 69; c) G. Müller, M. Klinga, M. Leskelä, B. Rieger, *Z. Anorg. Allg. Chem.* **2002**, *628*, 2839.
- [3] a) J. Zhang, M. Gandelman, D. Herrman, G. Leitus, L. J. W. Shimon, Y. Ben-David, D. Milstein, *Inorg. Chim. Acta* **2006**, *359*, 1955; b) R. J. Trovitch, E. Lobkovsky, P. J. Chirik, *Inorg. Chem.* **2006**, *45*, 7252.
- [4] E. M. Pelczar, T. J. Emge, K. Krogh-Jespersen, A. S. Goldman, *Organometallics* **2008**, *27*, 5759.
- [5] a) W.-S. W. DeRieux, A. Wong, Y. Schrodi, *J. Organomet. Chem.* **2014**, *772–773*, 60; b) S. Mazza, R. Scopelliti, X. Hu, *Organometallics* **2015**, *34*, 1538–1545.
- [6] a) B. Bichler, M. Glatz, B. Stöger, K. Mereiter, L. F. Veiros, K. Kirchner, *Dalton Trans.* **2014**, *43*, 14517; b) M. Glatz, B. Bichler, M. Mastalir, B. Stöger, K. Mereiter, M. Weil, E. Pittenauer, G. Allmaier, L. F. Veiros, K. Kirchner, *Dalton Trans.* **2015**, *44*, 281.
- [7] D. Benito-Garagorri, J. Wiedermann, M. Pollak, K. Mereiter, K. Kirchner, *Organometallics* **2007**, *26*, 217.
- [8] a) D. Benito-Garagorri, M. Puchberger, K. Mereiter, K. Kirchner, *Angew. Chem. Int. Ed.* **2008**, *47*, 9142; *Angew. Chem.* **2008**, *120*, 9282; b) D. Benito-Garagorri, L. G. Alves, M. Puchberger, K. Mereiter, L. F. Veiros, M. J. Calhorda, M. D. Carvalho, L. P. Ferreira, M. Godinho, K. Kirchner, *Organometallics* **2009**, *28*, 6902.
- [9] For examples of CO sensors with metal complexes, see: a) M. Itou, Y. Araki, O. Ito, H. Kido, *Inorg. Chem.* **2006**, *45*, 6114; b) A. Giulino, T. Gupta, M. Altman, S. Lo Schiavo, P. G. Mineo, I. L. Fragalà, G. Evmenenko, P. Dutta, M. E. van der Boom, *Chem. Commun.* **2008**, 2900; c) S. Paul, F. Amalraj, S. Radhakrishnana, *Synt. Met.* **2009**, *159*, 1019; d) M. E. Moragues, J. Esteban, J. V. Ros-Lis, R. Martínez-Mañez, M. D. Marcos, M. Martínez, J. Soto, F. Sancenón, *J. Am. Chem. Soc.* **2011**, *133*, 15762; e) J. Esteban, J. V. Ros-Lis, R. Martínez-Mañez, M. D. Marcos, M. Moragues, J. Soto, F. Sancenón, *Angew. Chem. Int. Ed.* **2010**, *49*, 4934; *Angew. Chem.* **2010**, *122*, 5054; f) M. E. Moragues, J. Esteban, J. V. Ros-Lis, R. Martínez-Mañez, M. D. Marcos, M. Martínez, J. Soto, F. Sancenón, *J. Am. Chem. Soc.* **2011**, *133*, 15762; g) M. E. Moragues, R. Montes-Robles, J. V. Ros-Lis, M. Alcañiz, J. Ibanez, T. Pardo, R. Martínez-Mañez, *Sens. Actuators, B* **2014**, *191*, 257.
- [10] C. W. Tate, A. deMello, A. D. Gee, S. Kealey, R. Vilar, A. J. P. White, N. J. Long, *Dalton Trans.* **2012**, *41*, 83.
- [11] a) D. W. Keogh, R. Poli, *J. Am. Chem. Soc.* **1997**, *119*, 2516; b) J.-L. Carreon, J. N. Harvey, *J. Am. Chem. Soc.* **2004**, *126*, 5789; c) N. Strickland, J. N. Harvey, *J. Phys. Chem. B* **2007**, *111*, 841.
- [12] For a review of open-shell complexes, see: R. Poli, *Chem. Rev.* **1996**, *96*, 2135.
- [13] N. J. Hardman, X. Fang, B. L. Scott, R. J. Wright, R. L. Martin, G. J. Kubas, *Inorg. Chem.* **2005**, *44*, 8306.
- [14] D. V. Stynes, Y. S. Hui, V. Chew, *Inorg. Chem.* **1982**, *21*, 1222.
- [15] J. Ellison, A. Nienstedt, S. C. Shoner, D. Barnhart, J. A. Cowen, J. A. Kovacs, *J. Am. Chem. Soc.* **1998**, *120*, 5691.
- [16] a) A. A. Danopoulos, D. Pugh, H. Smith, J. Saßmannshausen, *Chem. Eur. J.* **2009**, *15*, 5491; b) R. M. Henry, R. K. Shoemaker, R. H. Newell, G. M. Jacobsen, D. L. DuBois, M. Rakowski DuBois, *Organometallics* **2005**, *24*, 2481; c) J. Breuer, H.-W. Fruhauf, W. J. J. Smeets, A. L. Spek, *Inorg. Chim. Acta* **1999**, *291*, 438.
- [17] C. Holzhaecker, B. Stöger, M. D. Carvalho, L. P. Ferreira, E. Pittenauer, G. Allmaier, L. F. Veiros, S. Realista, A. Gil, M. J. Calhorda, D. Müller, K. Kirchner, *Dalton Trans.* **2015**, *44*, 13071.
- [18] This reaction was previously studied with the PBE functional, which considerably overestimated the stability of the low-spin species [Fe(PNP-*i*Pr)(CO)Cl₂] (**4a**).
- [19] For excellent reviews on MECPs and their location for transition-metal complexes, see: a) J. N. Harvey, R. Poli, K. M. Smith, *Coord. Chem. Rev.* **2003**, *238–239*, 347; b) R. Poli, J. N. Harvey, *Chem. Soc. Rev.* **2003**, *32*, 1.
- [20] J. N. Harvey, *Phys. Chem. Chem. Phys.* **2007**, *9*, 331.
- [21] R. J. Abraham, J. Fisher, P. Loftus, *Introduction to NMR Spectroscopy*, John Wiley & Sons, New York, **1988**.
- [22] D. D. Perrin, W. L. F. Armarego, *Purification of Laboratory Chemicals*, 3rd ed., Pergamon, New York, **1988**.
- [23] a) W. J. Knebel, R. J. Angelici, *Inorg. Chim. Acta* **1973**, *7*, 713; b) W. J. Knebel, R. J. Angelici, *Inorg. Chem.* **1974**, *13*, 632; c) E. W. Ainscough, A. M. Brodie, S. T. Wong, *J. Chem. Soc., Dalton Trans.* **1977**, 915.
- [24] a) S. K. Sur, *J. Magn. Reson.* **1989**, *82*, 169; b) D. F. Evans, *J. Chem. Soc.* **1959**, 2003.
- [25] APEX2, SAINT, SADABS, and TWINABS, Bruker AXS Inc., Madison, WI, **2012**.
- [26] G. M. Sheldrick, *Acta Crystallogr., Sect. A* **2008**, *64*, 112.
- [27] L. Palatinus, G. Chapuis, *J. Appl. Crystallogr.* **2007**, *40*, 786.
- [28] V. Petříček, M. Dušek, L. Palatinus, *Z. Kristallogr.* **2014**, *229*, 345.
- [29] C. F. Macrae, P. R. Edgington, P. McCabe, E. Pidcock, G. P. Shields, R. Taylor, M. Towler, J. van de Streek, *J. Appl. Crystallogr.* **2006**, *39*, 453.

- [30] M. J. Frisch, G. W. Trucks, H. B. Schlegel, G. E. Scuseria, M. A. Robb, J. R. Cheeseman, G. Scalmani, V. Barone, B. Mennucci, G. A. Petersson, H. Nakatsuji, M. Caricato, X. Li, H. P. Hratchian, A. F. Izmaylov, J. Bloino, G. Zheng, J. L. Sonnenberg, M. Hada, M. Ehara, K. Toyota, R. Fukuda, J. Hasegawa, M. Ishida, T. Nakajima, Y. Honda, O. Kitao, H. Nakai, T. Vreven, J. A. Montgomery Jr., J. E. Peralta, F. Ogliaro, M. Bearpark, J. J. Heyd, E. Brothers, K. N. Kudin, V. N. Staroverov, R. Kobayashi, J. Normand, K. Raghavachari, A. Rendell, J. C. Burant, S. S. Iyengar, J. Tomasi, M. Cossi, N. Rega, J. M. Millam, M. Klene, J. E. Knox, J. B. Cross, V. Bakken, C. Adamo, J. Jaramillo, R. Gomperts, R. E. Stratmann, O. Yazyev, A. J. Austin, R. Cammi, C. Pomelli, J. W. Ochterski, R. L. Martin, K. Morokuma, V. G. Zakrzewski, G. A. Voth, P. Salvador, J. J. Dannenberg, S. Dapprich, A. D. Daniels, Ö. Farkas, J. B. Foresman, J. V. Ortiz, J. Cioslowski, D. J. Fox, *Gaussian 09*, revision A.01, Gaussian, Inc., Wallingford CT, **2009**.
- [31] a) N. C. Handy, A. J. Cohen, *Mol. Phys.* **2001**, *99*, 403; b) W.-M. Hoe, A. Cohen, N. C. Handy, *Chem. Phys. Lett.* **2001**, *341*, 319; c) J. P. Perdew, K. Burke, M. Ernzerhof, *Phys. Rev. Lett.* **1997**, *78*, 1396; d) J. P. Perdew, K. Burke, M. Ernzerhof, *Phys. Rev. Lett.* **1996**, *77*, 3865.
- [32] a) M. Swart, *J. Chem. Theory Comput.* **2008**, *4*, 2057; b) J. Conradie, A. Ghosh, *J. Chem. Theory Comput.* **2007**, *3*, 689; c) J. Conradie, A. Ghosh, *J. Phys. Chem. B* **2007**, *111*, 12621.
- [33] a) U. Haeusermann, M. Dolg, H. Stoll, H. Preuss, *Mol. Phys.* **1993**, *78*, 1211; b) W. Kuechle, M. Dolg, H. Stoll, H. Preuss, *J. Chem. Phys.* **1994**, *100*, 7535; c) T. Leininger, A. Nicklass, H. Stoll, M. Dolg, P. Schwerdtfeger, *J. Chem. Phys.* **1996**, *105*, 1052.
- [34] a) A. D. McLean, G. S. Chandler, *J. Chem. Phys.* **1980**, *72*, 5639; b) R. Krishnan, J. S. Binkley, R. Seeger, J. A. Pople, *J. Chem. Phys.* **1980**, *72*, 650; c) P. J. Hay, *J. Chem. Phys.* **1977**, *66*, 4377; d) K. Raghavachari, G. W. Trucks, *J. Chem. Phys.* **1989**, *91*, 1062; e) R. C. Binning, L. A. Curtiss, *J. Comput. Chem.* **1995**, *16*, 6104; f) M. P. McGrath, L. Radom, *J. Chem. Phys.* **1991**, *94*, 511.
- [35] a) C. Peng, P. Y. Ayala, H. B. Schlegel, M. J. Frisch, *J. Comput. Chem.* **1996**, *17*, 49; b) C. Peng, H. B. Schlegel, *Isr. J. Chem.* **1994**, *33*, 449.
- [36] J. N. Harvey, M. Aschi, H. Schwarz, W. Koch, *Theor. Chem. Acc.* **1998**, *99*, 95.
- [37] S. Grimme, J. Antony, S. Ehrlich, H. J. Krieg, *J. Chem. Phys.* **2010**, *132*, 154104.
- [38] a) A. D. Becke, E. R. J. Johnson, *J. Chem. Phys.* **2005**, *122*, 154101; b) E. R. Johnson, A. D. Becke, *J. Chem. Phys.* **2005**, *123*, 24101; c) E. R. Johnson, A. D. Becke, *J. Chem. Phys.* **2006**, *124*, 174104.

Received: June 11, 2015

Published Online: September 30, 2015

Manuscript #3

"Synthesis and characterization of cationic dicarbonyl Fe(II) PNP pincer complexes"

Glatz, M., Schröder-Holzacker, C., Bichler, B. Schröder-Holzacker C.; Bichler B.; Stöger B.; Mereiter K.; Veiros L. F.; Kirchner K. *Monatsh. Chem.* **2016**, *147*, 1713-1719.

<https://doi.org/10.1007/s00706-016-1811-x>

Reproduced by permission of Springer Nature

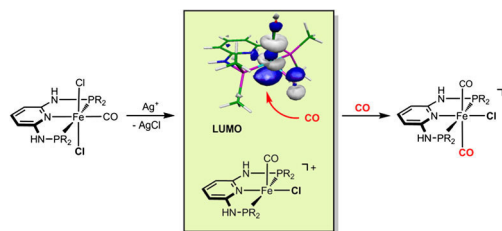
Synthesis and characterization of cationic dicarbonyl Fe(II) PNP pincer complexes

Mathias Glatz¹ · Christian Schröder-Holzacker¹ · Bernhard Bichler¹ ·
Berthold Stöger² · Kurt Mereiter² · Luis F. Veiros³ · Karl Kirchner¹

Received: 16 May 2016 / Accepted: 26 June 2016 / Published online: 6 August 2016
© The Author(s) 2016. This article is published with open access at Springerlink.com

Abstract In the present work, we have prepared a series of octahedral Fe(II) complexes of the type *trans*-[Fe(PNP)(CO)₂Cl]⁺—PNP are tridentate pincer-type ligands based on 2,6-diaminopyridine. These complexes are formed irrespective of the size of the substituents at the phosphorus sites and whether *cis*-[Fe(PNP)(Cl₂)(CO)] or *trans*-[Fe(PNP)(Cl₂)(CO)] are reacted with CO in the presence of 1 equiv of silver salts. X-ray structures of representative complexes are presented. Based on simple bonding considerations the selective formation of *trans*-dicarbonyl Fe(II) complexes is unexpected. In fact, DFT calculations confirm that *trans*-dicarbonyl complexes are indeed thermodynamically disfavored over the respective *cis*-dicarbonyl compounds, but are favored for kinetic reasons.

Graphical abstract



Keywords Iron complexes · PNP pincer ligands · Carbon monoxide · DFT calculations

Introduction

As part of our ongoing research on the synthesis and reactivity of iron(II) PNP pincer complexes [1–3], we recently prepared the cationic dicarbonyl complex *trans*-[Fe(PNP-*i*Pr)(CO)₂Cl]⁺ (PNP-*i*Pr = *N,N'*-bis(diisopropyl)-2,6-diaminopyridine) (*trans*-**2a**) as shown in Scheme 1 [4]. The formation of this complex was somewhat unexpected as it features two CO ligands in a mutual *trans* position. In fact, simple bonding considerations suggest that the unobserved *cis* isomers are the more stable one. This was indeed also supported by DFT calculations. This complex is interesting, since the *trans* CO arrangement makes one of the CO ligands comparatively labile which can be replaced by other potential ligands. Accordingly, *trans*-[Fe(PNP-*i*Pr)(CO)₂Cl]X with X = BF₄[−] turned out to be an efficient precatalyst for the coupling of aromatic aldehydes with ethyl diazoacetate to selectively give 3-hydroxyacrylates rather than β-keto esters [5].

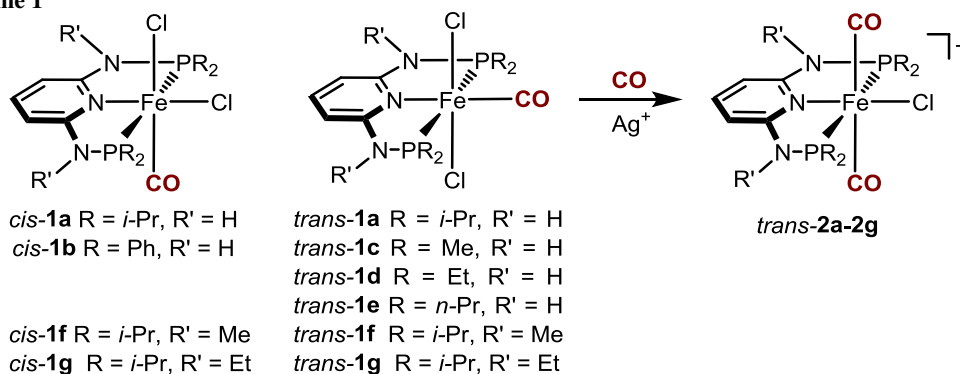
✉ Karl Kirchner
kkirch@mail.tuwien.ac.at

¹ Institute of Applied Synthetic Chemistry, Vienna University of Technology, Getreidemarkt 9/163, 1060 Vienna, Austria

² Institute of Chemical Technologies and Analytics, Vienna University of Technology, Getreidemarkt 9, 1060 Vienna, Austria

³ Centro de Química Estrutural, Instituto Superior Técnico, Universidade de Lisboa, Av. Rovisco Pais No. 1, 1049-001 Lisbon, Portugal

Scheme 1



In continuation of our studies on iron PNP complexes, we herein report on the synthesis and reactivity of a series of octahedral Fe(II) carbonyl complexes bearing both sterically little demanding as well as bulky PNP ligands in order to probe whether sterics influence the preference for a *trans*- over a *cis*-dicarbonyl arrangement. Moreover, we investigate the impact of the NR linker on the outcome of these reactions.

Results and discussion

Treatment of complexes *cis-1b* and *trans-1c–1g* (**1f** and **1g** are mixtures of *cis* and *trans* isomers) with 1 equiv of Ag⁺ salts (with SbF₆[−], BF₄[−], or CF₃SO₃[−] as counterions) in THF or acetone in the presence of CO at room temperature selectively afforded the cationic complexes *trans*-[Fe(κ^3 -P,N,P-PNP)(CO)₂X]⁺ (*trans-2b–2g*) in 78–98 % isolated yields (Scheme 1). The respective *cis*-dicarbonyl complexes were not observed and, hence, sterics and also the amine linker (NR) apparently do not influence the preference for a *trans*-dicarbonyl geometry. This is also supported by DFT calculations (vide infra). These complexes are thermally robust red solids that are air stable both in the solid state and in solution for several days. Characterization was accomplished by elemental analysis and ¹H, ¹³C{¹H}, ³¹P{¹H} NMR and IR spectroscopy. In addition, the solid state structures of *trans-2b*, *trans-2d*, *trans-2f*, and *trans-2g* were determined by single-crystal X-ray diffraction.

In the IR spectrum, as expected, the CO ligands exhibit only one band between 1979 and 2031 cm^{−1} for the mutually *trans* CO ligands which are assigned to the asymmetric CO stretching frequency. The symmetric CO stretching band is IR inactive and not observed. The ³¹P{¹H} NMR spectrum of complexes *trans-2b–2g* show singlet resonances at 85.0, 92.3, 100.7, 96.7, 130.6, and 132.8 ppm, respectively. In the ¹³C{¹H} NMR spectrum the two CO ligands exhibit a single low-intensity triplet

resonance in the range of 207.2–211.8 ppm, thus clearly revealing that the two CO ligands are *trans* to one another.

Structural views of *trans-2b*, *trans-2d*, *trans-2f*, and *trans-2g* are depicted in Figs. 1, 2, 3 and 4 with selected bond distances and angles reported in the captions. All complexes adopt a distorted octahedral geometry around the metal center with the CO ligands in *trans* position to one another. The PNP ligand is coordinated to the iron center in a typical tridentate meridional mode, with P–Fe–P angles between 167.8° and 169.1°. The C_(CO)–Fe–C_(CO) angles vary between 168.7° and 174.4°. The compounds with NH linkers show, as a typical feature, hydrogen bonds between the NH-groups of the cationic Fe(PNP) complexes and the counterions BF₄[−] and CF₃SO₃[−].

To better understand why *trans*-dicarbonyl complexes are preferred over *cis*-dicarbonyl complexes, DFT calculations were performed with the N²,N⁶-bis(dimethylphosphanyl)-pyridine-2,6-diamine ligand (PNP-Me) as model. The starting point of our calculations are the coordinatively unsaturated cationic intermediates [Fe(PNP-Me)(CO)Cl]⁺ (**A** and/or **B**), which are formed from *trans*-[Fe(κ^3 -P,N,P-PNP-Me)(CO)Cl₂] (*trans-1c*) upon irreversible removal of chloride with silver salts (Scheme 2). The analogous *cis* isomer is experimentally not accessible. The energy profile (DFT/OPBE) for the *cis/trans* isomerization of [Fe(PNP-Me)(CO)Cl]⁺ is shown in Fig. 5.

According to the calculations both cationic pentacoordinated intermediates **A** and **B** adopt a square pyramidal geometry where the Cl and the CO ligands, respectively, are in the apical position. The singlet ground state ¹**B** is the energetically favored species by 22.6 and 50.7 kJ mol^{−1}, respectively, over the singlet and triplet states of **A** (¹**A**, ³**A**) (Fig. 5). In the case of **B**, no stable triplet state was found. **A** and **B** were found to interconvert readily via two pathways. ¹**A** is able to isomerize along the spin singlet surface (*S* = 0) to give ¹**B** with a small energy barrier of 11.3 kJ mol^{−1}. This reaction proceeds via transition state ¹TS_{AB}. In the second pathway, ¹**A** undergoes two

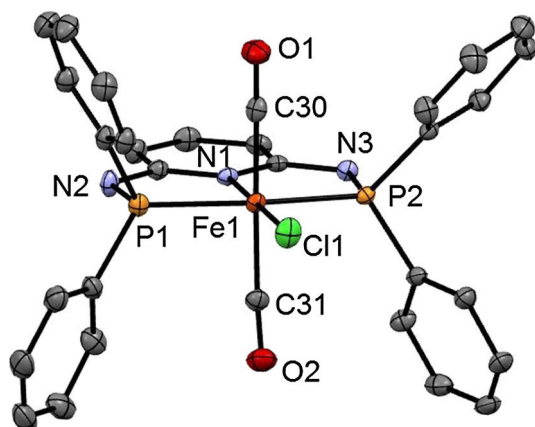


Fig. 1 Structural view of *trans*-[Fe(PNP-Ph)(CO)₂Cl]SbF₆ (*trans*-**2a**) showing 50 % thermal ellipsoids (H atoms and counterion omitted for clarity). Selected bond lengths (Å) and bond angles (°): Fe1–Cl1 2.3029(7), Fe1–P2 2.2190(7), Fe1–P1 2.2317(7), Fe1–C30 1.824(3), Fe1–C31 1.850(3), Fe1–N1 1.977(2), P2–Fe1–P1 168.33(3), C30–Fe1–C31 172.6(1)

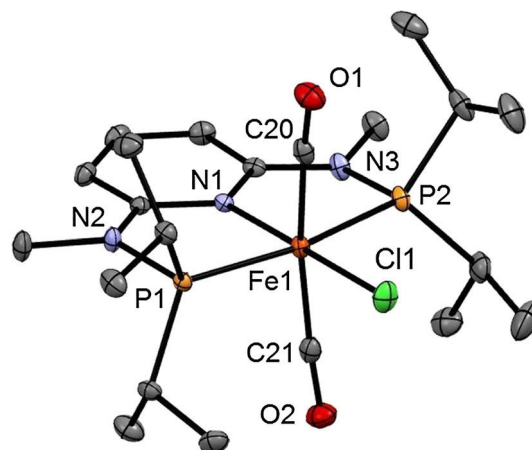


Fig. 3 Structural view of *trans*-[Fe(PNP^{Me}-iPr)(CO)₂Cl]BF₄ (*trans*-**2e**) showing 50 % thermal ellipsoids (H atoms and counterion omitted for clarity). Selected bond lengths (Å) and bond angles (°): Fe1–Cl1 2.3009(5), Fe1–P1 2.2507(5), Fe1–P2 2.2455(5), Fe1–N1 1.976(1), Fe1–C20 1.818(1), Fe1–C21 1.819(1), P1–Fe1–P2 168.33(2), C20–Fe1–C21 168.71(7)

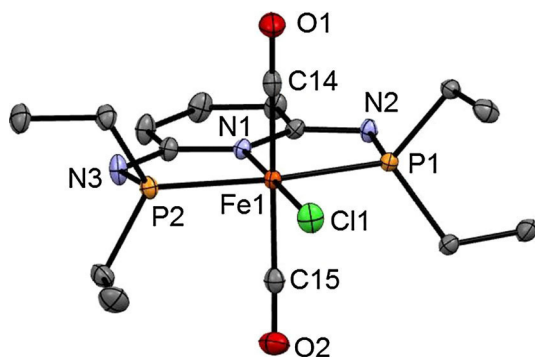


Fig. 2 Structural view of *trans*-[Fe(PNP-Et)(CO)₂Cl]CF₃SO₃ (*trans*-**2c**) showing 50 % thermal ellipsoids (H atoms and counterion omitted for clarity). Selected bond lengths (Å) and bond angles (°): Fe1–Cl1 2.3116(4), Fe1–P1 2.2265(4), Fe1–P2 2.2302(4), Fe1–N1 1.983(1), Fe1–C14 1.823(1), Fe1–C15 1.837(1), P1–Fe1–P2 167.82(2), C14–Fe1–C15 172.15(6)

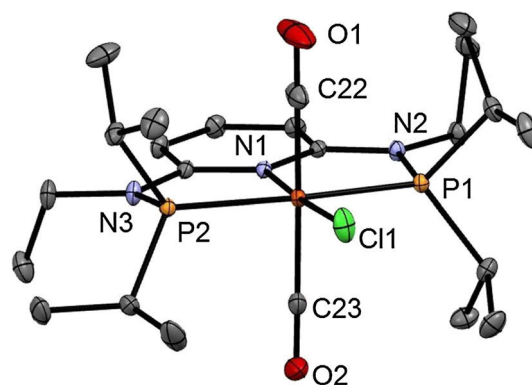


Fig. 4 Structural view of *trans*-[Fe(PNP^{Et}-iPr)(CO)₂Cl]BF₄ (*trans*-**2f**) showing 50 % thermal ellipsoids (H atoms and counterion omitted for clarity). Selected bond lengths (Å) and bond angles (°): Fe1–Cl1 2.3034(3), Fe1–P1 2.2494(3), Fe1–P2 2.2598(3), Fe1–N1 1.9713(7), Fe1–C22 1.8126(10), Fe1–C23 1.8316(8), P1–Fe1–P2 169.14(1), C22–Fe1–C23 174.40(5)

consecutive spin state changes (spin crossover) from $S = 0$ to $S = 1$ and back to $S = 0$. The minimum energy crossing point¹ between the potential energy surfaces of the two spin states $S = 0$ to $S = 1$ (**CP2**) is easily accessible lying merely 1.3 kJ mol^{−1} above ¹**A**. The second spin state change from $S = 1$ to $S = 0$ proceeds via **CP1** with a barrier of 19.3 kJ mol^{−1}.

¹ In the MECP both the energy as well as the geometry of the molecule are the same in the two spin states surfaces. Once that point (MECP) is reached, following the reaction coordinate, there is a given probability for the system to change spin state and hop from one PES to the other, giving rise to the “spin-forbidden” reaction. For more information about MECP and the kinetics of spin-forbidden reactions see for example Ref. [6].

Finally, the experimentally isolated *trans*-**2c** (which is actually is less stable than *cis*-**2c** by 17.2 kJ mol^{−1}) is formed by an essentially barrierless addition of CO to ¹**B** which is the most stable and predominant species lying 50.7 kJ mol^{−1} lower in energy than ¹**A**. In general, CO addition at singlet intermediates is generally more favorable than at triplet intermediates as can be seen by examining the frontier orbitals of the relevant species. The LUMO of the pentacoordinated intermediates with a singlet spin state (¹**A** and ¹**B**) are formed mainly by z^2 -type orbitals centered at the Fe-atom and pointing towards the empty coordination position (Fig. 5). Therefore, these orbitals are ready to receive a pair of electrons from a ligand that occupies the sixth coordination site (CO in this

Scheme 2

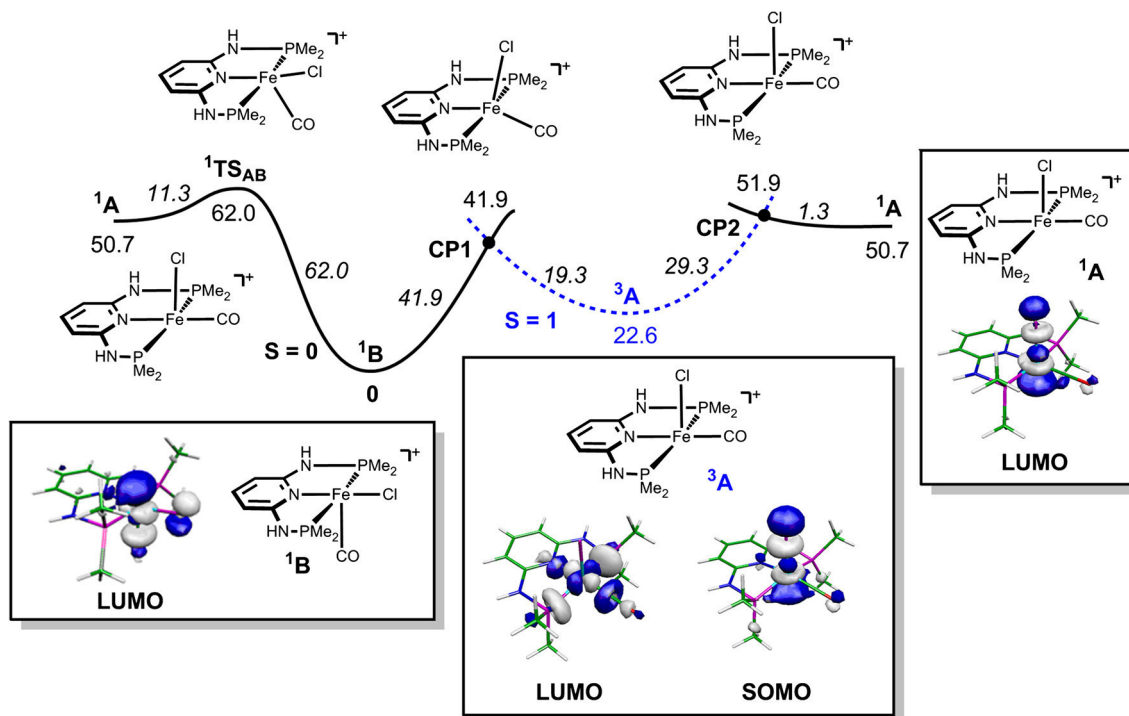
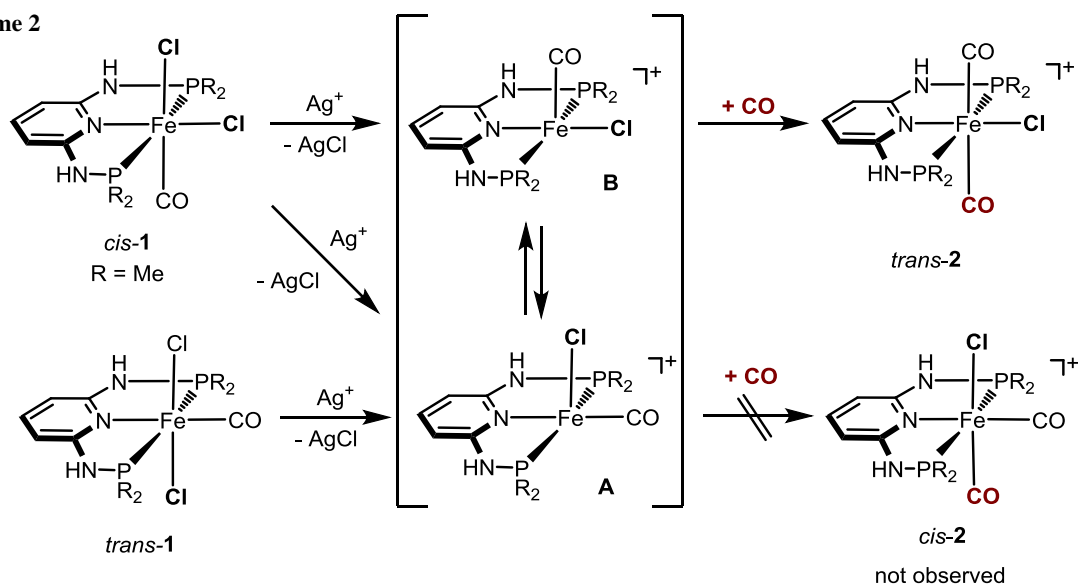


Fig. 5 Energy profile (DFT/OPBE) for the *cis/trans* isomerization of pentacoordinated intermediates $[\text{Fe}(\text{PNP-Me})(\text{CO})\text{Cl}]^+$ with the LUMO's and the SOMO of ^1A , ^1B , and ^3A , respectively. The energy values (kJ mol^{-1}) are referred to the cationic singlet intermediate

$[\text{Fe}(\text{PNP-Me})(\text{CO})\text{Cl}]^+$ (^1B). The plain curve corresponds to the spin singlet surface ($S = 0$) and the dashed curve corresponds to the spin triplet surface ($S = 1$)

case) and establish the corresponding σ -bond. In the case of spin triplet intermediate (^3A), this orbital is occupied being, in fact, the highest single occupied molecular orbital (SOMO) of this species (Fig. 5). This is easily available to receive the electron pair from an incoming CO rendering

addition of this ligand a difficult process. In fact, the first empty orbital (LUMO) in the case of the triplet intermediate corresponds to an x^2-y^2 -type orbital which is centered on the metal and is antibonding (σ^*) with respect to the four ligands in the equatorial plane.

Conclusion

In the present work we have prepared, spectroscopically and structurally characterized several octahedral iron(II) complexes of the type $trans\text{-}[\text{Fe}(\text{PNP})(\text{CO})_2\text{X}]^+$. These complexes are formed irrespective of the size of the substituents at the phosphorus sites and whether $cis\text{-}[\text{Fe}(\text{PNP})(\text{Cl}_2)(\text{CO})]$ or $trans\text{-}[\text{Fe}(\text{PNP})(\text{Cl}_2)(\text{CO})]$ are reacted with CO in the presence of 1 equiv of silver salts. Based on simple bonding considerations the selective formation of $trans\text{-}dicarbonyl$ Fe(II) complexes is unexpected. DFT calculations indeed confirm that $trans\text{-}dicarbonyl$ complexes are thermodynamically disfavored over the respective $cis\text{-}dicarbonyl$ compounds. The key to an understanding of this unexpected selectivity is the fact that upon irreversible removal of a chloride ligand from $[\text{Fe}(\text{PNP})(\text{CO})\text{Cl}_2]$ pentacoordinate intermediates $[\text{Fe}(\text{PNP})(\text{CO})\text{Cl}]^+$ of two conformations, one with the chloride in the apical and CO in the basal position (**A**) and vice versa (**B**), are formed. The subsequent carbonylation process depends strongly on the complex geometry of the 16e intermediates $[\text{Fe}(\text{PNP})(\text{CO})\text{Cl}]^+$, i.e., **A** vs. **B**, which in turn determines the spin state ($S = 0$ or $S = 1$) and consequently the reactivity and also the stability of these intermediates. According to calculations, **B** in the singlet ground state is the most stable and also kinetically the most accessible intermediate in solution. The formation of $trans\text{-}[\text{Fe}(\text{PNP})(\text{CO})_2\text{Cl}]^+$ is kinetically controlled with **1B** being the key intermediate. The mechanism deduced from DFT calculations is in full agreement with experimental findings.

Experimental

All manipulations were performed under an inert atmosphere of argon by using Schlenk techniques or in an MBraun inert-gas glovebox. The solvents were purified according to standard procedures [7]. The deuterated solvents were purchased from Aldrich and dried over 4 Å molecular sieves. Complexes $cis\text{-}[\text{Fe}(\kappa^3\text{P},N,P\text{-PNP-Ph})(\text{CO})\text{Cl}_2]$ (*cis-1b*), $trans\text{-}[\text{Fe}(\kappa^3\text{P},N,P\text{-PNP-Me})(\text{CO})\text{Cl}_2]$ (*trans-1c*), $trans\text{-}[\text{Fe}(\kappa^3\text{P},N,P\text{-PNP-Et})(\text{CO})\text{Cl}_2]$ (*trans-1d*), $trans\text{-}[\text{Fe}(\kappa^3\text{P},N,P\text{-PNP-}n\text{Pr})(\text{CO})\text{Cl}_2]$ (*trans-1e*), $cis/trans\text{-}[\text{Fe}(\text{PNP}^{\text{Me}}\text{-}i\text{Pr})(\text{CO})\text{Cl}_2]$ (*cis/trans-1f*), and $cis/trans\text{-}[\text{Fe}(\text{PNP}^{\text{Et}}\text{-}i\text{Pr})(\text{CO})\text{Cl}_2]$ (*cis/trans-1g*) were prepared according to the literature [8]. ^1H , $^{13}\text{C}\{^1\text{H}\}$, and $^{31}\text{P}\{^1\text{H}\}$ NMR spectra were recorded on Bruker AVANCE-250 and AVANCE-400 spectrometers. ^1H and $^{13}\text{C}\{^1\text{H}\}$ NMR spectra were referenced internally to residual protio-solvent and solvent resonances, respectively, and are reported relative to tetramethylsilane ($\delta = 0$ ppm). $^{31}\text{P}\{^1\text{H}\}$ NMR spectra were referenced externally to H_3PO_4 (85 %) ($\delta = 0$ ppm).

Trans-[(chloro)[N^2,N^6 -bis(diphenylphosphanyl)pyridine-2,6-diamine](dicarbonyl)iron(II)] tetrafluoroborate (*trans*- $[\text{Fe}(\kappa^3\text{P},N,P\text{-PNP-Ph})(\text{CO})_2\text{Cl}]\text{BF}_4$) (*trans-2b*, $\text{C}_{31}\text{H}_{25}\text{BClF}_4\text{FeN}_3\text{O}_2\text{P}_2$)

Complex *cis-1b* (200 mg, 0.316 mmol) was dissolved in 10 cm^3 THF, CO gas was bubbled through the solution and 62 mg AgBF_4 (0.316 mmol) was added. After 4 h the red solution was filtered over Celite and the solvent was evaporated. The red powder was washed with 20 cm^3 Et_2O and dried under vacuum. Yield 180 mg (85 %); ^1H NMR (acetone- d_6 , 20 °C): $\delta = 9.50$ (s, 2H, NH), 8.10 (m, 5H, Ph, py⁴), 7.71 (m, 18H, Ph, py^{3,5}) ppm; $^{13}\text{C}\{^1\text{H}\}$ NMR (CD_2Cl_2): $\delta = 207.2$ (t, $J = 25.8$ Hz, CO), 161.3 (py), 141.8 (py), 134.6–133.2 (Ph), 132.10 (Ph), 131.0–129.8 (Ph), 129.2 (t, $J = 5.4$ Hz, Ph), 102.2 (py) ppm; $^{31}\text{P}\{^1\text{H}\}$ NMR (acetone- d_6 , 20 °C): $\delta = 85.0$ ppm; IR (ATR, 20 °C): $\bar{\nu} = 2031$ ($\nu_{\text{C=O}}$) cm^{-1} .

Trans-[(chloro)[N^2,N^6 -bis(dimethylphosphanyl)pyridine-2,6-diamine](dicarbonyl)iron(II)] trifluoromethanesulfonate (*trans*- $[\text{Fe}(\kappa^3\text{P},N,P\text{-PNP-Me})(\text{CO})_2\text{Cl}]\text{CF}_3\text{SO}_3$) (*trans-2c*, $\text{C}_{12}\text{H}_{17}\text{ClF}_3\text{FeN}_3\text{O}_5\text{P}_2\text{S}$)

CO was bubbled through a suspension of 100 mg *trans-1b* (0.26 mmol) and 67 mg AgCF_3SO_3 (0.26 mmol) in 7 cm^3 acetone. The orange solution was then filtrated over Celite, evaporated to dryness and the obtained solid was washed with 10 cm^3 *n*-hexane. The orange powder was dried under reduced pressure. Yield 134 mg (98 %); ^1H NMR (acetone- d_6 , 20 °C): $\delta = 8.46$ (s, 2H, NH), 7.33 (t, $J_{\text{HH}} = 7.9$ Hz, 1H, py⁴), 6.23 (d, $J_{\text{HH}} = 8.0$ Hz, 2H, py^{3,5}), 2.38 (m, 12H, CH₃) ppm; $^{13}\text{C}\{^1\text{H}\}$ NMR (acetone- d_6 , 20 °C): $\delta = 210.3$ (t, $J_{\text{CP}} = 26.8$ Hz, CO), 162.4 (t, $J_{\text{CP}} = 7.5$ Hz, py), 141.9 (py), 101.1 (t, $J_{\text{CP}} = 3.8$ Hz, py), 18.9 (t, $J_{\text{CP}} = 17.2$ Hz, CH₃) ppm; $^{31}\text{P}\{^1\text{H}\}$ NMR (acetone- d_6 , 20 °C): $\delta = 92.3$ ppm; IR (ATR): $\bar{\nu} = 1979$ (ν_{CO}) cm^{-1} .

Trans-[(chloro)[N^2,N^6 -bis(diethylphosphanyl)pyridine-2,6-diamine](dicarbonyl)iron(II)] trifluoromethanesulfonate (*trans*- $[\text{Fe}(\kappa^3\text{P},N,P\text{-PNP-Et})(\text{CO})_2\text{Cl}]\text{CF}_3\text{SO}_3$) (*trans-2c*, $\text{C}_{16}\text{H}_{25}\text{ClF}_3\text{FeN}_3\text{O}_5\text{P}_2\text{S}$)

This compound was prepared analogously to *trans-2b* with 120 mg *trans-1c* (0.27 mmol) and 70 mg AgCF_3SO_3 (0.27 mmol) as starting materials. The orange product was dried under reduced pressure. Yield: 153 mg (97 %). Crystals were grown from an acetone solution of **2c** by slow diffusion of Et_2O . ^1H NMR (acetone- d_6 , 20 °C): $\delta = 8.49$ (2H, NH), 7.63 (1H, py⁴), 6.31 (d, $J_{\text{HH}} = 5.2$ Hz, 2H, py^{3,5}), 2.90 (4H, CH₂), 2.78 (4H, CH₂), 1.51 (12H, CH₃) ppm; $^{13}\text{C}\{^1\text{H}\}$ NMR (acetone- d_6 , 20 °C): $\delta = 210.5$ (t, $J_{\text{CP}} = 25.2$ Hz, CO), 161.8 (t, $J_{\text{CP}} = 6.9$ Hz, py), 141.1 (py), 100.3 (py), 23.4 (t, $J_{\text{CP}} = 15.3$ Hz, CH₂), 6.4 (CH₃) ppm; $^{31}\text{P}\{^1\text{H}\}$ NMR (acetone- d_6 , 20 °C): $\delta = 100.7$ ppm; IR (ATR): $\bar{\nu} = 2008$ (ν_{CO}) cm^{-1} .

Trans-[(chloro)[N^2, N^6 -bis(dipropylphosphanyl)pyridine-2,6-diamine](dicarbonyl)iron(II)] trifluoromethanesulfonate (*trans*-[Fe(κ^3P, N, P -PNP-*nPr*)(CO)₂Cl]CF₃SO₃) (*trans*-**2d**, C₂₀H₃₃ClF₃FeN₃O₅P₂S)

This compound was prepared analogously to *trans*-**2b** using 150 mg *trans*-**1d** (0.30 mmol) and 78 mg AgCF₃SO₃ (0.30 mmol) as starting materials. The red–orange product was dried under reduced pressure. Yield: 177 mg (92 %); ¹H NMR (acetone-*d*₆, 20 °C): δ = 8.41 (2H, NH), 7.47 (t, J_{HH} = 7.9 Hz, 1H, py⁴), 6.41 (d, J_{HH} = 7.6 Hz, 2H, py^{2,6}), 2.01 (m, 8H, CH₂), 1.58 (m, 8H, CH₂), 1.12 (t, J_{HH} = 7.1 Hz, 12H, CH₃) ppm; ¹³C{¹H} NMR (acetone-*d*₆, 20 °C): δ = 210.4 (t, J_{CP} = 25.6 Hz, CO), 161.7 (t, J_{CP} = 6.8 Hz, py), 140.9 (py), 100.2 (t, J_{CP} = 3.7 Hz, py), 32.8 (t, J_{CP} = 14.3 Hz, CH₂), 16.2 (CH₃), 15.0 (t, J_{CP} = 7.8 Hz, CH₂) ppm; ³¹P{¹H} NMR (acetone-*d*₆, 20 °C): δ = 96.7 ppm; IR (ATR): $\bar{\nu}$ = 2011 (ν_{CO}) cm⁻¹.

Trans-[(chloro)[N^2, N^6 -bis(diisopropylphosphanyl)- N^2, N^6 -dimethylpyridine-2,6-diamine](dicarbonyl)iron(II)] tetrafluoroborate (*trans*-[Fe(κ^3P, N, P -PNP^{Me}-*iPr*)(CO)₂Cl]BF₄) (*trans*-**2e**, C₂₁H₃₇BClF₄FeN₃O₂P₂)

CO was bubbled through a solution of 150 mg *cis/trans*-**1e** (0.30 mmol) and 59 mg AgBF₄ (0.30 mmol) in 15 cm³ of THF. The pink solution was stirred under CO atmosphere for 1 h; then the solvent was removed under reduced pressure. The residue was redissolved in 15 cm³ of CH₂Cl₂, filtered and the volume of the solvent was reduced to about 0.5 cm³. The product was precipitated by addition of 40 cm³ of pentane, collected on a glass frit, washed with 15 cm³ of *n*-pentane, and dried under vacuum. Yield: 141 mg (78 %); ¹H NMR (CD₂Cl₂, 20 °C): δ = 7.53 (t, $^3J_{HH}$ = 8.1 Hz, 1H, py⁴), 6.14 (d, $^3J_{HH}$ = 8.2 Hz, 2H, py^{3,5}), 3.19 (m, 4H, CH(CH₃)₂), 3.08 (s, 6H, NCH₃), 1.53–1.42 (m, 24H, CH(CH₃)₂) ppm; ¹³C{¹H} NMR (CD₂Cl₂, 20 °C): δ = 211.6 (t, $^2J_{CP}$ = 24.7 Hz, CO), 163.0 (vt, $^2J_{CP}$ = 7.4 Hz, py^{2,6}), 142.2 (s, py⁴), 100.2 (vt, $^3J_{CP}$ = 2.7 Hz, py^{3,5}), 35.4 (s, NCH₃), 32.0 (vt, $^1J_{CP}$ = 11.2 Hz, CH(CH₃)₂), 18.5 (s, CH(CH₃)₂), 17.7 (s, CH(CH₃)₂) ppm; ³¹P{¹H} NMR (CD₂Cl₂, 20 °C): δ = 130.6 ppm; IR (ATR): $\bar{\nu}$ = 2002 ($\nu_{C=O}$) cm⁻¹.

Trans-[(chloro)[N^2, N^6 -bis(diisopropylphosphanyl)- N^2, N^6 -diethylpyridine-2,6-diamine](dicarbonyl)iron(II)] tetrafluoroborate (*trans*-[Fe(κ^3P, N, P -PNP^{Et}-*iPr*)(CO)₂Cl]BF₄) (*trans*-**2f**, C₂₃H₄₁BClF₄FeN₃O₂P₂)

This complex was prepared analogously to *trans*-**2e** with 150 mg *cis/trans*-**1f** (0.29 mmol) and 56 mg AgBF₄ (0.29 mmol) as starting materials. Yield: 131 mg (75 %); ¹H NMR (CD₂Cl₂, 20 °C): δ = 7.54 (t, $^3J_{HH}$ = 8.2 Hz, 1H, py⁴), 6.17 (d, $^3J_{HH}$ = 8.2 Hz, 2H, py^{3,5}), 3.58 (m, 4H, NCH₂CH₃), 3.18 (m, CH(CH₃)₂), 1.49–1.10 (m, 30H, NCH₂CH₃, CH(CH₃)₂) ppm; ¹³C{¹H} NMR (CD₂Cl₂, 20 °C): δ = 211.8 (t, $^2J_{CP}$ = 24.8 Hz, CO), 162.3 (vt,

$^2J_{CP}$ = 6.9 Hz, py^{2,6}), 142.4 (s, py⁴), 101.2 (vt, $^3J_{CP}$ = 2.6 Hz, py^{3,5}), 43.3 (s, NCH₂CH₃), 31.4 (vt, $^1J_{CP}$ = 10.8 Hz, CH(CH₃)₂), 19.1 (s, CH(CH₃)₂), 17.8 (s, CH(CH₃)₂), 13.0 (s, NCH₂CH₃) ppm; ³¹P{¹H} NMR (CD₂Cl₂, 20 °C): δ = 132.8 ppm; IR (ATR): $\bar{\nu}$ = 2005 ($\nu_{C=O}$) cm⁻¹.

X-ray structure determination

X-ray diffraction data of *trans*-**2a**, *trans*-**2c**, *trans*-**2e**, and *trans*-**2f** (CCDC entries 1015363 (*trans*-**2a**), 1469956 (*trans*-**2c**), 1469957 (*trans*-**2e**), 1469958 (*trans*-**2f**)) were collected at T = 100 K in a dry stream of nitrogen on Bruker Kappa APEX II diffractometer systems using graphite-monochromatized Mo- $K\alpha$ radiation (λ = 0.71073 Å) and fine sliced φ - and ω -scans. Data were reduced to intensity values with SAINT and an absorption correction was applied with the multi-scan approach implemented in SADABS [9]. The structures of *trans*-**2c**, *trans*-**2e**, and *trans*-**2f** were solved by charge flipping using SUPERFLIP [10] and refined against with JANA2006 [11]. The structure of *trans*-**2a** was solved with direct methods and refined against F^2 with the SHELX software package [12]. Non-hydrogen atoms were refined anisotropically. The H atoms connected to C atoms were placed in calculated positions and thereafter refined as riding on the parent atoms. The H atoms of the amine functionalities were located in difference Fourier maps and freely refined. Molecular graphics were generated with the program MERCURY [13].

Computational details

Calculations were performed using the GAUSSIAN 09 software package, and the OPBE functional without symmetry constraints as already described previously [14].

Acknowledgments Open access funding provided by TU Wien (TUW). Financial support by the Austrian Science Fund (FWF) is gratefully acknowledged (Project No. P28866-N34). The X-ray center of the Vienna University of Technology is acknowledged for financial support and for providing access to the single-crystal diffractometer. LFV acknowledges Fundação para a Ciência e Tecnologia, UID/QUI/00100/2013.

Open Access This article is distributed under the terms of the Creative Commons Attribution 4.0 International License (<http://creativecommons.org/licenses/by/4.0/>), which permits unrestricted use, distribution, and reproduction in any medium, provided you give appropriate credit to the original author(s) and the source, provide a link to the Creative Commons license, and indicate if changes were made.

References

- Benito-Garagorri D, Puchberger M, Mereiter K, Kirchner K (2008) *Angew Chem Int Ed* 47:9142

2. Benito-Garagorri D, Alves LG, Puchberger M, Veiros LF, Calhorda MJ, Carvalho MD, Ferreira LP, Godinho M, Mereiter K, Kirchner K (2009) *Organometallics* 28:6902
3. Benito-Garagorri D, Kirchner K (2008) *Acc Chem Res* 41:201
4. Benito-Garagorri D, Alves LG, Veiros LF, Standfest-Hauser CM, Tanaka S, Mereiter K, Kirchner K (2010) *Organometallics* 29:4923
5. Alves L, Dazinger LG, Veiros LF, Kirchner K (2010) *Eur J Inorg Chem* 3160
6. Harvey JN (2007) *Phys Chem Chem Phys* 9:331
7. Perrin DD, Armarego WLF (1988) *Purification of laboratory chemicals*, 3rd edn. Pergamon Press, New York
8. Glatz M, Holz hacker C, Bichler B, Mastalir M, Stöger B, Mereiter K, Weil M, Veiros LF, Mösch-Zanetti NC, Kirchner K (2015) *Eur J Inorg Chem* 5053
9. Bruker computer programs (2012) APEX2, SAINT, and SADABS. Bruker AXS Inc, Madison
10. Palatinus L, Chapuis G (2007) *J Appl Cryst* 40:786
11. Petříček V, Dušek M, Palatinus L (2006) JANA2006, the crystallographic computing system. Institute of Physics, Praha
12. Spek AL (2009) *Acta Cryst D* 65:148
13. Macrae CF, Edgington PR, McCabe P, Pidcock E, Shields GP, Taylor R, Towler M, van de Streek J (2006) *J Appl Cryst* 39:453
14. Schröder-Holz hacker C, Stöger B, Pittenauer E, Allmaier G, Veiros LF, Kirchner K (2016) *Monatsh Chem.* doi:[10.1007/s00706-016-1731-9](https://doi.org/10.1007/s00706-016-1731-9)

Manuscript #4

“Chemoselective Hydrogenation of Aldehydes under Mild, Base-Free Conditions - Manganese Outperforms Rhenium”

Glatz M.; Stöger B.; Himmelbauer D.; Veiros L. F.; Kirchner K. *ACS Catal.* **2018**, 8, 4009-4016.

DOI: 10.1021/acscatal.8b00153

Reproduced by permission of ACS Catalysis

Copyright 2018 American Chemical Society

Chemoselective Hydrogenation of Aldehydes under Mild, Base-Free Conditions: Manganese Outperforms Rhenium

Mathias Glatz,[†] Berthold Stöger,[§] Daniel Himmelbauer,[†] Luis F. Veiros,[‡] and Karl Kirchner^{*,†,‡}

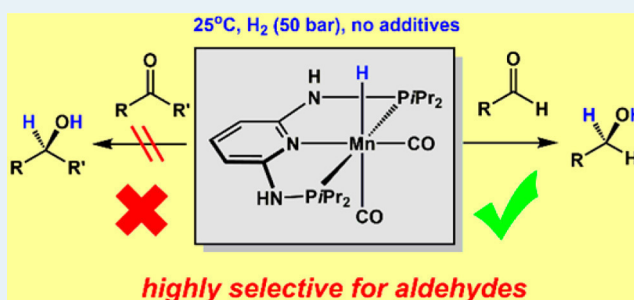
[†]Institute of Applied Synthetic Chemistry and [§]X-Ray Center, Vienna University of Technology, Getreidemarkt 9, A-1060 Vienna, Austria

[‡]Centro de Química Estrutural, Instituto Superior Técnico, Universidade de Lisboa, Av. Rovisco Pais No. 1, 1049-001 Lisboa, Portugal

Supporting Information

ABSTRACT: Several hydride Mn(I) and Re(I) PNP pincer complexes were applied as catalysts for the homogeneous chemoselective hydrogenation of aldehydes. Among these, [Mn(PNP-*i*Pr)(CO)₂(H)] was found to be one of the most efficient base metal catalysts for this process and represents a rare example which permits the selective hydrogenation of aldehydes in the presence of ketones and other reducible functionalities, such as C=C double bonds, esters, or nitriles. The reaction proceeds at room temperature under base-free conditions with catalyst loadings between 0.1 and 0.05 mol% and a hydrogen pressure of 50 bar (reaching TONs of up to 2000). A mechanism which involves an outer-sphere hydride transfer and reversible PNP ligand deprotonation/protonation is proposed. Analogous isoelectronic and isostructural Re(I) complexes were only poorly active.

KEYWORDS: hydrogenation, aldehydes, manganese, pincer complexes, DFT calculations



INTRODUCTION

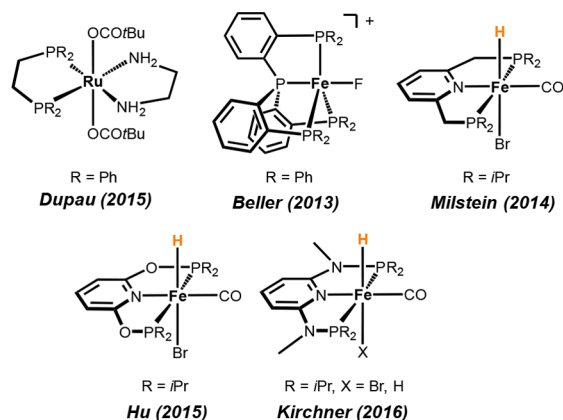
One environmentally friendly and sustainable method to prepare alcohols, which are valuable commodities for a large number of fine and bulk chemicals, is the catalytic hydrogenation of carbonyl compounds with dihydrogen.¹ Over the years, many highly efficient and active homogeneous catalysts based on precious but also non-precious metals have been described for this purpose (Scheme 1).² Especially catalysts which reveal full selectivity for aldehydes over ketones and/or alkenes^{3,4} are of

practical importance for the synthesis of flavors,⁵ fragrances,³ and pharmaceuticals.⁶

In the past couple of years, the development and advancement of hydrogenation catalysts based on earth-abundant, inexpensive non-precious metals experienced tremendous progress.⁷ In particular, iron- and manganese-based catalysts turned out to be highly active for the hydrogenation of carbonyl compounds, imines, and nitriles (Scheme 2).^{8–11} In the case of manganese, however, most hydrogenations proceed at relatively high catalyst loadings and elevated temperatures and, in addition, require large amounts of strong bases as additives. As yet, only iron-based systems proved to be reasonably chemoselective for the reduction of aldehydes, as shown in Scheme 1.^{12–14} We recently described the application of [Fe(PNP^{Me}-*i*Pr)(CO)(H)(Br)] and [Fe(PNP^{Me}-*i*Pr)(H)₂(CO)] as highly active catalysts for the homogeneous hydrogenation of aldehydes (Scheme 1).^{15,16}

In this paper, we describe an experimental and theoretical investigation of the chemoselective hydrogenation of aldehydes with dihydrogen using several hydride Mn(I) and Re(I) PNP pincer complexes as catalysts (Scheme 3). To the best of our knowledge, this is the first example of an efficient manganese-based selective hydrogenation of aldehydes which proceeds under mild and base-free conditions with low catalyst loadings. It

Scheme 1. Well-Defined Catalysts for the Chemoselective Hydrogenation of Aldehydes

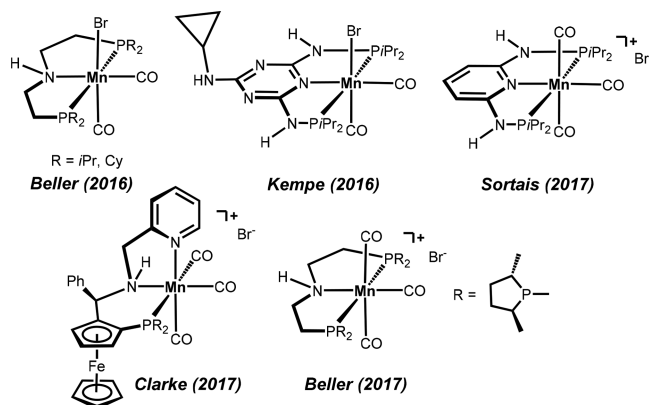
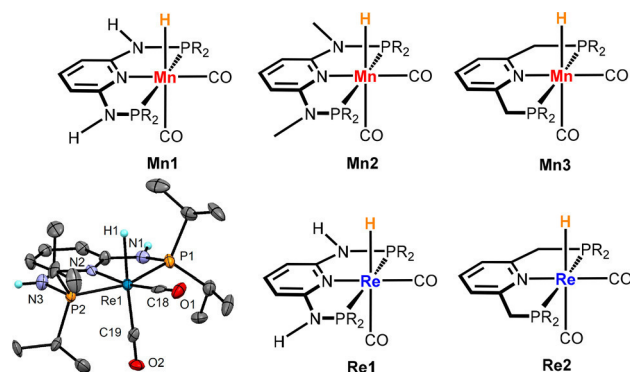


Received: January 12, 2018

Revised: March 20, 2018

Published: April 2, 2018

Scheme 2. Manganese Catalysts for the Hydrogenation of Ketones and Aldehydes

Scheme 3. PNP Pincer Complexes Tested as Catalysts for the Hydrogenation of Aldehydes (R = *i*Pr) and Structural View of Re1 Showing 30% Thermal Ellipsoids^a

^aSelected bond lengths (Å) and angles (°): Re1–P1 2.347(3), Re1–P2 2.342(3), Re1–N2 2.162(8), Re1–C18 1.87(1), Re1–C19 1.94(1), Re1–H1 1.91(5), P1–Re1–P2 158.2(1).

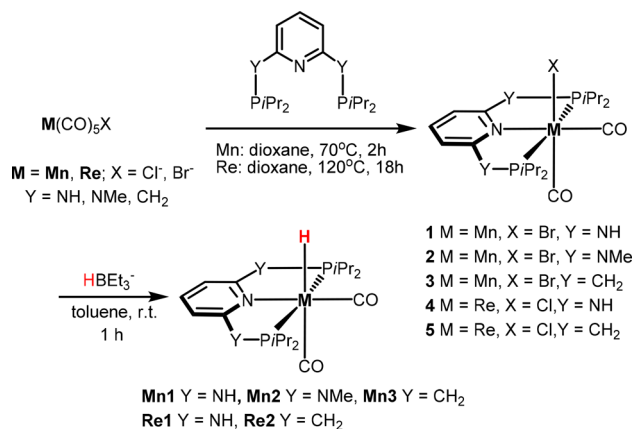
has to be noted that Re pincer complexes have rarely been used in (de)hydrogenation catalysis.^{17,18}

RESULTS AND DISCUSSION

The reaction of $[M(\text{CO})_5\text{X}]$ ($M = \text{Mn}$, $X = \text{Br}$; $M = \text{Re}$, $X = \text{Cl}$) with the respective PNP pincer ligands in dioxane at elevated temperatures afforded the neutral biscarbonyl complexes $[M(\text{PNP})(\text{CO})_2\text{X}]$ (**1–5**) (Scheme 4). Treatment of these intermediates with $\text{Na}[\text{HBET}_3]$ (1.1 equiv) in toluene afforded complexes **Mn1**, **Mn2**, **Mn3**, **Re1**, and **Re2**. The synthesis of **Mn1** and **Mn2** was already reported previously.¹⁹ All new complexes could be isolated in 77–95% isolated yields and were fully characterized by a combination of elemental analysis, ^1H , $^{13}\text{C}\{^1\text{H}\}$, and $^{31}\text{P}\{^1\text{H}\}$ NMR, and IR spectroscopy (see Supporting Information (SI)). In addition, the molecular structure of **Re1** was determined by X-ray crystallography (Scheme 3, bottom left).

The catalytic performance of **Mn1**, **Mn2**, **Mn3**, **Re1**, and **Re2** was then investigated for the hydrogenation of aldehydes. The experiments were performed in EtOH as solvent using 4-fluorobenzaldehyde as model substrate to find the most active catalyst and optimal hydrogenation reaction conditions (Table 1). No reaction took place in aprotic solvents such as THF or toluene at 50 bar H_2 , a catalyst loading of 1.0 mol%, and a reaction time of 18 h. In the absence of dihydrogen, the

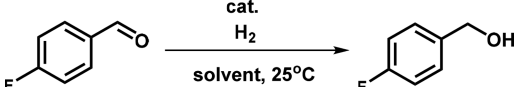
Scheme 4. Synthesis of Hydride Mn(I) and Re(I) PNP Pincer Complexes



hydrogenation of 4-fluorobenzaldehyde to yield 4-fluorobenzyl alcohol was not observed—no reaction took place. Thus, a possible transfer-hydrogenation mechanism in EtOH could be excluded. It has to be further emphasized that ketones, e.g., acetophenone and 4-fluoroacetophenone, did not react with any of the catalysts tested under the same reaction conditions described below.

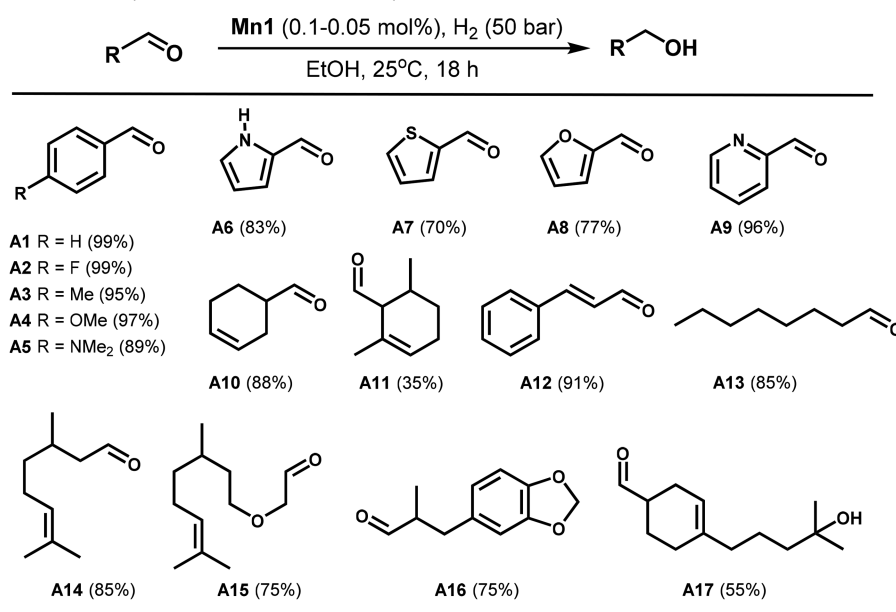
When **Mn1** (0.1 mol%) was used as catalyst, complete conversion was observed after 4 h under a hydrogen pressure of 30 bar (Table 1, entry 4). By lowering the catalyst loading to 0.05 mol%, quantitative conversion was achieved after 18 h at a hydrogen pressure of 50 bar (Table 1, entry 5). If the reaction was performed in the presence of 3 equiv of DBU (1,8-diazabicyclo[5.4.0]undec-7-ene) as external base, 4-fluorobenzyl alcohol was obtained in 52% yield after 48 h under a hydrogen pressure of 50 bar and a catalyst loading of 0.005 mol% (Table 1, entry 6). This corresponds to a turnover number (TON) of 10400. Complexes **Mn2** and **Mn3** showed no or poor reactivity, even with a catalyst loading of 1 mol% (Table 1, entries 7 and 8). Surprisingly, the Re(I) complexes **Re1** and **Re2** with 1 mol% catalyst loadings were poorly active, affording only 45 and 76%, respectively, of 4-fluorobenzyl alcohol (Table 1, entries 9 and 11). At 50 °C, 4-fluorobenzyl alcohol was obtained in 95% yield (Table 1, entry 10).

Once **Mn1** was determined to be the most active catalyst and its general applicability proved, various substrates were tested to establish scope and limitations (Table 2). The catalytic experiments were conducted in the presence of 0.1–0.05 mol% of catalyst at 25 °C and 50 bar hydrogen pressure, for a reaction time of 18 h, without addition of any additives. The best results could be obtained for aromatic aldehydes bearing electron-withdrawing halogen substituents as well as electron-donating groups such as 4-anisaldehyde and 4-tolylaldehyde on the phenyl ring (Table 2, A1–A5) where catalyst loadings of 0.05 mol% were employed. Heteroaromatic substrates as well as aliphatic aldehydes could be reduced quantitatively under the same reaction conditions but with a catalyst loading of 0.1 mol% (Table 2, A6–A17). Substrates with conjugated and non-conjugated C=C double bonds were also selectively hydrogenated. For instance, citronellal or linal, which are used in the flavor and fragrance industry (Table 2, A14–A17), as well as the more challenging α,β -unsaturated substrate cinnamaldehyde (Table 2, A12) were not hydrogenated. In order to investigate the catalyst's selectivity toward substrates with other unsaturated functionalities which can be easily hydrogenated, additional

Table 1. Hydrogenation of 4-Fluorobenzaldehyde with Several Manganese and Rhenium Catalysts^a


entry	cat.	solvent	S/C	P (bar)	t (h)	conversion (%) ^b	TON
1	Mn1	THF	1000	50	18		
2	Mn1	toluene	1000	50	18		
3	Mn1	EtOH	1000	30	1	54	540
4	Mn1	EtOH	1000	30	4	>99	1000
5	Mn1	EtOH	2000	50	18	>99	2000
6 ^c	Mn1	EtOH	20000	50	48	52	10400
7	Mn2	EtOH	100	50	18		
8	Mn3	EtOH	100	50	18	21	21
9	Re1	EtOH	100	50	18	86	86
10 ^d	Re1	EtOH	100	50	18	95	95
11	Re2	EtOH	100	50	18	76	76

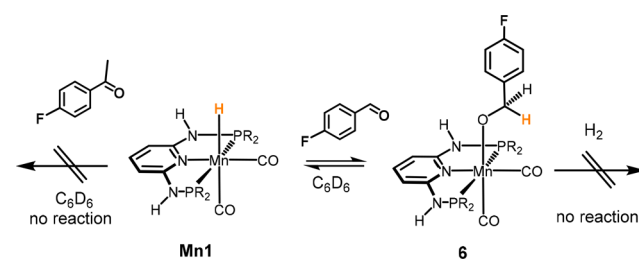
^aReaction conditions: catalysts (0.4–20.0 μmol), 4-fluorobenzaldehyde (2.0 mmol), EtOH (4 mL), 50 bar H₂, 25 °C. ^bDetermined by ¹⁹F NMR spectroscopy. ^cIn the presence of DBU (1.2 μmol , 3 equiv). ^dPerformed at 50 °C.

Table 2. Hydrogenation of Aldehydes A1–A17 with Catalyst Mn1^{a,b}

^aReaction conditions: A1–A5 (1.0 μmol , 0.05 mol% Mn1), A6–A17 (2.0 μmol , 0.1 mol% Mn1), aldehyde (2 mmol), EtOH (4 mL), 50 bar H₂, 25 °C, 18 h. ^bYields (in parentheses) based on integration of ¹H spectra using mesitylene as internal standard.

studies were carried out. Competitive experiments were carried out using equimolar mixtures of 4-fluorobenzaldehyde and the respective co-substrates at a catalyst-to-substrate ratio of 1:1000 with respect to the aldehyde. These studies showed that ketones, esters, alkynes, and nitrile groups were not hydrogenated. Moreover, these functionalities also did not interfere with the hydrogenation of the aldehyde moieties.

Stoichiometric experiments show that Mn1 reacts readily with aldehydes, even in aprotic solvents such as benzene or THF. The addition of 1 equiv of 4-fluorobenzaldehyde to a solution of the Mn(I) hydride Mn1 in C₆D₆ revealed the formation of a new but minor manganese species (Scheme 5). The concentration of this compound did not change over time but grew with increasing amount of added substrate. Thus, addition of up to 20 equiv of aldehyde was required to observe complete conversion of the manganese hydride complex. The new compound was tentatively assigned as the alkoxide complex 6, generated by

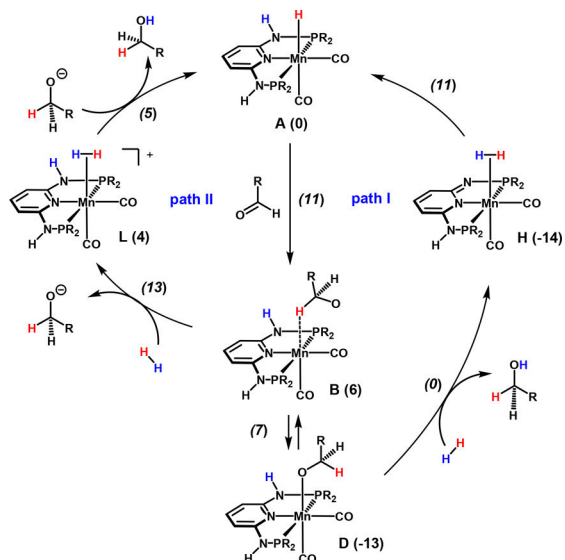
Scheme 5. Reaction of Mn1 with 4-Fluorobenzaldehyde and 4-Fluoroacetophenone in C₆D₆

insertion of the aldehyde into the metal hydride bond of Mn1. Compound 6 could not be isolated and exhibited singlet resonances at 115.8 and 140.9 ppm in the ¹⁹F{¹H} and ³¹P{¹H} NMR spectra, respectively (free 4-fluorobenzyl alcohol exhibits a singlet at 116.1 ppm in the ¹⁹F{¹H} NMR spectrum). In the IR

spectrum, **6** displays the expected two signals of the symmetric and asymmetric CO stretching frequency at 1925 and 1848 cm^{-1} (cf. 1873 and 1790 cm^{-1} in **Mn1**). However, no further reaction took place when a benzene (or THF) solution of the *in situ*-generated alkoxide complex **6** was exposed to dihydrogen. There was also no catalytic reaction if a 3:1 mixture of THF/EtOH was used. Accordingly, EtOH as solvent is not required for the insertion step but obviously plays a crucial role in the subsequent dihydrogen activation step. Moreover, **Mn1** did not react with 4-fluoroacetophenone in both aprotic and protic solvents.

The reaction mechanism was explored in detail by means of DFT calculations.²⁰ Benzaldehyde was taken as substrate and **Mn1** (**A** in the calculations) as active catalyst. An explicit ethanol molecule (solvent) was considered, providing a proton shuttle and H-bond stabilization of the intermediates. Two different paths were considered, as shown in a simplified manner in **Scheme 6**. The more likely one proceeds via participation of the

Scheme 6. Simplified Catalytic Cycles for Benzaldehyde Hydrogenation with Mn1^a



^aFree energies in kcal/mol are referred to **A** (**Mn1** + EtOH + benzaldehyde); transition state energies are given in italics; R = *i*Pr).

acidic N–H bond of the PNP ligand in a bifunctional mechanism (path I). This is supported by the fact that catalyst **Mn2**, bearing NMe linkers, is catalytically inactive and **Mn3**, featuring CH₂ linkers which are less acidic than the NH linkers in **Mn1**, is only poorly active (**Table 1**, entry 8).

A reasonable mechanism has been established by means of DFT calculations. The free energy profile for path I is depicted in **Figure 1**. The first step is the attack of the hydride ligand in complex **A** to the carbonyl C-atom of a free benzaldehyde molecule. The result is intermediate **B**, a species with the resulting alkoxide weakly bonded to the metal by one C–H bond. This is a fairly easy step with a barrier of 11 kcal/mol and a free energy balance of $\Delta G = 6$ kcal/mol, indicating that **B** is less stable than the initial reactants. The alkoxide in **B** can easily leave the metal following a dissociative path, through intermediate **C**. From here, the alkoxide may coordinate the metal by the O-atom, forming **D** through an easy process involving proton exchange with the solvent (**SI**, **Figure S1**). Importantly, the alkoxide complex **D** is 13 kcal/mol more stable than the initial reagents and represents the catalyst resting state. Naturally, there

can be proton exchange between the solvent, EtOH, and benzyl alkoxide. Thus, the subsequent species may be either one. Following the profile in **Figure 1**, the coordinated alkoxide in **D** is protonated by the N–H proton of the PNP arm, with assistance of the ethanol molecule, from **D** to **E**. This process has a barrier of 13 kcal/mol and is endergonic, with $\Delta G = 7$ kcal/mol. Intermediate **F** is 3 kcal/mol more stable than the reactants and features a dearomatized PNP ligand. The HOMO and LUMO of complex **F** are depicted in **Figure 2**. The HOMO corresponds to the ligand π -system, with a significant contribution of the lone pair of the deprotonated N-atom. The LUMO is essentially metal z^2 pointing toward the empty coordination position.

The reaction continues along the profile represented in **Figure 3**, **F'** being equivalent to **F** with a different relative orientation of the three molecules. Exchange of benzyl alcohol by one H₂ molecule produces intermediate **G**. Dihydrogen coordination is facile, with a barrier of only 1 kcal/mol (**TS_{GH}**) in a clearly exergonic step, $\Delta G = -9$ kcal/mol. The resulting intermediate **H** is an η^2 -H₂ complex, which is 14 kcal/mol more stable than the initial reagents. Rearrangement of the H-bond network between the H₂ complex and the nearby ethanol molecule changes **H** into **I**. In the final step, there is splitting of the H–H bond with re-protonation of the PNP N-atom and regeneration of the hydride ligand in **J**, corresponding to the initial reactant **A** and an ethanol molecule. The last step is exergonic, with **J** being 25 kcal/mol more stable than **A**. Despite the presence of an ethanol molecule acting as a proton shuttle, the associated barrier is significant ($\Delta G^\ddagger = 21$ kcal/mol). The highest barrier along path I is 25 kcal/mol, corresponding to the difference between intermediate **H**, the most stable one, and transition state **TS_{IJ}**.

For comparison, the first step of the mechanism was also calculated for acetophenone as substrate. The barrier for the attack of the hydride ligand in complex **A** to the carbonyl C-atom of a free acetophenone molecule is significantly higher than the one calculated for benzaldehyde (18 vs 11 kcal/mol, respectively; **SI**, **Figure S2**). This trend is in accordance with the fact that ketones are not hydrogenated under the same reaction conditions. The remarkable substrate selectivity was recently also explained by the relative stability of alkoxide intermediates formed upon aldehyde insertion into the metal–H bond in the case of related iron PNP pincer complexes based on DFT calculations.²¹ It has to be noted that the related Mn(I) PNP pincer complex [Mn(PNP-*i*Pr)(CO)₃]Br (**Scheme 2**) was shown to act as a catalyst for the hydrogenation of ketones but at a catalyst loading of 5 mol%, a temperature of 130 °C in the presence of 10 mol% base, and a hydrogen pressure of 50 bar in toluene as solvent.^{10d}

The alternative mechanism (path II) shares the first part in **Figure 1** until formation of the cationic intermediate **C**. Following the profile represented in **Figure 4**, addition of H₂ to **C** yields intermediate **K**. From here, coordination of dihydrogen is easy, with a barrier of merely 1 kcal/mol (**TS_{KL}**) in an exergonic step ($\Delta G = -8$ kcal/mol). The difference between the two mechanisms is that while here H₂ coordinates to complex [Mn(PNP)(CO)₂]⁺, producing the cationic dihydrogen complex [Mn(PNP)(η^2 -H₂)(CO)₂]⁺, in path I that process occurs with the neutral metallic species [Mn(PNP')(CO)₂], featuring a deprotonated PNP ligand (PNP'), and yields the corresponding neutral H₂ complex: [Mn(PNP')(η^2 -H₂)(CO)₂]. The mechanism proceeds from **L** with protonation of the free alkoxide by means of the coordinated H₂. The associated barrier (**TS_{LM}**) is negligible (1 kcal/mol), and the resulting species (**M**) is 13 kcal/

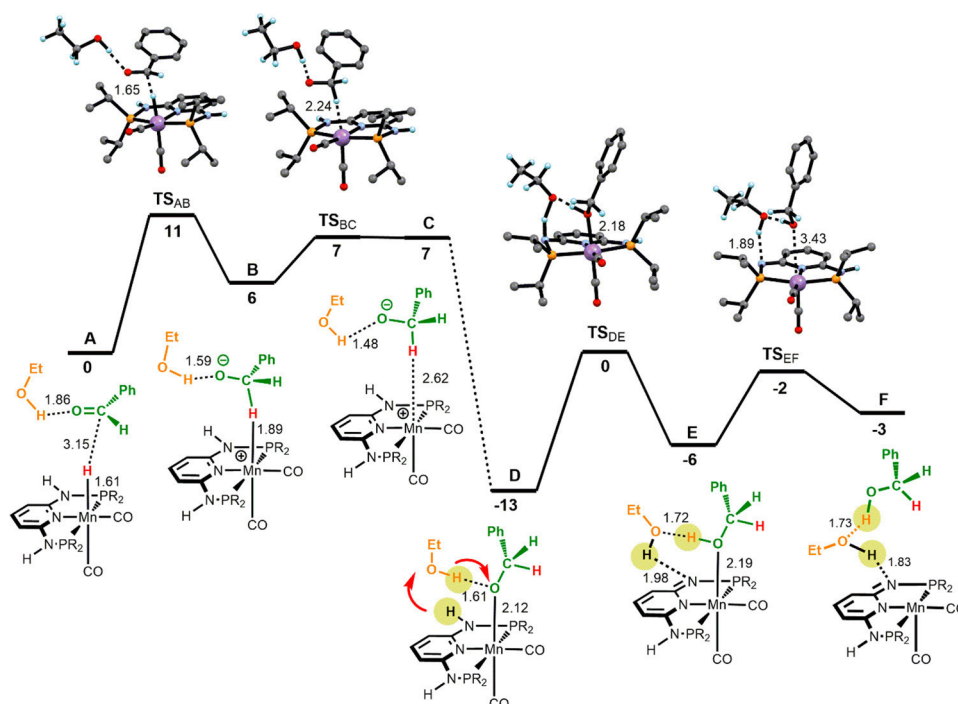


Figure 1. Free energy profile calculated for the hydrogenation of benzaldehyde catalyzed by the hydride complex **A** with ligand *N*-H bond participation. Free energies (kcal/mol) are referred to the initial reactants (**A**), and relevant distances (Å) are presented.

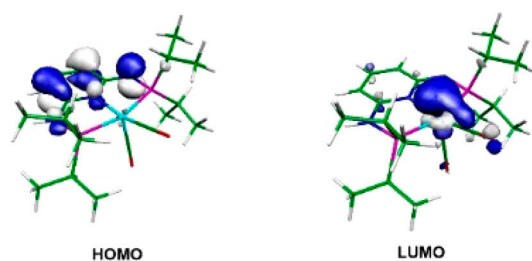


Figure 2. HOMO and LUMO of deprotonated **Mn1** (F in calculations).

mol more stable than **A**. The highest barrier in path II is 26 kcal/mol, measured between the O-coordinated alkoxide complex **D** and the highest following transition state **TS_{KL}**. This is the

transition state associated with H₂ coordination and formation of the dihydrogen complex in **L**. It has to be noted that the same reaction pathway was recently established for the chemoselective hydrogenation of aldehydes catalyzed by [Fe(PNP^{Me}-iPr)(CO)-(H)(Br)], where metal–ligand cooperation was not possible due to NMe linkers.¹⁵

In path I, alkoxide protonation is accomplished by the *N*-H proton in the PNP ligand, yielding a metallic fragment with a dearomatized PNP ligand. This corresponds to a bifunctional mechanism with participation of the PNP ligand that is further regenerated by the coordinated H₂ molecule. In path II, there is no participation of the PNP ligand, and alkoxide protonation is made directly by the coordinated H₂ molecule. The difference between the highest barriers calculated for the two mechanisms is

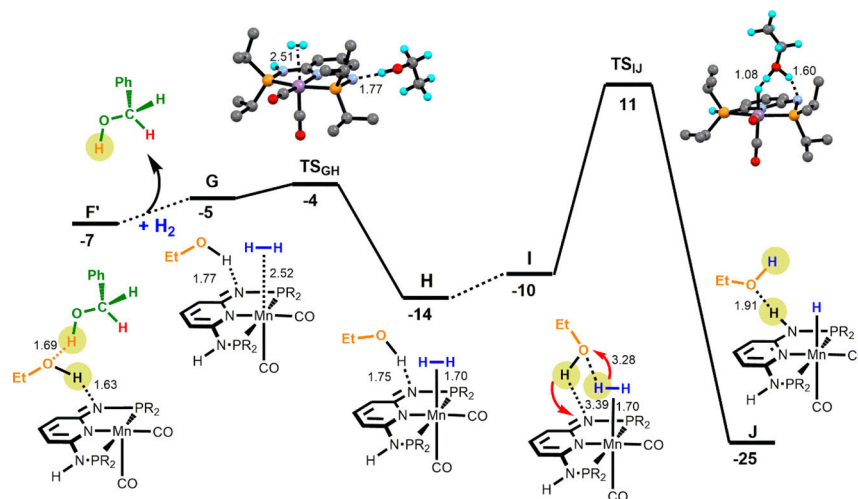


Figure 3. Free energy profile calculated for the hydrogenation of benzaldehyde catalyzed by the hydride complex **A** in a bifunctional mechanism with ligand *N*-H bond participation. The free energy values (kcal/mol) are referred to the initial reactants (**A**), and relevant distances (Å) are presented.

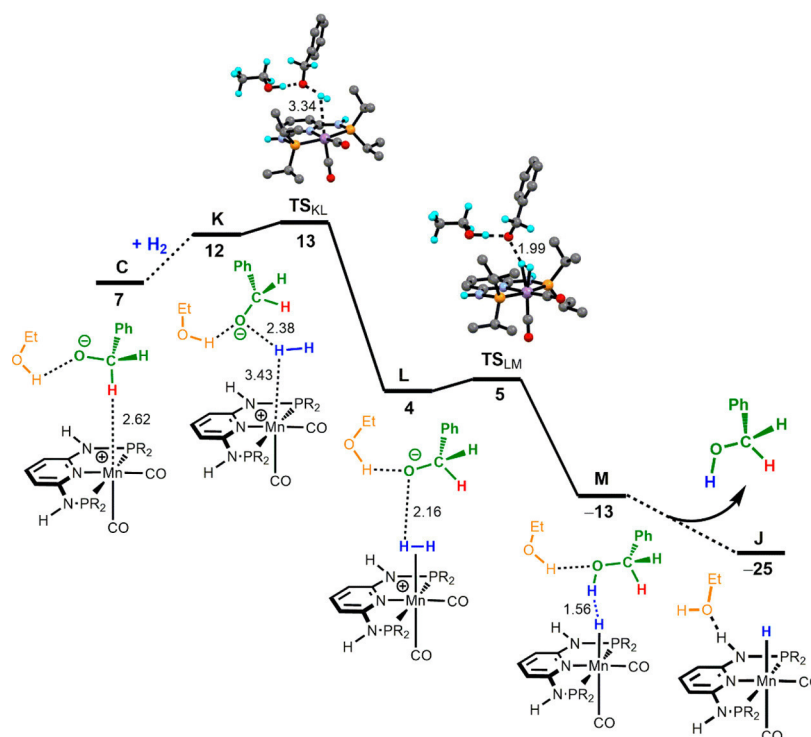


Figure 4. Free energy profile calculated for the hydrogenation of benzaldehyde catalyzed by the hydride complex A *without ligand N–H bond participation*. The free energy values (kcal/mol) are referred to the initial reactants (A), and relevant distances (Å) are presented.

only 1 kcal/mol (25 kcal/mol for path I, 26 kcal/mol for path II); thus, in principle, both could occur under the experimental conditions. If entropy corrections for non-standard conditions are considered, the total barrier for path I rises to 26.5 kcal/mol due to the lower molecularity of TS_{II} when compared to TS_{KL} and to the reaction conditions. This makes path I slightly less favorable than path II.

CONCLUSION

Several hydride Mn(I) and Re(I) PNP pincer complexes were prepared and tested as catalysts for the homogeneous chemoselective hydrogenation of aldehydes. [Mn(PNP-*i*Pr)(CO)₂(H)] (**Mn1**), based on the 2,6-diaminopyridine scaffold, where the *Pi*Pr₂ moieties of the PNP ligand connect to the pyridine ring via NH linkers, was found to be the most efficient catalyst for this process. The reaction is highly chemoselective also in the presence of other functional groups which can be hydrogenated, such as ketones, esters, alkynes, olefins, nitriles, and α,β -unsaturated double bonds. The low catalyst loadings (0.1–0.05 mol%), mild and base-free reaction conditions (25 °C, 50 bar H₂), and broad applicability make this catalyst interesting for the syntheses of fine and bulk chemicals. The catalysis works also with lower catalyst loadings (0.005 mol%) but requires then the addition of an external base. Based on experimental and computational studies, a bifunctional mechanism with participation of the PNP ligand (deprotonation/protonation) is proposed. An alternative mechanism without participation of the PNP ligand cannot be fully dismissed but seems to be less likely. Surprisingly, analogous isoelectronic and isostructural Re(I) complexes turned out to be only poorly active.

ASSOCIATED CONTENT

Supporting Information

The Supporting Information is available free of charge on the ACS Publications website at DOI: 10.1021/acscatal.8b00153.

Complete crystallographic data, ¹H, ¹³C{¹H}, and ³¹P{¹H} NMR spectra of all new complexes, and computational details (PDF)

Crystallographic details for **Re1** (CCDC entry 1815730) (CIF)

Coordinates of all optimized species (XYZ)

AUTHOR INFORMATION

Corresponding Author

*E-mail: karl.kirchner@tuwien.ac.at. Tel.: (+43) 1 58801 163611. Fax: (+43) 1 58801 16399.

ORCID

Karl Kirchner: 0000-0003-0872-6159

Notes

The authors declare no competing financial interest.

ACKNOWLEDGMENTS

Financial support by the Austrian Science Fund (FWF) is gratefully acknowledged (Project No. P29584-N28). L.F.V. acknowledges Fundação para a Ciência e Tecnologia, Projecto Estratégico - PEst-OE/QUI/UI0100/2013.

REFERENCES

- (1) (a) de Vries, J. G.; Elsevier, C. J., Eds. *Handbook of Homogeneous Hydrogenation*; Wiley-VCH: Weinheim, 2007. (b) Dupau, P. In *Organometallics as Catalysts in the Fine Chemical Industry*; Beller, M., Blaser, H. U., Eds.; Springer-Verlag: Berlin, 2012. (c) Johnson, N. B.; Lennon, I. C.; Moran, P. H.; Ramsden, J. A. *Industrial-Scale Synthesis and Applications of Asymmetric Hydrogenation Catalysts*. *Acc. Chem.*

Res. **2007**, *40*, 1291–1299. (d) Dub, P. A.; Ikariya, T. Catalytic Reductive Transformations of Carboxylic and Carbonic Acid Derivatives Using Molecular Hydrogen. *ACS Catal.* **2012**, *2*, 1718–1741.

(2) (a) Noyori, R.; Ohkuma, T. Rapid, productive and stereoselective hydrogenation of ketones. *Pure Appl. Chem.* **1999**, *71*, 1493–1501. (b) Noyori, R.; Ohkuma, T. Asymmetric Catalysis by Architectural and Functional Molecular Engineering: Practical Chemo- and Stereoselective Hydrogenation of Ketones. *Angew. Chem., Int. Ed.* **2001**, *40*, 40–73. (c) Noyori, R. Asymmetric Catalysis: Science and Opportunities (Nobel Lecture). *Angew. Chem., Int. Ed.* **2002**, *41*, 2008–2022. (d) Ohkuma, H.; Ooka, T.; Ikariya, R.; Noyori, R. Preferential hydrogenation of aldehydes and ketones. *J. Am. Chem. Soc.* **1995**, *117*, 10417–10418. (e) Baldino, S.; Facchetti, S.; Zanotti-Gerosa, A.; Nedden, H. G.; Baratta, W. Transfer Hydrogenation and Hydrogenation of Commercial-Grade Aldehydes to Primary Alcohols Catalyzed by 2-(Aminomethyl)pyridine and Pincer Benzo[h]quinoline Ruthenium Complexes. *ChemCatChem* **2016**, *8*, 2279–2288.

(3) Bonomo, L.; Kermorvan, L.; Dupau, P. Ruthenium-Catalyzed Highly Chemoselective Hydrogenation of Aldehydes. *ChemCatChem* **2015**, *7*, 907–910.

(4) (a) Casey, C. P.; Strotman, N. A.; Beetner, S. E.; Johnson, J. B.; Priebe, D. C.; Guzei, I. A. PPh₃-Substituted [2,5-Ph₂-3,4-Tol₂(η⁵-C₄COH)]Ru(CO)(PPh₃)₂H Exhibits Slower Stoichiometric Reduction, Faster Catalytic Hydrogenation, and Higher Chemoselectivity for Hydrogenation of Aldehydes over Ketones Than the Dicarboxyl Shvo Catalyst. *Organometallics* **2006**, *25*, 1236–1244. (b) Diab, L.; Smejkal, T.; Geier, J.; Breit, B. Supramolecular Catalyst for Aldehyde Hydrogenation and Tandem Hydroformylation–Hydrogenation. *Angew. Chem., Int. Ed.* **2009**, *48*, 8022–8026.

(5) (a) Surburg, H., Panten, J., Eds. *Common Fragrance and Flavor Materials*; Wiley-VCH: Weinheim, 2006. (b) Saudan, L. A. Hydrogenation Processes in the Synthesis of Perfumery Ingredients. *Acc. Chem. Res.* **2007**, *40*, 1309–1319.

(6) (a) Smith, A. B.; Barbosa, J.; Wong, W.; Wood, J. L. Total Syntheses of (+)-Trienomycins A and F via a Unified Strategy. *J. Am. Chem. Soc.* **1996**, *118*, 8316–8328. (b) Kobayakawa, Y.; Nakada, M. J. Enantioselective total synthesis of (A)-cyathin B2. *J. Antibiot.* **2014**, *67*, 483–485.

(7) Bullock, R. M., Ed. *Catalysis Without Precious Metals*; Wiley-VCH: Weinheim, 2010.

(8) (a) Maji, B.; Barman, M. K. Recent Developments of Manganese Complexes for Catalytic Hydrogenation and Dehydrogenation Reactions. *Synthesis* **2017**, *49*, 3377–3393. (b) Garbe, M.; Junge, K.; Beller, M. Homogeneous Catalysis by Manganese-Based Pincer Complexes. *Eur. J. Org. Chem.* **2017**, *2017*, 4344–4362. (c) Kallmeier, F.; Kempe, R. Manganese Complexes for (De)Hydrogenation Catalysis: A Comparison to Cobalt and Iron Catalysts. *Angew. Chem., Int. Ed.* **2018**, *57*, 46–60. (d) Zell, T.; Langer, R. From ruthenium to iron and manganese - a mechanistic view on challenges and design principles of base metal hydrogenation catalysts. *ChemCatChem* **2018**, DOI: 10.1002/cctc.201701722. (e) Filonenko, G. A.; van Putten, R.; Hensen, E. J. M.; Pidko, E. A. Catalytic (de)hydrogenation promoted by non-precious metals – Co, Fe and Mn: recent advances in an emerging field. *Chem. Soc. Rev.* **2018**, *47*, 1459–1483.

(9) Fe-catalyzed hydrogenation reactions: (a) Federsel, C.; Boddien, A.; Jackstell, R.; Jennerjahn, R.; Dyson, P. J.; Scopelliti, R.; Laurency, G.; Beller, M. A Well-Defined Iron Catalyst for the Reduction of Bicarbonates and Carbon Dioxide to Formates, Alkyl Formates, and Formamides. *Angew. Chem., Int. Ed.* **2010**, *49*, 9777–9780. (b) Langer, R.; Leitus, G.; Ben-David, Y.; Milstein, D. Efficient hydrogenation of ketones catalyzed by an iron pincer complex. *Angew. Chem., Int. Ed.* **2011**, *50*, 2120–2124. (c) Langer, R.; Iron, M. A.; Konstantinovskii, L.; Diskin-Posner, Y.; Leitus, G.; Ben-David, Y.; Milstein, D. Iron Borohydride Pincer Complexes for the Efficient Hydrogenation of Ketones under Mild, Base-Free Conditions: Synthesis and Mechanistic Insight. *Chem. - Eur. J.* **2012**, *18*, 7196–7209. (d) Ziebart, C.; Federsel, C.; Anbarasan, P.; Jackstell, R.; Baumann, W.; Spannenberg, A.; Beller, M. Well-Defined Iron Catalyst for Improved Hydrogenation of Carbon Dioxide and Bicarbonate. *J. Am. Chem. Soc.* **2012**, *134*, 20701–20704.

(e) Fleischer, S.; Zhou, S.; Junge, K.; Beller, M. General and Highly Efficient Iron-Catalyzed Hydrogenation of Aldehydes, Ketones, and α,β -Unsaturated Aldehydes. *Angew. Chem., Int. Ed.* **2013**, *52*, 5120–5124. (f) Srimani, D.; Diskin-Posner, Y.; Ben-David, Y.; Milstein, D. Iron Pincer Complex Catalyzed, Environmentally Benign, E-Selective Semi-Hydrogenation of Alkynes. *Angew. Chem., Int. Ed.* **2013**, *52*, 14131–14134. (g) Wienhofer, G.; Baseda-Kruger, M.; Ziebart, C.; Westerhaus, F. A.; Baumann, W.; Jackstell, R.; Junge, K.; Beller, M. Hydrogenation of nitroarenes using defined iron–phosphine catalysts. *Chem. Commun.* **2013**, *49*, 9089–9091. (h) Bornschein, C.; Werkmeister, S.; Wendt, B.; Jiao, H.; Alberico, E.; Baumann, W.; Junge, H.; Junge, K.; Beller, M. Mild and selective hydrogenation of aromatic and aliphatic (di)nitriles with a well-defined iron pincer complex. *Nat. Commun.* **2014**, *5*, 4111. (i) Chakraborty, S.; Dai, H.; Bhattacharya, P.; Fairweather, N. T.; Gibson, M. S.; Krause, J. A.; Guan, H. Iron-Based Catalysts for the Hydrogenation of Esters to Alcohols. *J. Am. Chem. Soc.* **2014**, *136*, 7869–7872. (j) Chakraborty, S.; Lagaditis, P. O.; Förster, M.; Bielinski, E. A.; Hazari, N.; Holthausen, M. C.; Jones, W. D.; Schneider, S. Well-Defined Iron Catalysts for the Acceptorless Reversible Dehydrogenation-Hydrogenation of Alcohols and Ketones. *ACS Catal.* **2014**, *4*, 3994–4003. (k) Lagaditis, P. O.; Sues, P. E.; Sonnenberg, J. E.; Wan, K. Y.; Lough, A. J.; Morris, R. H. Iron(II) Complexes Containing Unsymmetrical P-N-P' Pincer Ligands for the Catalytic Asymmetric Hydrogenation of Ketones and Imines. *J. Am. Chem. Soc.* **2014**, *136*, 1367–1380. (l) Werkmeister, S.; Junge, K.; Wendt, B.; Alberico, E.; Jiao, H.; Baumann, W.; Junge, H.; Gallou, F.; Beller, M. Hydrogenation of Esters to Alcohols with a Well-Defined Iron Complex. *Angew. Chem., Int. Ed.* **2014**, *53*, 8722–8726. (m) Bertini, F.; Mellone, I.; Ienco, A.; Peruzzini, M.; Gonsalvi, L. Iron(II) Complexes of the Linear rac-Tetraphos-1 Ligand as Efficient Homogeneous Catalysts for Sodium Bicarbonate Hydrogenation and Formic Acid Dehydrogenation. *ACS Catal.* **2015**, *5*, 1254–1265. (n) Rivada-Wheelaghan, O.; Dauth, A.; Leitus, G.; Milstein, D.; Diskin-Posner, Y. Synthesis and Reactivity of Iron Complexes with a New Pyrazine-Based Pincer Ligand, and Application in Catalytic Low-Pressure Hydrogenation of Carbon Dioxide. *Inorg. Chem.* **2015**, *54*, 4526–4538. (o) Zhang, Y.; MacIntosh, A. D.; Wong, J. L.; Bielinski, E. A.; Williard, P. G.; Mercado, B. Q.; Hazari, N.; Bernskoetter, W. H. Iron catalyzed CO₂ hydrogenation to formate enhanced by Lewis acid co-catalysts. *Chem. Sci.* **2015**, *6*, 4291–4299. (p) Gorgas, N.; Stöger, B.; Veiros, L. F.; Pittenauer, E.; Allmaier, G.; Kirchner, K. Efficient Hydrogenation of Ketones and Aldehydes Catalyzed by Well-Defined Iron(II) PNP Pincer Complexes: Evidence for an Insertion Mechanism. *Organometallics* **2014**, *33*, 6905–6914.

(10) Mn-catalyzed hydrogenations of ketones and aldehydes: (a) Elangovan, S.; Topf, C.; Fischer, S.; Jiao, H.; Spannenberg, A.; Baumann, W.; Ludwig, R.; Junge, K.; Beller, M. Selective Catalytic Hydrogenations of Nitriles, Ketones, and Aldehydes by Well-Defined Manganese Pincer Complexes. *J. Am. Chem. Soc.* **2016**, *138*, 8809–8814. (b) Kallmeier, F.; Irrgang, T.; Diel, T.; Kempe, R. Highly Active and Selective Manganese C=O Bond Hydrogenation Catalysts: The Importance of the Multidentate Ligand, the Ancillary Ligands, and the Oxidation State. *Angew. Chem., Int. Ed.* **2016**, *55*, 11806–11809. (c) Widegren, M. B.; Harkness, G. J.; Slawin, A. M. Z.; Cordes, D. B.; Clarke, M. L. A Highly Active Manganese Catalyst for Enantioselective Ketone and Ester Hydrogenation. *Angew. Chem., Int. Ed.* **2017**, *56*, 5825–5828. (d) Bruneau-Voisine, A.; Wang, D.; Roisnel, T.; Darcel, C.; Sortais, J.-P. Hydrogenation of ketones with a manganese PN³P pincer pre-catalyst. *Catal. Commun.* **2017**, *92*, 1–4. (e) Garbe, M.; Junge, K.; Walker, S.; Wei, Z.; Jiao, H.; Spannenberg, A.; Bachmann, S.; Scalone, M.; Beller, M. Manganese(I)-Catalyzed Enantioselective Hydrogenation of Ketones Using a Defined Chiral PNP Pincer Ligand. *Angew. Chem., Int. Ed.* **2017**, *56*, 11237–11241.

(11) (a) Perez, M.; Elangovan, S.; Spannenberg, A.; Junge, K.; Beller, M. Molecularly Defined Manganese Pincer Complexes for Selective Transfer Hydrogenation of Ketones. *ChemSusChem* **2017**, *10*, 83–86. (b) Zirakzadeh, A.; de Aguiar, S. R. M. M.; Stöger, B.; Widhalm, M.; Kirchner, K. Enantioselective Transfer Hydrogenation of Ketones Catalyzed by a Manganese Complex Containing an Unsymmetrical Chiral PNP' Tridentate Ligand. *ChemCatChem* **2017**, *9*, 1744–1748.

- (c) Espinosa-Jalapa, N. A.; Nerush, A.; Shimon, L. J. W.; Leitus, G.; Avram, L.; Ben-David, Y.; Milstein, D. Manganese-Catalyzed Hydrogenation of Esters to Alcohols. *Chem. - Eur. J.* **2017**, *23*, 5934–5938.
- (d) Elangovan, S.; Garbe, M.; Jiao, H.; Spannenberg, A.; Junge, K.; Beller, M. Non-Pincer-Type Manganese Complexes as Efficient Catalysts for the Hydrogenation of Esters. *Angew. Chem.* **2016**, *128*, 15590–15594.
- (e) Bertini, F.; Glatz, M.; Gorgas, N.; Stöger, B.; Peruzzini, M.; Veiros, L. F.; Kirchner, K.; Gonsalvi, L. Carbon dioxide hydrogenation catalysed by well-defined Mn(I) PNP pincer hydride complexes. *Chem. Sci.* **2017**, *8*, 5024–5029.
- (f) van Putten, R.; Us lamin, E. A.; Garbe, M.; Liu, C.; Gonzalez-de-Castro, A.; Lutz, M.; Junge, K.; Hensen, E. J. M.; Beller, M.; Lefort, L.; Pidko, E. A. Non-Pincer-Type Manganese Complexes as Efficient Catalysts for the Hydrogenation of Esters. *Angew. Chem., Int. Ed.* **2017**, *56*, 7531–7534.
- (g) Kar, S.; Goepfert, A.; Kothandaraman, J.; Prakash, G. K. S. Manganese-Catalyzed Sequential Hydrogenation of CO₂ to Methanol via Formamide. *ACS Catal.* **2017**, *7*, 6347–6351.
- (12) Wienhofer, G.; Westerhaus, F. A.; Junge, K.; Ludwig, R.; Beller, M. A Molecularly Defined Iron-Catalyst for the Selective Hydrogenation of α,β -Unsaturated Aldehydes. *Chem. - Eur. J.* **2013**, *19*, 7701–7707.
- (13) Zell, T.; Ben-David, Y.; Milstein, D. Highly efficient, general hydrogenation of aldehydes catalyzed by PNP iron pincer complexes. *Catal. Sci. Technol.* **2015**, *5*, 822–826.
- (14) Mazza, S.; Scopelliti, R.; Hu, X. Chemoselective Hydrogenation and Transfer Hydrogenation of Aldehydes Catalyzed by Iron(II) PONOP Pincer Complexes. *Organometallics* **2015**, *34*, 1538–1545.
- (15) (a) Gorgas, N.; Stöger, B.; Veiros, L. F.; Kirchner, K. Highly Efficient and Selective Hydrogenation of Aldehydes: A Well-Defined Iron(II) Catalyst exhibits Noble Metal Activity. *ACS Catal.* **2016**, *6*, 2664–2672. (b) Brünig, J.; Csendes, Z.; Weber, S.; Gorgas, N.; Bittner, R. W.; Limbeck, A.; Bica, K.; Hoffmann, H.; Kirchner, K. Chemoselective Supported Ionic Liquid Phase (SILP) Aldehyde Hydrogenation Catalyzed by an Fe(II) PNP Pincer Complex. *ACS Catal.* **2018**, *8*, 1048–1051.
- (16) Wei, D.; Roisnel, T.; Darcel, C.; Clot, E.; Sortais, J.-B. Hydrogenation of Carbonyl Derivatives with a Well-Defined Rhenium Precatalyst. *ChemCatChem* **2017**, *9*, 80–83.
- (17) For rhenium-catalyzed (de)hydrogenation reactions, see: (a) Piehl, P.; Pena-Lopez, M.; Frey, A.; Neumann, H.; Beller, M. Hydrogen autotransfer and related dehydrogenative coupling reactions using a rhenium(I) pincer catalyst. *Chem. Commun.* **2017**, *53*, 3265–3268. (b) Schleker, P. P. M.; Honeker, R.; Klankermayer, J.; Leitner, W. Catalytic Dehydrogenative Amide and Ester Formation with Rhenium–Triphos Complexes. *ChemCatChem* **2013**, *5*, 1762–1764. (c) Jin, H.; Xie, J.; Pan, C.; Zhu, Z.; Cheng, Y.; Zhu, C. Rhenium-Catalyzed Acceptorless Dehydrogenative Coupling via Dual Activation of Alcohols and Carbonyl Compounds. *ACS Catal.* **2013**, *3*, 2195–2198. (d) Vogt, M.; Nerush, A.; Iron, M. A.; Leitus, G.; Diskin-Posner, Y.; Shimon, L. J. W.; Ben-David, Y.; Milstein, D. Activation of Nitriles by Metal Ligand Cooperation. Reversible Formation of Ketimido- and Enamido-Rhenium PNP Pincer Complexes and Relevance to Catalytic Design. *J. Am. Chem. Soc.* **2013**, *135*, 17004–17018. (e) Abdukader, A.; Jin, H.; Cheng, Y.; Zhu, C. Rhenium-catalyzed amination of alcohols by hydrogen transfer process. *Tetrahedron Lett.* **2014**, *55*, 4172–4174. (f) Vogt, M.; Nerush, A.; Diskin-Posner, Y.; Ben-David, Y.; Milstein, D. Reversible CO₂ binding triggered by metal–ligand cooperation in a rhenium(I) PNP pincer-type complex and the reaction with dihydrogen. *Chem. Sci.* **2014**, *5*, 2043–2051. (g) Mazzotta, M. G.; Xiong, M.; Abu-Omar, M. M. Carbon Dioxide Reduction to Silyl-Protected Methanol Catalyzed by an Oxorhenium Pincer PNN Complex. *Organometallics* **2017**, *36*, 1688–1691.
- (18) (a) Rao, G. K.; Korobkov, I.; Gabidullin, B.; Richeson, D. Employing a neutral “PN3P” pincer to access *mer*-Re(I) tricarbonyl complexes: Autoionization of a halo ligand and the role of an N-R (R = H, Me) substituent. *Polyhedron* **2018**, *143*, 62–69. (b) Choualeb, A.; Maccaroni, E.; Blacque, O.; Schmalle, H. W.; Berke, H. Rhenium Nitrosyl Complexes for Hydrogenations and Hydrosilylations. *Organometallics* **2008**, *27*, 3474–3481.
- (19) (a) Mastalir, M.; Glatz, M.; Gorgas, N.; Stöger, B.; Pittenauer, E.; Allmaier, G.; Veiros, L. F.; Kirchner, K. Divergent Coupling of Alcohols and Amines Catalyzed by Isoelectronic Hydride Mn^I and Fe^{II} PNP Pincer Complexes. *Chem. - Eur. J.* **2016**, *22*, 12316–12320. (b) Mastalir, M.; Glatz, M.; Pittenauer, E.; Allmaier, G.; Kirchner, K. Sustainable Synthesis of Quinolines and Pyrimidines Catalyzed by Manganese PNP Pincer Complexes. *J. Am. Chem. Soc.* **2016**, *138*, 15543–15546. (c) Mastalir, M.; Pittenauer, E.; Allmaier, G.; Kirchner, K. Manganese-Catalyzed Aminomethylation of Aromatic Compounds with Methanol as Sustainable C1 Building Block. *J. Am. Chem. Soc.* **2017**, *139*, 8812–8815.
- (20) (a) Parr, R. G.; Yang, W. *Density Functional Theory of Atoms and Molecules*; Oxford University Press: New York, 1989. (b) Free energy values were obtained at the PBE0/VDZP level using the Gaussian 09 package. All calculations included solvent effects (ethanol) using the PCM/SMD model. A full account of the computational details and a complete list of references are provided as SI.
- (21) Morello, G. R.; Hopmann, K. H. A Dihydride Mechanism Can Explain the Intriguing Substrate Selectivity of Iron-PNP-Mediated Hydrogenation. *ACS Catal.* **2017**, *7*, 5847–5855.

Manuscript #5

“Activation of Carbon Dioxide by Hydride Mn and Re PNP Pincer Complexes”

Glatz M., Haager L.; Pecak J.; Stöger B.; Kirchner K. *Organometallics*, **2018**, manuscript in preparation.

Activation of Carbon Dioxide by Hydride Mn and Re PNP Pincer Complexes

Mathias Glatz,^a Jan Pecak,^a Lena Haager,^a Berthold Stöger,^b Karl Kirchner*^a

^aInstitute of Applied Synthetic Chemistry, Vienna University of Technology, Getreidemarkt 9/163, A-1060 Wien, Austria.

^bX-Ray Center, Vienna University of Technology, Getreidemarkt 9, A-1060 Vienna, Austria.

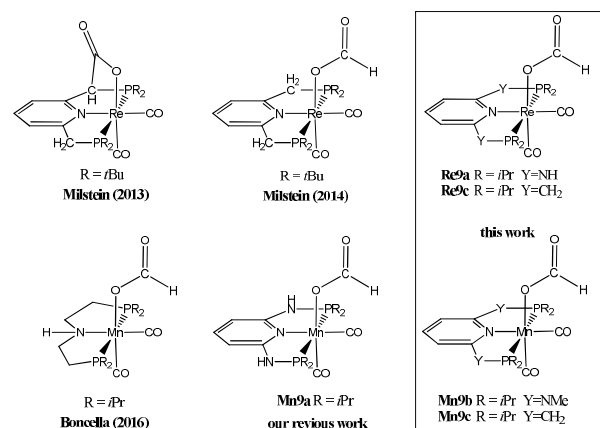
Supporting Information

ABSTRACT: The synthesis several formiato Mn(I) and Re(I) PNP pincer is described. Notably, most of them are formed from their relative hydrido compounds by insertion of gaseous CO₂ into the metal-hydrogen bond. This is a key process for utilization of carbon dioxide as a sustaining C1 building block. Throughout, the synthetic pathway, starting from M(CO)₅X (M = Mn, Re; X = Cl, Br) and a variety of six different PNP pincer ligands is investigated. Thereby, a rare example of a cationic 16 electron manganese complex [Mn(PNP)(CO)₂]⁺ and its deprotonated analogue was found. The structure of all isolated products is highly depending on sterics and bi-functionality of the ligands. With our findings we believe to deliver an advanced understanding of Group 7 PNP pincer chemistry.

INTRODUCTION

Pincer complexes of group 7 transition metals (Mn, Re) experienced a rising interest in homogeneous catalysis during the last couple of years. The ever thriving goal of sustainable catalysis, replacing precious metals in large scale applications inspired the field of base metal catalysis. Earth abundant and non-toxic metals like Fe, Ti and Mn are prominent candidates for this challenging goal. Pincer ligands proved to be a powerful support to achieve noble-metal-like reactivity on Fe(II) complexes. Well established catalytic systems for reductions, oxidations, couplings and transformations were reported in the last decade. Isoelectronic Mn(I) systems are fairly poor studied, and caught the attention of several groups very recently. Herein we describe the synthesis and reactivity of several Mn(I) formiato complexes and discuss the underlying chemistry to its related homologue Re(I).

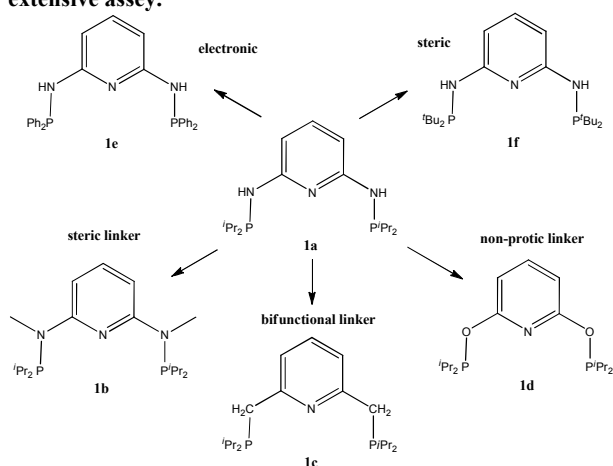
Scheme 1. Examples of Rhenium and Manganese PNP formiato-carbonyl complexes.



The first insertion of CO₂ into a Mn-H bond was evidenced back in 1994 by Berke et. al.¹ An analogous reaction for a Re-H bond was done by the research group of Roveda in 2005.² While manganese PNP pincer complexes enjoy a rising interest during the last years in catalysis, its later homologue Re is little studied in this manner. The latest efficient catalysis, hydrogenation of aldehydes and ketones by Re(I) pincers was presented by Sortais.³ The nucleophilicity of Re pincers was exemplified by Milstein, binding electrophiles like nitriles and CO₂ by metal-ligand cooperation.⁴ The high catalytic potential of formiato intermediates was shown in our previous work, by reduction of carbondioxide with H₂ to formic acid.⁵

In this paper, we investigate the fundamental reactivity and coordinative nature of a series of Mn(I) and Re(I) PNP pincer complexes, based on the ligand system. For this purpose, we selected six pyridine-backed PNP pincer ligands **1a-f**, which are well known pincer research⁵ (scheme 2). This selection changes in electronics and sterics of the phosphorus donors, as well as functional varieties in the linking groups. This piece of work includes complexation of ligands **1a-f** with precursors of general formula [M(CO)₅X] (M = Mn, Re; X = Cl, Br). Reaction conditions and ligands take influence in the products formed. The study also led to a rare cationic low-valent 16-electron Mn(I) complex, and its deprotonated neutral form. The earliest report on a 16 electron manganese PNP complex dates back to 2009, in a comparative work on Mn(I) and Re(I) with anionic ligands by Nocera.⁶ The relative hydrido-complexes [M(κ³P,N,P-PNP)(CO)₂H], revealed impressive nucleophilic character. Gaseous CO₂ readily inserts into the metal-hydrogen bond in solution. Four new PNP formiato-complexes of type [M(κ³P,N,P-PNP)(CO)₂OCHO] are isolated and characterized.

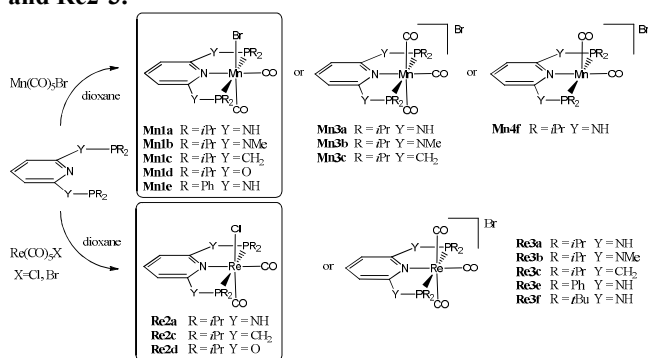
Scheme 2. Pyridine PNP Pincer Ligands used throughout this extensive assey.



RESULTS AND DISCUSSION

For our initial synthetic approach, PNP ligands **1a-f** were reacted with group 7 carbonyl precursors $\text{Mn}(\text{CO})_5\text{Br}$ and $\text{Re}(\text{CO})_5\text{Br}$ in dioxane. Complexes **Mn1a,d** and **Mn1c** were already reported in previous works from Boncella and Beller.⁷ Notably, the outcome of the major product was highly depending on the reaction temperature (70°C or 120°C), period (2-18h) and also varied from the ligand-system used, displayed in scheme 4. Speaking for the manganese complexes **Mn1-4**, reaction at lower temperatures and short reaction times preferred the formation of cationic species **Mn3** of type $[\text{Mn}(\kappa^3P,N,P\text{-PNP})(\text{CO})_3]\text{Br}$. All of these off-white compounds share a similar spectroscopic character, exhibiting three carbonyl stretching frequencies, one weak band and at

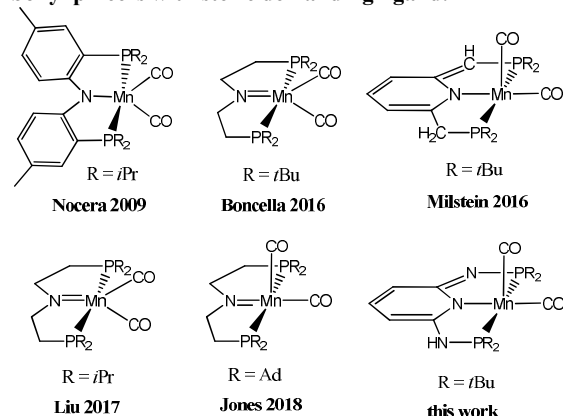
Scheme 5. Synthesis of the Mn and Re Complexes Mn1-4 and Re2-3.



2034-2028 cm^{-1} and two strong bands ν_{CO} at 1941-1916 cm^{-1} . As a matter of resolution, the latter two bands, are superimposed in some cases (e.g. **Mn3b**), resulting in one broad intense signal. In $^{13}\text{C}\{^1\text{H}\}$ NMR, the three CO ligands give rise to two low field triplets located at 221.0-216.9 ppm and 215.4-207.4 ppm of higher intensity, indicating the CO in trans position to the pyridine. Due to the magnetic nature of ^{55}Mn ($s = 5/2$), the triplets are not always fully resolved, ending up in a rather broad multiplet. $^{31}\text{P}\{^1\text{H}\}$ NMR displays an expected broad singlet, ranging from 156.5 to 88.3 ppm. Harsher reaction conditions applied in a sealed reaction flask, supported the formation of the neutral *cis*-dicarbonyl complex **Mn1** of type

cis- $[\text{Mn}(\kappa^3P,N,P\text{-PNP})(\text{CO})_2\text{Br}]$, yellow-orange colored. Notably, ligands **1a**, **1d** and **1e** were exclusively isolated in this coordination state, independent on the reaction conditions. In a recent publication, Boncella et al described, the transformation of **Mn3a** to **Mn1a** after thermal treatment. The spectroscopic properties of complexes **Mn1** are comparable with its literature known compounds **Mn1a,c,d**. By the usage of dioxane, as a high boiling and coordinating solvent, we were able to isolate all complexes **Mn1** in quantitative yield. The two intense CO bands ν_{CO} at 1943-1908 cm^{-1} and 1875-1814 cm^{-1} display at lower wavelengths, the greater the π -acceptor tendency of the phosphine donor is. Compared to the cationic complexes **Mn3**, the chemical shift of the $^{31}\text{P}\{^1\text{H}\}$ NMR resonance is shifted low field at 230.4-85.8 ppm. The broad two resonances of the two CO ligands in are shifted high field, ranging from 230.0-229.6 ppm and 225.7-222.9 ppm. In strong contrast, the reaction mixture of ligand **1f** and $\text{Mn}(\text{CO})_5\text{Br}$ always ended up forming a turbid suspension. Workup of the violet solid via filtration, revealed a new cationic 16 electron species **Mn4f** of general formula $[\text{Mn}(\kappa^3P,N,P\text{-PNP}^{\text{NH-}t\text{Bu}})(\text{CO})_2]\text{Br}$. The x-ray crystal structure propounded a square pyramidal geometry with Mn-C bonding distances of 1.739 Å and 1.730 Å. A previously reported iso-electronic PNP complex from Jones and coworkers⁸, exhibiting an aliphatic backbone, features a very similar structure. Due to the fact, that Jones ligand exploited two adamantly residues at the donor sites, it is suggested that the formation of $(\kappa^3P,N,P\text{-PNP})(\text{CO})_2]\text{Br}$ is exclusively nature to a bulky ligand structure. This unexpected

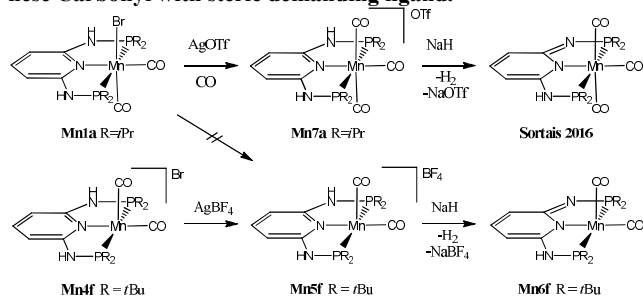
Scheme 6. Examples of neutral 16-electron Manganese Carbonyl pincers with steric demanding ligand.



outcome, drew our interest for further investigation. Other newly found examples of 16 electron Mn pincer complexes from Boncella, Liu and Milstein⁹ are neutral, result from a deprotonated anionic ligand backbone. The crystallographic data of **Mn4f** was of poor quality, as well as solubility and signal intensity in NMR analysis. Therefore **Mn4f** was converted into its better soluble BF_4 -salt $[\text{Mn}(\kappa^3P,N,P\text{-PNP}^{\text{NH-}t\text{Bu}})(\text{CO})_2]\text{BF}_4$ **Mn5f** of similar structure. The Mn-C bonding distances turned out to have become slightly longer 1.754 Å and 1.787 Å. This finding is related, to an absence of hydrogen bonding interaction of the halide ion Br⁻. The CO ligands of **Mn4f** display two characteristic ν_{CO} bands in the solid state IR spectrum, at 1927 and 1860 cm^{-1} . **Mn5f**, with good spectral resolution, shows three ν_{CO} bands at 1936, 1865 and 1856 cm^{-1} . Contrary, the CO resonance in $^{13}\text{C}\{^1\text{H}\}$ NMR shows only one signal at 235.6 and 234.9 ppm, which reflects an equilibrium in solution. Colorless crystals were harvested from a

solution in EtOD- d_6 after 2 weeks, which was just sufficient for a ^1H , $^{31}\text{P}\{^1\text{H}\}$ NMR, as well as an IR spectrum. The dataset of this compound concurs with the small impurities observed in the NMR spectra of **Mn4f**. In agreement with the pattern of the ν_{CO} in the IR analysis (2020 cm^{-1} (w), 1912 cm^{-1} (s)), this solidifies the assumption of a cationic tricarbonyl $[\text{Mn}(\kappa^3P,N,P\text{-PNP}^{\text{NH-}i\text{Bu}})(\text{CO})_3]\text{Br}$. In a comparative reaction, complex **Mn1a** was treated with halophile Ag^+ -salts, to

Scheme 4. Synthesis and deprotonation of 16-electron Manganese Carbonyl with steric demanding ligand.



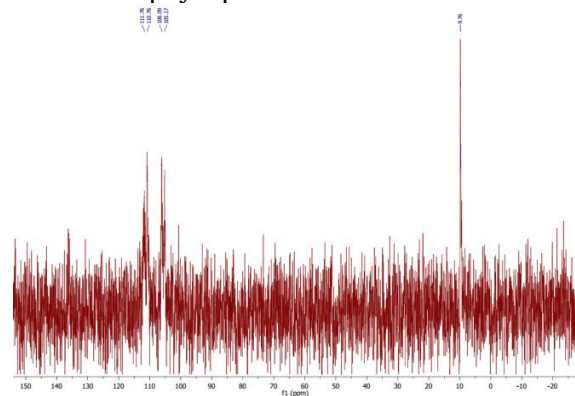
obtain a structure of type **Mn7a**. This less bulky ligand system, yields a different result. The bis-carbonyl-bromido complex **Mn1a** formed the cationic tris-carbonyl complex **Mn7a** in <50% yield. Under CO atmosphere, complex **Mn7a** is isolated quantitatively. Beside minor variations, the spectroscopic data of **Mn7a** is matching with those of **Mn3a**. Deprotonation of **Mn4-5f** yields a neutral 16 electron dicarbonyl, while **Mn7a** prefers the 18 electron tris-carbonyl as reported by Sortais.¹⁰ $^{31}\text{P}\{^1\text{H}\}$ NMR of **Mn6e** monitors a *AB* coupling pattern, slightly shifted high field ($P_{A,B} = 145.7, 142.2\text{ ppm}$, $J_{PP} = 84.5\text{ Hz}$). The two IR carbonyl frequencies ν_{CO} are shifted to low wavelengths ($\nu_{\text{CO}} = 1913, 1838\text{ cm}^{-1}$) and the single CO triplet in $^{13}\text{C}\{^1\text{H}\}$ NMR is decently shifted low field at 238.2 .

The reaction of ligands **1a-f** with $\text{Re}(\text{CO})_5\text{Br}$ afforded less variety of products, obtaining preferably the cationic tris-carbonyl complex $[\text{Mn}(\kappa^3P,N,P\text{-PNP})(\text{CO})_3]\text{Br}$ **Re3**. Results of the spectroscopic characterization, are corresponds with data published by Richeson.¹¹ Three (or two if superimposed) ν_{CO} bands at $2068\text{-}2031\text{ cm}^{-1}$ (w), $1966\text{-}1910\text{ cm}^{-1}$ (s), a singlet in $^{31}\text{P}\{^1\text{H}\}$ NMR located at $120.9\text{-}48.6\text{ ppm}$ and two CO multiplets in $^{13}\text{C}\{^1\text{H}\}$ NMR ranging from $198.2\text{-}194.6\text{ ppm}$ and $196.6\text{-}188.3\text{ ppm}$ are observed as expected. Ligand **1d** led to mixtures, and was not further investigated. However, switching of the precursor towards $\text{Re}(\text{CO})_5\text{Cl}$, plus longer reaction times at higher temperature enabled us to isolate three neutral bis-carbonyl chlorido complexes **Re2** of conformation *cis*- $[\text{Re}(\kappa^3P,N,P\text{-PNP})(\text{CO})_2\text{Cl}]$. Using a slightly modified ligand, Richeson and coworkers also observed, that the utilization $\text{Re}(\text{CO})_5\text{Cl}$ instead of $\text{Re}(\text{CO})_5\text{Br}$ facilitated the formation of *cis*- $[\text{Re}(\kappa^3P,N,P\text{-PNP})(\text{CO})_2\text{Cl}]$. A comparison between complexes **Re2** and its manganese bromo-analogues **Mn1** reveals a shift of the two CO bands ν_{CO} in the IR at $1928\text{-}1900\text{ cm}^{-1}$ and $1848\text{-}1804\text{ cm}^{-1}$. NMR shifts $^{31}\text{P}\{^1\text{H}\}$ NMR and $^{13}\text{C}\{^1\text{H}\}$ NMR are located clearly high field at $184\text{-}52\text{ ppm}$ or $208.9\text{-}203.6\text{ ppm}$ and $199.2\text{-}195.3\text{ ppm}$ respectively.

Synthesis of PNP Formiato Complexes *cis*- $[\text{M}(\kappa^3P,N,P\text{-PNP})(\text{CO})_2\text{OCHO}]$ (M = Re, Mn)

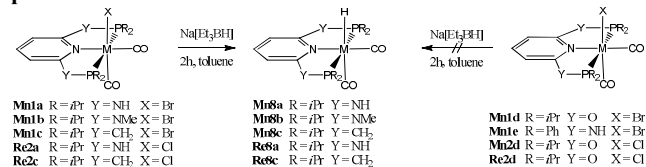
The stated formiato complexes **Mn8** and **Re8** are prepared from their relative hydrido complexes *cis*- $[\text{M}(\kappa^3P,N,P\text{-PNP})(\text{CO})_2\text{H}]$. Documented standard procedures, using $\text{Na}[\text{Et}_3\text{BH}]$ (1M in THF) in toluene led to five *cis*-dicarbonyl hydrido complexes **Mn8** and **Re8**. The expected ligand exchange was only accomplished with ligands **1a-c**. None of the tris-carbonyls **Mn3**, **Re3** did form a hydride at all. Attempts to obtain or even detect a hydrido-complex, exhibiting phosphito ligand **1d** were without success. Also the chloride-manganese dicarbonyl **Mn2d**, which was synthesized for comparison, undertook no change upon addition of hydride reagent. The acidity of the NH group of **Mn2e** is prone to deprotonation. This may be explained by the electron withdrawing manner of Ph-groups as a decent π -acceptor at the phosphorus site.

Scheme 7. $^{31}\text{P}\{^1\text{H}\}$ NMR spectrum of Mn1e after addition of a solution of $\text{Na}[\text{Et}_3\text{BH}]$



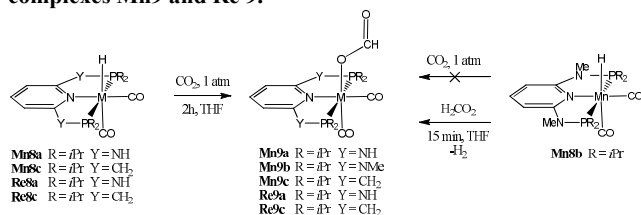
Two sets of broad multiplets at 111.3 and 105.6 ppm , as well as free ligand **1e** were monitored via $^{31}\text{P}\{^1\text{H}\}$ NMR in C_6D_6 after addition of a 1M solution of $\text{Na}[\text{Et}_3\text{BH}]$. A characteristic feature of the ^1H NMR spectra of **Mn8** and **Re8** is the high-field shift of the proton attached to the metal center, giving rise to triplets at -2.56 to -3.84 ppm for rhenium and -4.27 to -6.27 ppm for manganese. The signals in $^{31}\text{P}\{^1\text{H}\}$ NMR are shifted low field, relative to the starting material. $^{31}\text{P}\{^1\text{H}\}$ resonances of **Mn8** ranges from 185.5 to 110.8 ppm , and 103.5 to 56.1 for **Re8**. The two resonances in $^{13}\text{C}\{^1\text{H}\}$ NMR are also shifted low field, while the two ν_{CO} bands are centered at lower wavelengths. Detailed characterization and interpretation was recently published. Insertion of one gaseous CO_2

Scheme 8. Synthesis of manganese and rhenium hydrido complexes



molecule into the metal-hydrogen bond is achieved in solution under very mild conditions (rt, 1 atm CO_2). Pale-yellow complexes **Mn9a,c** and **Re9a,c** are readily obtained in quantitative yields via this procedure. Complex **Mn9b**, as the steric most hindered hydrido-complex, is supposedly inhibited from a kinetic point of view. Still, **Mn9b** could be isolated with an alternative protocol, by addition of formic acid to a solution of **Mn8b** in C_6H_6 . A common feature for all characterized

Scheme 9. Synthesis of manganese and rhenium formiato complexes Mn9 and Re 9.



formiato complexes **9** is a particularly low field shifted O=C-H resonance in ¹H NMR, down to 9.16 ppm for **Mn9c**. IR spectroscopy demonstrates *cis*-configuration for all complexes if two strong ν_{CO} bands of 1929-1906 cm⁻¹ and 1844-1816 cm⁻¹. Compared to ¹³C{¹H} NMR resonance of molecular CO₂ (125-124 ppm), the signal is significantly shifted low field between 169.6 and 167.7 ppm. ³¹P{¹H} NMR resonances are shifted high field, comparably similar to halogen complexes **Mn1-2** and **Re1-2**. The coordination of the formiato ligand via the oxygen atom is evidenced by x-ray crystallography of **Mn9a**.

CONCLUSION

This comparative study, the complexation of group 7 pentacarbonyl-halides (Mn, Re) by a series of six different PNP pincer ligands was investigated. Beside [M(κ³P,N,P-PNP)(CO)₂X] and [M(κ³P,N,P-PNP)(CO)₃]X, also an unusual example of a 16-electron complex [Mn(κ³P,N,P-PNP^{NH}-*t*Bu)(CO)₂]⁺ was isolated with steric demanding moieties. Deprotonation provided the corresponding neutral complex [M(κ³P,N,P-PNP^{NH}-*t*Bu)(CO)₂]. Reaction temperature and nature of the ligand are crucial driving forces for the structure of the formed product. Only a fraction of the isolated compounds, forms hydrido-complexes [M(κ³P,N,P-PNP)(CO)₂H]. With the objective to activate gaseous CO₂, formiato-carbonyl complexes of the type [M(κ³P,N,P-PNP)(CO)₂OCHO] were obtained. With this proof of concept, all these newly reported formiates (M = Mn, Re) [M(κ³P,N,P-PNP)(CO)₂OCHO] are promising for catalytic applications, incorporating CO₂ as a sustainable C1 source.

EXPERIMENTAL SECTION

General. All manipulations were performed under an inert atmosphere of argon by using Schlenk techniques or in an MBraun inert-gas glovebox. The solvents were purified according to standard procedures.²⁷ The deuterated solvents were purchased from Aldrich and dried over 4 Å molecular sieves. The ligands 1a-1f were prepared according to the literature. ¹H, ¹³C{¹H}, and ³¹P{¹H} NMR spectra were recorded on Bruker AVANCE-250 and AVANCE-600 spectrometers. ¹H and ¹³C{¹H} NMR spectra were referenced internally to residual protio-solvent, and solvent resonances, respectively, and are reported relative to tetramethylsilane (δ = 0 ppm). ³¹P{¹H} NMR spectra were referenced externally to H₃PO₄ (85%) (δ = 0 ppm).

X-ray Structure Determination. X-ray diffraction data of **1**, **2and3** [CCDC entries 1491438-1491440] were collected at T = 100 K in a dry stream of nitrogen on a Bruker Kappa APEX II diffractometer system using graphite-monochromatized Mo-Kα radiation (λ = 0.71073 Å) and fine sliced φ- and ω-scans. Data were reduced to intensity values with SAINT and an absorption correction was applied with the multi-scan approach implemented in SADABS.⁴⁴ The structures were solved by charge flipping using SUPERFLIP⁴⁵ and refined against F with JANA2006.⁴⁶ Non-hydrogen atoms were refined anisotropically. Generally, H atoms were placed in calculated positions and thereafter refined as riding on the parent C atoms. H atoms con-

nected to the metals were located in the difference Fourier maps and freely refined. The hydride and one CO ligand in **3** were modelled as occupationally disordered. The W-C and W-H distances of the positions with the lower occupancy (32.44%) were restrained to 1.640(1) and 1.700(1) Å.

ASSOCIATED CONTENT

Supporting Information

The Supporting Information is available free of charge on the ACS Publications website at DOI: .

NMR spectra and crystallographic data, atomic coordinates for DFT optimized structures (PDF)
X-ray crystallographic data (CIF)

AUTHOR INFORMATION

Corresponding Author

*K.K.: e-mail, kkirch@mail.tuwien.ac.at, tel (+43) 1 58801 163611; fax (+43) 1 58801 16399.

Notes

The authors declare no competing financial interest.

ACKNOWLEDGMENT

Financial support by the Austrian Science Fund (FWF) is gratefully acknowledged (Project No. P28866-N34) and LFW acknowledges Fundação para a Ciência e Tecnologia, UID/QUI/00100/2013. The X-ray center of the Vienna University of Technology is acknowledged for financial support and for providing access to the single-crystal diffractometer.

REFERENCES

- (1) Nietlispach D.; Bosch H. W.; Berke H. Chem. Ber. **1994**, 127, 2403-2415.
- (2) Albertin G.; Antoniutti S.; Roveda G.; Inorg. Chim. Acta **2005**, 358, 3093-3105.
- (3) Wei D.; Roisnel T.; Darcel C.; Clot E.; Sortais J.-B. Chem. Cat. Chem. **2017**, 9, 80-83.
- (4) (a) Vogt M.; Nerush A.; Iron M. A.; Leitus G.; Diskin-Posner Y.; Shimon L. J. W.; Ben-David Y. Milstein D. JACS **2013**, 135, 17004-17018. (b) Vogt M.; Nerush A.; Diskin-Posner Y.; Ben-David Y. Milstein D. Chem. Sci. **2014**, 5, 2043-2051.
- (5) (a) Leung W.-P.; Ip Q. W.-Y.; Wong S.-Y.; Mak T. C. W. Organometallics **2003**, 22, 4604-4609. (b) Salem H.; Shimon L. J. W.; Posner-Diskin Y.; Leitus G.; Ben-David Y.; Milstein D. Organometallics **2009**, 28, 4791-4806. (c) Benito-Garagorri D.; Becker E.; Wiedermann J.; Lackner W.; Pollak M.; Mereiter K.; Kisala J.; Kirchner K. Organometallics **2006**, 25, 1900-1913. (d) Öztöpcü Ö.; Holzhaecker C.; Puchberger M.; Weil M.; Mereiter K.; Veiros L. F.; Kirchner K. Organometallics **2013**, 32, 3042-3052. (e) Schirmer, W.; Flörke, U.; Haupt, H.-J. Z. Anorg. Allg. Chem. **1987**, 545, 83-97. (f) Schirmer, W.; Flörke, U.; Haupt, H.-J. Z. Anorg. Allg. Chem. **1989**, 574, 239-255.
- (6) Bertini F.; Glatz M.; Gorgas N.; Stöger B.; Peruzini M.; Veiros L. F.; Kirchner K.; Gonsalvi L. Chem. Sci. **2017**, 8, 524-5029.
- (7) Radosevich A. T.; Melnick J. G.; Stoian S. A.; Bacciu D.; Chen C.-H.; Foman B. M.; Ozerov O. V. Nocera D. G. Inorg. Chem. **2009**, 48, 9214-9221.
- (8) (a) Tondreau A. M.; Boncella J. M. Polyhedron **2016**, 116, 96-104. (b) Neumann J.; Elangovan S.; Spannenberg A.; Junge K.; Beller M. Chem. Eur. J. **2017**, 23, 5410-5413.
- (9) Kulkarni N. V.; Brennessel W. W.; Jones W. D. ACS Catal. **2018**, 8, 997-1002.
- (10) (a) Tondreau A. M.; Boncella J. M. Organometallics **2016**, 35, 2049-2052. (b) Fu S.; Shao Z.; Wang Y.; Liu Q. JACS **2017**, 139, 11941-11948. (c) Mukherjee A.; Nerush A.; Leitus G.; Shimon L. J. W.; Ben-David Y.; Jalapa N. A. E.; Milstein D. JACS **2016**, 138, 4298-4301.

- (10) Bruneau-Voisine A.; Wang D.; Dorcet V.; Roisnel T.; Darcel C.; Sortais J.-B. *J. Catal.* **2017**, *347*, 57-62.
- (11) Rao K. R.; Korobkov I.; Gabidullin B.; Richeson D. *Polyhedron*, **2018**, in press.

Activation of Carbon Dioxide by Hydride Mn and Re PNP Pincer Complexes. The synthesis several formiato Mn(I) and Re(I) PNP pincer is described. Notably, most of them are formed from their relative hydrido compounds by insertion of gaseous CO₂ into the metal-hydrogen bond. This is a key process for utilization of carbon dioxide as a sustaining C1 building block. Throughout, the synthetic pathway, starting from M(CO)₅X (M = Mn, Re; X = Cl, Br) and a variety of six different PNP pincer ligands is investigated. Thereby, a rare example of a cationic 16 electron manganese complex [Mn(PNP)(CO)₂]⁺ and its deprotonated analogue was found. The structure of all isolated products is highly depending on sterics and bi-functionality of the ligands. With our findings we believe to deliver an advanced understanding of Group 7 PNP pincer chemistry

1 Supporting Information

2

3 Activation of Carbon Dioxide by Group by Mn and Re PNP Pincer 4 Complexes 7

5 Mathias Glatz,^a Jan Pecak,^a Lena Haager,^a Berthold Stoeger,^b and Karl Kirchner^{*, a}

6 ^aInstitute of Applied Synthetic Chemistry, Vienna University of Technology, Getreidemarkt 9/163, A-
7 1060 Wien, Austria.

8 ^bX-Ray Center, Vienna University of Technology, Getreidemarkt 9, A-1060 Wien, Austria.

9

10

11	General experimental information	S3
12	Synthesis of <i>cis</i> -[Mn(PNP ^{Me} - <i>i</i> Pr)(CO) ₂ Br] (Mn1b)	S3
13	Synthesis of <i>cis</i> -[Mn(PNP ^{NH} -Ph)(CO) ₂ Br] (Mn1e)	S3
14	Synthesis of <i>cis</i> -[Mn(PNP ^O - <i>i</i> Pr)(CO) ₂ Cl] (Mn2d)	S4
15	Synthesis of <i>cis</i> -[Re(PNP ^O - <i>i</i> Pr)(CO) ₂ Cl] (Re2d)	S4
16	Synthesis of [Mn(PNP ^{NMe} - <i>i</i> Pr)(CO) ₃]Br (Mn3b)	S4
17	Synthesis of [Mn(PNP ^{CH2} - <i>i</i> Pr)(CO) ₃]Br. (Mn3c)	S5
18	Synthesis of [Re(PNP ^{NH} - <i>i</i> Pr)(CO) ₃]Br (Re3a)	S5
19	Synthesis of [Re(PNP ^{NMe} - <i>i</i> Pr)(CO) ₃]Br (Re3b)	S5
20	Synthesis of [Re(PNP ^{NH} - <i>t</i> Bu)(CO) ₃]Br Re3f	S5
21	Synthesis of [Re(PNP ^{NH} -Ph)(CO) ₃]Br Re3e	S6
22	Synthesis of [Re(PNP ^{CH2} - <i>i</i> Pr)(CO) ₃]Cl (Re3c)	S6
23	Synthesis of [Mn(PNP ^{NH} - <i>t</i> Bu)(CO) ₂]Br Mn4f	S6
24	Synthesis of [[Mn(PNP ^{NH} - <i>t</i> Bu)(CO) ₂]BF ₄ 5f	S7
25	Synthesis of [Mn(PNP ^N - <i>t</i> Bu)(CO) ₂] Mn6f	S7

1	Synthesis of $[\text{Mn}(\text{PNP}^{\text{NH}}-i\text{Pr})(\text{CO})_3]\text{OTf}$ Mn7a.....	S7
2	Synthesis of <i>cis</i> - $[\text{Mn}(\text{PNP}^{\text{NH}}-i\text{Pr})(\text{CO})_2\text{OCHO}]$ Mn9a.....	S8
3	Synthesis of <i>cis</i> - $[\text{Mn}(\text{PNP}^{\text{NMe}}-i\text{Pr})(\text{CO})_2\text{OCHO}]$ Mn9b.....	S8
4	Synthesis of <i>cis</i> - $[\text{Mn}(\text{PNP}^{\text{CH}_2}-i\text{Pr})(\text{CO})_2\text{OCHO}]$ Mn9c	S8
5	Synthesis of <i>cis</i> - $[\text{Re}(\text{PNP}^{\text{NH}}-i\text{Pr})(\text{CO})_2\text{OCHO}]$ Re9a.....	S8
6	Synthesis of <i>cis</i> - $[\text{Re}(\text{PNP}^{\text{CH}_2}-i\text{Pr})(\text{CO})_2\text{OCHO}]$ Re9c.....	S9
7	References	S9

8

1 **General experimental information.** All manipulations were performed under an inert atmosphere of
 2 argon by using Schlenk techniques or in a MBraun inert-gas glovebox. Hydrogen (99.999% purity)
 3 was purchased from Messer Austria and used as received. The solvents were purified according to
 4 standard procedures.¹ The deuterated solvents were purchased from Aldrich and dried over 4 Å
 5 molecular sieves. All aldehyde substrates were obtained from commercial sources and purified by
 6 distillation prior to use. PNP pincer ligands **1a-f** were synthesized according to literature known
 7 procedures.² Complexes *cis*-[Mn(PNP^{NH}-*i*Pr)(CO)₂H] **Mn8a**, *cis*-[Mn(PNP^{Me}-*i*Pr)(CO)₂H] **Mn8b**,³ *cis*-
 8 *cis*-[Mn(PNP^{CH₂}-*i*Pr)(CO)₂H] **Mn8c**, *cis*-[Re(PNP^{NH}-*i*Pr)(CO)₂H] **Re8a**, *cis*-[Re(PNP^{CH₂}-*i*Pr)(CO)₂H]
 9 **Re8c**,⁴ were prepared according to the literature.⁵ ¹H, ¹³C{¹H}, ¹⁹F{¹H}, and ³¹P{¹H} NMR spectra were
 10 recorded on Bruker AVANCE-250, 400, and AVANCE-600 spectrometers. ¹H and ¹³C{¹H} NMR
 11 spectra were referenced internally to residual protio-solvent, and solvent resonances, respectively,
 12 and are reported relative to tetramethylsilane (δ = 0 ppm). ³¹P{¹H} NMR spectra were referenced
 13 externally to H₃PO₄ (85%) (δ = 0). ¹⁹F{¹H} NMR spectra referenced externally to trifluoro
 14 toluene(0.05%) (δ = 0 ppm).

15 Synthesis

16 ***cis*-[Mn(PNP^{Me}-*i*Pr)(CO)₂Br] (Mn1b).** PNP^{Me}-*i*Pr **1b** (185 mg, 0.50 mmol) and Mn(CO)₅Br
 17 (137 mg, 0.50 mmol) are stirred in a closed vessel at 120°C in dioxane (15 ml) for 18 h. The
 18 suspension is evaporated to dryness and the solid washed with *n*-pentane (20 ml). The yellow powder
 19 is dried under reduced pressure. Crystals suitable for x-ray diffraction were grown by slow diffusion of
 20 *n*-pentane into a solution of acetone. Yield: 250 mg (89 %). Anal. Calcd. for C₂₁H₃₇BrMnN₃O₂P₂
 21 (560.33). C, 45.01; H, 6.66; N, 7.50. Found: C, 45.00; H, 6.66; N, 7.47. ¹H NMR (600 MHz, δ, acetone-
 22 d₆, 20 °C) 7.57 (t, *J*_{HH} = 8.0 Hz, 1H, py⁴), 6.28 (d, *J*_{HH} = 8.1 Hz, 2H, py^{3,5}), 3.23 (s, 6H, NCH₃), 3.09 (dt,
 23 *J* = 14.0, 7.2 Hz, 2H, CH), 2.98 (dt, *J* = 13.2, 6.8 Hz, 2H, CH), 1.65 (dd, *J* = 14.9, 7.1 Hz, 6H, CH₃),
 24 1.54 (dd, *J* = 14.7, 7.3 Hz, 6H, CH₃), 1.49 (dd, *J* = 16.9, 7.1 Hz, 6H, CH₃), 1.22 (dd, *J* = 13.3, 7.0 Hz,
 25 6H, CH₃). ¹³C{¹H} NMR (151 MHz, δ, acetone-d₆, 20 °C) 229.6 (m, CO), 222.9 (m, CO), 162.7 (vt, *J*_{CP}
 26 = 10.4 Hz, py^{2,6}), 139.3 (s, py⁴), 97.6 (vt, *J*_{CP} = 3.1 Hz, py^{2,6}), 35.3 (vt, *J*_{CP} = 2.6 Hz, NCH₃), 33.7 (vt,
 27 *J*_{CP} = 8.9 Hz, CH), 30.2 (vt, *J*_{CP} = 11.1 Hz, CH), 21.9 (s, CH₃), 19.5 (s, CH₃), 17.9 (s, CH₃), 17.7 (vt, *J*_{CP}
 28 = 5.4 Hz, CH₃). ³¹P{¹H} NMR (101 MHz, δ, acetone-d₆, 20 °C) 155.6 (s, 2P). IR (ATR, cm⁻¹): 1929
 29 (ν_{CO}), 1853 (ν_{CO}).

30
 31 ***cis*-[Mn(PNP^{NH}-Ph)(CO)₂Br] (Mn1e).** PNP^{NH}-Ph **1e** (191 mg, 0.50 mmol) and Mn(CO)₅Br (137
 32 mg, 0.50 mmol) are stirred in dioxane (10 ml) for 2 h at 80°C. The yellow solution is evaporated to
 33 dryness and the solid washed 3 times with *n*-pentane (15 ml). The yellow powder is finally dried under
 34 reduced pressure. Crystals suitable for x-ray diffraction were grown by slow diffusion of *n*-pentane into
 35 a solution of acetone. Yield: 317 mg (95 %). Anal. Calcd. for C₃₁H₂₅BrMnN₃O₂P₂ (668.34). C, 55.71; H,
 36 3.77; N, 6.29. Found: C, 55.73; H, 3.80; N, 6.25. ¹H NMR (250 MHz, δ, acetone-d₆, 20 °C) 9.52 (m,
 37 2H, NH), 7.84 (m, 4H, ph^{2,6}), 7.57 (m, 4H, ph^{2,6}), 7.42 (m, 13H, ph^{3,4,5}, py⁴), 6.56 (d, *J*_{HH} = 7.8 Hz, 2H,
 38 py^{3,5}). ¹³C{¹H} NMR (151 MHz, δ, acetone-d₆, 20 °C) 230.0 (m, CO), 223.5 (m, CO), 160.5 (vt, *J*_{CP} =
 39 10.8 Hz, py^{2,6}), 140.5 (vt, *J*_{CP} = 22.8 Hz, ph¹), 139.1 (s, py⁴), 136.6 (vt, *J*_{CP} = 22.5 Hz, ph¹), 132.9 (vt,

1 $J_{CP} = 5.9$ Hz, $\text{ph}^{2,6}$), 130.58 (s, ph), 129.7 (vt, $J_{CP} = 6.0$ Hz, $\text{ph}^{2,6}$), 129.6 (s, ph), 129.4 (s, ph), 128.2
 2 (vt, $J_{CP} = 4.6$ Hz, $\text{ph}^{3,5}$), 128.1 (s, ph), 127.6 (vt, $J_{CP} = 5.0$ Hz, $\text{ph}^{3,5}$), 99.2 (vt, $J_{CP} = 3.6$ Hz, $\text{ph}^{3,5}$).
 3 $^{31}\text{P}\{^1\text{H}\}$ NMR (101 MHz, δ , acetone- d_6 , 20 °C) 115.2 (s, 2P). IR (ATR, cm^{-1}): 1922 (ν_{CO}), 1841 (ν_{CO}).

4 ***cis*-[Mn(PNP^O-*i*Pr)(CO)₂Cl] (Mn2d)**. PNP^O-*i*Pr **1d** (137 mg, 0.40 mmol) and Mn(CO)₅Br (110
 5 mg, 0.40 mmol) are stirred in dioxane (10 ml) for 2 h at 80°C. The yellow solution is evaporated to
 6 dryness and the solid washed 3 times with *n*-pentane (15 ml). The yellow powder is finally dried under
 7 reduced pressure. Crystals suitable for x-ray diffraction were grown by slow evaporation of a saturated
 8 solution (CH₂Cl₂/*n*-pentane) in argon atmosphere. Yield: 197 mg (92 %). Anal. Calcd. for
 9 C₁₉H₃₁BrMnNO₄P₂ (489.79). C, 46.59; H, 6.38; N, 2.86. Found: C, 46.55; H, 6.36; N, 2.88. ^1H NMR
 10 (250 MHz, δ , acetone- d_6 , 20 °C) 7.84 (t, $J_{HH} = 8.1$ Hz, 1H, py^4), 6.86 (d, $J_{HH} = 8.1$ Hz, 2H, $\text{py}^{3,5}$), 3.61
 11 (m, 2H, CH), 3.03 (m, 4H, CH), 1.56-1.20 (m, 24H, CH₃). $^{13}\text{C}\{^1\text{H}\}$ NMR (151 MHz, δ , acetone- d_6 , 20
 12 °C) 228.6 (m, CO), 224.3 (m, CO), 163.5 (vt, $J_{CP} = 5.6$ Hz, $\text{py}^{2,6}$), 142.9 (s, py^4), 108.8 (s, $\text{py}^{3,5}$), 27.3
 13 (vt, $J_{CP} = 7.4$ Hz, CH), 17.0 (vt, $J_{CP} = 3.6$ Hz, CH₃), 16.9 (vt, $J_{CP} = 4.1$ Hz, CH₃), 16.5 (s, CH₃), 15.5 (s,
 14 CH₃). $^{31}\text{P}\{^1\text{H}\}$ NMR (101 MHz, δ , acetone- d_6 , 20 °C) 232.2 (s, 2P). IR (ATR, cm^{-1}): 1943 (ν_{CO}), 1875
 15 (ν_{CO}).

16 ***cis*-[Re(PNP^O-*i*Pr)(CO)₂Cl] (Re2d)**. PNP^O-*i*Pr **1d** 136 mg (0.4 mmol) and Re(CO)₅Cl (144 mg,
 17 0.4 mmol) are stirred in a closed vessel at 120°C in dioxane (15 ml) for 18 h. The suspension is
 18 evaporated to dryness and the solid washed with Et₂O (10 ml) and *n*-pentane (20 ml). Crystals
 19 suitable for x-ray diffraction were grown by slow diffusion of *n*-pentane in acetone. Yield: 228 mg (92
 20 %). Anal. Calcd. for C₁₉H₃₁ClNO₄P₂Re (621.06). C, 36.74; H, 5.03; N, 2.26. Found: C, 36.84; H, 5.08;
 21 N, 2.23. ^1H NMR (600 MHz, δ , acetone- d_6 , 20 °C) 7.76 (t, $J_{HH} = 8.1$ Hz, 1H, py^4), 6.80 (d, $J_{HH} = 8.1$ Hz,
 22 2H, $\text{py}^{3,5}$), 3.59 (m, 2H, CH), 2.89 (m, 2H, CH), 1.29 (dd, $J = 12.9, 7.0$ Hz, 6H, CH₃), 1.23 (m, 12H,
 23 CH₃), 1.09 (dd, $J = 15.1, 7.2$ Hz, 6H, CH₃). $^{13}\text{C}\{^1\text{H}\}$ NMR (151 MHz, δ , acetone- d_6 , 20 °C) 203.6 (m,
 24 CO), 193.9 (m, CO), 163.2 (vt, $J_{CP} = 3.7$ Hz, $\text{py}^{2,6}$), 143.4 (s, py^4), 102.8 (vt, $J_{CP} = 1.9$ Hz, $\text{py}^{3,5}$), 27.9
 25 (vt, $J_{CP} = 12.0$ Hz, CH), 17.6 (vt, $J_{CP} = 5.3$ Hz, CH), 17.1 (vt, $J_{CP} = 4.6$ Hz, CH₃), 16.7 (s, CH₃), 15.0 (s,
 26 CH₃). $^{31}\text{P}\{^1\text{H}\}$ NMR (101 MHz, δ , acetone- d_6 , 20 °C) 184.7 (2P). IR (ATR, cm^{-1}): 1928 (ν_{CO}), 1848
 27 (ν_{CO}).

28 **[Mn(PNP^{NMe}-*i*Pr)(CO)₃]Br (Mn3b)**. PNP^{NMe}-*i*Pr **1b** (185 mg, 0.50 mmol) and Mn(CO)₅Br (137
 29 mg, 0.50 mmol) are stirred at 80°C in dioxane (15 ml) for 2 h. The suspension is evaporated to
 30 dryness and the solid washed with *n*-pentane (20 ml). The pale powder is dried under reduced
 31 pressure. Crystals suitable for x-ray diffraction were grown by slow diffusion of *n*-pentane into a
 32 solution of acetone. Yield: 285 mg (97 %). Anal. Calcd. for C₂₁H₃₇BrMnN₃O₃P₂ (588.34). C, 44.91; H,
 33 6.34; N, 7.14. Found: C, 44.94; H, 6.34; N, 7.15. ^1H NMR (600 MHz, δ , dms_o- d_6 , 20 °C) 7.80 (t, $J_{HH} =$
 34 8.0 Hz, 1H, py^4), 6.47 (d, $J_{HH} = 8.1$ Hz, 2H, $\text{py}^{3,5}$), 3.36 (m, 4H, CH), 3.17 (s, 6H, NCH₃), 1.39 (dd, $J =$
 35 17.8, 6.5 Hz, 6H, CH₃), 1.19 (dd, $J = 14.3, 6.8$ Hz, 6H, CH₃). $^{13}\text{C}\{^1\text{H}\}$ NMR (151 MHz, δ , dms_o- d_6 , 20
 36 °C) 220.3 (m, CO), 215.4 (m, CO), 162.1 (vt, $J_{CP} = 8.3$ Hz, $\text{py}^{2,6}$), 142.3 (s, py^4), 100.0 (s, $\text{py}^{3,5}$), 35.2
 37 (s, NCH₃), 32.5 (vt, $J_{CP} = 12.0$ Hz, CH), 18.8 (s, CH₃), 18.6 (vt, $J_{CP} = 5.4$ Hz, CH₃). $^{31}\text{P}\{^1\text{H}\}$ NMR (101
 38 MHz, δ , acetone- d_6 , 20 °C) 156.5 (s, broad, 2P). IR (ATR, cm^{-1}): 2034 (ν_{CO}), 1929 (ν_{CO}).

1 **[Mn(PNP^{CH₂–iPr})(CO)₃]Br. (Mn3c)** PNP^{CH₂–iPr} (172 mg, 0.50 mmol) and Mn(CO)₅Br (137 mg,
 2 0.50 mmol) are stirred at 80°C in dioxane (15 ml) for 2 h. The suspension is evaporated to dryness
 3 and the solid washed with Et₂O (15 ml) and *n*-pentane (15 ml). The colorless powder is dried under
 4 reduced pressure. Crystals suitable for x-ray diffraction were grown by a solution of CH₂Cl₂ with *n*-
 5 pentane. Yield: 265 mg (95 %). Anal. Calcd. for C₂₂H₃₅BrMnNO₃P₂ (558.31). C, 47.33; H, 6.32; N,
 6 2.51. Found: C, 47.32; H, 6.32; N, 2.46. ¹H NMR of [Mn(PNP^{CH₂–iPr})(CO)₃]OTf (250 MHz, δ, acetone-
 7 d₆, 20 °C) 7.94 (t, *J*_{HH} = 7.5 Hz, 1H, py⁴), 7.68 (d, *J*_{HH} = 7.4 Hz, 2H, py^{3,5}), 4.11 (d, *J*_{HH} = 8.5 Hz, 2H,
 8 CH₂), 3.73 (d, *J*_{HH} = 8.9 Hz, 2H, CH₂), 2.82 (dt, *J* = 14.5, 7.3 Hz, 2H, CH), 2.32 (m, 2H, CH), 1.45-1.21
 9 (m, 24H, CH₃). ¹³C{¹H} NMR (151 MHz, δ, dms_o-d₆, 20 °C) 216.9 (m, CO), 207.4 (m, CO), 163.3 (m,
 10 py^{2,6}), 140.0 (s, py⁴), 122.6 (m, py^{2,6}), 51.9 (s, CH₂), 27.4 (vt, *J*_{CP} = 11.4 Hz, CH), 18.7 (d, *J*_{CP} = 20.1
 11 Hz, CH), 7.6 (s, CH₃). ³¹P{¹H} NMR (101 MHz, δ, dms_o-d₆, 20 °C) 88.3(s, 2P). IR (ATR, cm⁻¹): 2028
 12 (ν_{CO}), 1937 (ν_{CO}), 1916 (ν_{CO}).

13 **[Re(PNP^{NH–iPr})(CO)₃]Br (Re3a).** PNP-*iPr* **1a** (206 mg, 0.6 mmol) and Re(CO)₅Br (244 mg, 0.6
 14 mmol) are stirred in dioxane (10 ml) for 2 h at 80°C. The suspension is evaporated to dryness and the
 15 solid washed 3 times with *n*-pentane (15 ml). The colourless powder is finally dried under reduced
 16 pressure. Yield: 394 mg (95%). Anal. Calcd. for C₂₀H₃₃BrN₃O₃P₂Re (691.55). C, 34.74; H, 4.81; N,
 17 6.08. Found: C, 34.80; H, 4.83; N, 6.09. ¹H NMR (250 MHz, δ, dms_o-d₆, 20 °C) 9.21 (m, 2H, NH), 7.54
 18 (t, *J*_{HH} = 8.0 Hz, 1H, py⁴), 6.46 (d, *J*_{HH} = 8.1 Hz, 2H, py^{3,5}), 2.68 (m, 4H, CH), 1.35 (dd, *J* = 17.2, 6.9 Hz,
 19 12H, CH₃), 1.21 (dd, *J* = 17.6 Hz, 7.3 Hz, 12H, CH₃). ¹³C{¹H} NMR (63 MHz, δ, dms_o-d₆, 20 °C) 196.0
 20 (m, CO), 191.0 (vt, *J*_{CP} = 9.2 Hz, CO), 162.3 (vt, *J*_{CP} = 6.0 Hz, py^{2,6}), 141.8 (s, py⁴), 99.4 (s, py^{3,5}), 31.4
 21 (vt, *J*_{CP} = 15.9 Hz, CH), 18.9 (s, CH₃). ³¹P{¹H} NMR (101 MHz, δ, dms_o-d₆, 20 °C) 93.8 (2P). IR (ATR,
 22 cm⁻¹): 2045 (ν_{CO}), 1926 (ν_{CO}).

23 **[Re(PNP^{NMe–iPr})(CO)₃]Br (Re3b).** PNP^{NMe–iPr} **1b** (222 mg, 0.60 mmol) and Re(CO)₅Br (244
 24 mg, 0.60 mmol) are stirred in dioxane (10 ml) for 2 h at 80°C. The pale suspension is evaporated to
 25 dryness and the solid washed 3 times with *n*-pentane (15 ml). The off white powder is finally dried
 26 under reduced pressure. Crystals suitable for x-ray diffraction were grown by slow diffusion of *n*-
 27 pentane in acetone. Yield: 405 mg (94 %). Anal. Calcd. for C₂₂H₃₇BrN₃O₃P₂Re (719.61). C, 36.72; H,
 28 5.18; N, 5.84. Found: C, 36.72; H, 5.18; N, 5.82. ¹H NMR (600 MHz, δ, acetone-d₆, 20 °C) 7.90 (t, *J*_{HH}
 29 = 8.3 Hz, 1H, py⁴), 6.65 (d, *J*_{HH} = 8.3 Hz, 2H, py^{3,5}), 3.39 (m, 6H, NCH₃), 2.94 (m, 4H, CH), 1.46 (dd, *J*
 30 = 19.8 Hz, 6.9 Hz, 12H, CH₃), 1.22 (dd, *J* = 19.8 Hz, 6.9 Hz, 12H, CH₃). ¹³C{¹H} NMR (151 MHz, δ,
 31 acetone-d₆, 20 °C) 194.6 (m, CO), 190.8 (t, *J*_{CP} = 9.3 Hz, CO), 163.1 (vt, *J*_{CP} = 7.2 Hz, py^{2,6}), 142.0 (s,
 32 py⁴), 100.2 (vt, *J*_{CP} = 2.6 Hz, py^{3,5}), 35.4 (s, NCH₃), 32.25 (vt, *J*_{CP} = 15.2 Hz, CH), 19.2 (vt, *J*_{CP} = 4.6
 33 Hz, CH₃), 17.9 (s, CH₃). ³¹P{¹H} NMR (101 MHz, δ, acetone-d₆, 20 °C) 120.9 (s, 2P). IR (ATR, cm⁻¹):
 34 2045 (ν_{CO}), 1925 (ν_{CO}).

35 **[Re(PNP^{NH–tBu})(CO)₃]Br Re3f.** PNP^{NH–tBu} **1f** (199 mg, 0.50 mmol) and Re(CO)₅Br (203 mg,
 36 0.50 mmol) are stirred in dioxane (10 ml) for 2 h at 80°C. The pale suspension is evaporated to
 37 dryness and the solid washed 3 times with *n*-pentane (15 ml) and Et₂O (15 ml). The colourless powder
 38 is finally dried under reduced pressure. Crystals suitable for x-ray diffraction were grown by slow
 39 diffusion of *n*-pentane in acetone. Yield: 360 mg (96 %). Anal. Calcd. for C₂₄H₄₁BrN₃O₃P₂Re (747.66).

1 C, 38.55; H, 5.53; N, 5.62. Found: C, 38.52,41; H, 5.50; N, 5.63. ^1H NMR (250 MHz, δ , dms -d_6 , 20
 2 $^\circ\text{C}$) 9.04 (m, 2H, NH), 7.58 (t, $J_{\text{HH}} = 7.9$ Hz, 1H, py^4), 6.63 (d, $J_{\text{HH}} = 7.9$ Hz, 2H, $\text{py}^{3,5}$), 1.42 (m, 36H,
 3 CH_3). $^{13}\text{C}\{^1\text{H}\}$ NMR (151 MHz, δ , dms -d_6 , 20 $^\circ\text{C}$) 197.2 (s, CO), 196.6 (t, $J_{\text{CP}} = 8.5$ Hz, CO), 162.8 (s,
 4 $\text{py}^{2,6}$), 142.4 (s, py^4), 100.1 (s, $\text{py}^{3,5}$), 42.0 (vt, $J_{\text{CP}} = 10.9$ Hz, C_q), 29.6 (vt, $J_{\text{CP}} = 2.4$ Hz, CH_3). $^{31}\text{P}\{^1\text{H}\}$
 5 NMR (101 MHz, δ , dms -d_6 , 20 $^\circ\text{C}$) 116.0 (s, 2P). IR (ATR, cm^{-1}): 2034 (ν_{CO}), 1925 (ν_{CO}), 1910 (ν_{CO}).

6 **[Re(PNP^{NH}-Ph)(CO)₃]Br Re3e.** PNP-Ph **1e** (287 mg, 0.6 mmol) and $\text{Re}(\text{CO})_5\text{Br}$ (244 mg, 0.6
 7 mmol) are stirred in dioxane (10 ml) for 2 h at 80 $^\circ\text{C}$. The suspension is evaporated to dryness and the
 8 solid washed 3 times with Et_2O (20 ml). The colourless powder is finally dried under reduced pressure.
 9 Crystals suitable for x-ray diffraction were grown from a solution in EtOH by slow diffusion of *n*-
 10 pentane. Yield: 468 mg (94%). Anal. Calcd. for $\text{C}_{32}\text{H}_{25}\text{BrN}_3\text{O}_3\text{P}_2\text{Re}$ (827.62). C, 46.44; H, 3.04; N,
 11 5.08. Found: C, 46.53; H, 3.10; N, 5.02. ^1H NMR (600 MHz, δ , dms -d_6 , 20 $^\circ\text{C}$) 10.71 (m, 2H, NH),
 12 7.82-7.71 (m, 8H, $\text{ph}^{2,6}$), 7.63-7.57 (m, 13H, py^4 , $\text{ph}^{3,5}$), 6.89 (d, $J_{\text{HH}} = 8.1$ Hz, $\text{py}^{3,5}$). $^{13}\text{C}\{^1\text{H}\}$ NMR (151
 13 MHz, δ , dms -d_6 , 20 $^\circ\text{C}$) 195.5 (s, CO), 188.3 (vt, $J_{\text{CP}} = 8.8$ Hz, CO), 161.5 (vt, $J_{\text{CP}} = 7.6$ Hz, $\text{py}^{2,6}$),
 14 142.4 (s, py^4), 136.2 (vt, $J_{\text{CP}} = 30.0$ Hz, C_q), 132.3 (s, ph^4), 130.7 (vt, $J_{\text{CP}} = 7.0$ Hz, $\text{ph}^{2,6}$), 129.7 (vt,
 15 $J_{\text{CP}} = 5.4$ Hz, $\text{ph}^{3,5}$), 100.1 (s, $\text{py}^{3,5}$), 42.0 (vt, $J_{\text{CP}} = 10.9$ Hz, C_q), 29.6 (vt, $J_{\text{CP}} = 2.4$ Hz, CH_3). $^{31}\text{P}\{^1\text{H}\}$
 16 NMR (101 MHz, δ , dms -d_6 , 20 $^\circ\text{C}$) 65.4 (2P). IR (ATR, cm^{-1}): 2068 (ν_{CO}), 1966 (ν_{CO}), 1917 (ν_{CO}).

17 **[Re(PNP^{CH2}-iPr)(CO)₃]Cl (Re3c).** PNP^{CH2}-iPr **1c** (136 mg, 0.4 mmol) and $\text{Re}(\text{CO})_5\text{Cl}$ (144 mg,
 18 0.4 mmol) are stirred in dioxane (10 ml) for 2 h at 80 $^\circ\text{C}$. The suspension is evaporated to dryness and
 19 the solid washed 3 times with *n*-pentane (15 ml). The colourless powder is finally dried under reduced
 20 pressure. Crystals suitable for x-ray diffraction were grown by slow diffusion of *n*-pentane in CH_2Cl_2 .
 21 Yield: 251 mg (97%). Anal. Calcd. for $\text{C}_{22}\text{H}_{35}\text{ClNO}_3\text{P}_2\text{Re}$ (645.13). C, 40.96; H, 5.47; Cl, 5.50; N, 2.17.
 22 Found: C, 40.98; H, 5.47; N, 2.16. ^1H NMR (600 MHz, δ , dms -d_6 , 20 $^\circ\text{C}$) 8.02 (t, $J_{\text{HH}} = 7.7$ Hz, 1H,
 23 py^4), 7.66 (d, $J_{\text{HH}} = 7.8$ Hz, 2H, $\text{py}^{3,5}$), 4.26 (m, 4H, CH_2), 2.60 (m, 4H, CH), 1.24 (dd, $J = 16.2$, 7.0 Hz,
 24 12H, CH_3), 1.12 (dd, $J = 16.4$ Hz, 7.2 Hz, 12H, CH_3). $^{13}\text{C}\{^1\text{H}\}$ NMR (151 MHz, δ , dms -d_6 , 20 $^\circ\text{C}$)
 25 198.2 (m, CO), 193.8 (vt, $J_{\text{CP}} = 8.3$ Hz, CO), 165.0 (vt, $J_{\text{CP}} = 3.0$ Hz, $\text{py}^{2,6}$), 140.6 (s, py^4), 122.3 (vt, J_{CP}
 26 = 4.6 Hz, $\text{py}^{3,5}$), 42.1 (vt, $J_{\text{CP}} = 13.9$ Hz, CH_2), 27.7 (vt, $J_{\text{CP}} = 14.3$ Hz, CH_3), 18.9 (vt, $J_{\text{CP}} = 13.3$ Hz,
 27 CH_3). $^{31}\text{P}\{^1\text{H}\}$ NMR (101 MHz, δ , dms -d_6 , 20 $^\circ\text{C}$) 48.6 (2P). IR (ATR, cm^{-1}): 2041 (ν_{CO}), 1936 (ν_{CO}),
 28 1916 (ν_{CO}).

29 **[Mn(PNP^{NH}-tBu)(CO)₂]Br Mn4f.** PNP-tBu **1f** (200 mg, 0.50 mmol) and $\text{Mn}(\text{CO})_5\text{Br}$ (137 mg,
 30 0.50 mmol) are stirred in dioxane (15 ml) at 80 $^\circ\text{C}$ for 4 h. The insoluble precipitate is isolated via
 31 filtration by a glass frit (por. 3) The solid is washed 2 times with THF (15 ml) and *n*-pentane (15 ml)
 32 and finally dried under reduced pressure zu obtain a violet powder. Crystals suitable for x-ray
 33 diffraction were grown by slow diffusion of Et_2O into a solution of acetone/DMSO (3:1). Yield: 280 mg
 34 (95 %). Anal. Calcd. for $\text{C}_{23}\text{H}_{41}\text{BrMnN}_3\text{O}_2\text{P}_2$ (588.38). C, 46.95; H, 7.02; N, 7.14. Found: C, 46.99; H,
 35 6.99; N, 7.13. ^1H NMR (250 MHz, δ , dms -d_6 , 20 $^\circ\text{C}$) 9.14 (m, 2H, NH), 7.74 (m, 1H, py^4), 6.63 (d, J_{HH}
 36 = 8.9 Hz, 2H, $\text{py}^{3,5}$), 1.36 (m, 36H, CH_3). $^{13}\text{C}\{^1\text{H}\}$ NMR (151 MHz, δ , dms -d_6 , 20 $^\circ\text{C}$) 235.6 (vt, J_{CP}
 37 = 17.8 Hz, CO), 165.6 (vt, $J_{\text{CP}} = 8.6$ Hz, $\text{py}^{2,6}$), 144.6 (s, py^4), 99.6 (m, $\text{py}^{3,5}$), 28.4 (m, , CH_3), 26.7 (m,
 38 C_q). $^{31}\text{P}\{^1\text{H}\}$ NMR (101 MHz, δ , dms -d_6 , 20 $^\circ\text{C}$) 147.6 (s, 2P). IR (ATR, cm^{-1}): 1936 (ν_{CO}), 1865 (ν_{CO}),
 39 1856 (ν_{CO}).

1 **[Mn(PNP^{NH}-*t*Bu)(CO)₂]BF₄ 5f.** PNP-*t*Bu **1f** (200 mg, 0.50 mmol) and Mn(CO)₅Br (137 mg,
 2 0.50 mmol) are stirred in dioxane (15 ml) at 80 °C for 4 h. The dark solid is filtered with a glass frit (por.
 3 3), washed with Et₂O (15 ml) and dried under reduced pressure. The violet powder is stirred with
 4 AgBF₄ (98 mg, 0.5 mmol) in acetone (10 ml) for 1 h. The insoluble precipitate are removed by filtration
 5 over celite and the solution is evaporated to dryness. The solid is washed with Et₂O (15 ml) and *n*-
 6 pentane (15 ml) and finally dried under reduced pressure zu obtain a soluble violet powder. Crystals
 7 suitable for x-ray diffraction were grown by slow diffusion of *n*-pentane into a solution of acetone/EtOH
 8 (1:1). Yield: 245 mg (82 %). Anal. Calcd. for C₂₃H₄₁BF₄MnN₃O₂P₂ (595.28). C, 46.41; H, 6.94; N, 7.06.
 9 Found: C, 46.44; H, 6.95; N, 7.05. ¹H NMR (250 MHz, δ, acetone-d₆, 20 °C) 8.49 (m, 2H, NH), 7.76 (t,
 10 1H, J_{HH} = 8.0 Hz, py⁴), 6.80 (d, J_{HH} = 8.0 Hz, 2H, py^{3,5}), 1.36 (m, 36H, CH₃). ¹³C{¹H} NMR (151 MHz, δ,
 11 acetone-d₆, 20 °C) 234.9 (vt, J_{CP} = 17.2 Hz, CO), 165.2 (vt, J_{CP} = 8.3 Hz, py^{2,6}), 144.4 (s, py⁴), 99.8 (vt,
 12 J_{CP} = 3.2 Hz, py^{3,5}), 39.7 (vt, J_{CP} = 8.6 Hz, C_q), 27.7 (vt, J_{CP} = 2.0 Hz, CH₃). ³¹P{¹H} NMR (101 MHz, δ,
 13 acetone-d₆, 20 °C) 148.6 (s, 2P). IR (ATR, cm⁻¹): 1936 (ν_{CO}), 1865 (ν_{CO}), 1856 (ν_{CO}).

14 **[Mn(PNP^N-*t*Bu)(CO)₂] Mn6f.** To a suspension of **5f** [Mn(PNP^{NH}-*t*Bu)(CO)₂]Br (118 mg, 0.20
 15 mmol) in THF (15 ml), NaH (11 mg, 0.46 mmol) are added. The suspension turns deep blue after 10
 16 min and is stirred for 2h. Insoluble solids are removed by filtration over celite. The solvent is then
 17 removed under reduced pressure. The crude product is redissolved in *n*-pentane (20 ml), filtered over
 18 celite and evaporated to dryness zu obtain a blue powder. Yield: 96 mg (95 %). Anal. Calcd. for
 19 C₂₃H₄₀MnN₃O₂P₂ (507.20). C, 54.44; H, 7.94; N, 8.28. Found: C, 54.45; H, 7.99; N, 8.22. ¹H NMR (250
 20 MHz, δ, C₆D₆, 20 °C) 6.91 (t, J_{HH} = 7.4 Hz, 1H, py⁴), 6.79 (d, J_{HH} = 8.4 Hz, 1H, py³), 5.13 (d, J_{HH} = 6.9
 21 Hz, 1H, py⁵), 4.27 (d, J_{HH} = 6.7 Hz, 1H, NH), 1.36 (d, J_{HP} = 13.0 Hz, 18H, CH₃), 0.94 (d, J_{HP} = 13.7 Hz,
 22 18H, CH₃). ¹³C{¹H} NMR (151 MHz, δ, C₆D₆, 20 °C) 238.2 (vt, J_{CP} = 16.2 Hz, CO), 174.6 (vdd, J_{CP} =
 23 8.4, 2.8 Hz, py²), 162.0 (vdd, J_{CP} = 12.7, 8.7 Hz, py⁶), 139.6 (s, py⁴), 108.6 (vd, J_{CP} = 20.9 Hz, py³),
 24 85.7 (vd, J_{CP} = 7.1 Hz, py⁵), 118.1 (s, py^{3,5}), 39.4 (d, J_{CP} = 23.7 Hz, C_q), 38.2 (d, J_{CP} = 15.7 Hz, C_q),
 25 28.5 (d, J_{CP} = 3.7 Hz, CH₃), 27.9 (d, J_{CP} = 5.5 Hz, CH₃). ³¹P{¹H} NMR (101 MHz, δ, C₆D₆, 20 °C) 145.7
 26 (A), 142.2 (B) (AB, J_{PP} = 84.5 Hz, 2P). IR (ATR, cm⁻¹): 1913 (ν_{CO}), 1838 (ν_{CO}).

27 **[Mn(PNP^{NH}-*i*Pr)(CO)₃]OTf Mn7a.** PNP^{NH}-*i*Pr **1a** (170 mg, 0.50 mmol), Mn(CO)₅Br (137 mg,
 28 0.50 mmol) and AgOTf (129 mg, 0.5 mmol) are stirred at 80 °C in dioxane (15 ml) for 4 h. The
 29 suspension is evaporated to dryness and the solid washed with Et₂O (15 ml) and *n*-pentane (15 ml).
 30 The colorless powder is dried under reduced pressure. Crystals suitable for x-ray diffraction were
 31 grown by slow diffusion of *n*-pentane into a solution of acetone. Yield: 250 mg (89 %). Anal. Calcd. for
 32 C₂₁H₃₃F₃MnN₃O₆P₂S (629.45). C, 40.07; H, 5.28; N, 6.68. Found: C, 40.12; H, 5.31; N, 6.66. ¹H NMR
 33 (400 MHz, δ, acetone-d₆, 20 °C) 8.28 (m, 2H, NH), 7.50 (t, J_{HH} = 8.0 Hz, 1H, py⁴), 6.55 (d, J_{HH} = 8.0
 34 Hz, 2H, py^{3,5}), 2.93 (m, 4H, CH), 1.53 (dd, J = 16.3, 7.0 Hz, 12H, CH₃), 1.43 (dd, J = 17.1, 7.3 Hz,
 35 12H, CH₃). ¹³C{¹H} NMR (151 MHz, δ, acetone-d₆, 20 °C) 221.0 (m, CO), 215.4 (m, CO), 161.0 (vt, J_{CP}
 36 = 7.4 Hz, py^{2,6}), 141.0 (s, py⁴), 99.8 (vt, J_{CP} = 3.3 Hz, py^{2,6}), 30.9 (m, CH), 17.59 (s, CH₃), 17.58 (s,
 37 CH₃). ³¹P{¹H} NMR (101 MHz, δ, acetone-d₆, 20 °C) 133.4 (s, 2P). IR (ATR, cm⁻¹): 2043 (ν_{CO}), 1941
 38 (ν_{CO}), 1927 (ν_{CO}).

1 **cis-[Mn(PNP^{NH}-iPr)(CO)₂OCHO] Mn9a.** This compound was already published in an earlier
 2 manuscript. For convenience of the reader, the procedure and spectroscopic dataset is repeated here.
 3 **Mn8a** *cis*-[Mn(PNP^{NH}-iPr)(CO)₂H] (225 mg, 0.5 mmol) was dissolved in CH₂Cl₂ and the solution
 4 purged with CO₂ (1 atm) for 1 min. An off white suspension is formed and after 15 min the solid was
 5 collected in a glass frit and dried under reduced pressure. Yield: 255 mg (99%). Anal. Calcd. for
 6 C₂₀H₃₆MnN₃O₅P₂ (515.40). C, 46.61; H, 7.04; N, 8.15. Found: C, 46.70; H, 7.10; N, 8.02. ¹H NMR (250
 7 MHz, δ, C₆D₆, 20 °C) 8.21 (s, 1H, HCOO), 8.19 (b, 2H, NH), 7.33 (t, *J*_{HH} = 7.8 Hz, 1H, py⁴), 6.28 (d,
 8 *J*_{HH} = 7.8 Hz, 2H, py^{3,5}), 2.51 (m, 2H, CH), 2.23 (m, 2H, CH), 1.41-0.96 (m, 24H, CH₃). ¹³P{¹H} NMR
 9 (101 MHz, δ, DMSO-*d*₆, 20 °C) 136.7 (s). IR (ATR, cm⁻¹): 1923 (ν_{CO}), 1842 (ν_{CO}), 1593 (ν_{CO}). ¹³C{¹H}
 10 NMR (151 MHz, δ, acetone-*d*₆, 20 °C) 230.3 (m, CO), 225.6 (m, CO), 168.3 (s, COOH), 162.0 (vt, *J*_{CP}
 11 = 4.7 Hz, py^{2,6}), 139.6 (s, py⁴), 97.9 (s, py^{3,5}), 26.7 (vt, *J*_{CP} = 12.6 Hz, CH), 26.3 (vt, *J*_{CP} = 8.1 Hz, CH),
 12 19.4 (vt, *J*_{CP} = 3.2 Hz, CH₃), 18.8 (s, CH₃), 18.6 (m, CH₃), 17.1 (s, CH₃).

13 **cis-[Mn(PNP^{NMe}-iPr)(CO)₂ OCHO] Mn9b.** A solution of **Mn8b** Mn(PNP^{NMe}-iPr)(CO)₂H (96 mg,
 14 0.2 mmol) and formic acid (30 mg, 0.44 mmol) is stirred in benzene (5 ml) for 10 min. The solvent is
 15 reduced under reduced pressure and the solid washed with *n*-pentane (2 x 5 ml). The powder is finally
 16 dried under reduced pressure zu obtain a pale yellow powder. Yield: 105 mg (quantitative). Anal.
 17 Calcd. for C₂₂H₃₈MnN₃O₄P₂ (525.44). C, 50.29; H, 7.29; N, 8.00. Found: C, 50.35; H, 7.35; N, 7.94. ¹H
 18 NMR (250 MHz, δ, acetone-*d*₆, 20 °C) 8.19 (s, 2H, HCOO), 7.78 (m, 2H, NH), 7.36 (t, *J*_{HH} = 8.0 Hz, 1H,
 19 py⁴), 6.43 (dd, *J*_{HH} = 8.0 Hz, 1.7 2H, py^{3,5}), 2.68 (m, 2H, CH), 2.46 (m, 2H, CH), 1.41 (dd, *J*_{HH} = 17.7
 20 Hz, 7.0 Hz, 6H, CH₃), 1.34 (dd, *J*_{HH} = 13.3 Hz, 7.0 Hz, 6H, CH₃), 1.41 (m 12H, CH₃). ¹³C{¹H} NMR (151
 21 MHz, δ, acetone-*d*₆, 20 °C) 228.7 (m, CO), 224.4 (m, CO), 169.6 (s, COOH), 163.0 (m, py^{2,6}), 139.9 (s,
 22 py⁴), 97.6 (s, py^{3,5}), 24.6 (s, NCH₃), 30.9 (vt, *J*_{CP} = 6.0 Hz, CH), 30.1 (vt, *J*_{CP} = 11.5 Hz, CH), 19.0 (m,
 23 CH), 18.3 (m, CH₃), 18.2 (m, CH₃), 18.0 (m, CH₃). ³¹P{¹H} NMR (101 MHz, δ, acetone-*d*₆, 20 °C) 157.8
 24 (s, 2P). IR (ATR, cm⁻¹): 1929 (ν_{CO}), 1844 (ν_{CO}), 1573 (ν_{COOH}).

25 **cis-[Mn(PNP^{CH2}-iPr)(CO)₂OCHO] Mn9c.** A solution of **Mn8c** Mn(PNP^{CH2}-iPr)(CO)₂H (90 mg,
 26 0.2 mmol) in benzene (5 ml) is stirred under CO₂ atmosphere (1 atm) for 2 h. The solvent is reduced
 27 under reduced pressure and the solid washed with *n*-pentane (2 x 5 ml). The powder is finally dried
 28 under reduced pressure zu obtain a pale yellow powder. Yield: 50 mg (quantitative). Anal. Calcd. for
 29 C₂₂H₃₆MnNO₄P₂ (495.41). C, 53.34; H, 7.32; N, 2.83. Found: C, 53.35; H, 7.31; N, 2.86. ¹H NMR (250
 30 MHz, δ, C₆D₆, 20 °C) 9.16 (s, 2H, HCOO), 6.76 (t, *J*_{HH} = 6.7 Hz, 1H, py⁴), 6.46 (d, *J*_{HH} = 7.3 Hz, 2H,
 31 py^{3,5}), 3.16 (m, 2H, CH₂), 2.91 (m, 2H, CH₂), 1.16 (m, 18H, CH), 1.13 (dd, *J*_{HH} = 12.5 Hz, 7.3 Hz, 6H,
 32 CH₃). ¹³C{¹H} NMR (151 MHz, δ, C₆D₆, 20 °C) 232.3 (m, CO), 228.4 (m, CO), 169.6 (s, COOH), 163.5
 33 (vt, *J*_{CP} = 5.7 Hz, py^{2,6}), 135.9 (s, py⁴), 119.7 (vt, *J*_{CP} = 4.3 Hz, py^{3,5}), 38.81 (vt, *J*_{CP} = 7.1 Hz, CH₂), 25.5
 34 (vt, *J*_{CP} = 10.0 Hz, CH), 24.5 (vt, *J*_{CP} = 6.3 Hz, CH), 19.0 (s, CH₃), 18.9 (s, CH₃), 18.8 (s, CH₃) 18.1 (s,
 35 CH₃). ³¹P{¹H} NMR (101 MHz, δ, C₆D₆, 20 °C) 91.7 (s, 2P). IR (ATR, cm⁻¹): 1912 (ν_{CO}), 1825 (ν_{CO}),
 36 1587 (ν_{COOH}).

37 **cis-[Re(PNP^{NH}-iPr)(CO)₂OCHO] Re9a.** A solution of **Re8a** Re(PNP^{NH}-iPr)(CO)₂H (45 mg,
 38 0.08 mmol) in benzene (2 ml) is stirred under CO₂ atmosphere (1 atm) for 2 h. The solvent is reduced
 39 under reduced pressure and the solid washed with *n*-pentane (2 x 5 ml). The powder is finally dried

1 under reduced pressure zu obtain a pale yellow powder. Yield: 58 mg (quantitative). Anal. Calcd. for
 2 $C_{20}H_{34}ReN_3O_4P_2$ (628.66). C, 38.21; H, 5.45; N, 6.68. Found: C, 38.25; H, 5.14; N, 6.66. 1H NMR (250
 3 MHz, δ , acetone- d_6 , 20 °C) 8.19 (s, 2H, $HCOO$), 7.78 (m, 2H, NH), 7.36 (t, $J_{HH} = 8.0$ Hz, 1H, py^4), 6.43
 4 (dd, $J_{HH} = 8.0$ Hz, 1.7 2H, $py^{3,5}$), 2.68 (m, 2H, CH), 2.46 (m, 2H, CH), 1.41 (dd, $J_{HH} = 17.7$ Hz, 7.0 Hz,
 5 6H, CH_3), 1.34 (dd, $J_{HH} = 13.3$ Hz, 7.0 Hz, 6H, CH_3), 1.41 (m 12H, CH_3). $^{13}C\{^1H\}$ NMR (151 MHz, δ ,
 6 acetone- d_6 , 20 °C) 206.8 (m, CO), 197.8 (m, CO), 167.7 (s, COOH), 162.4 (vt, $J_{CP} = 7.5$ Hz, $py^{2,6}$),
 7 139.5 (s, py^4), 97.7 (s, $py^{3,5}$), 27.6 (vt, $J_{CP} = 15.4$ Hz, CH), 26.8 (vt, $J_{CP} = 12.2$ Hz, CH), 19.1 (vt, $J_{CP} =$
 8 4.2 Hz, CH), 18.6 (s, CH_3), 18.2 (s, CH_3), 16.0 (s, CH_3). $^{31}P\{^1H\}$ NMR (101 MHz, δ , acetone- d_6 , 20 °C)
 9 103.5 (s, 2P). IR (ATR, cm^{-1}): 1925 (ν_{CO}), 1839 (ν_{CO}), 1594 (ν_{COOH}).

10 **cis-[Re(PNP^{CH₂)-iPr)(CO)₂OCHO] Re9c.}** A solution of **Re8c** $Re(PNP^{CH_2-iPr})(CO)_2H$ (45 mg,
 11 0.08 mmol) in benzene (2 ml) is stirred under CO_2 atmosphere (1 atm) for 2 h. The solvent is reduced
 12 under reduced pressure and the solid washed with *n*-pentane (2 x 5 ml). The powder is finally dried
 13 under reduced pressure zu obtain a pale yellow powder. Yield: 58 mg (quantitative). Anal. Calcd. for
 14 $C_{22}H_{36}ReNO_4P_2$ (626.68). C, 42.16; H, 5.79; N, 2.24. Found: C, 42.20; H, 5.80; N, 2.24. 1H NMR (250
 15 MHz, δ , C_6D_6 , 20 °C) 8.89 (s, 2H, $HCOO$), 6.88 (t, $J_{HH} = 7.8$ Hz, 1H, py^4), 6.52 (d, $J_{HH} = 7.7$ Hz, 2H,
 16 $py^{3,5}$), 3.33 (dt, $J_{HH} = 16.4$ Hz, 4.1 Hz, 2H, CH_2), 3.33 (dt, $J_{HH} = 16.4$ Hz, 3.8 Hz, 2H, CH_2), 2.10 (m, 4H,
 17 CH), 1.13 (dd, $J_{HH} = 15.5$ Hz, 7.3 Hz, 12H, CH_3), 1.03 (dd, $J_{HH} = 15.4$ Hz, 7.5 Hz, 6H, CH_3), 0.93 (dd,
 18 $J_{HH} = 13.6$ Hz, 7.1 Hz, 6H, CH_3). $^{13}C\{^1H\}$ NMR (151 MHz, δ , C_6D_6 , 20 °C) 208.2 (m, CO), 202.5 (m,
 19 CO), 169.4 (s, COOH), 164.6 (vt, $J_{CP} = 4.3$ Hz, $py^{2,6}$), 136.5 (s, py^4), 119.8 (vt, $J_{CP} = 4.2$ Hz, $py^{3,5}$),
 20 41.7 (vt, $J_{CP} = 10.6$ Hz, CH_2), 26.8 (vt, $J_{CP} = 13.6$ Hz, CH), 25.0 (vt, $J_{CP} = 10.7$ Hz, CH), 19.3 (s, CH_3),
 21 19.1 (s, CH_3), 17.7 (s, CH_3). $^{31}P\{^1H\}$ NMR (101 MHz, δ , C_6D_6 , 20 °C) 56.1 (s, 2P). IR (ATR, cm^{-1}): 1906
 22 (ν_{CO}), 1816 (ν_{CO}), 1621 (ν_{COOH}).

23 References

- 24 1 Perrin, D.D.; Armarego, W. L. F. *Purification of Laboratory Chemicals*, 3rd ed.; Pergamon: New
 25 York, **1988**.
- 26 2 (a) Leung W.-P.; Ip Q. W.-Y.; Wong S.-Y.; Mak T. C. W. *Organometallics* **2003**, *22*, 4604-4609.
 27 (b) Salem H.; Shimon L. J. W.; Posner-Diskin Y.; Leitus G.; Ben-David Y.; Milstein D.
 28 *Organometallics* **2009**, *28*, 4791-4806. (c) Benito-Garagorri D.; Becker E.; Wiedermann J.;
 29 Lackner W.; Pollak M.; Mereiter K.; Kisala J.; Kirchner K. *Organometallics* **2006**, *25*, 1900-1913.
 30 (d) Öztöpcü Ö.; Holzacker C.; Puchberger M.; Weil M.; Mereiter K.; Veiros L. F.; Kirchner K.
 31 *Organometallics* **2013**, *32*, 3042-3052. (e) Schirmer, W.; Flörke, U.; Haupt, H.-J. Z. Anorg. Allg.
 32 Chem. **1987**, *545*, 83-97. (f) Schirmer, W.; Flörke, U.; Haupt, H.-J. Z. Anorg. Allg. Chem. **1989**,
 33 *574*, 239-255.
- 34 3 Mastalir M.; Glatz M.; Gorgas N.; Stöger B.; Pittenauer E.; Allmaier G.; Veisor L. F.; Kirchner K.
 35 Chem. Eur. J. **2016**, *22*, 12316-12320.
- 36 4 Glatz M.; Stöger B.; Himmelbauer D.; Veiros L. F.; Kirchner K. *ACS Catal.* **2018**, *8*, 4009-4016.

37

38

3 Conclusion and Closing Words

In summary, a series of 2,6-diaminopyridine (DAP) base PNP pincer complexes have been synthesized and applied in Fe(II) and Mn(I) chemistry. In several comparative studies, the influence of size and electronics was investigated. General procedures for preparation of phosphine precursors have been applied.

The unusual substance class of octahedral κ^3, κ^2 -[Fe(PNP)₂X]⁺ complexes, made up of two PNP pincer ligands in different bonding modes, has been characterized. Unlike earlier estimations, it has been proven, that the nature of these cationic complexes is purely steric driven. The *cis* configuration of the pyridines is stabilized by intramolecular hydrogen bonding between the amino groups and pyridine nitrogen. The non-coordinated phosphine site, points away from the coordination center and is prone to oxidation by molecular sulfur and oxygen. Polar solvents or abstraction of a coordinated halide, results in the irreversible formation of the thermodynamic stable dicationic κ^3, κ^2 -[Fe(PNP)₂X]²⁺ complexes. κ^3, κ^2 -[Fe(PNP)₂X]⁺ of very small ligands undergo this rearrangement immediately and cannot be isolated in pure form.

The configuration of κ^3, κ^2 -[Fe(PNP)₂X]⁺ complexes leads to high stress and distortion of ideal octahedral geometry. The PNP ligand in bidentate coordination mode is therefore labile and can be substituted by other donors. Carbon monoxide (CO) proved to displace the labile PNP ligand to form stable Fe(II) carbonyl complexes [Fe(PNP)(CO)X₂]. These complexes were not accessible with non-bulky phosphines before. The reaction does not proceed, when a perfect octahedral structure is apparent. The carbonyl ligands of complexes [Fe(PNP)(CO)X₂] are also labile can be removed upon thermal treatment. This process is also steric driven – the temperatures and time needed are higher, the smaller the ligands are.

The formation of cationic carbonyl complexes [Fe(PNP)(CO)₂X]⁺ is achieved by polar solvents or halide abstraction under CO atmosphere. The *trans* configuration of the CO ligands is always isolated as the most stable isomer. This was independent on the ligand and starting material.

Manganese(I) complexes of type [Mn(PNP)(CO)₂X] and [Mn(PNP)(CO)₃]⁺ have been synthesized. The major product was strongly depending on the reaction conditions and ligand backbone. Hydrido complexes of type [Mn(PNP)(CO)₂H] have been prepared and were only approachable from [Mn(PNP)(CO)₂X] as a precursor. The hydrido complex [Mn(PNP^{NH}-iPr)(CO)₂H] performed extremely well as pre-catalyst for selective hydrogenation of aldehydes. A substrate scope included over a dozen natural and synthetic aldehydes. The catalysis proceeded only in protic solvents, and is highly depending on ligand-metal cooperation. Turnover numbers (TONs) of

10,000 have been accomplished. Analogue Re(I) compounds showed only low grade performance.

A general study on Mn(I) and Re(I) PNP pincer chemistry was done by investigating the activation of carbon dioxide (CO_2). Mn(I) forms stable 16 electron complexes of general formula $[\text{Mn}(\text{PNP})(\text{CO})_2]^+$ and $[\text{Mn}(\text{PNP})(\text{CO})_2]$ upon deprotonation. Rhenium complexes preferably formed cationic tricarbonyl complexes $[\text{Re}(\text{PNP})(\text{CO})_3]^+$. Hydrido complexes of both metals were synthesized and showed impressive reactivity towards gaseous CO_2 . An 1,2-insertion led to the formation of formiato complexes $[\text{Mn}(\text{PNP})(\text{CO})_2\text{OCHO}]$ and $[\text{Re}(\text{PNP})(\text{CO})_2\text{OCHO}]$.

The overall knowledge collected in this work, describes the interaction between a well-established ligand system and base metal. This understanding can contribute to solidify the application of iron catalysts abroad. Although many applications have been found for base metals, a practical use to replace precious metals is still distant. Even though, the raw metals themselves are of superb ecologic value, the precursors, procedures and especially ligands are intensive in costs and resources. The true value of this fundamental research is the challenging quest to find key leading structures, which inherit promising reactivity. Once this goal is accomplished, the easy-to-study systems can be optimized step by step towards actual sustainable compounds. Therefore, information like how to trim stability, exchange ligands, improve the rate determining step is so valuable for future application. The era of iron is has already experienced 20 years of constant improvements and success and will for sure see a rising interest and demand. The manganese era is just beginning, and the fact that is has similarities with iron in reactivity is a benefit in its early evolution. It would be pleasure to see these contributions be a part of a prospective turnaround in homogeneous catalysis.

4 State of Contribution

Manuscript #1

The investigation of κ^3, κ^2 Fe PNP complexes was started by Bernhard Bichler on the PNP-Ph ligand system. The extension of the scope of κ^3, κ^2 Fe PNP complexes was the authors initiative, using other non-bulky phosphines as well as the investigation of reactivity. This included all syntheses, characterization and simulation of NMR spectra. *N*-substituted 2,6-diaminopyridine precursors were provided by Matthias Mastalir. X-ray measurements were done by Stöger, Weil and Mereiter, ESI-MS measurements were done by Pittenauer.

Manuscript #2

Based on the previous results on κ^3, κ^2 -Fe PNP complexes, the aim of the research was to isolate Fe(II) PNP carbonyl complexes with sterically non-demanding phosphines. The syntheses, reactivity and characterization were done by the author. Experiments on the reversible release of CO were carried out by Bernhard Bichler. Some complexes were synthesized by Christian Holzacker. *N*-substituted 2,6-diaminopyridine precursors were provided by Matthias Mastalir. X-ray measurements were done by Stöger, Weil and Mereiter. DFT calculations and graphics were provided by Veiros and Kirchner.

Manuscript #3

The synthesis and observation cationic dicarbonyl Fe(II) PNP pincer complexes was done by Bernhard Bichler and Christian Holzacker based on PNP-*i*Pr and PNP-Ph. All additional work on a comparative study a wide range of ligands was done by the author. X-ray measurements were done by Stöger and Weil. DFT calculations and graphics were provided by Veiros and Kirchner.

Manuscript #4

Synthesis characterization and application of the catalyst were all done by the author. X-ray measurements were done by Stöger and Himmelbauer. DFT calculations and graphics were provided by Veiros and Kirchner.

Manuscript #5

Synthesis and characterization of all compounds were done by the author. Lena Haager contributed essential results as part of her bachelor thesis. X-ray measurements were done by Stöger and Pecak. DFT calculations and graphics were provided by Veiros and Kirchner.

5 References

- [1] Special issues accounted to abundant, non-precious metal catalysis. (a) "Earth abundant metals in Homogeneous Catalysis", *Acc. Chem. Res.* **2015**, 48, 9. (b) "Spotlight on non-precious Metal Catalysis", *Process Res. Dev.* **2015**, 19, 10.
- [2] Greenwood N. N.; Earnshaw A. *Chemistry of the Elements*, **1997**, Butterworth-Heinemann, Oxford, 2nd edn.
- [3] Van Koten G. *Pure Appl. Chem.* **1989**, 61, 1681-1694.
- [4] For essentials of Coordination Chemistry see: Janik C.; Meyer H.-J.; Gudat D.; Alsfasser R.; *Moderne Anorganische Chemie*, de Gruyter, Berlin, 4. Auflage, **2012**.
- [5] (a) Peris E.; Loch J. A.; Mata J.; Crabtree R. H. *Chem. Commun.* **2001**, 0, 201-202. (b) Tulchinsky Y.; Iron M. A.; Botoshansky M. Gandelman M. *Nat. Chem.* **2011**, 3, 525-531. (c) Basauri-Molina M.; Hernandez-Ortega S.; Morales-Morales D. *Eur. J. Inorg. Chem.* **2014**, 27, 4619-4625.
- [6] Moulton C. J.; Shaw B. L. *J. Chem. Soc., Dalton Trans* **1976**, 1020-1024.
- [7] (a) Crocker C.; Errington R. J.; McDonald W. S.; Odell K. J.; Shaw B. L.; Goodfellow R. J. *J. Chem. Soc. Chem. Commun.* **1979**, 498-499. (b) Crocker C.; Errington R. J.; Markham R.; Moulton C. J.; Odell K. J.; Shaw B. L.; *J. Am. Chem. Soc.* **1980**, 201, 4373-4379. (c) Crocker C.; Empsall H. D.; Errington R. J.; Hyde E. M.; McDonald W. S.; Markham R.; Norton M. C.; Shaw B. L.; Weeks B. *J. Chem. Soc. Dalton Trans.* **1982**, 7, 1217-1224.
- [8] (a) Albrecht M.; van Koten G.; *Angew. Chem. Int. Ed.* **2001**, 40, 33750-3781. (b) van der Boom M. E.; Milstein D. *Chem. Rev.* **2003**, 103, 1759-1792. (c) Morales-Morales D.; *Rev. Soc. Quim. Mex.* **2004**, 48, 338-346. (d) Morales-Morales D.; Jensen C. M. *The Chemistry of Pincer Compounds*, Elsevier, Amsterdam, 1st edn, **2007**. (e) Selander N.; Szabo K. *J. Chem. Rev.* **2011**, 111, 2048-2076.
- [9] (a) Kelly W. S. J.; Ford G. H.; Nelson S. M. *J. Chem. Soc. A*, **1971**, 388-396. (b) Dalhoff W. V.; Nelson S. M. *J. Chem. Soc. A*; **1971**, 2184-2190.
- [10] (a) Giannoccaro P.; Vasapollo G.; Sacco A. *J. Chem. Soc., Chem. Commun.* **1980**, 1136-1137. (b) Vasapollo G.; Nobile C. F.; Sacco A. *J. Organomet. Chem.* **1985**, 3, 435-441.
- [11] (a) Leung W.-P.; Ip Q. W.-Y.; Wong S.-Y.; Mak T. C. W. *Organometallics* **2003**, 22, 4604-4609. (b) Salem H.; Shimon L. J. W.; Posner-Diskin Y.; Leitun G.; Ben-David Y.; Milstein D. *Organometallics* **2009**, 28, 4791-4806. (c) Benito-Garagorri D.; Becker E.; Wiedermann J.; Lackner W.; Pollak M.; Mereiter K.; Kisala J.; Kirchner K. *Organometallics* **2006**, 25, 1900-1913. (d) Öztopcu Ö.; Holzhaecker C.; Puchberger M.; Weil M.; Mereiter K.; Veiros L. F.; Kirchner K. *Organometallics* **2013**, 32, 3042-3052. (e) Schirmer, W.; Flörke, U.; Haupt, H.-J. *Z. Anorg. Allg. Chem.* **1987**, 545, 83-97. (f) Glatz M.; Bichler B.; Mastalir M.; Stöger B.; Weil M.; Mereiter K.; Pittenauer E.; Allmeier G.; Veiros L. F.; Kirchner K. *Dalton Trans.* **2015**, 44, 281-294.
- [12] Blase H.-U.; Indolese A.; Schnyder A.; *Curr. Science.* **2000**, 78, 1336-1344.
- [13] Recommended textbook: Crabtree, *Organometallic Chemistry of the Transition Elements*, Wiley, New York, 5th edn, **2009**.

[14] (a) Tolman C. A. *Chem. Rev.* **77**, 3, 313-348. (b) Poe A. J. *New. J. Chem.* **2013**, 37, 2957-2964.

[15] Gorenstein D.; *Phosphorous – 31 NMR*, Elsevier, Amsterdam, 1st edn, **2012**.

[16] Corey E.; *General methods for the construction of complex molecules*. Pure and Applied Chemistry, **2009**, 14, 19-28.

[17] (a) Weferling N. *Z. Anorg. Allg. Chem.* **1987**, 548, 55-62. (b) Gusev D. G.; Madott M.; Dolgushin F. M.; Lyssenko K. A.; Antipin M. Y. *Organometallics* **2000** 19, 1734-1739.

[18] a) Voskuil W.; Arens J. F. *Org. Synth.* **1968**, 48, 47-50. (b) Issleb K.; Seidel W.; *Chem. Ber.* **1959**, 92, 2681-2694. (c) Fild M.; Stelzer O.; Schmutzler R.; *Inorg Synth.* **1973**, 14, 4-9. (d) Eisenträger F.; Göthlich A.; Gruber I.; Heiss H.; Kiener C. A.; Krüger C.; Notheis J. U.; Rominger F.; Scherhag G.; Schultz M.; Straub B.; Volland M. A. O.; Hofmann P. *New J. Chem.* **2003**, 27, 540-550.

[19] (a) Wolfsberger W. *J. Organomet. Chem.* **1989**, 317, 167-173. (b) McEwen W. E.; Janes B. A.; Knapczyk J. W.; Kyllingstad V. L.; Shiao W.-I.; Shore S.; Smith J. H. *J. Am. Chem. Soc.* **1978**, 100, 7304-7311. (c) Yudina K. S., Medved T. Y.; Kabachnik M. I. *Izv. Akad. Nauk SSR, Ser. Khim.* **1954**. (1966).

[20] Busacca C. A.; Lorenz J. C.; Grinberg N.; Haddad N.; Hrapchak M.; Latli B.; Lee H.; Sabila P.; Saha A.; Sarvestani M.; Shen S.; Varsolona R.; Wei X.; Senanayake C. H. *Org. Lett.* **2005**, 7, 4277-4280.

[21] (a) Kuchen W., Buchwald H. *Angew. Chem.* **1957**, 69, 307-308. (b) Issleb K.; Frohlich H. O. *Z. Naturforsch.* **1959**, 14b, 249-350. (c) Wittenberg D.; Gilman H.; *J. Org. Chem.* **1958**, 23, 1063-1064. (d) Gulyas H.; Benet-Buchholz J.; Escudero-Adan E. C.; Freixa Z.; van Leeuwen P. W. N. M. *Chem. Eur. J.* **2007**, 13, 3424-3430.

[22] Holz J.; Monsees A.; Kadyrov R.; Börner A. *Synlett* **2007**, 4, 599-602.

[23] Tian L.; Qui H.; Pun V. C.; Lin H.; Ge E.; Chan J. C.; Louie. K.; Ho K.; Yu II. T. S. *Am. J. Respir. Crit. Care Med.* **2013**, 188, 1240-1245.

[24] (a) Mond L.; Langer C.; Quinke F. *J. Chem. Soc. Trans.* **1890**, 57, 749-753. (b) Trout W. E. *J. Chem. Educ.* **1934**, 14, 453-459.

[25] See textbook: Astruc D.; *Organometallic Chemistry and Catalysis*, 1st edn., Springer, Berlin, **2007**.

[26] (a) Itou M.; Araki Y.; Ito O.; Kido H.; *Inorg. Chem.* **2006**, 45, 6114-6116. (b) Moragues M. E.; Esteban J.; Ros-Lis J. V.; Martinez-Manez R.; Marcos M. D.; Martinez M.; Soto J.; Sanceon F. *J. Am. Chem. Soc.* **2001**, 133, 15762-15772.

[27] Hermann A. *Physikalische Blätter*, **1965**, 21, 168-171.

[28] (a) Bolm C.; Legros J.; Pailh J. L.; Zani L. *Chem. Rev.* **2004**, 104, 6217-6254. (b) Fürstner A.; Martin R. *Chem. Lett.* **2005**, 34, 624-629. (c) Enthaler S., Junge K., Beller M. *Angew. Chem. Int. Ed.* **2008**, 47, 3317-3321. (d) Bauer E. B. *Curr. Org. Chem.* **2008**, 12, 1341-1369.

[29] (a) Bhattacharya P.; Guan H. *Comments Inorg. Chem.* **2011**, 32, 88-112. (b) Zell T.; Milstein D. *Acc. Chem. Res.* **2015**, 48, 1979-1994. (c) Bauer G.; Hu X. *Inorg. Chem. Front.* **2016**, 3, 741-765.

[30] (a) Jorgensen C. K. *Coord. Chem. Rev.* **1966**, 1, 164-176. (b) Grützmacher H. *Angew. Chem. Int. Ed.* **2008**, 47, 1814-1818. (c) van der Vlugt J. *Eur. J. Inorg.*

Chem. **2012**, 363-375. (d) Blanchard S.; Derat E.; Murr M. D-E.; Fensterbank L.; Malacria M.; Mouries-Mansuy V. *Eur. J. Inorg. Chem.* **2012**, 376-389.

[31] (a) Nelson S. M.; Dahlhoff W. V. *J. Chem. Soc. (A)* **1971**, 2184-2190. (b) Giannoccaro P.; Vasapollo G.; Nobile C. F.; Sacco A. *Inorg. Chim. Acta* **1982**, 61, 69-75. (c) Zhang J.; Gandelman M.; Herrman D.; Leitus G.; Shimon L. J. W.; Ben-David Y.; Milstein D. *Inorg. Chim. Acta* **2006**, 359, 1955-1960. (d) Benito-Garagorri D.; Wiedermann J.; Pollak M.; Mereiter K.; Kirchner K. *Organometallics* **2007**, 26, 217-222. DeRieux W-S. W.; Wong A.; Schrodi Y. *J. Organomet. Chem.* **2014**, 772-773, 60-67.

[32] (a) Trovitch R. J.; Lobkovsky E.; Chirik P. *J. Inorg. Chem.* **2006**, 45, 7252-7260. (b) Pelczar E. M.; Emge T. J.; Krogh-Jespersen K. Goldman A. S. *Organometallics* **2008**, 27, 5759-5767.

[33](a) Benito-Garagorri D.; Puchberger M.; Mereiter K. Kirchner K. *Angew. Chem. Int. Ed.* **2008**, 47, 9142-9145. (b) Benito-Garagorri D.; Alves L. G.; Puchberger M.; Mereiter K.; Veiros L. F.; Calhorda M. J.; Carvalho M. D.; Ferreira L. P.; Godinho M. Kirchner K. *Organometallics* **2009**, 28, 6902-6914. (c) Benito-Garagorri D.; Alves L. G.; Veiros L. F.; Standfest-Hauser C. M.; Tanaka S.; Mereiter K.; Kirchner K. *Organometallics* **2010**, 29, 4932-4942.

[34] Pecak J.; Glatz M.; Stöger B.; Roland B.; Hoffmann H.; Atkins A.; Gonzalez L.; Kirchner K. *Polyhedron* **2018**, 143, 94-98.

[35] (a) Bichler B.; Glatz M.; Stöger B.; Mereiter K.; Veiros L. F.; Kirchner K. *Dalton Trans.* **2014**, 43, 14517-14519. (b) Holzhaecker C.; Stöger B.; Carvalho M. D.; Ferreira L. P.; Pittenauer E.; Allmaier G.; Veiros L. F.; Realista S.; Gil A.; Calhorda M. J.; Müller D.; Kirchner K. *Dalton Trans.* **2015**, 44, 13071-13086.

[36] (a) Langer R.; Leigus G.; Ben-David Y.; Milstein D. *Angew. Chem. Int. Ed.* **2011**, 50, 2120-2124. (b) Gorgas N.; Stöger B.; Veiros L. F.; Pittenauer E.; Allmeier G.; Kirchner K. *Organometallics* **2014**, 33, 6905-6914. (c) Mazza S.; Scopelliti, R.; Hu X. *Organometallics* **2015**, 34, 1538-1545. (d) Gorgas N.; Stöger B.; Veiros L. F.; Kirchner K. *ACS Catal.* **2016**, 6, 2664-2672

[37] Smith A. D.; Saini A.; Singer L. M.; Phadke N.; Findlater M. *Polyhedron* **2016**, 114, 286-291.

[38] Heim L. E.; Konnerth H.; Prechtl M. H. G. *Green Chem.* **2017**, 19, 2347-2355.

[39] (a) Rivada-Wheelaghan, Dauth A., Leitus G.; Diskin-Posner Y.; Milstein D. *Inorg. Chem.* **2015**, 54, 4526-4538. (b) Bertini F.; Gorgas N.; Stöger B.; Peruzzini M.; Veiros L. F.; Kirchner K.; Gonsalvi L. *ACS Catal.* **2016**, 6, 2889-2893.

[40](a) Fillman K. L.; Bielinsky E. A.; Schmeier T. J.; Nevset J. C.; Woodruff T. M.; Pan C. J.; Takase M. K.; Hazari N.; Neidig M. L. *Inorg. Chem.* **2014**, 53, 6066-6072. (b) Koehne I.; Schmeier T. J.; Bielinsky E. A.; Pan C. J.; Lagaditis P. O.; Bernskoetter W. H.; Takase M. K.; Würtele C.; Hazari N.; Schneider S. *Inorg. Chem.* **2014**, 53, 2133-2143.

[41] (a) Alberico E.; Sponholz P.; Cordes C.; Nielsen M.; Drexler H.-J.; Baumann W.; Junge H.; Beller M. *Angew. Chem. Int. Ed.* **2013**, 52, 14162-14166. (b) Lagaditis P. O.; Sues P. E.; Sonnenberg J. F.; Wan K. Y.; Lough A. J.; Morris R. H. *J. Am. Chem. Soc.* **2014**, 136, 1367-1380.

[42](a) Chakraborty S.; Dai H.; Bhattacharya P.; Fairweather N. T.; Gibson M. S.; Krause J. A.; Guan H. *J. Am. Chem. Soc.* **2014**, 136, 7869-7872. (b) Werkmeister S.; Junge K.; Wendt B.; Alberico E.; Jiao H.; Baumann W.; Junge H.; Gallou F.; Beller M. *Angew. Chem. Int. Ed.* **2014**, 53, 8722-8726. (c) Elangovan S.; Wendt B.; Topf C.; Bachmann S.; Scalone M.; Spannenberg A.; Jiao H.; Baumann W.; Junga K.; Beller M. *Adv. Synth. Catal.* **2016**, 358, 820-825.

[43](a) Ingleson M. J.; Fullmer B. C.; Buschhorn D. T.; Fan H.; Pink M.; Huffman J. C.; Caulton K. G. *Inorg. Chem.* **2008**, 47, 407-409. (b) Adhikari D.; Basuli F.; Fan H.; Huffman J. C.; Pink M.; Mindiola D. J. *Inorg. Chem.* **2008**, 47, 4439-4441. (d) Kuriyama S.; Arashiba K.; Nakajima K.; Matsuo Y.; Tanaka H.; Ishii K.; Yoshizawa K.; Nishibayashi Y. *Nature Commun.* **2016**, 7, 21181. (d) Ehrlich Nico, Kreye M.; Baabe D.; Schweyen P.; Freytag M.; Jones P. G.; Walter M. D. *Inorg. Chem.* **2017**, 56, 8415-8422.

[44] (a) Thompson C. V.; Arman H. D.; Tonzetich Z. J. *Organometallics* **2017**, 46, 1795-1802. (b) Thompson C. V.; Davis I.; DeGayner J. A.; Arman H. D.; Tonzetich Z. J. *Organometallics* **2017**, 36, 4928-4935. (c) Thompson C. V.; Arman H. D.; Tonzetich Z. J. *Organometallics* **2017**, 36, 1795-1802.

[45] (a) Katsuki T. *Coord. Chem. Rev.* **1995**, 140, 189-214. (b) Valyaev D.; Lavigne G.; Lugan N. *Coord. Chem. Rev.* **2016**, 308, 192-235. (c) Liu W.; Ackermann L. *ACS Catal* **2016**, 6, 3743-3752.

[46] (a) Maji B.; Barman M. K. *Synthesis* **2017**, 49, 3377-3393. (b) Garbe M.; Junge K.; Beller M. *Eur. J. Org. Chem.* **2017**, 30, 4344-4362. (c) Filonenko G. A.; van Putten R.; Hensen E. J. M.; Pidko E. A. *Chem. Soc. Rev.* **2018**, 47, 1459-1483

[47] Dahl L. F.; Ishishi E.; Rundle R. E. *J. Chem. Phys.* **1957**, 26, 1750-1751.

[48] (a) Reimer K. J.; Shaver A. *Inorg. Synth.* **1979**, 19, 159. (b) Reimer K. J.; Shaver A. *Inorg. Synth.* **1990**, 28.

[49] Radosevich A. T.; Melnick J. G.; Stoian S. A.; Bacciu D.; Chen C.-H.; Foxman B. M.; Ozerov O. V.; Nocera D. G. *Inorg. Chem.* **2009**, 48, 9214-9221.

[50] Bacciu D.; Chen C.-H.; Surawatanawong P.; Foxman B. M.; Ozerov O. V. *Inorg. Chem.* **2010**, 49, 5328-5334.

[51] (a) Tondreau A. M.; Boncella J. M. *Polyhedron* **2016**, 116, 96-104. (b) Tondreau A. M.; Boncella J. M. *Organometallics* **2016**, 35, 2049-2052.

[52] (a) Mastalir M.; Glatz M.; Gorgas N.; Stöger B.; Pittenauer E.; Allmaier G.; Veiros L, F.; Kirchner K. *Chem. Eur. J.* **2016**, 22, 12316-12320. (b) Mukherjee A.; Nerush A.; Leitus G.; Shimon L. J. W.; Ben-David Y.; Japala N. A. E.; Milstein D. *J. Am. Chem. Soc.* **2016**, 138, 4298-4301. (c) Elangovan S. Topf C.; Fisher S.; Jiao H.; Spannenberg A.; Baumann W.; Ludwig R.; Junge K.; Beller M. *J. Am. Chem. Soc.* **2016**, 138, 8809-8814 (d) Kallmeier F.; Irrgang T.; Dietel T.; Kempe R. *Angew. Chem. Int. Ed.* **2016**, 55, 11806-11809.

[53] (a) Mastalir M.; Glatz M.; Pittenauer E.; Allmaier G.; Kirchner K. *J. Am. Chem. Soc.* **2016**, 138, 15543-15546. (b) Deibl N.; Kempe R. *Angew. Chem. Int. Ed.* **2017**, 56, 1663-1666.

[54] a) Bruneau-Voisine A.; Wang D.; Dorcet V.; Roisnel T.; Darcel C.; Sortais J.-B. *J. Catal.* **2017**, 347, 57-62. b) Neumann J.; Elangovan S.; Spannenberg A.; Junge

K.; Beller M. *Chem. Eur. J.* **2017**, 23, 5410-5413. Mastalir M.; Pittenauer E.; Allmaier G.; Kirchner K. *J. Am. Chem. Soc.* **2017**, 139, 8812-8815.

[55] (a) Tondreau A. M.; Boncella J. M. *Organometallics* **2016**, 25, 2049-2052.
(b) Bertini F.; Glatz M.; Gorgas N.; Stöger B.; Peruzzini M.; Beiros L.; Kirchner K.; Gonsalvi L. *Chem. Sci* **2017**, 8, 5024-5029.

6 List of Figures

Figure 1: Basic structure of a pincer ligand and coordination to a metal center.....	2
Figure 2: Synthesis of PCP pincer complexes by Shaw	2
Figure 3: Applications of precious metal pincer complexes	3
Figure 4: Versatility of 2,6-substituted pyridine moiety	3
Figure 5: PNP pincer ligands used in this work	4
Figure 6: Retrosynthetic analysis of a PNP pincer with CH ₂ linkers	4
Figure 7: Synthetic concept for the preparation of tertiary phosphine precursors.....	5
Figure 8: Illustration of σ -donor/ π -acceptor interaction in metal-CO complexes	6
Figure 9: Selection of pentacoordinated Fe(II) PNP dichloro complexes.....	7
Figure 10: Synthesis of Fe(0) PNP biscarbonyl complexes	7
Figure 11: Reversible binding of CO by an iron(II) PNP pincer complex	8
Figure 12: Fe(II) PNP pincer complexes with bidentate (κ^2) bonding modes.....	9
Figure 13: Pre-catalysts for hydrogenation of ketones and aldehydes	10
Figure 14: Pre-catalysts for hydrogenation of ketones and aldehydes	10
Figure 15: Hydrosilylation of secondary alcohols.....	11
Figure 16: Hydrogenation of CO ₂ catalyzed by Fe(II) PNP pincer complexes	11
Figure 17: Hydrogenation of esters to alcohols catalyzed by Fe(II) PNP pincer complex	12
Figure 18: Iron PNP complexes with anionic ligand system	12
Figure 19: Synthesis of manganese-pentacarbonyl halide	13
Figure 20: The first manganese(I) PNP pincer complexes by Nocera and Ozerov....	14
Figure 21: Reactivities of neutral Mn(I) PNP pincer complexes.....	15
Figure 22: Mn(I) PNP pincer complexes in reductive chemistry	16
Figure 23: Formal mechanism of the hydrogenation mechanism on C=O double bond	16
Figure 24: Multicomponent pyrimidine and quinoline synthesis catalyzed by Mn(I) PNP pincer complexes	17
Figure 25: Alkylation of amines by methanol, catalyzed by Mn(I)	17
Figure 26: Synthesis of Mn(I) PNP formate pincer complexes	18

7 Abbreviation

PCP	Pincer ligand with phosphorus, carbon and phosphorus donors
PNP	Pincer ligand with phosphorus, nitrogen and phosphorus donors
CO	Carbon monoxide
PR ₂	Fragment of a tertiary phosphine with two organic substituents
<i>n</i> Bu, <i>i</i> Pr, <i>t</i> Bu, Cy	1-butane, <i>iso</i> -butane, <i>tert</i> -butane, cyclohexane
TFA	Trifluoro acetic acid
MO	Molecular orbital
[Et ₃ BH] ⁻	Triethylborohydride (Superhydride®)
DFT	Density functional theory
THF	Tetrahydrofuran
TON	Turnover number
k ³ , k ²	Chelate ligand in tri- / bidentate coordination mode
bipy	bipyridine
NMR	Nuclear magnet resonance
IR	Infrared
HOTf	Triflic acid

8 Reprint Permissions

Download the [Royal Society of Chemistry licence to publish](#) ([/globalassets/05-journals-books-databases/journal-authors-reviewers/licences-copyright-permissions/royal-society-of-chemistry-licence-to-publish.pdf](#))

Rights retained by authors

When the author accepts the exclusive licence to publish for a journal article, he/she retains certain rights that may be exercised without reference to the Royal Society of Chemistry.

Reproduce/republish portions of the article (including the abstract).

Photocopy the article and distribute such photocopies and distribute copies of the PDF of the article for personal or professional use only (the Royal Society of Chemistry makes this PDF available to the corresponding author of the article upon publication. Any such copies should not be offered for sale. Persons who receive or access the PDF mentioned above must be notified that this may not be made available further or distributed.).

Adapt the article and reproduce adaptations of the article for any purpose other than the commercial exploitation of a work similar to the original.

Reproduce, perform, transmit and otherwise communicate the article to the public in spoken presentations (including those that are accompanied by visual material such as slides, overheads and computer projections).

The author(s) must submit a written request to the Royal Society of Chemistry for any use other than those specified above.

All cases of republication/reproduction must be accompanied by an [acknowledgement](#) ([/journals-books-databases/journal-authors-reviewers/licences-copyright-permissions/#reuse-permission-requests](#)) of first publication of the work by the Royal Society of Chemistry, the wording of which depends on the journal in which the article was published originally. The acknowledgement should also include a hyperlink to the article on the Royal Society of Chemistry website.

The author also has some rights concerning the deposition of the whole article.

Deposition and sharing rights

The following details apply only to authors accepting the standard licence to publish. Authors who have accepted one of the open access licences to publish, or are thinking of doing so, should refer to the [details for open access deposition rights](#) ([/journals-books-databases/open-access/#choose](#)).

When the author accepts the licence to publish for a journal article, he/she retains certain rights concerning the deposition of the whole article. This table summarises how you may distribute the accepted manuscript and version of record of your article.

Sharing rights	Accepted manuscript	Version of record
Share with individuals on request, for personal use	✓	✓
Use for teaching or training materials	✓	✓
Use in submissions of grant applications, or academic requirements such as theses or dissertations	✓	✓
Share with a closed group of research collaborators, for example via an intranet or privately via a scholarly communication network (/journals-books-databases/open-access/green-open-access/#share)	✓	✓
Share publicly via a scholarly communication network that has signed up to STM sharing principles	⌘	×
Share publicly via a personal website, institutional repository (/journals-books-databases/open-access/green-open-access/#share), or other not-for-profit repository	⌘	×
Share publicly via a scholarly communication network that has not signed up to STM sharing principles	×	×

⌘ Accepted manuscripts may be distributed via repositories after an embargo period of 12 months

If you are a reader looking for the terms of use for information published by the Royal Society of Chemistry under our standard licence to publish please refer our [terms of use](#) ([/journals-books-databases/librarians-information/products-prices/licensing-terms-and-conditions/#non-commercial-terms](#)).

We are members of the CHORUS initiative, and therefore make the Accepted manuscript version of articles describing research funded by participating funders publicly available on our web site after an embargo period of 12 months. This is effective for research published from 1st March 2018 onwards. Unless otherwise noted on the article the Accepted manuscript is licensed under the terms of our standard license to publish and is subject to our standard [reuse terms](#) ([/journals-books-databases/librarians-information/products-prices/licensing-terms-and-conditions/#non-commercial-terms](#)).

Re-use permission requests

Material published by the Royal Society of Chemistry and other publishers is subject to all applicable copyright, database protection, and other rights. Therefore, for any publication, whether printed or electronic, permission must be obtained to use material for which the author(s) does not already own the copyright. This material may be, for example, a figure, diagram, table, photo or some other image.

Author reusing their own work published by the Royal Society of Chemistry

You do not need to request permission to reuse your own figures, diagrams, etc. that were originally published in a Royal Society of Chemistry publication. However, permission should be requested for use of the whole article or chapter except if reusing it in a thesis. If you are including an article or book chapter published by us in your thesis please ensure that your co-authors are aware of this.

Reuse of material that was published originally by the Royal Society of Chemistry must be accompanied by the appropriate acknowledgement of the publication. The form of the acknowledgement is dependent on the journal in which it was published originally, as detailed in 'Acknowledgements'.

Material published by the Royal Society of Chemistry to be used in another of our publications

Authors contributing to our publications (journal articles, book or book chapters) do not need to formally request permission to reproduce material contained in another Royal Society of Chemistry publication. However, permission should be requested for use of a whole article or chapter. For all cases of reproduction the correct acknowledgement of the reproduced material should be given. The form of the acknowledgement is dependent on the journal in which it was published originally, as detailed in the 'Acknowledgements' section.

Acknowledgements —

The Royal Society of Chemistry publishes some journals in partnership with, or on behalf of, other organisations; these journals require a specific wording of the acknowledgement when work is reproduced from them. The text for the acknowledgement for these journals, and the standard wording to be used by all other journals are given below.

Standard acknowledgement

Reproduced from Ref. XX with permission from the Royal Society of Chemistry.

Non-standard acknowledgements

Reproduction of material from NJC (New Journal of Chemistry)

Reproduced from Ref. XX with permission from the Centre National de la Recherche Scientifique (CNRS) and the Royal Society of Chemistry.

Reproduction of material from Photochemical & Photobiological Sciences (PPS)

Reproduced from Ref. XX with permission from the European Society for Photobiology, the European Photochemistry Association, and the Royal Society of Chemistry.

Reproduction of material from PCCP (Physical Chemistry Chemical Physics)

Reproduced from Ref. XX with permission from the PCCP Owner Societies.

Reproduction of material from Inorganic Chemistry Frontiers

Reproduced from Ref. XX with permission from the Chinese Chemical Society (CCS), Peking University (PKU), and the Royal Society of Chemistry.

Reproduction of material from Organic Chemistry Frontiers

Reproduced from Ref. XX with permission from the Chinese Chemical Society (CCS), Shanghai Institute of Organic Chemistry (SIOC), and the Royal Society of Chemistry.

Reproduction of material from articles in the Journal Archive from Geochemical Transactions

Reproduced from Ref. XX with permission from the American Chemical Society, Division of Geochemistry and the Royal Society of Chemistry.

Using third party material in Royal Society of Chemistry publications

We must ensure that the material we publish does not infringe the copyright of others. We require the author(s) to obtain, at the earliest opportunity, the relevant permissions that might be needed from third parties to include material that belongs to someone else.

Please contact the publisher/copyright owner of the third party material to check how they wish to receive permission requests. Please plan to submit your request well ahead of publication of your material.

The most common procedures for permission requests are outlined below.

- A number of publishers have opted out of receiving express permissions as long as they fall under the rules of the [STM Permission Guidelines](http://www.stm-assoc.org/copyright-legal-affairs/permissions/permissions-guidelines) (<http://www.stm-assoc.org/copyright-legal-affairs/permissions/permissions-guidelines>).
- If they do not fall into the category above, the majority of publishers now use RightsLink from the Copyright Clearance Center (CCC) to process their requests.
- Other publishers have their own permission request forms and/or specify what information they need to process any permission request.

JOHN WILEY AND SONS LICENSE TERMS AND CONDITIONS

Feb 15, 2018

This Agreement between Mathias Glatz ("You") and John Wiley and Sons ("John Wiley and Sons") consists of your license details and the terms and conditions provided by John Wiley and Sons and Copyright Clearance Center.

License Number	4290191370448
License date	Feb 15, 2018
Licensed Content Publisher	John Wiley and Sons
Licensed Content Publication	European Journal of Inorganic Chemistry
Licensed Content Title	FeII Carbonyl Complexes Featuring Small to Bulky PNP Pincer Ligands – Facile Substitution of κ^2P,N -Bound PNP Ligands by Carbon Monoxide
Licensed Content Author	Mathias Glatz,Christian Holzhaecker,Bernhard Bichler,Matthias Mastalir,Berthold Stöger,Kurt Mereiter,Matthias Weil,Luis F. Veiros,Nadia C. Mösch-Zanetti,Karl Kirchner
Licensed Content Date	Sep 30, 2015
Licensed Content Pages	13
Type of use	Dissertation/Thesis
Requestor type	Author of this Wiley article
Format	Print and electronic
Portion	Full article
Will you be translating?	No
Title of your thesis / dissertation	The Role of Sterics and Electronics of PNP-Pincer Ligands in Iron(II), Manganese(I) and Re(I) Pincer-Chemistry
Expected completion date	Mar 2018
Expected size (number of pages)	150
Requestor Location	Mathias Glatz Staudach 216 Hartberg, Styria 8230 Austria Attn: Mathias Glatz
Publisher Tax ID	EU826007151
Total	0.00 EUR

Terms and Conditions

TERMS AND CONDITIONS

This copyrighted material is owned by or exclusively licensed to John Wiley & Sons, Inc. or one of its group companies (each a "Wiley Company") or handled on behalf of a society with which a Wiley Company has exclusive publishing rights in relation to a particular work (collectively "WILEY"). By clicking "accept" in connection with completing this licensing transaction, you agree that the following terms and conditions apply to this transaction (along with the billing and payment terms and conditions established by the Copyright Clearance Center Inc., ("CCC's Billing and Payment terms and conditions"), at the time that you opened your RightsLink account (these are available at any time at <http://myaccount.copyright.com>).

Terms and Conditions

- The materials you have requested permission to reproduce or reuse (the "Wiley Materials") are protected by copyright.
- You are hereby granted a personal, non-exclusive, non-sub licensable (on a stand-alone basis), non-transferable, worldwide, limited license to reproduce the Wiley Materials for the purpose specified in the licensing process. This license, **and any CONTENT (PDF or image file) purchased as part of your order**, is for a one-time use only and limited to any maximum distribution number specified in the license. The first instance of republication or reuse granted by this license must be completed within two years of the date of the grant of this license (although copies prepared before the end date may be distributed thereafter). The Wiley Materials shall not be used in any other manner or for any other purpose, beyond what is granted in the license. Permission is granted subject to an appropriate acknowledgement given to the author, title of the material/book/journal and the publisher. You shall also duplicate the copyright notice that appears in the Wiley publication in your use of the Wiley Material. Permission is also granted on the understanding that nowhere in the text is a previously published source acknowledged for all or part of this Wiley Material. Any third party content is expressly excluded from this permission.
- With respect to the Wiley Materials, all rights are reserved. Except as expressly granted by the terms of the license, no part of the Wiley Materials may be copied, modified, adapted (except for minor reformatting required by the new Publication), translated, reproduced, transferred or distributed, in any form or by any means, and no derivative works may be made based on the Wiley Materials without the prior permission of the respective copyright owner. **For STM Signatory Publishers clearing permission under the terms of the [STM Permissions Guidelines](#) only, the terms of the license are extended to include subsequent editions and for editions in other languages, provided such editions are for the work as a whole in situ and does not involve the separate exploitation of the permitted figures or extracts,** You may not alter, remove or suppress in any manner any copyright, trademark or other notices displayed by the Wiley Materials. You may not license, rent, sell, loan, lease, pledge, offer as security, transfer or assign the Wiley Materials on a stand-alone basis, or any of the rights granted to you hereunder to any other person.
- The Wiley Materials and all of the intellectual property rights therein shall at all times remain the exclusive property of John Wiley & Sons Inc, the Wiley Companies, or their respective licensors, and your interest therein is only that of having possession of and the right to reproduce the Wiley Materials pursuant to Section 2 herein during the continuance of this Agreement. You agree that you own no right, title or interest in or to the Wiley Materials or any of the intellectual property rights therein. You shall have no rights hereunder other than the license as provided for above in Section 2. No right, license or interest to any trademark, trade name, service mark or other branding ("Marks") of WILEY or its licensors is granted hereunder, and you agree that you shall not assert any such right, license or interest with respect thereto
- NEITHER WILEY NOR ITS LICENSORS MAKES ANY WARRANTY OR REPRESENTATION OF ANY KIND TO YOU OR ANY THIRD PARTY, EXPRESS, IMPLIED OR STATUTORY, WITH RESPECT TO THE MATERIALS OR THE ACCURACY OF ANY INFORMATION CONTAINED IN THE MATERIALS, INCLUDING, WITHOUT LIMITATION, ANY IMPLIED WARRANTY OF MERCHANTABILITY, ACCURACY, SATISFACTORY QUALITY, FITNESS FOR A PARTICULAR PURPOSE, USABILITY, INTEGRATION OR NON-INFRINGEMENT AND ALL SUCH WARRANTIES ARE HEREBY EXCLUDED BY WILEY AND ITS LICENSORS AND WAIVED BY YOU.

- WILEY shall have the right to terminate this Agreement immediately upon breach of this Agreement by you.
- You shall indemnify, defend and hold harmless WILEY, its Licensors and their respective directors, officers, agents and employees, from and against any actual or threatened claims, demands, causes of action or proceedings arising from any breach of this Agreement by you.
- IN NO EVENT SHALL WILEY OR ITS LICENSORS BE LIABLE TO YOU OR ANY OTHER PARTY OR ANY OTHER PERSON OR ENTITY FOR ANY SPECIAL, CONSEQUENTIAL, INCIDENTAL, INDIRECT, EXEMPLARY OR PUNITIVE DAMAGES, HOWEVER CAUSED, ARISING OUT OF OR IN CONNECTION WITH THE DOWNLOADING, PROVISIONING, VIEWING OR USE OF THE MATERIALS REGARDLESS OF THE FORM OF ACTION, WHETHER FOR BREACH OF CONTRACT, BREACH OF WARRANTY, TORT, NEGLIGENCE, INFRINGEMENT OR OTHERWISE (INCLUDING, WITHOUT LIMITATION, DAMAGES BASED ON LOSS OF PROFITS, DATA, FILES, USE, BUSINESS OPPORTUNITY OR CLAIMS OF THIRD PARTIES), AND WHETHER OR NOT THE PARTY HAS BEEN ADVISED OF THE POSSIBILITY OF SUCH DAMAGES. THIS LIMITATION SHALL APPLY NOTWITHSTANDING ANY FAILURE OF ESSENTIAL PURPOSE OF ANY LIMITED REMEDY PROVIDED HEREIN.
- Should any provision of this Agreement be held by a court of competent jurisdiction to be illegal, invalid, or unenforceable, that provision shall be deemed amended to achieve as nearly as possible the same economic effect as the original provision, and the legality, validity and enforceability of the remaining provisions of this Agreement shall not be affected or impaired thereby.
- The failure of either party to enforce any term or condition of this Agreement shall not constitute a waiver of either party's right to enforce each and every term and condition of this Agreement. No breach under this agreement shall be deemed waived or excused by either party unless such waiver or consent is in writing signed by the party granting such waiver or consent. The waiver by or consent of a party to a breach of any provision of this Agreement shall not operate or be construed as a waiver of or consent to any other or subsequent breach by such other party.
- This Agreement may not be assigned (including by operation of law or otherwise) by you without WILEY's prior written consent.
- Any fee required for this permission shall be non-refundable after thirty (30) days from receipt by the CCC.
- These terms and conditions together with CCC's Billing and Payment terms and conditions (which are incorporated herein) form the entire agreement between you and WILEY concerning this licensing transaction and (in the absence of fraud) supersedes all prior agreements and representations of the parties, oral or written. This Agreement may not be amended except in writing signed by both parties. This Agreement shall be binding upon and inure to the benefit of the parties' successors, legal representatives, and authorized assigns.
- In the event of any conflict between your obligations established by these terms and conditions and those established by CCC's Billing and Payment terms and conditions, these terms and conditions shall prevail.
- WILEY expressly reserves all rights not specifically granted in the combination of (i) the license details provided by you and accepted in the course of this licensing

transaction, (ii) these terms and conditions and (iii) CCC's Billing and Payment terms and conditions.

- This Agreement will be void if the Type of Use, Format, Circulation, or Requestor Type was misrepresented during the licensing process.
- This Agreement shall be governed by and construed in accordance with the laws of the State of New York, USA, without regards to such state's conflict of law rules. Any legal action, suit or proceeding arising out of or relating to these Terms and Conditions or the breach thereof shall be instituted in a court of competent jurisdiction in New York County in the State of New York in the United States of America and each party hereby consents and submits to the personal jurisdiction of such court, waives any objection to venue in such court and consents to service of process by registered or certified mail, return receipt requested, at the last known address of such party.

WILEY OPEN ACCESS TERMS AND CONDITIONS

Wiley Publishes Open Access Articles in fully Open Access Journals and in Subscription journals offering Online Open. Although most of the fully Open Access journals publish open access articles under the terms of the Creative Commons Attribution (CC BY) License only, the subscription journals and a few of the Open Access Journals offer a choice of Creative Commons Licenses. The license type is clearly identified on the article.

The Creative Commons Attribution License

The [Creative Commons Attribution License \(CC-BY\)](#) allows users to copy, distribute and transmit an article, adapt the article and make commercial use of the article. The CC-BY license permits commercial and non-

Creative Commons Attribution Non-Commercial License

The [Creative Commons Attribution Non-Commercial \(CC-BY-NC\) License](#) permits use, distribution and reproduction in any medium, provided the original work is properly cited and is not used for commercial purposes.(see below)

Creative Commons Attribution-Non-Commercial-NoDerivs License

The [Creative Commons Attribution Non-Commercial-NoDerivs License](#) (CC-BY-NC-ND) permits use, distribution and reproduction in any medium, provided the original work is properly cited, is not used for commercial purposes and no modifications or adaptations are made. (see below)

Use by commercial "for-profit" organizations

Use of Wiley Open Access articles for commercial, promotional, or marketing purposes requires further explicit permission from Wiley and will be subject to a fee.

Further details can be found on Wiley Online Library

<http://olabout.wiley.com/WileyCDA/Section/id-410895.html>

Other Terms and Conditions:

v1.10 Last updated September 2015

Questions? customercare@copyright.com or +1-855-239-3415 (toll free in the US) or +1-978-646-2777.



RightsLink®

[Home](#)[Create Account](#)[Help](#)**SPRINGER NATURE**

Title: Synthesis and characterization of cationic dicarbonyl Fe(II) PNP pincer complexes

Author: Mathias Glatz, Christian Schröder-Holzacker, Bernhard Bichler et al

Publication: Monatshefte für Chemie/Chemical Monthly

Publisher: Springer Nature

Date: Jan 1, 2016

Copyright © 2016, Springer Nature

LOGIN

If you're a **copyright.com user**, you can login to RightsLink using your copyright.com credentials. Already a **RightsLink user** or want to [learn more?](#)

Creative Commons

The request you have made is considered to be non-commercial/educational. As the article you have requested has been distributed under a Creative Commons license (Attribution-Noncommercial), you may reuse this material for non-commercial/educational purposes without obtaining additional permission from Springer Nature, providing that the author and the original source of publication are fully acknowledged (please see the article itself for the license version number). You may reuse this material without obtaining permission from Springer Nature, providing that the author and the original source of publication are fully acknowledged, as per the terms of the license. For license terms, please see <http://creativecommons.org/>.

[BACK](#)[CLOSE WINDOW](#)

Copyright © 2018 [Copyright Clearance Center, Inc.](#) All Rights Reserved. [Privacy statement](#). [Terms and Conditions](#). Comments? We would like to hear from you. E-mail us at customercare@copyright.com

**RightsLink**®[Home](#)[Create Account](#)[Help](#)

Title: Chemoselective Hydrogenation of Aldehydes under Mild, Base-Free Conditions - Manganese Outperforms Rhenium

Author: Mathias Glatz, Berthold Stöger, Daniel Himmelbauer, et al

Publication: ACS Catalysis

Publisher: American Chemical Society

Date: Apr 1, 2018

Copyright © 2018, American Chemical Society

LOGIN

If you're a **copyright.com user**, you can login to RightsLink using your copyright.com credentials. Already a **RightsLink user** or want to [learn more?](#)

PERMISSION/LICENSE IS GRANTED FOR YOUR ORDER AT NO CHARGE

This type of permission/license, instead of the standard Terms & Conditions, is sent to you because no fee is being charged for your order. Please note the following:

- Permission is granted for your request in both print and electronic formats, and translations.
- If figures and/or tables were requested, they may be adapted or used in part.
- Please print this page for your records and send a copy of it to your publisher/graduate school.
- Appropriate credit for the requested material should be given as follows: "Reprinted (adapted) with permission from (COMPLETE REFERENCE CITATION). Copyright (YEAR) American Chemical Society." Insert appropriate information in place of the capitalized words.
- One-time permission is granted only for the use specified in your request. No additional uses are granted (such as derivative works or other editions). For any other uses, please submit a new request.

[BACK](#)[CLOSE WINDOW](#)

Copyright © 2018 [Copyright Clearance Center, Inc.](#) All Rights Reserved. [Privacy statement.](#) [Terms and Conditions.](#) Comments? We would like to hear from you. E-mail us at customercare@copyright.com

9 Curriculum Vitae (CV)

Personal Data

First- and Last Name: Mathias Glatz, MSc.

Date of Birth: 11.05.1989

Nationality: Austria



Education

03/2014 – 5/2018 University Assistant, TU Vienna

Dissertation (PhD) at the institute of applied synthesis (IAS)

Doctoral Thesis: field of organometallic chemistry and catalysis.

„The Role of Sterics and Electronics of PNP Pincer Ligands in Iron(II) and Manganese(I) Pincer-Chemistry”

10/2011 - 12/2013 Master Study (chemistry), TU Graz

Master Thesis: field of organometallic chemistry

„Characterization of new Fe(II) PNP Pincer Complexes with sterically nondemanding Phosphine-Residues

03/2008 – 10/2011 Bachelor Study (chemistry), TU Graz

Bachelor Thesis: field of analytical chemistry

„Determination of Metal Impurities in Pharmaceuticals with ICP-MS”

2007 - 2008 Military service, Pinkafeld, Burgenland

2003 - 2007 Diploma matriculation BORG Hartberg

Main Focus: Life Science and Computer Science

1999 - 2003 Secondary School in Hartberg (Sports)

Job Experience

2013 – now University Assistant at Vienna University of Technology

2010-2013 Tutor in various lab courses at TU Graz und TU Vienna

general, analytic, organic and inorganic chemistry

- 08/2010 AGRANA Fruit Corporate Gleisdorf (Internship) Product Development
- 08/2009 Prolactal (Internship) Quality Assurance
- 08/2008 Durmont Carpet Factory (Internship) Quality Assurance

Languages

- German mother tongue
- English business fluent
- French basic level

Hobbies

Sports American Football, Ultimate Frisbee, Radfahren

Economy and Technology security and bond exchange, computer hardware

Gastronomy Scotch Single Malt Whisky, Carribean Rum

Scientific Presentations

Poster-Presentation: 17th Austrian Chemistry Days in Salzburg “Highly Efficient and Selective Hydrogenation of Aldehydes Catalyzed by Manganese and Rhenium PNP Pincer Complexes” (2017)

Poster-Presentation: 34th Congress Organometallic Chemistry Group (GEQO) in Girona, Spanien “Novel PNP-Pincer Based Mn(I) Catalysts – selective Hydrogenation of Aldehydes under Mild, Basefree Conditions” (2016)

Poster-Presentation: 15th Belgian Organic Synthesis Symposium (BOSS) in Antwerpen, Belgien “Novel PNP-Pincer Based Mn(I) Catalysts – selective Hydrogenation of Aldehydes under Mild, Basefree Conditions” (2016)

Poster-Presentation: 14th Belgian Organic Synthesis Symposium (BOSS) in Louvain-la-Neuve, Belgien “2,6-Diaminopyridine Based PNP Pincers – the Study of a convenient Ligand System with Tremendous Steric and Electronic Versatility” (2014)

Poster-Presentation: 15th Austrian Chemistry Days in Graz, Österreich „Lability of iron(II) PNP Pincer Complexes – κ^3 versus κ^2 Bonding Modes of PNP Ligands” (2013)

Poster-Presentation: 14th Austrian Chemistry Days in Linz, „Determination of Metal Impurities in Pharmaceuticals with ICP-MS” (2011)

Publikationen

Paper "Chemoselective Hydrogenation of Aldehydes under Mild, Base-Free Conditions - Manganese Outperforms Rhenium". **Glatz M.**; Stoeger B.; Himmelbauer D.; Veiros L. F.; Kirchner K. *ACS Catal.* **2018**, 8, 4009-4016.

Paper "Non-order-disorder allotwinning of rhenium pincer complex cis-Re[(PNPCH₂-iPr)(CO)₂Cl]". **Glatz M.**; Stöger B.; Kirchner K. *Acta Cryst.* **2017**, B73, 941-949.

Paper "Visible light-induced cis/trans isomerization of dicarbonyl Fe(II) PNP pincer complexes". Pecak J.; **Glatz M.**; Stoeger B.; Bittner R.; Hoffmann H.; Atkins A.; Gonzalez L.; Kirchner K. *Polyhedron* **2018**, 143, 94-98.

Paper "Crystal structure of the tetrahydrofuran disolvate of a 94:6 solid solution of [N₂,N₆-bis(di-tert-butylphosphanyl)pyridine-2,6-diamine]dibromidomanganese(II) and its monophosphine oxide analogue". Rotter M.; Mastalir M.; **Glatz M.**; Stöger B.; Kirchner K. *Acta Cryst.* **2017**, E73, 1308-1311.

Paper "Carbon dioxide hydrogenation catalysed by well-defined Mn(I) PNP pincer hydride complexes". Bertini F.; **Glatz M.**; Gorgas N.; Stöger B.; Peruzzini M.; Veiros L. F.; Kirchner K.; Gonsalvi L. *Chem. Sci.* **2017**, 8, 5024-5029.

Paper "Sustainable Synthesis of Quinolines and Pyrimidines Catalyzed by Manganese PNP Pincer Complexes". Mastalir M.; **Glatz M.**; Pittenauer E.; Allmaier G.; Kirchner K. *J. Am. Chem. Soc.* **2016**, 138, 15543-15546.

Paper "Crystal structure of hexakis(dimethyl suloxido-κO)manganese(II) diiodide". **Glatz M.**; Schroffenegger M.; Weil M.; Kirchner K. *Acta Cryst.* **2016**, E72, 904-906.

Paper "Synthesis and characterization of cationic dicarbonyl Fe(II) PNP pincer complexes". **Glatz M.**; Schröder-Holzhacker C.; Bichler B.; Stöger B.; Mereiter K.; Veiros L. F.; Kirchner K. *Monatsh Chem.* **2016**, 147, 1713-1719.

Paper "Divergent Coupling of Alcohols and Amines Catalyzed by Isoelectronic Hydride MnI and FeII PNP Pincer Complexes". Mastalir M.; Glatz M.; Gorgas N.; Stöger B.; Veiros L. F.; Kirchner K. *Chem. Eur. J.* **2016**, 22, 12316-12320.

Paper "Crystal structure of bis[μ-2-(diisopropylphosphoryl)propan-2-olato-κ³O1,O2:O1]bis[chloridooxidovanadium(IV)]". **Glatz M.**; Stöger B.; Weil M.; Kirchner K. *Acta Cryst.* **2016**, E72, 785-788.

Paper "Synthesis, characterization and reactivity of vanadium, chromium, and manganese PNP pincer complexes". Mastalir M.; **Glatz M.**; Stöger B.; Weil M.; Pittenauer E.; Allmaier G.; Kirchner K. *Inorg. Chim. Acta.* **2017**, 455, 707-714.

Paper "A convenient solvothermal synthesis of Group 6 PNP pincer tricarbonyl complexes". Mastalir M.; de Aguiar S. R. M. M.; **Glatz M.**; Stöger B.; Kirchner K. *Organometallics* **2016**, 35, 229-232.

Paper "Twinning of three Fe-PNP pincer complexes interpreted according to order-disorder (OD) theory". Bichler B.; Schröder-Holzhacker C.; **Glatz M.**; Stöger B.; Kirchner K. *Acta Cryst.* **2015**, B71, 524-534.

Paper "Fell Carbonyl Complexes Featuring Small to Bulky PNP Pincer Ligands - Facile Substitution of κ^2 P,N-Bound PNP Ligands by Carbon Monoxide". **Glatz M.**; Schröder-Holzhacker C.; Bichler B.; Mastalir M.; Stöger B.; Mereiter K.; Weil M.; Veiros L. F.; Mösch-Zanetti N. C.; Kirchner K. *Eu. J. Inorg. Chem.* **2015**, 30, 5053-5065.

Paper "Iron(II) complexes featuring κ^3 - and κ^2 -bound PNP pincer ligands - the significance of sterics". **Glatz M.**; Bichler B.; Mastalir M.; Stöger B.; Weil M.; Mereiter K.; Pittenauer E.; Allmaier G.; Veiros L. F.; Kirchner K. *Dalton Trans.* **2015**, 44, 281-294.

Paper "An iron(II) complex featuring κ^3 and labile κ^2 -bound PNP pincer ligands - striking differences between CH₂ and NH spacers". Bichler B.; **Glatz M.**; Stöger B.; Mereiter K.; Veiros L. F.; Kirchner K. *Dalton Trans.* **2014**, 43, 14517-14519.